

POLITECNICO DI TORINO

Area dell'Ingegneria
Corso di Laurea Magistrale in Ingegneria Civile

Tesi di Laurea Magistrale

**Advanced characterization of asphalt mixtures
containing devulcanized rubber modified binders**



Relatori:

prof. Davide Dalmazzo
prof. Ezio Santagata
ing. Michele Lanotte
prof. M. Emin Kutay

Candidato:

Michele Salvianti

Luglio 2018

*Alla famiglia
che ho,
che ho trovato,
e che ho scelto.*

Abstract

In questa dissertazione finale è stata sviluppata una caratterizzazione avanzata di due diverse miscele di conglomerato bituminoso, contenenti bitumi modificati con polverino di gomma devulcanizzata e SBS, attraverso prove di modulo dinamico, Flow Number e SCB. Gli stessi test sono stati effettuati su altre due miscele di controllo contenenti bitumi modificati con il solo SBS, e alcuni campioni di ogni miscela sono stati immersi in acqua per 40 giorni per valutare il danno da umidità. I dati raccolti attraverso questi test sono stati usati come input per il progetto “mechanistic-empirical” di nuove pavimentazioni con l’ausilio del software di AASHTOWARE *Pavement ME Design*. Completa l’analisi una ricostruzione digitale attraverso fotogrammetria in 3D della Ligament Area dei campioni SCB testati per trovare il suo valore esatto e valutare eventuali differenze nell’accuratezza dei risultati.

Abstract

In this final dissertation an advanced characterization of two different asphalt mixtures, containing devulcanized rubber modified binders, has been developed through Dynamic Modulus, Flow Number and SCB tests. The same tests have been developed on other two control mixtures containing SBS modified binders, and several samples of each mixture have been drowned for 40 days in water to evaluate moisture damage. Data gathered through these tests have been used as inputs for mechanistic-empirical designs of new pavements using AASHTOWare's Pavement ME Design software. To complete the analysis, a digital 3D reconstruction of the Ligament Area of SCB tested samples have been developed through photogrammetry to find its exact value and evaluate differences in results accuracy.

Index

1	INTRODUCTION	13
2	LITERATURE REVIEW	17
2.1	Recycled Tire Rubber (RTR) Modified Bitumens: from an environmental problem to an engineering material	17
2.1.1	Bitumen – Rubber interaction	17
2.1.2	Rubber processing	17
2.1.3	CR-modified binders production: “Wet” technology	18
2.1.4	CR-modified binders production: “Dry” technology	20
2.1.5	CR-modified binders conclusions and DVR modification proposition	20
2.2	Devulcanized Rubber (DVR)	20
2.2.1	What is Devulcanized Rubber (DVR)?	21
2.2.2	Rubber devulcanization’s main technologies	22
2.3	MSU’s characterization of DVR-modified binders	23
2.3.1	Background	23
2.3.2	Modified binders production	23
2.3.3	Continuous high PG determination	24
2.3.4	Continuous intermediate PG determination	24
2.3.5	Continuous low PG determination	24
2.3.6	Multiple Stress Creep Recovery (MSCR) tests	25
2.3.7	Asphalt mixtures design	25
3	MECHANISTIC-EMPIRICAL DESIGN OF PAVEMENT STRUCTURES	27
3.1	Background	27
3.1.1	Limitations of the AASHTO Guide	27
3.1.2	Benefits of a Mechanistic-Empirical procedure	28
3.1.3	Principles of a mechanistic procedure	28
3.1.4	Design general approach	30
3.1.5	Hierarchical design inputs	31
3.2	Design Analysis for new and reconstructed flexible pavements: an overview	32
3.2.1	Design process	32
3.2.2	Trial design inputs and site conditions	33
3.2.3	Design inputs: processing over design analysis period	33
3.2.4	Pavement Response models	34
3.2.5	Incremental distress and damage accumulation	34
3.2.6	Distress prediction	35
3.2.7	Smoothness (IRI) prediction	37
3.2.8	Assessment of performance and design modification	38

3.2.9	Design reliability	38
3.2.10	Life cycle costs estimation	38
3.3	Inputs for new flexible pavement design.....	38
3.3.1	General information	39
3.3.2	Site/project identification	39
3.3.3	Analysis parameters	40
3.3.4	Traffic.....	40
3.3.5	Climate	41
3.3.6	Pavement structure	41
3.4	Flexible pavement design procedure.....	41
3.4.1	Trial design parameters	41
3.4.2	Pavement response model	42
3.4.3	Performance prediction	44
3.5	Design inputs: material characterization.....	55
3.5.1	Introduction	55
3.5.2	Material factors considered	56
3.5.3	Material categories	56
3.5.4	Input characterization (asphalt materials).....	57
3.5.5	Overview of E* estimation: Master Curve and Shift Factors.....	58
3.5.6	Binder viscosity.....	58
3.5.7	Asphalt aging.....	58
3.5.8	Implementation at Input level 1.....	59
3.5.9	Poisson's Ratio for bituminous materials.....	60
3.5.10	Other HMA material properties.....	60
3.6	MEPD software: AASHTOWare Pavement ME Design	62
4	RESEARCH PLAN.....	65
4.1	Objectives.....	65
4.2	Standard and advanced mixtures characterization.....	66
4.2.1	Dynamic Modulus and Flow Number	66
4.2.2	Moisture damage evaluation.....	66
4.2.3	Resistance to Cracking and Actual Ligament Area determination.....	67
4.3	Materials.....	68
4.3.1	Binders.....	68
4.3.2	Aggregates.....	69
4.3.3	Mixtures.....	70
4.4	Volumetric Characterization	70
4.4.1	Samples' G_{mm} and mass determination	70

4.4.2	Samples compaction, cutting and air void content determination.....	71
4.4.3	Sieve analysis.....	73
4.4.4	Binder content determination: Ignition Test.....	73
4.4.5	SCB samples geometry.....	74
4.5	Complex Modulus E^*	75
4.5.1	Overview.....	75
4.5.2	Testing samples for Complex Modulus.....	75
4.5.3	$ E^* $ Mastercurves development.....	76
4.6	Flow Number.....	77
4.6.1	Using Time Temperature Superposition for faster Repeated Load Permanent Deformation tests.....	78
4.7	<i>Pavement ME Design</i> data implementation and design simulation.....	79
4.8	Intermediate-temperature IL-SCB testing.....	81
4.8.1	Introduction.....	81
4.8.2	Flexibility Index determination.....	82
4.8.3	I-FIT software and MSU-developed MATLAB model.....	83
4.8.4	SCB test procedure.....	84
5	DATA ANALYSIS AND RESULTS.....	93
5.1	Volumetric and geometric characterization.....	93
5.1.1	Gmm determination.....	93
5.1.2	Binder content.....	94
5.1.3	Sieve analysis.....	94
5.1.4	SCB geometric characterization.....	96
5.1.5	Air voids content.....	98
5.2	Dynamic Modulus $ E^* $	99
5.3	Flow Number tests.....	103
5.4	<i>PavementME Design</i> data implementations and projects.....	108
5.4.1	Comparison (1) and (2): DVR vs. HS and DRY vs. WET.....	111
5.4.2	Comparison (3): Illinois vs. Arizona climate station.....	111
5.5	IL-SCB tests.....	112
6	CONCLUSIONS AND FUTURE RESEARCH.....	121
	Acknowledgments.....	123
	Bibliography and sites visited.....	125
	APPENDIX.....	127

List of Figures

Figure 1: Percentage of Roads in Good or Fair Condition in the Paved Aid System. (Report of the Michigan Transportation Asset Management Council)	13
Figure 2: Lansing area roads condition (Michigan TAMC)	14
Figure 3: Aggregates after ignition test.....	15
Figure 4: Crumb Rubber (Memon, 2011)	18
Figure 5: Maintenance and User cost comparison between asphalt mixes (AC) and Asphalt-Rubber mixes (ARAC). (Lo Presti, 2013)	19
Figure 6: Vulcanization process.....	21
Figure 7: Devulcanization process	22
Figure 8: Witczak's multilayer model	29
Figure 9: MEPD official guide stages (MEPD Guide)	31
Figure 10: Bottom-up fatigue cracking (MEPD Guide).....	36
Figure 11: Surface-down fatigue cracking (MEPD Guide)	36
Figure 12: Horizontal analysis of standard traffic.....	43
Figure 13: Deformation - Number of repetitions graph (MEPD Guide).....	49
Figure 14: Major material categories (MEPD Guide, Table 2.2.2).....	57
Figure 15: Asphalt materials input levels (MEPD Guide)	58
Figure 16: Laboratory test data for E* needed at Input level 1 (MEPD Guide)	59
Figure 17: Laboratory test data for creep compliance needed at Input level 1 (MEPD Guide)..	60
Figure 18: Pavement ME Design software	62
Figure 19: Pavement ME Design structural inputs	62
Figure 20: Pavement ME default climate stations	63
Figure 21: Pavement ME Design traffic inputs.....	63
Figure 22: Processes' Flow Chart.....	66
Figure 23: High-speed mixer	69
Figure 24: Low-speed mixer	69
Figure 25: Loose mixtures	71
Figure 26: Superpave Giratory Compactor (SGC).....	72
Figure 27: E*/FN samples.....	73
Figure 28: NCAT Asphalt Content Furnace	74
Figure 29: SCB samples ready for testing.....	75
Figure 30: Pavement ME Design project layers, detail.....	80
Figure 31: Reference climate stations – Illinois.....	81
Figure 32: Load-Displacement curve for SCB tests.....	82
Figure 33: I-FIT interface.....	83
Figure 34: I-FIT report example	84
Figure 35: MSU model report example	84
Figure 36: Tested SCB sample.....	86
Figure 37: Sample ready for Actual Ligament Area determination.....	87
Figure 38: Importing video data on 3DF Zephyr Free	88
Figure 39: Sparse point cloud	88
Figure 40: Dense point cloud.....	89
Figure 41: Actual Ligament Area, different views	89
Figure 42: Netfabb mesh implementation.....	90
Figure 43: Mesh scaled and rotated	91
Figure 44: ALA calculated values.....	91
Figure 45: Sieve Analyses.....	96
Figure 46: 3E1 and 4E1 E* mastercurves comparisons.....	100

Figure 47: 3E1 and 4E1 DVR DRY/WET E* mastercurves comparisons.....	101
Figure 48: 3E1 and 4E1 HS DRY/WET E* mastercurves comparisons.....	102
Figure 49: E* Data Quality Statistics Requirements.....	103
Figure 50: Permanent Deformation comparisons for 3E1 and 4E1 mixtures.....	105
Figure 51: Permanent Deformation comparisons for 3E1 HS and 4E1 HS mixtures	106
Figure 52: Permanent Deformation comparisons for 3E1 DVR and 4E1 DVR mixtures.....	107
Figure 53: Total ESALs during pavement's design life.....	108
Figure 54: Illinois' air temperature	109
Figure 55: Asphalt Dynamic Modulus input.....	109
Figure 56: DVR DRY (left) and HS DRY (right) design's distress report.....	111
Figure 57: DVR WET (left) and HS WET (right) design's distress report.....	111
Figure 58: DVR DRY (left) and HS DRY (right), Arizona design's distress report	111
Figure 59: Fracture Energy average for each SCB data analysis model	117
Figure 60: Flexibility Index average for each SCB data analysis model	117
Figure 61: Slope vs. Ligament Area, MSU model	118
Figure 62: Slope vs. Ligament Area, MSU model with 3D analysis	119
Figure 63: Slope vs. Ligament Area, IFIT model	120

1 INTRODUCTION

As of July 7, 2015, the Michigan State Trunkline Highway System holds 9,669 miles of state highways, including those designed as Interstate, US Highways or State Trunkline highways¹. Unfortunately, as it can be seen from *Figure 1*, the percentage of roads in good or fair condition in the Paved Federal Aid System has dropped from 87.8% in 2004 to 60.7% on January 2016².

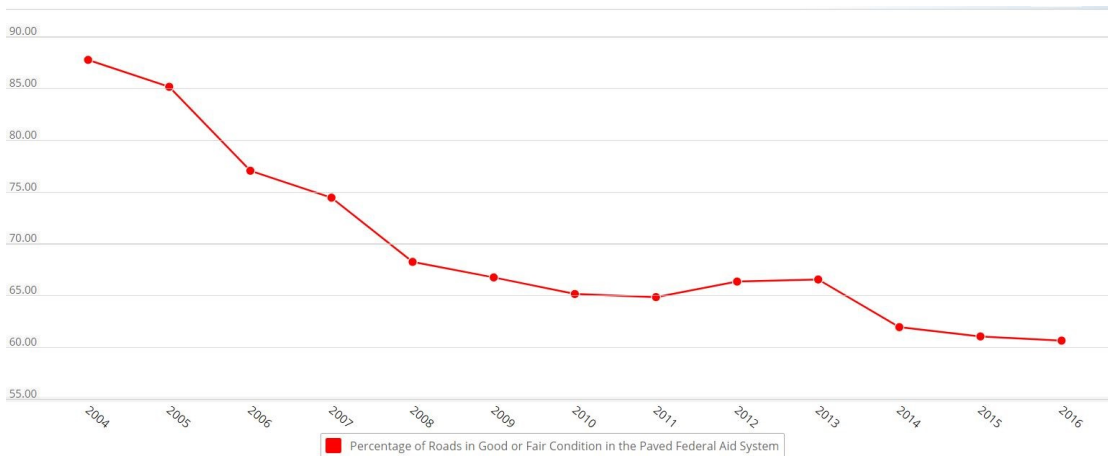


Figure 1: Percentage of Roads in Good or Fair Condition in the Paved Aid System. (Report of the Michigan Transportation Asset Management Council)

Figure 2 gives a better understanding of the critical condition of roads, this time in the capital city (Lansing) area: the roads in poor or fair condition (in red and yellow) are without any doubt the majority of those analyzed by Michigan TAMC (Transportation Asset Management Council).

That's why Michigan Department of Transportation (MDOT) is currently trying, through funded projects to the major Michigan universities, to avoid further degradation of the State road network and improve performance and design life of new infrastructures.

¹ Christopher J. Bessert, 'Michigan Highways: Introduction', 2017
<<http://www.michiganhighways.org/introduction.html>> [accessed 24 October 2017]; *Total Michigan Mileage*, 2017.

² (Percentage of Roads in Good or Fair Condition on the Paved Federal Aid System | Michigan - Open Performance, 2016)

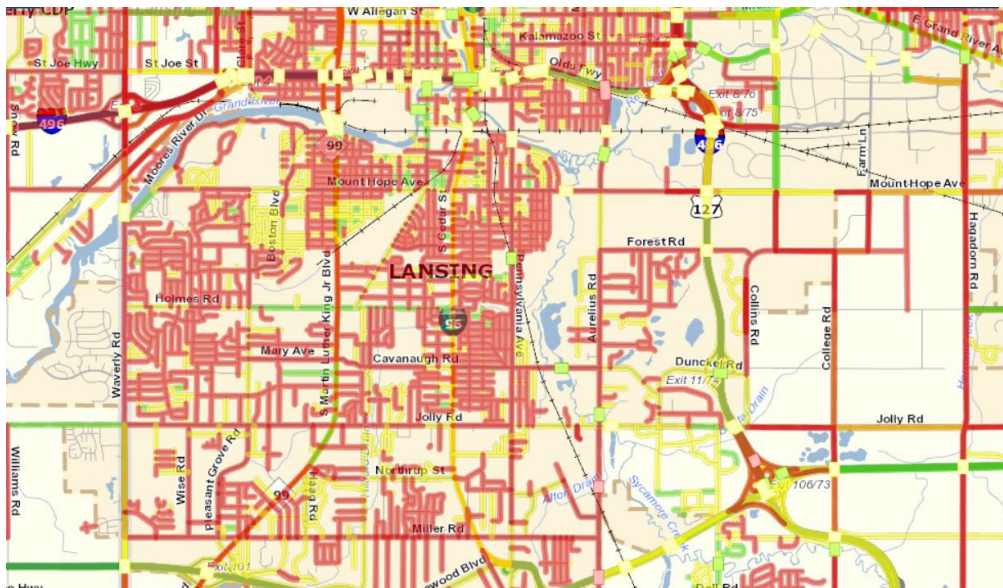


Figure 2: Lansing area roads condition (Michigan TAMC)

Besides fatigue cracking and rutting, the particularly severe climate in Michigan during the year plays a major role in roads' distresses: high rate of precipitations all year long and very low temperature in winter lead to freeze-thaw cycles that affect mechanical properties of the asphalt pavements³.

Considering all these elements, Michigan State University is currently working on studying innovative materials or developing ways to improve Michigan asphalt's mechanical properties and to prolong its life, as well as analyzing and monitoring existing roads. Examples are studies and funded projects on chip seals⁴, foamed binders⁵, or Devulcanized Rubber modified binders⁶.

In particular, Devulcanized Rubber (DVR) modified binders have been the subject of a long project sponsored by MDOT, started with lab tests on these binders and on

³ 'Michigan Average Climate Data', 2018 <<https://www.usclimatedata.com/climate/michigan/united-states/3192#>> [accessed 21 March 2018].

⁴ M. Ozdemir, U., Hibner, D., Kutay, M. E., and Lanotte, 'Image Processing Techniques For Determination Of Aggregate Embedment Depth In Chip Seals', in *96th Transportation Research Board Annual Meeting* (Washington, D.C., 2017).

⁵ M.E. Ozturk, H.I. and Kutay, 'Effect of Foamed Binder Characteristics on Warm Mix Asphalt (WMA) Performance', in *Proceedings of 93rd Annual Transportation Research Board Conference* (Washington, D.C., 2014).

⁶ M. E. Kocak, S., & Kutay, 'Combined Effect of SBS and Devulcanized Rubber (DVR) Modification on Performance Grade and Fatigue Cracking Resistance of Asphalt Binders', in *8th RILEM International Conference on Mechanisms of Cracking and Debonding in Pavements* (Springer Netherlands, 2016), pp. 269–74.

DVR-modified asphalt mixtures, and later with the construction of a section of a road in the town adjacent to the University⁷.

Since using DVR-modified asphalt mixtures is a very innovative project, and since MDOT raised some doubts on the effective improvement of using them for the construction of new roads, several other tests on those mixtures were needed. In addition to that, MSU researchers believe that one of the main issues with the bad condition of Michigan roads is the quality of the aggregates. *Figure 3* shows some of the aggregates taken from one of the mixtures after an ignition test: their shape is round, smooth and with almost no angles or faces at all, making it very unlikely to develop some shear force once mixed with bitumen and compacted.



Figure 3: Aggregates after ignition test

The reason for this particular shape could be found in the source of most of Michigan aggregates: due to the strong presence of water in the country (lakes, rivers...), the main part of the aggregates are fluvial ones, strongly worn out by water and with poor mechanical characteristics. Moreover, aggregate suppliers usually avoid giving particular information about their sources: that's why few or none information about aggregates' composition are available.

Another step of the research, then, would have been recreating the mixtures using both DVR-modified bitumen recreated at MSU and high-quality aggregates from trusted suppliers at Politecnico di Torino. Unfortunately, due to unplanned delays and binder shipping difficulties, this last step has not been developed and was not included in this thesis.

The present work aims to improve the knowledge and the existing database of mechanical characteristics and performances for these innovative mixtures through

⁷ Michele Lanotte and M Emin Kutay, *Evaluation of De-Vulcanized Rubber (DVR) Modified Hot Mix Asphalt (HMA) Pavement*, 2017.

advanced tests like Complex Modulus, Flow Number, Semi-Circular Bending and Moisture Susceptibility. This last analysis was developed by repeating the tests on samples left in water for 40 days, trying to maximize the moisture damage.

Data gathered through these tests have been used as input on a software that implements the Mechanistic-Empirical Pavement Design principles, to evaluate differences between the mixtures focusing not only on raw or processed data after the tests but on several virtual road designs: in this way differences on the various predicted permanent deformations at the end of the design lives of pavements could be highlighted. The thermal or fatigue cracking evaluation, although automatically developed by the software, has not been taken in consideration since no tests were developed to characterize the material in that sense (e.g. Push-Pull or Indirect Tensile Strength tests)

In place of the comparison between “made in USA” and “made in Italy” mixtures, a thorough SCB analysis of the mixtures studied at MSU was developed, along with 3D digital reproduction of the Ligament Area of the tested samples to evaluate whether this new element could help minimizing the data dispersion and lack of accuracy. This advanced SCB analysis has also been taken as a reference to complete the characterization of the mixtures on a “cracking point of view”, in place of more specific tests.

In the first part of this dissertation several topics of interest have been reviewed, starting from a literature review on crumb rubber modified binder and going through researches on DVR-modified binders and DVR-modified asphalt mixtures developed mostly at MSU. The following topic is an introduction of the mechanistic-empirical design of pavements that has been used in this dissertation, followed by an overview on the software used to analyze the final data. In the fourth chapter, the actual research plan explains in detail the objectives, the materials used and the tests carried on the samples: this section will follow the asphalt sample from the volumetric characterization all the way to its most advanced characterizations such as Flow Number, Complex Modulus and SCB tests. Instead, *Data Analysis* deals with the technical aspects of the data processing, showing how the research was practically developed after the data gathering: this includes both summaries of tests’ inputs and outputs, along with comments on the most peculiar results. In the end, in *Conclusions* all the results of the many tests are compared and discussed.

2 LITERATURE REVIEW

2.1 Recycled Tire Rubber (RTR) Modified Bitumens: from an environmental problem to an engineering material

Vehicles' end of life tires, due to their volume and durability, are the largest sources of waste in western countries: 355 million tires are produced in Europe every year, and many millions of them have been illegally stored or dumped with skyrocketing risks for the environment and human health. In addition to that, the annual estimated cost of this kind of waste in Europe is 600 million €. That's why many researchers have looked for a way to transform this high-maintenance and dangerous scrap all around the world into something useful⁸.

Tires are the product of more than a century of innovation and technology improvements, made essentially of elastomeric compounds held together by fabric and steel that ensure all the good performances we are used to look for in a good set of tires.

2.1.1 Bitumen – Rubber interaction

Some studies show different conclusions on bitumen – rubber interaction: some claim it is not chemical⁹ while some others state that the binder viscosity increases not only because of the rubber particles¹⁰. This interaction includes the rubber partial dissolution into the bitumen and the absorption of the aromatic phase within the polymers at high temperatures (160-220 °C), forming a material similar to a gel.

Moreover, if the rubber is kept at high temperatures for too long, a depolymerisation process will begin, causing rubber dispersion into the bitumen: its components are brought back to a liquid phase decreasing stiffness and complex modulus. If this process continues, a complete destruction of the binder network will take place.

2.1.2 Rubber processing

First of all, for end-of-life tires' (ELT) rubber to be suitable in asphalt development, it needs a size reduction through ambient, cryogenic or wet-ambient grinding.

⁸ Davide Lo Presti, 'Recycled Tyre Rubber Modified Bitumens for Road Asphalt Mixtures : A Literature Review Q', *Construction and Building Materials*, 49 (2013), 863–81
<<https://doi.org/10.1016/j.conbuildmat.2013.09.007>>.

⁹ M. Heitzman, 'Design and Construction of Asphalt Paving Materials with Crumb Rubber Modifier', *Transportation Research Record*, 1992.

¹⁰ H. Bahia and R Davis, 'Effect of Crumb Rubber Modifiers (CRMs) on Performance Related Properties of Asphalt Binders', *AAPT 1994*, 1994.

At first the rubber is reduced to 1- or 2-inch size while removing contamination from steel or fibers, then further grinded with an ambient ground mill or cooling it with liquid nitrogen (*Figure 4*). Further reduction of size leads to Crumb Rubber, the most common additive for asphalt binders which are mixed with the bitumen using “Wet” or “Dry” technologies.

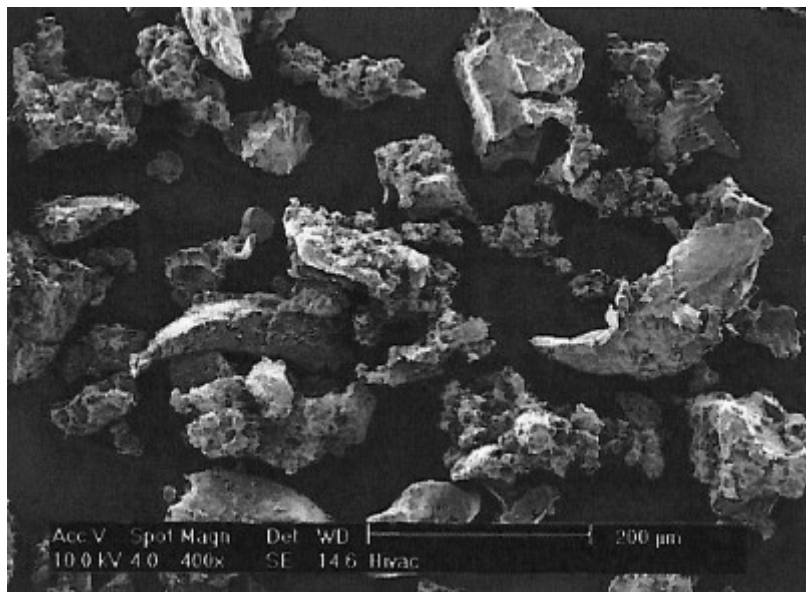


Figure 4: Crumb Rubber (Memon, 2011)

2.1.3 CR-modified binders production: “Wet” technology

Through an accurate mechanical mixing, the dispersion of CR particles in the bitumen takes place at 175 – 225 °C, developing two different products: “asphalt rubber” and “terminal blend” binders.

Temperature, CR selection and amount and mixing procedures are some of the factors that can modify CR-modified binders produced using “Wet” technology.

2.1.3.1 Asphalt Rubber

The first kind of binders are kept at high temperatures (150 – 215 °C) directly after mixing for 45-60 minutes to ensure interaction between the components: the resulting material is a gel-like composite material in which rubber particles are still distinguishable in the matrix. These binders are called “high viscosity” (not less than 1500 cP at 177 or 190 °C) and have at least 15% of CR (usually 18-22%). For United States, asphalt rubber binders are to be produced following ASTM D6114, which specifies also rubber

characteristics (for example, it must have less than 0.75% moisture and free flowing and specific gravity of 1.15 ± 0.05) and base binder requirements).

Asphalt rubber mixtures have shown major reductions in fatigue cracking and improvements in rutting resistance, with lower maintenance needs, costs and noise generation. Since aging effects are reduced, the increased durability of these pavements is another advantage in choosing this kind of binders.

However, drawbacks are not absent at all: high viscosity binders make pavement construction more difficult, since the temperature is crucial. Moreover, asphalt rubber storage is a major issue due to the low stability of the product: tanks with agitation facilities are needed to ensure a homogeneous dispersion of rubber particles if the product is not used within 4 hours from production. Higher initial costs are also to take into account, and the difference in maintenance cost is not to be seen in less than 15 years (*Figure 5*).

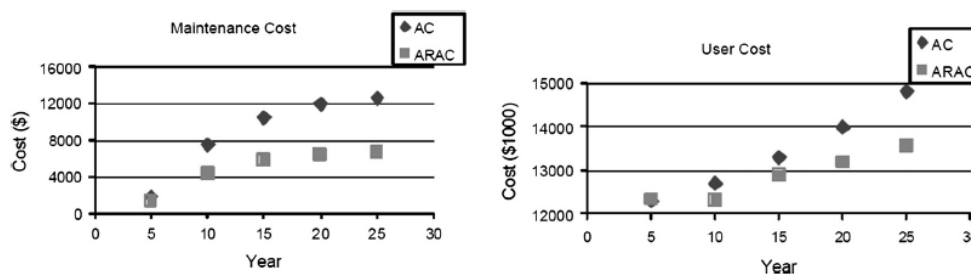


Figure 5: Maintenance and User cost comparison between asphalt mixes (AC) and Asphalt-Rubber mixes (ARAC). (Lo Presti, 2013)

2.1.3.2 Terminal Blend

“Terminal blend” binders, because of the thinner size of the CR used (0.3 mm), show a lower viscosity and original rubber particles are not to be seen in the final product, with less problems in terms of stability. That’s why this kind of binders is also called “No-Agitation” for its ability to keep the rubber particles dispersed also when stored. Terminal blends binders nowadays include up to 25% CR and they don’t require any changes in the asphalt plants (like reaction tanks).

Even if Terminal blend HMAs show a reduced performance life compared to Asphalt rubber HMAs (since binder content is 2 – 5% less), the main advantages are the binder’s portability and, as said before, minor storage and mixing costs: contractors could easily switch for this kind of binder in their manufacturing process without too much of a hassle.

2.1.4 CR-modified binders production: “Dry” technology

During “Dry” modification, CR is added as an additive right in the asphalt production facility: rubber is not mixed with binder at all, and it becomes a substitute for a small mineral aggregate percentage. That’s why a major issue for this kind of HMA is the difficult dispersion of it inside the aggregates matrix since CR has a very lower density (1.15 g/cm³, compared to aggregates’ 2.65 g/cm³). Another issue is the CR’s aromatic phase absorption, that continues also during transportation and implementation of the final asphalt product.

CR percentages on total aggregates weight are around 1-3%.

HMAs produced using this kind of binders have shown susceptibility to surface damage because of absorption. In gap-graded and open-graded mixtures, moreover, the higher air voids volume has to be taken into account, but it is suggested to use Crumb rubber with less than 2 mm size, because the use of bigger crumbs raises the risk of cracking in the final HMA¹¹.

For all these concerns, “Dry” technology is currently not used that much, and further studies have not been developed.

2.1.5 CR-modified binders conclusions and DVR modification proposition

CR modification of binders, and especially the wet-process products, should be the first choice for every company or road authority¹². Further studies are to be made, but initial costs seem to be compensated by results of lifecycle cost analyses.

This dissertation, however, aims to further evaluate an innovative material that could bypass all the drawbacks of HMAs using CR-modified binders stated in the previous paragraphs, such as Dry technologies bad performances, excessive viscosity of Asphalt rubber binders and overall stability problems or bad rubber-binder interaction: Devulcanized Rubber-modified binders.

2.2 Devulcanized Rubber (DVR)

An average car/truck tire is made of vulcanized rubber: raw rubber is a soft and sticky material with a low tensile strength and elasticity, so atomic bridges composed of

¹¹ M C Zanetti and others, ‘Characterization of Crumb Rubber from End-of-Life Tyres for Paving Applications’, *Waste Management*, 45 (2015), 161–70 <<https://doi.org/10.1016/j.wasman.2015.05.003>>.

¹² Presti.

sulphur or carbon-carbon bonds link the polymer chains together to form a new thermoset material (*Figure 6*). By doing so, stresses applied will deform this new material, but when stress is released the rubber will return to the original shape.

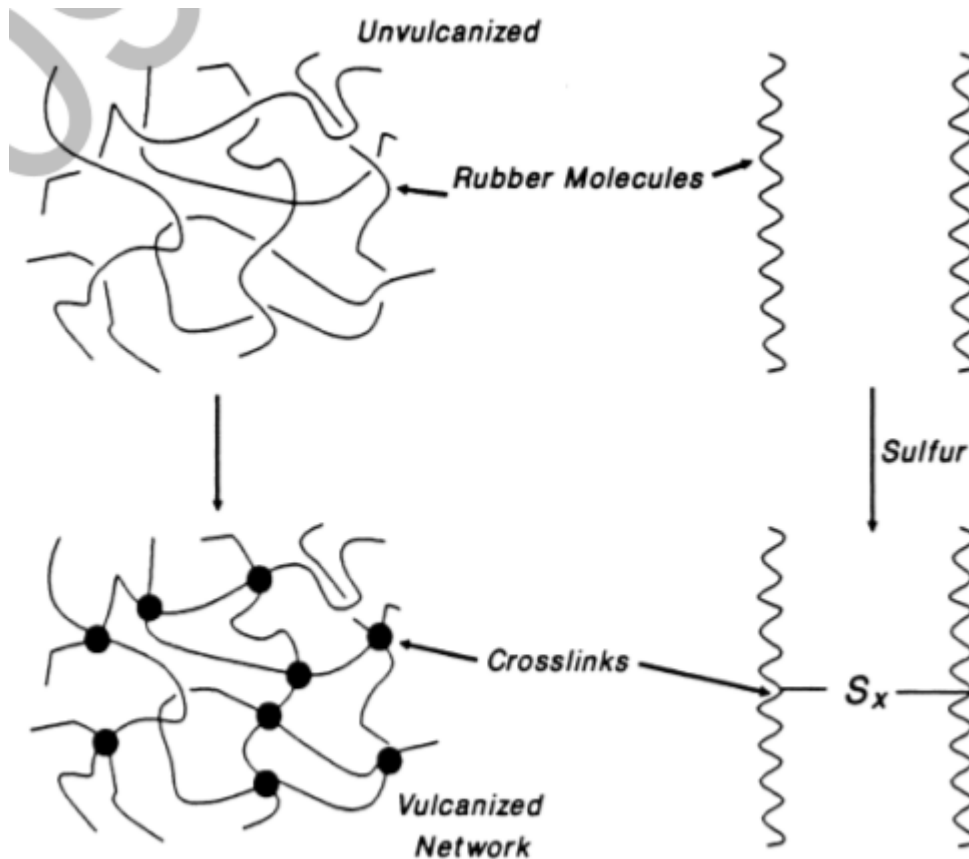


*Figure 6: Vulcanization process*¹³

2.2.1 What is Devulcanized Rubber (DVR)?

Devulcanization refers to a process in which the sulfidic crosslink bonds in the vulcanized rubber cleave totally or partially (*Figure 7*). Devulcanization of tire rubbers, ideally, would end into developing a substitute for virgin rubber, cheaper and more environmental-friendly, since those crosslink bonds can be created again.

¹³ C. Tzoganakis and M. Meysami, 'Thermo- mechanical Devulcanization of Tire Rubber Crumb with Supercritical CO₂: Devulcanized Rubber Properties', *IPR*, 2009.

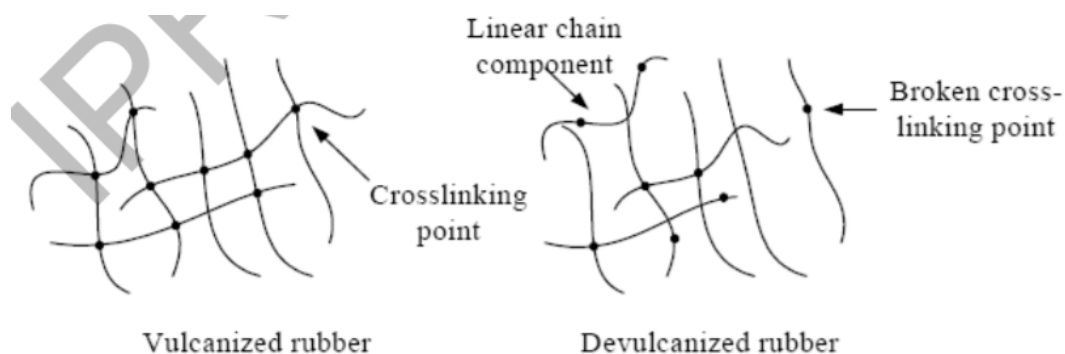


Figure 7: Devulcanization process¹⁴

This process can be achieved through chemical, ultrasonic, microwave, or biological methods¹⁵.

2.2.2 Rubber devulcanization's main technologies

- Chemical: organic solvents, oils and inorganic compounds are used as devulcanizing agents, under high pressure and temperature. Many of these processes have not been tested on a large scale, and sometimes they request much time. Inorganic compounds, especially, may cause pollution and/or become hazardous.
- Ultrasonic: in the late 80s it was discovered that using 50 kHz ultrasonic waves on vulcanized rubber could break C-S and S-S bonds in just 20 minutes¹⁶. In the following years the ultrasonic devulcanization process has been adjusted and it has become fast (rate is 1 second), simple, efficient and free of chemicals.
- Microwave: using this kind of energy means applying heat on the rubber quickly and uniformly, even if this process requires specific physical properties and expensive equipment.
- Biological: different kinds of microorganisms attack the sulfur bonds in rubber, like *Acidithiobacillus* or *P. furiosus*¹⁷, *Nocardia* and *C. subvermispra*¹⁸.

¹⁴ Tzoganakis and Meysami.

¹⁵ Tzoganakis and Meysami.

¹⁶ M. Okuda and Y. Hatano, 'Japanese Patent Application 62,121,741', 1987.

¹⁷ K. Bredberg, 'Sulphur-Utilizing Microorganisms in Biotechnological Applications—Rubber Recycling and Vanadium Reduction' (Lund University, 2003).

¹⁸ S. Sato, 'DeVulcanization of Polyisoprene Rubbers by Wood Rot Fungi' (Prague, Czech Republic, 2003) <<https://www.imc.cas.cz/sympo/42micros/poster1.htm#P09>>.

2.3 MSU's characterization of DVR-modified binders

2.3.1 Background

Over the last years, Michigan State University's Advanced Asphalt Characterization Labs investigated the performance of recently introduced De-Vulcanized Rubber (DVR) modified asphalt binder, mixtures, and a field test section located on Hagadorn Road in East Lansing, Michigan¹⁹.

The steps followed in the investigation have been:

- Laboratory testing of modified binders,
- Asphalt mixtures design and performance testing,
- QC/QA testing of field cores.

2.3.2 Modified binders production

Other than DVR itself, the additives used for the investigation were two types of SBS polymers (bound styrene 31% and 30% by mass, while 10% and 30% for vinyl) called respectively AT1101 and LCY3710 and one type of #20 mesh crumb rubber (CR) from recycled tire rubber (RTR) to evaluate the differences with DVR modified bitumen. The binder used was a base bitumen (PG58-28).

DVR and CR modified binders were prepared using different dosages: 3%, 6%, and 9%. The reason for this choice is the equivalent PG modification impacts of SBS modified binders (1% SBS = 3% CR). Moreover, the cost of a unit of SBS is a third of a DVR unit. In addition, other combination have been prepared and tested: 1% SBS+3% DVR/CR, 1% SBS+6% DVR/CR, 2% SBS+3% DVR/CR, 2% SBS+6% DVR/CR.

SBS binder modification was performed by using high and low shear mixers in two consecutive steps, first milled into the hot base binder (163°C) at 5000 RPM for 30 minutes and then kept at 1000 rpm for 120 minutes at 180°C. After 90 minutes a cross-linker (XL) agent is added at a weight ratio of 20 to 1.

DVR modification followed the same steps as the SBS one, only the DVR:XL ratio differs (40:1).

CR modification required only low shear mixing: CR particles are added to the base binder at 180°C and mixed for 60 minutes at 1000 RPM.

¹⁹ Lanotte and Kutay.

Combined SBS-DVR and SBS-CR modifications followed similar steps: those elements are first mixed separately with bitumen at high speed and then blended together in the low shear mixer.

This study adopted linear interpolation between absolute highest passing and lowest failure temperatures for all three continuous PGs (high, intermediate and low), although other various and more complex procedures exist.

2.3.3 Continuous high PG determination

All binders were tested both in original and short-term conditions to figure out the high PGs, and after linear interpolation was used to determine continuous high PGs. The smaller of these values was assigned as the continuous high PG. The impact of aging during the modification was negligible: continuous high PG if the original aged binder was almost equal to that of the RTFO-aged unmodified binder.

In the first two phases of the testing, the bitumen modified with the two different SBS polymers (AT1101 and LCY3710) were analyzed separately, and eventually AT1101 performed better than LCY3710, increasing the high PG by about 9 degrees at 2%. This may be due to the interference of the high vinyl content of the second polymer.

Afterward, two levels of combinations were analyzed: the first level included 2% SBS modification and replacement of 1% SBS with 3% RTR while the second level included 3% SBS modification and replacement of either the same as level 1 or 2% SBS with 6% RTR. The aim was to obtain the same or even better continuous high PG for the choice of the right modification.

2.3.4 Continuous intermediate PG determination

Continuous intermediate PG was determined to investigate the fatigue cracking behavior of the binders: lesser the intermediate PG, better the binder would perform. However, it's a very vague parameter and needs to be accompanied by performance tests.

DVR modification alone did not affect the parameter; better results were achieved while combined with SBS.

2.3.5 Continuous low PG determination

Continuous low PG was determined according to stiffness and logarithmic creep rate values obtained from BBR tests conducted at various temperatures and using linear interpolation method.

The aged binders obtained the highest value since aging made the binder stiffer, and increasing SBS content improved the value too with an increasing trend.

2.3.6 *Multiple Stress Creep Recovery (MSCR) tests*

MSCR tests were performed instead of elastic recovery tests, both at high PG temperatures and location temperatures.

Although there was not a clear trend for high PG testing temperature, the increasing percentage of RTR yielded better Jnr3.2 results. However, results at regional temperatures showed that the differences between individual and combined modifications were within a close proximity to each other.

2.3.7 *Asphalt mixtures design*

Laboratory tests were performed on DVR and SBS modified HMAs following the general guidelines of Michigan Department of Transportation (MDOT)'s Superpave specifications. Two mixtures were proposed and tested for the top course (4E1) and two for the leveling course (3E1). The HMAs were subjected to the full standard mix-design process.

Two binders were produced in the laboratory and used for the mix-design process:

- Polymer modified binder (2% SBS) with Continuous PG 69.5°C and
- DVR modified binder (7% DVR + 2% SBS + 0.4% Cross-linker) with Continuous PG 75.3°C.

The Job Mix Formulas in the attachments section of this research bear the exact mix/aggregates gradation, G_{mm} , G_{mb} and bitumen percentage used for the construction of the field test section and the lab samples.

These mixtures were subjected to different tests to evaluate and compare performances with respect to low-temperature and fatigue cracking and rutting. Additionally, they were tested in uniaxial compression mode at different temperatures and loading frequencies in order to get their linear viscoelastic $|E^*|$ master curves.

3 MECHANISTIC-EMPIRICAL DESIGN OF PAVEMENT STRUCTURES

Due to the lack of knowledge in Italy about the Mechanistic-Empirical (ME) Design of Pavements, giving the reader an overview to it was necessary: in the following paragraphs the most important features of this innovative process for new flexible pavements are described and the focus of the material characterization will be on the asphalt layers.

For all many other aspects of the ME design, such as inputs for all other layers (foundation, subgrade...), rigid pavements or rehabilitated ones, please see the official Mechanistic-Empirical Pavement Design Guide (MEPDG).

3.1 Background

Mechanistic-Empirical Design represents a major change in the way pavement design is performed. The designer first considers site conditions (traffic, climate, subgrade etc.) and construction conditions in proposing a trial design for a new pavement. The trial design is then evaluated for adequacy through the prediction of key distresses and smoothness, and if the design doesn't meet desired performance criteria it is revised and the evaluation process repeated as necessary. This approach makes it possible to optimize the design and ensure that specific distresses will not develop in the pavement. In addition to that, the format of the model leaves the door open to future changes in materials, design concepts, computers and so on.

3.1.1 *Limitations of the AASHTO Guide*

The *AASHTO Guide for Design of Pavement Structures* is currently the primary document used to design highway pavements in the US: between 1995 and 1997 the Federal Highway Administration's National Pavement Review found that about 80% of States use the 1972, 1986 or 1993 editions of the AASHTO Guide, developed on 1950's AASHO Road Test data with few refinements. Even if the Guide has served the US transportation well for decades, it has recently shown some limitations such as for:

- Traffic loading: heavy truck traffic design volume levels have increased about 10 to 20 times since the 1960's Interstate system design. Thus, the designer nowadays must extrapolate the design methodology far beyond the data and experience currently available.

- Surfacing materials: for the original Road Test, only one HMA has been used.

- Construction and drainage: pavement designs, materials, and construction were representative of those used at the time.

- Design life: the long-term effects of climate and aging of materials were not addressed (the AASHO Road Test was conducted over just 2 years).

- Performance: rutting, thermal cracking and fatigue were not fully considered as they are nowadays.

And many more related to subgrade, base course, truck characterization, reliability etc.

3.1.2 Benefits of a Mechanistic-Empirical procedure

One of the major concerns of the previous AASHTO design procedure was the inability to incorporate significant materials properties into the design procedure. In addition, various design features cannot be directly considered. The flexible pavement procedure cannot determine the required thickness of asphalt bound material to limit fatigue cracking. This lack of materials/design properties consideration can lead to early failures.

The mechanistic-empirical design procedure provides the tools for evaluating the effect of variations in materials on pavement performance, providing a rational relationship between construction and materials specification and the design of the pavement structure.

3.1.3 Principles of a mechanistic procedure

“Mechanistic” refers to the application of the principles of engineering mechanics, which leads to a rational design process. Yoder and Witczak in the 70s²⁰ stated that three elements must be considered fully: the theory used to predict the assumed failure or distress parameter, the evaluation of the materials properties applicable to the selected theory, and the determination of the relationship between the magnitude of the parameter in question to the performance level desired.

Generally, the analytical solution to the state of stress or strain within a pavement using the multi-layered elastic theory makes several assumptions, like (*Figure 8*):

- The material properties of each layer are homogeneous.

²⁰ E. J. Yoder and M. W. Witczak, *Principles of Pavement Design* (John Wiley & Sons, 1975).

- Each layer has a finite vertical thickness except for the lowest layer, an infinite thickness in the other directions and is isotropic.
- At the interface of each layer full friction is developed.
- There are no surface shearing forces.

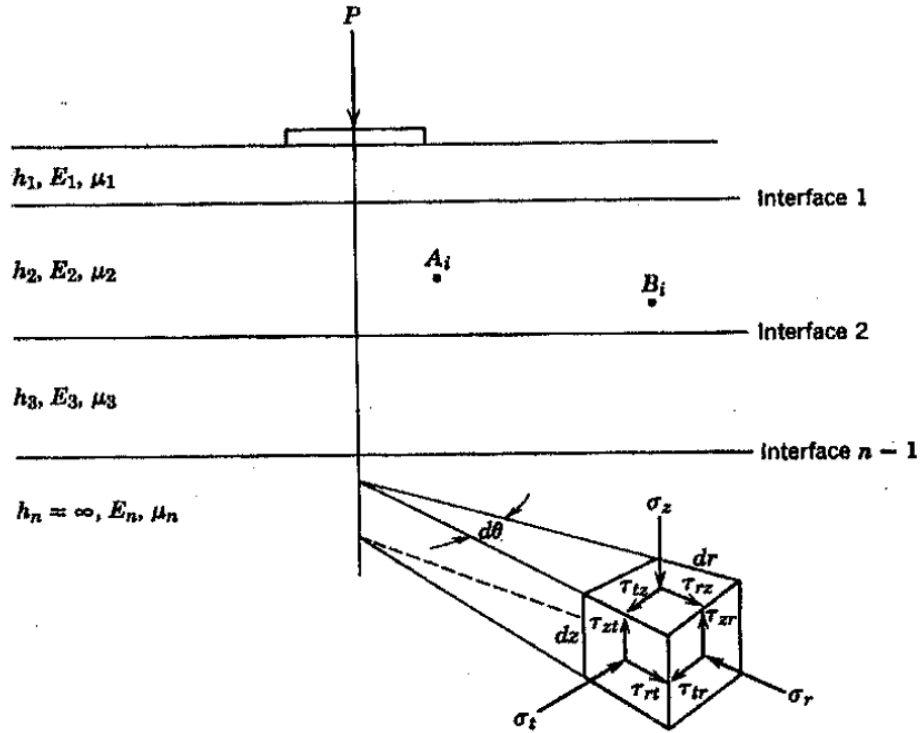


Figure 8: Witzak's multilayer model

At a given point within any layer, static equilibrium requires that nine stresses exist, acting on vertical (z), radial (r), and tangential (t) planes. These stresses are comprised of three normal stresses ($\sigma_z, \sigma_r, \sigma_t$) acting perpendicular to the element faces and six shearing stresses ($\tau_{rt}, \tau_{tr}, \tau_{rz}, \tau_{zr}, \tau_{tz}, \tau_{zt}$) acting parallel to the faces. Besides, the shear stresses acting on intersecting faces are equal for equilibrium, and there exists an orientation such that the shear stresses acting on each face are zero.

The strains may be determined as:

$$\varepsilon_z = \left(\frac{1}{E}\right) [\sigma_z - \mu(\sigma_r + \sigma_t)] \quad (1)$$

$$\varepsilon_r = \left(\frac{1}{E}\right) [\sigma_r - \mu(\sigma_z + \sigma_t)] \quad (2)$$

$$\varepsilon_t = \left(\frac{1}{E}\right) [\sigma_t - \mu(\sigma_r + \sigma_z)] \quad (3)$$

From these equations, three major properties of the pavement behavior can be found: the relationship between stress and strain (linear or nonlinear), the time dependency of strain under a constant stress level (viscous or non-viscous), and the degree to which the material can rebound or recover strain after stress removal (plastic or elastic).

3.1.4 Design general approach

There are three major stages in the Mechanistic-Empirical design:

- Stage 1: Development of input variables. During this stage, potential strategies are identified for consideration in the analysis stage, including the required foundation for the pavement. Also, materials characterization and traffic input data are developed. The Enhanced Integrated Climate Model (EICM) is used to model temperature and moisture within each pavement layer and the subgrade, considering hourly climatic data from weather stations across the USA (temperature, precipitation, solar radiation, cloud cover, and wind speed). The pavement layer temperature and moisture predictions from the EICM are calculated hourly over the design period and used in various ways to estimate material properties for the foundation and pavement layers throughout the design life.

- Stage 2: Structural/performance analysis. It's an iterative step, beginning with the selection of an initial trial design created by the designer, obtained from an existing design procedure, or from a general catalog. It requires initial estimates of layer thickness, geometric features, initial smoothness, pavement materials characteristics, and many other inputs. The trial section is analyzed incrementally over time using the pavement response and distress models, and the outputs of the analysis are accumulated damage the expected amount of distress and smoothness over time. If the trial design does not meet the performance criteria, modifications are made and the analysis re-run until a satisfactory result is obtained.

- Stage 3: Evaluation of alternatives. It includes an engineering analysis and life-cycle cost analysis of the alternative.

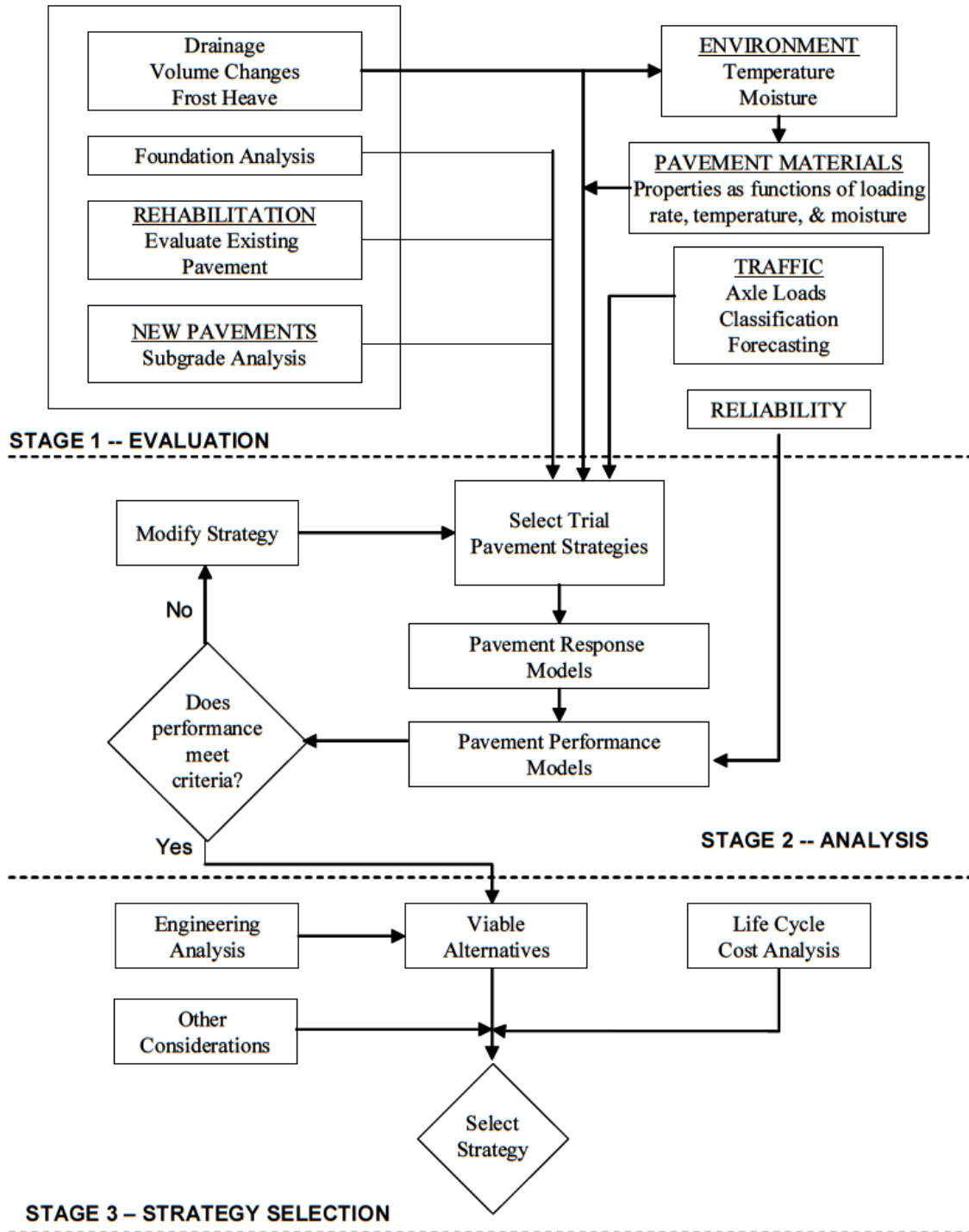


Figure 9: MEPD official guide stages (MEPD Guide)

3.1.5 Hierarchical design inputs

The hierarchical approach used in the Mechanistic-Empirical Design is nowhere to be found in existing versions of the AASHTO guides: it provides the designer with a lot of flexibility in obtaining the design inputs for a design project based on the criticality of

the project and the available resources regarding traffic, materials and environmental inputs.

Three levels of inputs are provided, but only Level 1 has been used in the following analyses: it provides for the highest level of accuracy and inputs would typically be used for designing heavily trafficked pavements. Level 1 material input require laboratory or field testing, such as the dynamic modulus testing of hot-mix asphalt concrete, site-specific axle load spectra data collections, or nondestructive deflection testing.

3.2 Design Analysis for new and reconstructed flexible pavements: an overview

The mechanistic-empirical design of new and reconstructed flexible pavements requires an iterative hands-on approach by the designer. The designer must select a trial design and then analyze the design in detail to determine if it meets the performance criteria established by the designer. The flexible pavement performance measures considered in this guide include permanent deformation (rutting), fatigue cracking (both bottom-up and top-down), thermal cracking, and smoothness (International Roughness Index or IRI). If the trial design does not satisfy the performance criteria, the design is modified and reanalyzed until the design does satisfy all criteria. The designs that meet the applicable performance criteria are then considered feasible from a structural and functional viewpoint and can be further considered for other evaluations such as life cycle cost analysis.

3.2.1 Design process

The main steps in the design process include the following:

a) Assemble a trial design for specific site conditions defining subgrade support, asphalt concrete and other paving material properties, traffic loads, climate, pavement type and design and construction features.

b) Establish criteria for acceptable pavement performance at the end of the design period (i.e., acceptable levels of rutting, fatigue cracking, thermal cracking, and IRI).

c) Select the desired level of reliability for each of the applicable performance indicators, like reliability levels for rutting, cracking and IRI.

d) Process input to obtain monthly values of traffic inputs and seasonal variations of material and climatic inputs needed in the design evaluations for the entire design period.

e) Compute structural responses (stresses and strains) using multilayer elastic theory or finite element based pavement response models for each axle type and load and for each damage-calculation increment throughout the design period.

f) Calculate accumulated distress and/or damage at the end of each analysis period for the entire design period.

g) Predict key distresses (rutting, bottom-up/top-down fatigue cracking, thermal cracking) at the end of each analysis period throughout the design life using the calibrated mechanistic-empirical performance models provided.

h) Predict smoothness (IRI) as a function of initial IRI, distresses that accumulate over time, and site factors at the end of each analysis increment.

i) Evaluate the expected performance of the trial design at the given reliability level.

j) If the trial design does not meet the performance criteria, modify the design and repeat the steps 4 through 9 above until the design does meet the criteria.

3.2.2 Trial design inputs and site conditions

An acceptable design is determined by iteratively analyzing and modifying trial designs until all performance criteria are satisfied over the analysis period. In addition to this, the designer must provide inputs for the project site conditions including subgrade properties, traffic and climatic data.

A major difficulty in obtaining adequate design inputs is that the desired project specific information is not generally available at the design stage and must often be estimated several years in advance of construction.

3.2.3 Design inputs: processing over design analysis period

The raw design inputs have to be processed to obtain seasonal values of the traffic, material and climatic inputs needed for each analysis increment in the design evaluations. Analysis inputs that are required on a seasonal basis consist of the following:

- Average daily number of single, tandem, tridem and quad axles in each axle weight category for each month

- Temperatures within the asphalt layer. Average temperature values for the analysis period are used to determine the temperature-dependent asphalt stiffness for rutting and fatigue cracking predictions. Hourly temperature values are needed for thermal cracking prediction. A minimum of 1 year's weather station data is required.

- Average moduli values of all unbound layers (base, subbase, subgrade) for each analysis period.

3.2.4 *Pavement Response models*

The purpose of the flexible pavement response model is to determine the structural response of the pavement system due to traffic loads and environmental influences. Environmental influences may be direct (e.g., strains due to thermal expansion and/or contraction) or indirect via effects on material properties (e.g., changes in stiffness due to temperature and/or moisture effects).

The outputs of these models are the stresses, strains and displacements within the pavement layers. Critical pavement response variables include tensile horizontal strain at the bottom/top of the HMA layer or compressive vertical stresses/strain within the various materials' layers from HMA to subgrade.

Each pavement response variable must be evaluated at the critical location within the pavement layer where the parameter is at its most extreme value. For a single wheel loading, the critical location can usually be determined by inspection.

Two flexible pavement analysis methods have been implemented in the Design Guide. For cases in which all materials in the pavement structure can realistically be treated as linearly elastic, multilayer elastic theory is used to determine the pavement response. Multilayer elastic theory provides an excellent combination of analysis features, theoretical rigor, and computational speed for linear pavement analyses. In cases where the unbound material nonlinearity is also considered, a nonlinear finite element procedure is used instead for determining the pavement stresses, strains, and displacements.

3.2.5 *Incremental distress and damage accumulation*

The trial design is analyzed for adequacy by dividing the target design life into shorter design analysis periods or increments beginning with the traffic opening month. Within each increment (each analysis period), all factors that affect pavement responses and damage (traffic levels, asphalt concrete modulus, base and subbase moduli and subgrade modulus) are held constant. Critical stress and/or strain values for each distress type are determined for each analysis increment. These values are converted to incremental distresses, either in absolute terms (e.g., incremental rut depth) or in terms of a damage index (e.g., fatigue cracking). Incremental distresses and/or damage are

summed over all increments and output at the end of each analysis period by the Design Guide software.

3.2.6 Distress prediction

The cumulative distress calculated in the previous section forms the basis for evaluating the structural adequacy of trial designs. The structural distresses considered are:

- Bottom up fatigue (alligator)
- Surface-down fatigue (longitudinal) cracking
- Permanent deformation (rutting)
- Thermal cracking

While rutting is predicted in absolute terms, the other distresses are predicted in terms of a damage index, which is a mechanistic parameter representing the load associated damage within the pavement structure. When “damage” is very small the pavement structure would not be expected to exhibit significant cracking. As computed “damage” increases, visible cracking can be expected to develop. The incremental damage is accumulated for each analysis period using Miner’s law. The cumulative damage is converted to physical cracking using calibrated models that relate the calculated damage to observable distresses. Calibrated distress prediction models were developed using the LTPP database and other long-term pavement performance data obtained for a wide range of flexible pavement structures located in a variety of climatic conditions and subject to various traffic and environmental loading situations.

3.2.6.1 Bottom-up fatigue cracking

It first shows up as short longitudinal cracks in the wheel path that quickly spread and become interconnected. These cracks initiate at the bottom of the HMA layer and propagate to the surface under repeated load applications.

This kind of cracking is a result of the repeated bending of the HMA layer under traffic. With continued bending, the tensile stresses and strains cause cracks to initiate at the bottom of the layer and then propagate to the surface, as in the following picture:

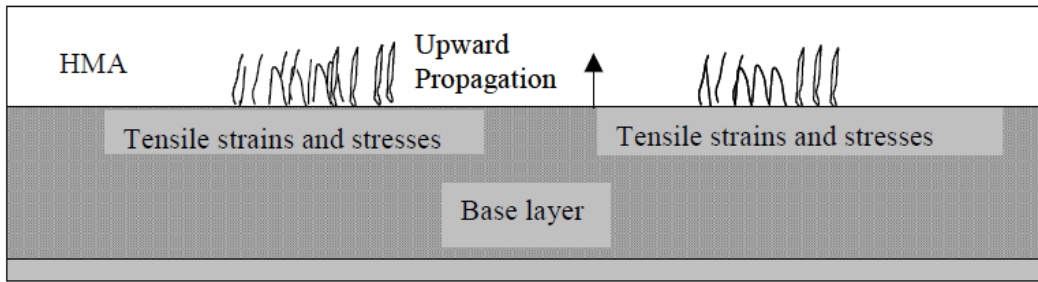


Figure 10: Bottom-up fatigue cracking (MEPD Guide)

The reasons for high tensile strains and stresses to occur at the bottom of the HMA layer can be a relatively thin or weak layer for the magnitude and repetitions of the wheel loads, higher wheel loads and tire pressures, soft spots or areas in unbound aggregate base materials or weak aggregate base/subbase layers caused by inadequate compaction.

3.2.6.2 Surface-down fatigue cracking (longitudinal)

There is increasing evidence that suggests load-related cracks do initiate at the surface and propagate downward. Some of the suggested mechanisms are:

- Wheel load induced tensile stresses and strains and strains that occur at the surface and cause cracks to initiate and propagate in tension. Aging of the HMA surface mixture accelerates this crack initiation-propagation process
- Shearing of the HMA surface mixture caused from radial tires with high contact pressures near the edge of the tire. This leads to cracks to initiate and propagate both in shear and tension
- Severe aging of the HMA mixture near the surface resulting in high stiffness and when combined with high contact pressures, adjacent to the tire loads, cause the cracks to initiate and propagate

The downward fatigue cracking mechanism is illustrated in the next *Figure 11*:

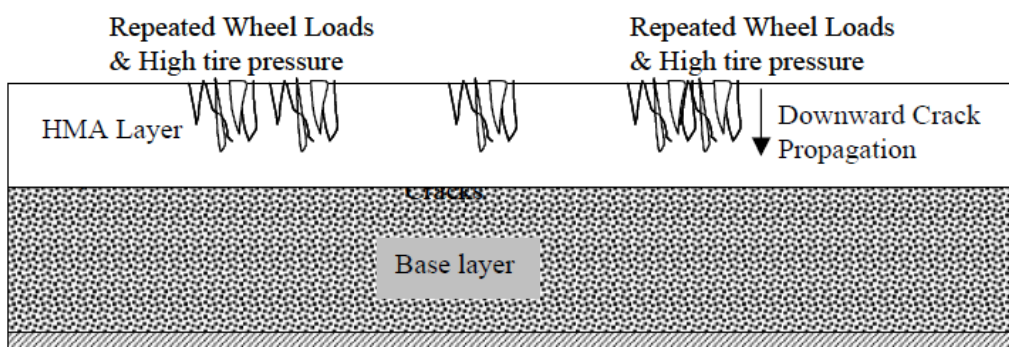


Figure 11: Surface-down fatigue cracking (MEPD Guide)

3.2.6.3 *Permanent deformation (rutting)*

This is a surface depression in the wheel paths caused by inelastic or plastic deformations in the pavement layers and subgrade. These plastic deformations are typically the result of densification or one-dimensional compression and consolidation and lateral movements or plastic flow of materials from wheel loads. Rutting can be of two types:

- **One dimensional densification or vertical compression:** A rut depth caused by material densification is a depression near the center of the wheel path without an accompanying hump on either side of the depression. Densification of materials is generally caused by excessive air voids or inadequate compaction for any of the bound or unbound layers. This allows the underlying layers to compact when subjected to traffic loads.
- **Lateral flow or plastic movement:** A rut caused by the lateral flow of material is a depression near the center of the wheel path with shear upheavals on either side of the depression. This type of rut depth usually results in a moderate to high severity level of rutting. Lateral flow or the plastic movement of materials will occur in those mixtures with inadequate shear strength and/or large shear stress states due to the traffic loads on the specific pavement cross-section used.

3.2.6.4 *Thermal cracking*

Thermal cracks typically appear as transverse cracks on the pavement surface roughly perpendicular to the pavement centerline. These cracks can be caused by shrinkage of the HMA surface due to low temperatures, hardening of the asphalt, and/or daily temperature cycles.

Cracks that result from the coldest in temperature are referred to as low temperature cracking. Cracking that result from thermal cycling is generally referred to as thermal fatigue cracking.

3.2.7 *Smoothness (IRI) prediction*

The IRI over the design period depends upon the initial as-constructed profile of the pavement from which the initial IRI is computed and upon the subsequent development of distresses over time. These distresses include rutting, bottom-up/top-down fatigue cracking, and thermal cracking for flexible pavements. The IRI model uses the distresses predicted using the models previously analyzed, initial IRI, and site factors

to predict smoothness over time. The site factors include subgrade and climatic factors to account for the roughness caused by shrinking or swelling soils and frost heave conditions. IRI is estimated incrementally over the entire design period.

3.2.8 Assessment of performance and design modification

The designs are obtained iteratively in a mechanistic design procedure that follows these steps:

- a) Establish performance criteria (level of rutting, cracking and smoothness at the end of the design life and the reliability)
- b) Assemble a trial design
- c) Predict performance over the design life
- d) Evaluate the predicted performance against the design requirements
- e) If the design criteria are not satisfied, revise design and repeat steps c) and d)

3.2.9 Design reliability

Design reliability for the individual pavement distress models (i.e., rutting, bottom-up cracking, top-down cracking, and thermal cracking) are based on the standard error of the estimates of each individual model obtained through the calibration process. These estimates of error include a combined input variability, variability in the construction process, and model or pure error. The desired level of reliability is specified along with the acceptable level of distress at the end of design life in defining the performance requirements for a pavement design.

3.2.10 Life cycle costs estimation

After a trial design has passed the structural (distress) and functional (smoothness) requirements, it becomes a technically feasible design alternative. At this point, the pavement can be analyzed for its life cycle costs for comparison with other feasible designs. The predicted distress and IRI of the feasible design alternatives can be used in estimating the mean lives of the design alternatives and their standard deviations, along with a designer-defined maintenance and rehabilitation policy, in conducting a life cycle cost analysis.

3.3 Inputs for new flexible pavement design

Input data used for the design of new flexible pavements are categorized as follows:

- General information
- Site/project identification
- Analysis parameters
- Traffic
- Climate
- Drainage and surface properties
- Pavement structure

3.3.1 General information

The following inputs define the analysis period and type:

- Design life: expected pavement design life (years)
- Base/subgrade construction month: the approx. month in which the base and subgrade are anticipated to be constructed. This input establishes the $t=0$ for the climatic model. The moisture regime within the unbound layers and subgrade is assumed to be at optimum too.
 - HMA construction month: this input defines the $t=0$ for the HMA material aging model and the thermal cracking model.
 - Traffic opening month: the expected month in which the pavement will be opened to traffic. This value defines the climatic conditions at the time of opening to traffic, which affects the temperature and moisture gradients as well as the layer moduli values, including subgrade. The analysis begins with the month entered (i.e., first day of month is assumed). This input establishes $t=0$ for incremental damage and incremental distress calculations.
 - Pavement type – Flexible: determines the method of design evaluations and the applicable performance models.

3.3.2 Site/project identification

This group of inputs includes the following:

- Project location, defines the climatic conditions for the pavement design
- Project identification
- Functional class of the pavement, from Interstate to Local street, helps determining the default vehicle class distribution and the selection of the vehicle operating speed.

3.3.3 *Analysis parameters*

- Initial IRI

Initial IRI defines the smoothness of the pavement. It's highly dependent on the project smoothness specifications and has a significant impact on the long-term ride quality of the pavement.

- Performance criteria

The flexible design is based on surface-down and bottom-up fatigue cracking of the asphalt surface, HMA thermal cracking, fatigue cracking in chemically stabilized layers, permanent deformation for both the asphalt layers and the total pavement, and pavement smoothness (IRI). The performance criteria for each distress will depend on the tolerance for the amount of cracking over the design period and also on the reliability level. A brief description of performance criteria for each distress will follow:

- A. *Surface-down fatigue cracking*: maximum allowable length of longitudinal cracking per mile of pavement that is permitted to occur over the design period (generally 1000 ft per mile of pavement).
- B. *Bottom-up fatigue cracking*: maximum area of alligator cracking expressed as a percentage of the total lane area that is permitted to occur over the design period (generally 25 to 50 percent of the total lane area).
- C. *Thermal cracking*: maximum length of transverse cracking per mile of pavement that is permitted to occur over the design period (generally 1000 ft per mile of pavement).
- D. *Total permanent deformation*: maximum rut depth in the wheel path (generally from 0.3 to 0.5 inches).
- E. *Smoothness*: acceptable IRI at the end of design life (generally from 150 to 250 in/mile).

3.3.4 *Traffic*

The basic data needed are AADTT, directional distribution factor, lane distribution factor and operational speed of vehicles. In addition to that, more adjustments are needed such as traffic growth factors or hourly truck traffic distribution and axle load distribution factors.

3.3.5 *Climate*

The following weather-related information is required and provided by weather station data for a given site:

- Hourly air temperature over the design period.
- Hourly precipitation over the design period.
- Hourly wind speed over the design period.
- Hourly percentage sunshine over the design period.
- Hourly ambient relative humidity values.
- Seasonal or constant water table depth at the project site.

The climatic inputs are combined with the pavement material properties, layer thicknesses, and drainage-related inputs to yield the following information:

- Hourly profiles of temperature distribution through the asphalt layers.
- Hourly temperature and moisture profiles (including frost depth calculations) through other pavement layers.
- Monthly or semi-monthly (during frozen or recently frozen periods) predictions of layer moduli for asphalt, unbound base/subbase, and subgrade layers.
- Annual freezing index values.
- Mean annual number of wet days.
- Number of freeze-thaw cycles.

3.3.6 *Pavement structure*

Will be detailed in the following paragraphs.

3.4 Flexible pavement design procedure

The design methodology used is based upon mechanistic-empirical approaches to predict all the distress types previously stated (fatigue fracture, permanent deformation, thermal cracking). Also IRI is estimated as a functional performance criterion.

3.4.1 *Trial design parameters*

The designer must first select an initial trial pavement structure for design using guidance. The designer must identify the pavement cross section and specify the layer material types and layer thicknesses for the initial pavement section to be analyzed.

He must next decide whether a seasonal analysis is required. If a seasonal analysis is not selected, all non-HMA layers will be assumed to have constant values of E_i and μ_i (modulus and Poisson's ratio) throughout the entire analysis period.

If the EICM option is selected for the seasonal analysis, the program internally generates environmental adjustment factors for the resilient modulus values entered by the user to estimate the seasonal material variation on monthly or semi-monthly intervals.

For the monthly seasonal values option instead, the designer must enter modulus and moisture values for each month for the entire year. The input modulus values are used directly in the pavement response model.

The next important decision is the selection of the design performance criteria for each distress type. The specific information required for the design performance criteria depends upon whether a deterministic or reliability design analysis has been selected. In a deterministic analysis, only two pieces of information are needed for the pavement analysis: the limiting design value for the distress (or IRI), and the design life.

3.4.2 *Pavement response model*

Inputs to the response models include:

- Pavement geometry
- Layer thickness
- Environment
- Temperature vs. depth for each season
- Moisture vs. depth for each season
- Material properties
- Elastic properties
- Nonlinear properties
- Traffic
- Load spectrum
- Tire contact pressure distributions and areas

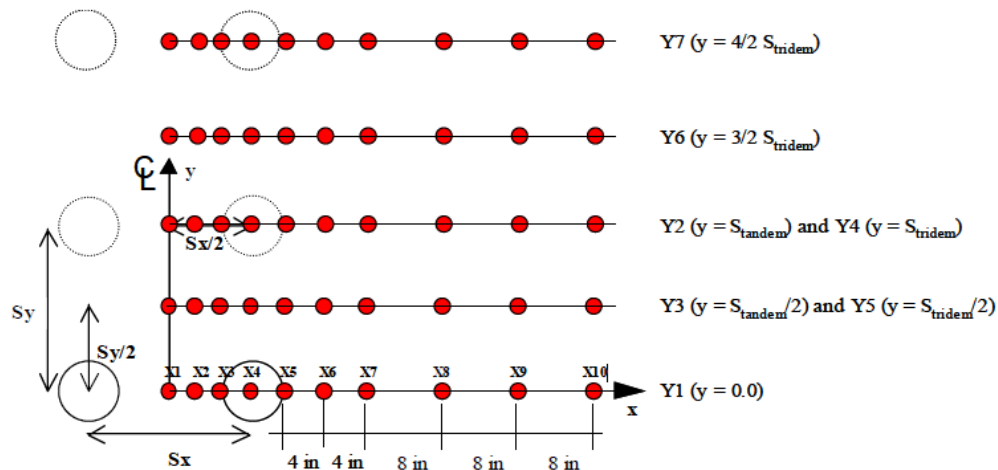
The outputs from the pavement response model are the stresses, strains and displacements within the pavement layers as we previously mentioned.

Two flexible pavement analysis methods have been implemented: for cases in which all materials in the pavement structure can realistically be treated as linearly elastic, the JULEA multilayer elastic theory program is used to determine the pavement response. JULEA provides an excellent combination of analysis features, theoretical rigor, and

computational speed for linear pavement analyses. In cases where the unbound material nonlinearity is also considered, the DSC2D nonlinear finite element code is used instead for determining the pavement stresses, strains, and displacements.

Also, for performance prediction, it is important to identify the locations in the pavement system that will result in the maximum damage over the entire analysis period. However, for mixed traffic conditions it is not possible to specify in advance the maximum damage location. To overcome this problem, the Guide software defines the analysis locations where the maximum damage is most likely to occur under mixed traffic. Damage is calculated at all these locations, and the performance prediction is based on conditions at the location producing the maximum damage.

Figure 12 represents schematics for horizontal analysis locations and regular traffic:



Computed Responses

- Single
 - Response 1 = Y1
- Tandem
 - Response 1 = Y1 + Y2
 - Response 2 = 2 * Y3
- Tridem
 - Response 1 = Y1 + 2 * Y4
 - Response 2 = 2 * Y5 + Y6
- Quad
 - Response 1 = Y1 + 2 * Y4 + Y7
 - Response 2 = 2 * Y5 + 2 * Y6

Figure 12: Horizontal analysis of standard traffic

3.4.3 Performance prediction

The Design Guide methodology for performance prediction is based upon an incremental damage approach. Distress or damage is estimated and accumulated for each analysis interval. An analysis interval of one month is defined as the basic unit for estimating the damage. However, the analysis interval reduces to semi-monthly during freeze and thaw periods because of the rapid change in the modulus under these conditions. The change in temperature and moisture conditions directly affects the material response and hence the performance.

3.4.3.1 Permanent deformation: overview

Permanent deformation is associated with rutting in the wheel path, which develops gradually as the number of load repetitions accumulate. Rutting normally appears as longitudinal depressions in the wheel paths accompanied by small upheavals to the sides. The width and depth of the rutting profile is highly dependent upon the pavement structure, traffic matrix and quantity and environment. Major problems can be associated with changes in roads' profiles due to differential consolidation altering the surface level:

- Transverse profile: Rutting modifies drainage characteristics and reduces runoff capability, Water creates conditions for aquaplaning of vehicles and reduces skid resistance of the surface course. In colder environments snow and ice removal is impeded.
- Longitudinal profile: differential permanent deformations increase roughness and reduce the serviceability of the road.

With time and enhanced technical capabilities and knowledge it became quite clear to design engineers that the total permanent deformation was a product of cumulative ruts occurring in all layers of the pavement system.

In the Design Guide a predictive rutting system is available to evaluate the permanent deformation within all rut susceptible layers in the pavement within the analysis period.

Regardless of the material type considered, there are generally three distinct stages for the permanent deformation behavior of pavement materials under a given set of material, load and environmental conditions, which can be described as follows:

- Primary stage: high initial level of rutting, with a decreasing rate of plastic deformations, predominantly associated with volumetric change.

- Secondary stage: small rate of rutting exhibiting a constant rate of change of rutting that is also associated with volumetric changes; however, shear deformations increase at increasing rate.

- Tertiary stage: high level of rutting associated with plastic deformations under no volume change conditions.

The primary stage is modeled using an extrapolation of the secondary stage trend. The tertiary stage is not taken into account since the tests are extremely difficult and time consuming, and also lack a prediction methodology for implementation.

True plastic shear deformations are not modeled within the system. In addition, no permanent deformation is assumed to occur for chemically stabilized materials and bedrock.

The damage of rutting is estimated for each subseason at the mid-depth of each sublayer within the pavement system: after verifying the type of layer, the system applies the model corresponding to the material type of the sublayer and computes the plastic strain accumulated at the end of each subseason with the following equation:

$$RD = \sum_{i=1}^{nsublayers} \varepsilon_p^i h^i \quad (4)$$

where

RD is the pavement permanent deformation,

nsublayers is the number of sublayers,

ε_p^i is the total plastic strain in sublayer I,

h^i is the thickness of sublayer I.

The process is repeated for each load level, subseason, and month of the analysis period.

For asphalt mixtures, the laboratory model form selected is:

$$\frac{\varepsilon_p}{\varepsilon_r} = a_1 T^{a_2} N^{a_3} \quad (5)$$

where

ε_p is the accumulated plastic strain at N repetitions of load (in/in),

ε_r is the resilient strain of the asphalt material as a function of mix properties, temperature and time rate of loading (in/in),

N is the number of load repetitions,

T is Temperature (degF),

a_i are non-linear regression coefficients.

The final model is:

$$\frac{\epsilon_p}{\epsilon_r} = k_1 10^{-3.4488} N^{0.479244} \quad (6)$$

where a depth parameter k_1 has been introduced to provide as accurate a rut depth prediction model as possible.

The total rutting in the pavement structure is equal to the sum of the individual layer permanent deformation for each season: the one in the asphalt layer (already explained) and those in granular base / subbase and subgrade layers (not shown).

Some of the factors affecting the permanent deformation are listed below:

- HMA layer thickness
- HMA layer dynamic modulus
- Binder grade in the HMA mixture
- Air voids
- Effective binder content
- Base type
- Base thickness
- Base stiffness
- Traffic load, contact area and tire pressure
- Traffic operating speed
- Traffic wander
- Temperature and environmental conditions

While many of the parameters above remain constant throughout the design period (e.g., layer thickness), others vary seasonally, monthly, hourly, or with pavement age.

3.4.3.2 *Permanent deformation: procedure step by step*

1. Tabulate input data

All input data required is explained in the DESIGN INPUTS chapter

2. Process traffic data

The traffic inputs are first processed to determine the expected number of single, tandem, tridem, and quad axles in each month within the design period.

3. Process temperature profile data

The solution sequence from the EICM provides temperature data at intervals of 0.1 hours (6 minutes) over the analysis period. This temperature distribution for a given month can be represented by a normal distribution. The frequency diagram obtained from the EICM represents the distribution at a specific depth and time.

Temperatures in a given month, though, may have extreme temperatures (even at a low frequency of occurrence) that could be significant for rutting: using the average temperature value will not capture the damage caused by these extreme temperatures. That's why the temperatures over a given interval are divided into five different sub-seasons, and for each of these the sub-layer temperature is defined by a temperature that represents 20% of the frequency distribution of the pavement temperature. This sub-season will also represent those conditions when 20% of the monthly traffic will occur.

4. Process monthly moisture conditions data

EICM calculates the moisture content and corrects for the moisture change in the unbound layer.

5. Calculate stress

The following increments are considered:

- Pavement age – by year
- Season – by month
- Load configuration – axle type
- Load level – discrete load levels in 1000 to 3000 lb increments, depending on axle type
- Temperature – pavement temperature for the HMA dynamic modulus.

The vertical resilient strain at any given depth is defined by knowledge of the three-dimensional stress state and the elastic properties of the HMA layer from:

$$\varepsilon_{rz} = \frac{1}{E^*} (\sigma_z - \mu\sigma_x - \mu\sigma_y) \quad (7)$$

E^* is expressed as a function of the mix properties, temperature, and time of the load pulse. Knowledge of the predicted vertical resilient strain at any point allows for the direct calculation of the plastic strain ε_p at any given point after N repetitions.

The incremental rut depth for each sublayer in the HMA layer can be found from:

$$\Delta RD_i = \varepsilon_{pi} \times \Delta h_i \quad (8)$$

And in the end, the total layer rut depth can be found by summing all incremental ΔRD_i

$$RD = \sum_{i=1}^N \Delta RD_i \quad (9)$$

6. Calculate permanent deformation

For the general solution, permanent deformation is estimated for each layer at each computational location using pavement responses calculated at the mid-depth of each sublayer. This is done at locations defined by the analysis module for regular traffic. In the following model description, the equivalent number of load cycles for each subseason is found by solving the permanent deformation model for N with the deformation accumulated up to and the material properties and load conditions prevailing in the current subseason:

$$\varepsilon_p = f(\varepsilon_r, T, N) \quad (10)$$

where:

ε_p is the total plastic strain (in/in),

ε_r is the resilient strain which is related to the dynamic modulus (E^*) of the mix and other mixture properties (in/in),

T is temperature (degF),

N is the total number of load cycles (given axle type and load).

In the following graph, the total plastic strain $\varepsilon_{p,i-1}$ at the end of subseason $i-1$ corresponds to a total number of traffic repetitions N_{i-1} (point A). In the next subseason i , the layer temperature is T_i and resilient strain for load and material conditions prevailing in i is $\varepsilon_{r,i}$ (Figure 13).

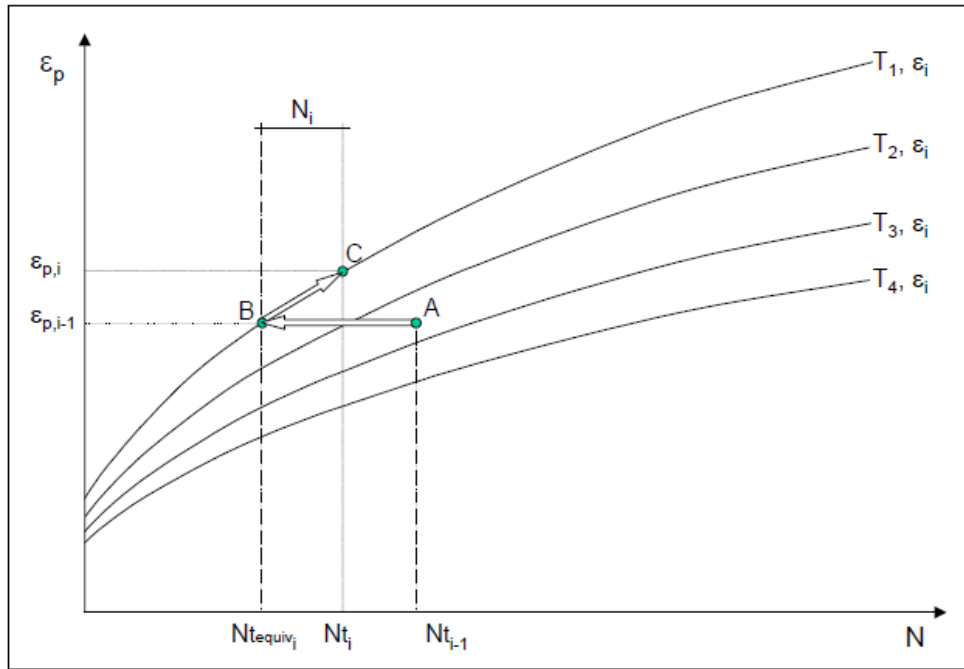


Figure 13: Deformation - Number of repetitions graph (MEPD Guide)

At the beginning of the next subseason i (point B), there is an equivalent number of traffic repetitions N_{teqi} that is associated with the total deformation at the end of subseason $i-1$ but under conditions prevailing in the new sub-season ($T_l \ \epsilon_{r,i}$). The approach is necessary because models for permanent deformation provide an estimate of the total deformation rather than the increment in plastic strain due to seasonal traffic.

By adding the number of traffic repetitions at season i (N_i) to the total equivalent number of repetitions N_{teqi} , using the specific material model, it is possible to estimate point C, which corresponds to the total plastic strain at the end of sub-season i .

3.4.3.3 Modification of Flexible Design to Reduce Permanent deformation

If the predicted rutting in the HMA layer is greater than the design requirements, the trial design must be modified to increase structural capacity and for the quality of materials used in all layers. The first thing that the engineer needs to accomplish is to critically evaluate the initial predicted rut depth quantities by layer and material type in the first (trial) design run.

One major design consideration would be to increase the quality of the HMA layer being placed. The direct factor that can be controlled is to increase the HMA mixture stiffness (modulus) by increasing the mix Master Curve location using a stiffer grade of

binder or less asphalt and insuring that field compaction specifications are fully complied with.

Moreover, the majority of all rutting in the HMA layer will generally occur within the top 3- to 5-in. Thus, if a poor quality HMA mixture is being used, increasing the thickness of this poor-quality layer will not decrease the rutting in the HMA layer.

3.4.3.4 *Fatigue Cracking: overview*

The action of repeated traffic loads induces tensile and shear stresses in the bound layers, which eventually lead to a loss in the structural integrity. Repeated load or fatigue initiates cracks at points where the critical tensile strains and stresses occur, which are affected by the stiffness of the layer and the load configuration. Once the damage initiates at the critical location, the continued action of traffic eventually causes these cracks to propagate through the entire bound layer.

It has been common to assume that fatigue cracking normally initiates at the bottom of the asphalt layer and propagates to the surface (bottom-up cracking). This is due to the bending action of the pavement layer that results in flexural stresses to develop at the bottom of the bound layer. However,

numerous studies have also demonstrated that it may also be initiated from the top and propagates down (top-down cracking), probably due to critical tensile and/or shear stresses developed at the surface and caused by extremely large contact pressures at the tire edges-pavement interface.

The Guide utilizes an approach that models both the top-down and bottom-up cracking, based on calculating the fatigue damage at the surface and at the bottom of each asphalt layer. The fatigue damage is then correlated using calibration data to the fatigue cracking.

Estimation of fatigue damage is based upon Miner's Law, which states that damage is given by the following relationship:

$$D = \sum_{i=1}^T \frac{n_i}{N_i} \quad (11)$$

where:

D is the damage,

T is the total number of periods,

n_i is the actual traffic for period I ,

N_i is the traffic allowed under conditions prevailing in i .

The commonly used mathematical relationship used for fatigue characterization has the following form:

$$N_f = 0.00432 \cdot k'_1 \cdot C \left(\frac{1}{\varepsilon_t} \right)^{3.9492} \cdot \left(\frac{1}{E} \right)^{1.281} \quad (12)$$

where:

N_f is the number of repetitions to fatigue cracking,

ε_t is the tensile strength at the critical location,

E is the stiffness of the material,

k'_1 is the correction for different asphalt layer thickness,

C is a “laboratory to field” adjustment factor.

The final transfer function to calculate the fatigue top-down cracking from the fatigue damage is:

$$FC_{top} = \left(\frac{1000}{1 + e^{7-3.5 \cdot \text{Log}(D \cdot 100)}} \right) \cdot 10.56 \quad (13)$$

where

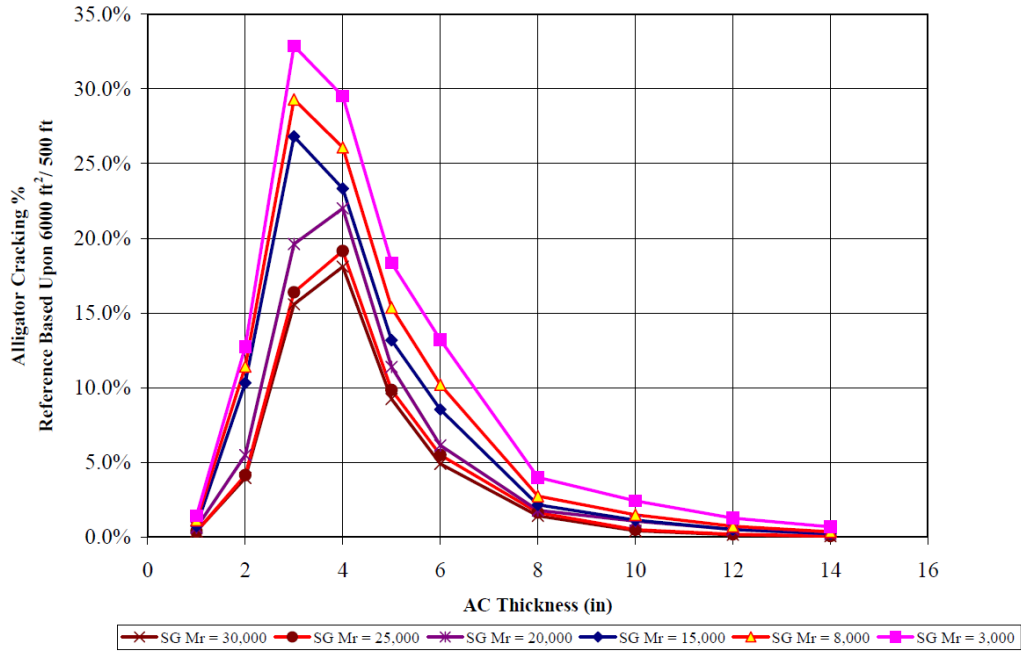
FC_{top} is top-down fatigue cracking, ft/mile,

D is top-down fatigue damage.

The transfer function for bottom-up cracking will not be analyzed here since it's very similar to the previous one.

The factors affecting fatigue cracking in flexible pavements are the same previously explained for rutting, plus traffic load repetitions.

As a note, the following graph illustrates an extremely important fact regarding the distribution of alligator fatigue cracking for flexible pavements: the magnitude of alligator cracking is directly related to the thickness of the HMA layer: the greatest potential for fatigue fracture is associated to layers 3- to 5-in thickness range. However, very thin HMA layers may have other major distresses like repetitive shear deformations, leading to permanent deformation or excessive rutting.



3.4.3.5 Fatigue cracking prediction procedure

The process follows exactly the steps previously listed for rutting until 5., where this time the software calculates critical tensile strain with the following equation, similar to the rutting one:

$$\varepsilon_{rx,y} = \frac{1}{E^*} (\sigma_{x,y} - \mu\sigma_{y,x} - \mu\sigma_z) \quad (14)$$

And 6. calculates fatigue cracking with the function described earlier.

3.4.3.6 Modification of flexible design to reduce fatigue cracking

As previously said, the designer can decrease alligator fatigue cracking by increasing the thickness of the HMA layers. Moreover, the greater the effective volume of bitumen and the lower the air voids will result in an increase in HMA fatigue life, and a reduced E_i/E_{i+1} ratio will decrease the likelihood of fatigue damage.

The difference between top-down and bottom-up cracking is a key issue to appreciate: in general, the presence of thick and /or stiff layers in the upper portion of the structural pavement cross section will tend to cause an increase in tensile surface strain and therefore longitudinal surface cracking. This is completely opposite trend for the alligator cracking.

3.4.3.7 Thermal cracking model: overview

The amount of transverse cracking expected in the pavement system is predicted by relating the crack depth to an amount of cracking (crack frequency) by the following expression:

$$C_f = \beta_1 \cdot N\left(\frac{\log C/h_{ac}}{\sigma}\right) \quad (15)$$

where

C_f is the observed amount of thermal cracking,

β_1 is the regression coefficient determined through field calibration,

$N(z)$ is the standard normal distribution evaluated at z ,

σ is the standard deviation of the log of the depth of cracks,

C is crack depth,

h_{ac} is the thickness of asphalt layer.

3.4.3.8 Structural response modeling for thermal cracking

The following factors affect the magnitude of the thermal cracking prediction in the HMA layer:

- Temperature-depth profile within the asphalt layer
- Creep compliance
- Creep compliance test temperature
- Tensile strength
- Mixture VMA
- Aggregate coefficient of thermal contraction
- Mix coefficient of thermal contraction
- HMA layer thickness
- Air voids
- VFA
- Intercept of binder viscosity-temperature relationship at RTFO condition
- Penetration at 77 °F

The thermal cracking increment defined in the Guide was determined equal to one month to account for those cases as follows:

- Temperature-depth profile within the asphalt layer: the general approach is to use the EICM as the climatic algorithm to determine the temperature-depth profile at hourly time intervals over the entire analysis period.

- Creep compliance: evaluated at 0 °C, -10 °C and -20 °C. It accounts for the linear visco-elastic properties on which the thermal cracking analysis is based on.

3.4.3.9 Thermal cracking prediction procedure

1. Gathering input data

The thermal cracking approach developed requires characterization of asphalt mixes in Indirect Tensile (IDT) mode. Key visco-elastic properties of the asphalt mixture are measured, like the creep compliance, using indirect tensile tests at one or three temperatures, and the indirect tensile strength.

2. Development of the master creep compliance curve

Enhanced data analysis techniques are claimed to provide accurate evaluations of the time-temperature shift factor (a_T) and creep compliance model statistical fitting technique, as well as the development of the creep compliance master curve (CCMC).

3. Prediction of thermal stresses

Using viscoelastic transformation theory, the compliance can be related to the relaxation modulus. Knowledge of this parameter allows for the prediction of the thermal stress within the asphalt layer.

The relaxation modulus function is obtained by transforming the creep compliance function:

$$E(\xi) = \sum_{i=1}^{N+1} E_i \cdot e^{-\xi/\lambda_i} \quad (16)$$

where

$E(\xi)$ is the relaxation modulus at reduced time ξ ,

E_i, λ_i are parameters for master relaxation modulus curve.

Knowledge of the relaxation modulus function allows for the computation of the thermal stresses:

$$\sigma(\xi) = \int_0^{\xi} E(\xi - \xi') \frac{d\varepsilon}{d\xi} d\xi' \quad (17)$$

where

$\sigma(\xi)$ is stress at reduced time ξ ,

$E(\xi - \xi')$ is the relaxation modulus at reduced time $\xi - \xi'$,

ε is the strain at reduced time ξ ,

ξ' is a variable of integration.

4. Growth of the thermal crack length computation

Fracture mechanics is used to compute the growth of the thermal crack length. This is accomplished by knowledge of the stress intensity factor, K , as well as the A and n fracture parameters obtained from the creep compliance and strength of the mixture.

5. Length of thermal cracks computation

The degree of cracking is predicted from an assumed relationship between the probability distribution of the log of the crack depth to HMA layer thickness ratio and the percent of cracking.

The maximum amount of thermal cracking assumed is 400 ft per 500 ft of pavement length.

3.5 Design inputs: material characterization.

Of all inputs required by MEPD models, only “material characterization” will be analyzed in this dissertation, since it’s been carried out thoroughly through sample testing. For information about all other inputs (like climate, traffic...) and their related models see *Mechanistic-Empirical Pavement Design Guide*.

Information about climate and traffic needed for this study has been found in the software database.

3.5.1 Introduction

To better understand the material requirements, the following subcategories have been developed: material properties required for computing pavement responses, additional materials inputs to the distress/transfer functions and additional materials inputs required for climatic modeling.

The first kind of material properties predict the states of stress, strain and displacement within the pavement when subjected to an external wheel load: they include elastic modulus (E) and Poisson’s ratio (μ) of the material.

The second category includes all the materials-related inputs that enter the distress or smoothness models directly, such as load-related fatigue fracture (top-down and bottom-up), permanent deformation and transverse fracture.

The last category includes materials-related inputs that enter the climatic module to help determine the temperature and moisture profiles through the pavement cross-section,

like plasticity index, porosity, grain size, absorptivity, coefficient of thermal expansion etc.

3.5.2 *Material factors considered*

Materials can be fully described using the following attributes:

a. “Time-dependent properties”: due to chemical and physical forces, influence of climate, onset of fracture or deformation. Chemical and physical hardening of asphalt binders due to its aging, curing caused by the evaporation of moisture within asphalt emulsion systems. These enhancements usually increase the modulus and strength of the material. Physical hardening of an asphalt layer leads to lowering the states of stress in an underlying layer and the chance of rutting.

Materials that are subjected to load-related fatigue distress, however, may also experience a severe degradation of properties with time and load repetitions, developing microcracks and leading to a reduced modulus. This reduced modulus will result in an increase in stress states within the pavement.

b. “Time-Temperature effects”: since asphalt is a viscoelastic-plastic material, its modulus may approach that of an unbound granular material at high temperatures and long loading rates, while at cold temperatures and short load rates the material will behave in a pure elastic mode, with a modulus near to the one of a PCC material. Both cases will be taken into account.

The rate of load effect upon material response is a function not only of the vehicular speed, but also of the location of the material within the pavement structure. In general, as one proceeds deeper into the pavement, the length of the stress pulse acting on a given material will increase, suggesting that the time of the load pulse will also increase.

c. “Non-Linear behavior”: if the value of the elastic modulus depends on the state of the stress in the material, that one is considered non-linear. The guide will consider as non-linear only base/subbase and subgrade materials at the most advanced levels of M-E analysis.

3.5.3 *Material categories*

The M-E analysis groups materials in the following six categories and various subcategories:

<u>Asphalt Materials</u> Hot Mix Asphalt (HMA)—Dense Graded Central Plant Produced In-Place Recycled Stone Matrix Asphalt (SMA) Hot Mix Asphalt—Open Graded Asphalt Hot Mix Asphalt—Sand Asphalt Mixtures Cold Mix Asphalt Central Plant Processed In-Place Recycled <u>PCC Materials</u> Intact Slabs Fractured Slabs Crack/Seat Break/Seat Rubblized <u>Chemically Stabilized Materials</u> Cement Stabilized Aggregate Soil Cement Lime Cement Fly Ash Lime Fly Ash Lime Stabilized Soils Open graded Cement Stabilized Aggregate	<u>Non-Stabilized Granular Base/Subbase</u> Granular Base/Subbase Sandy Subbase Cold Recycled Asphalt (used as aggregate) RAP (includes millings) Pulverized In-Place Cold Recycled Asphalt Pavement (HMA plus aggregate base/subbase) <u>Subgrade Soils</u> Gravelly Soils (A-1:A-2) Sandy Soils Loose Sands (A-3) Dense Sands (A-3) Silty Sands (A-2-4:A-2-5) Clayey Sands (A-2-6; A-2-7) Silty Soils (A-4:A-5) Clayey Soils Low Plasticity Clays (A-6) Dry-Hard Moist Stiff Wet/Sat-Soft High Plasticity Clays (A-7) Dry-Hard Moist Stiff Wet/Sat-Soft <u>Bedrock</u> Solid, Massive and Continuous Highly Fractured, Weathered
---	---

Figure 14: Major material categories (MEPD Guide, Table 2.2.2)

One of the more complicated groups is “Asphalt Materials,” because the response and behavior of these materials are heavily influenced by temperature, time rate of load, method of mixture, the mixing process, and the degree of damage of the material (new versus rehabilitated pavement systems). In reality, this category may include material subgroups for which a great deal of historical information is available concerning typical modulus, Poisson’s ratio, strength, fracture and permanent deformation properties.

3.5.4 Input characterization (asphalt materials)

The primary stiffness property of interest for asphalt materials is the time-temperature dependent dynamic modulus (E^*). The following table provides a summary of the procedures at various input hierarchical levels to derive E^* :

Material Group Category	Input Level	Description
Asphalt Materials	1	<ul style="list-style-type: none"> • Conduct E^* (dynamic modulus) laboratory test (NCHRP 1-28A) at loading frequencies and temperatures of interest for the given mixture. • Conduct binder complex shear modulus (G^*) and phase angle (δ) testing on the proposed asphalt binder (AASHTO T315) at $\omega = 1.59$ Hz (10 rad/s) over a range of temperatures. • From binder test data estimate Ai-VTSi for mix-compaction temperature. • Develop master curve for the asphalt mixture that accurately defines the time-temperature dependency including aging.
	2	<ul style="list-style-type: none"> • No E^* laboratory test required. • Use E^* predictive equation. • Conduct G^*-δ on the proposed asphalt binder (AASHTO T315) at $\omega = 1.59$ Hz (10 rad/s) over a range of temperatures. The binder viscosity or stiffness can also be estimated using conventional asphalt test data such as Ring and Ball Softening Point, absolute and kinematic viscosities, or using the Brookfield viscometer. • Develop Ai-VTSi for mix-compaction temperature. • Develop master curve for asphalt mixture that accurately defines the time-temperature dependency including aging.
	3	<ul style="list-style-type: none"> • No E^* laboratory testing required. • Use E^* predictive equation. • Use typical Ai-VTS- values provided in the Design Guide software based on PG, viscosity, or penetration grade of the binder. • Develop master curve for asphalt mixture that accurately defines the time-temperature dependency including aging.

Figure 15: Asphalt materials input levels (MEPD Guide)

3.5.5 Overview of E^* estimation: Master Curve and Shift Factors

For level 1 analysis, master curves and the corresponding shift factors for E^* can be developed experimentally by shifting laboratory frequency sweep test data. For characterization of E^* mastercurves see *Research Plan* of this dissertation.

3.5.6 Binder viscosity

The binder viscosity at the temperature of interest can be determined (at unaged conditions) from the ASTM viscosity temperature relationship defined by:

$$\log \log \eta = A + VTS \log T_R \quad (18)$$

where

η is the viscosity,

T_R is the temperature,

A is the regression intercept,

VTS is the regression slope of viscosity temperature susceptibility.

At level 1, A and VTS parameters can be estimated from the DSR test data conducted in accordance to AASHTO T315.

3.5.7 Asphalt aging

The effect of aging is incorporated into the determination of dynamic modulus using the Global Aging System, that provides models that describe the change in viscosity that occurs during mixing and compaction, as well as long-term aging. It includes four models:

- “Original to mix/lay-down” model: accounts for the short-term aging that occurs during mixing and compaction.
- “Surface aging” model: predicts the viscosity of the binder at the surface of the pavement after any period of time.
- “Air void adjustment” model: adjusts the surface viscosity for different air void contents.
- “Viscosity-depth” model: determines viscosity as a function of depth along with the previous models.

The output of the Global Aging System is a prediction of the binder viscosity at any time and any depth in the pavement system.

3.5.8 Implementation at Input level 1

3.5.8.1 Required test data

At this level actual laboratory test data are required to develop the master curve and shift factors, shown in the following table:

Temperature, °F	Mixture E^* and δ^1				Binder G^* and δ^2 1.59 Hz
	0.1 Hz	1 Hz	10 Hz	25 Hz	
10	X	X	X	X	
25					
40	X	X	X	X	X
55					X
70	X	X	X	X	X
85					X
100	X	X	X	X	X
115					X
130	X	X	X	X	X

¹ Testing to be performed in accordance with NCHRP 1-28A.

² Testing to be performed in accordance with AASHTO T315.

Figure 16: Laboratory test data for E^* needed at Input level 1 (MEPD Guide)

To account for short-term aging that occurs during mixing and compaction, the mixture testing should be performed after short-term oven aging in accordance with

AASHTO R30, and the binder testing should be performed after Rolling Thin Film Oven Test aging (AASHTO T240) in accordance with AASHTO T315.

The mixture data consist of dynamic modulus frequency sweep tests on replicate specimens (100 mm diameter and 150 mm height) for five temperatures and four rates of loading. Additionally, binder complex modulus and phase angle data are needed over a range of temperatures for a loading rate of 1.59 Hz.

3.5.9 Poisson’s Ratio for bituminous materials

The Poisson’s Ratio for bituminous road materials ranges between 0.15 and 0.50, as a function of temperature. At input level 1 it would be estimated from laboratory testing, however the use of correlation or typical assumed values for analysis can be considered satisfactory.

3.5.10 Other HMA material properties

3.5.10.1 Tensile strength

At level 1 actual test data for tensile strength at 14°F is required, in accordance with AASHTO T322, “Determining the Creep Compliance and Strength of Hot Mix Asphalt (HMA) Using the Indirect Tensile Test Device.”

3.5.10.2 Creep compliance

At level 1 actual test data for HMA creep compliance is required. The specific data requirements are presented in the following table. Testing should be done in accordance with AASHTO T322.

Time of Loading	Temperature, °F		
	-4	14	32
1	X	X	X
2	X	X	X
5	X	X	X
10	X	X	X
20	X	X	X
50	X	X	X
100	X	X	X

Figure 17: Laboratory test data for creep compliance needed at Input level 1 (MEPD Guide)

3.5.10.3 Coefficient of thermal contraction

The Design Guide software computes CTC internally using the HMA volumetric properties such as VMA and the thermal contraction coefficient for the aggregates. The model used to estimate CTC for asphalt concrete mixtures is shown in the following equation:

$$L_{MIX} = \frac{VMA \cdot B_{ac} + V_{AGG} \cdot B_{AGG}}{3 \cdot V_{TOTAL}} \quad (19)$$

where

L_{MIX} is the linear coefficient of thermal contraction of the mixture,

B_{ac} is the volumetric coefficient of thermal contraction of the asphalt cement in the solid state,

B_{AGG} is the volumetric coefficient of thermal contraction of the aggregate,

VMA is the percent volume of voids in the mineral aggregate,

V_{AGG} is the percent volume of aggregate in the mixture,

V_{TOTAL} is 100%.

3.5.10.4 Surface shortwave absorptivity

It depends on a layer's composition, color and texture. This quantity directly correlates with the amount of available solar energy absorbed by the pavement surface: lighter and more reflective surfaces tend to have lower shortwave absorptivity and vice versa. At level 1 it is recommended that this parameter be estimated through laboratory testing since there are no current AASHTO certified standards.

3.5.10.5 Thermal conductivity and Heat capacity

Thermal conductivity K is the quantity of heat that flows normally across a surface of unit area per unit time and per unit of temperature gradient. The moisture content has an influence upon the thermal conductivity of asphalt concrete. If the moisture content is small, the differences between the unfrozen, freezing and frozen thermal conductivity are small.

The heat capacity is the actual amount of heat energy Q necessary to change the temperature of a unit mass by one degree.

At level 1 a direct measurement is recommended for both of those properties above.

3.6 MEPD software: AASHTOWare Pavement ME Design

The software chosen for this study, that implements MEPD principles and models, is AASHTOWare's *Pavement ME Design*: this software, through its interface and tools, guide designers through this particular design process, giving a better understanding and evaluating the design life of many kinds of pavements.

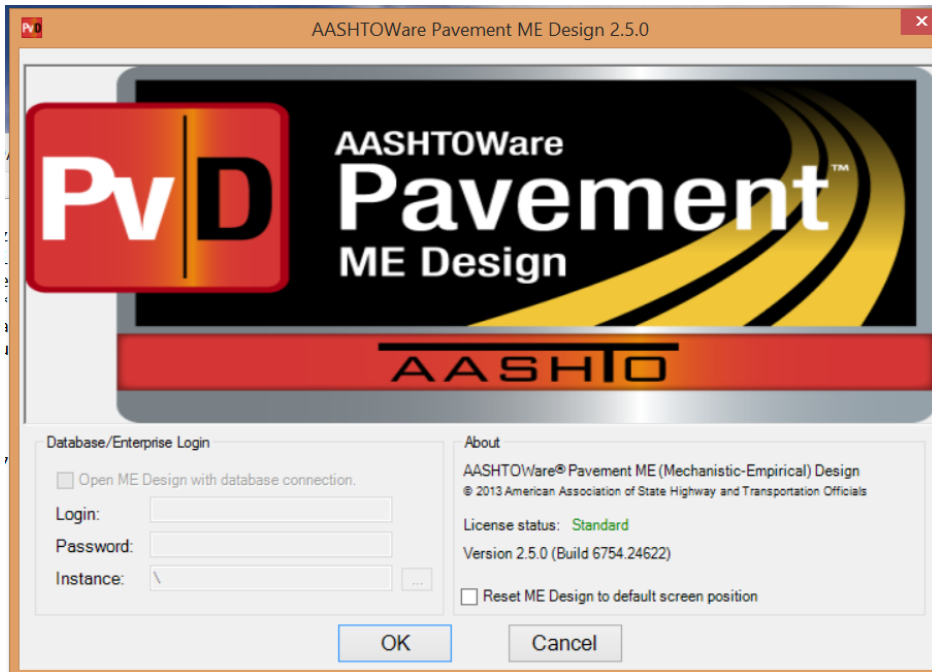


Figure 18: Pavement ME Design software

The pavement structure is represented by layers, and one can initially choose between new or overlay flexible or PCC superstructure and later put all the structural inputs (see Figure 19 for an example of a flexible pavement with two layers of asphalt).

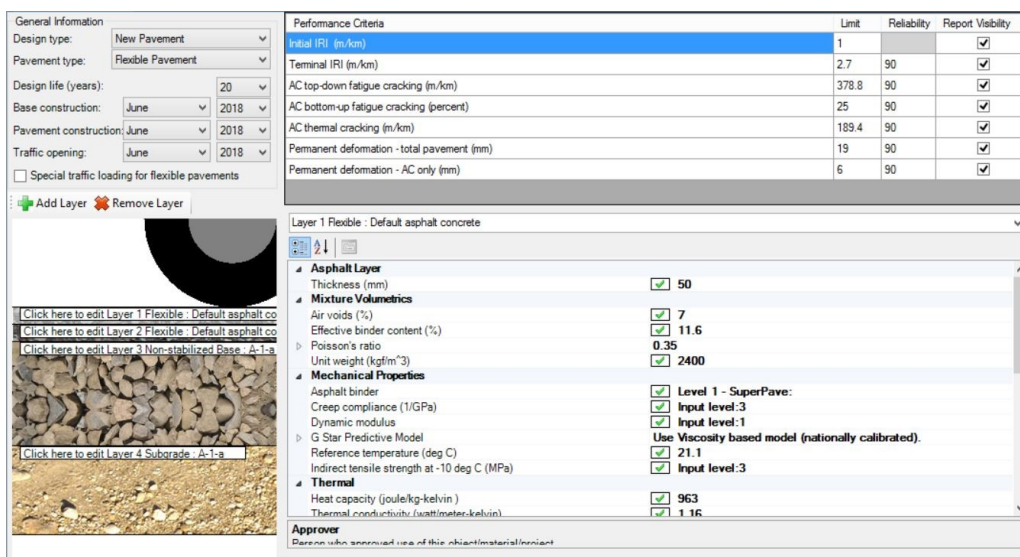


Figure 19: Pavement ME Design structural inputs

The inputs and their accuracy and precision, as in the MEPDG, depend on the input level chosen. As previously said, in this case Input level 1 (site-specific values) has been chosen for Dynamic modulus and permanent deformation's Beta coefficients. These values can be copy-pasted, imported from a database or through .xml files.

Values for climate can be found in the database if none is available: one can select from 8 different default climate stations around the United States (*Figure 20*) or upload manually climate data.



Figure 20: Pavement ME default climate stations

The same thing happens for traffic data: one can change the default heavy vehicles traffic and axles per truck distribution manually, along with many very specific information like wheels spacing or tire pressure.

DVR_DRY:Project DVR_DRY:Traffic DVR_DRY:Single DVR_DRY:Tandem DVR_DRY:Tridem DVR_DRY:Quad

Vehicle Class Distribution and Growth

Vehicle Class	Distribution (%)	Growth Rate (%)	Growth Function
Class 4	3.3	3	Linear
Class 5	34	3	Linear
Class 6	11.7	3	Linear
Class 7	1.6	3	Linear
Class 8	9.9	3	Linear
Class 9	36.2	3	Linear

Monthly Adjustment

Month	Class 4	Class 5	Class 6	Class 7	Class 8	Class 9	Class 10	Class 11	Class 12	Class 13
January	1	1	1	1	1	1	1	1	1	1
February	1	1	1	1	1	1	1	1	1	1
March	1	1	1	1	1	1	1	1	1	1
April	1	1	1	1	1	1	1	1	1	1
May	1	1	1	1	1	1	1	1	1	1
June	1	1	1	1	1	1	1	1	1	1

Axles Per Truck

Vehicle Class	Single	Tandem	Tridem	Quad
Class 4	1.62	0.39	0	0
Class 5	2	0	0	0
Class 6	1.02	0.99	0	0
Class 7	1	0.26	0.83	0
Class 8	2.38	0.67	0	0
Class 9	1.13	1.93	0	0
Class 10	1.19	1.09	0.89	0

AAADTT
 Two-way AADTT 4000
 Number of lanes 2
 Percent trucks in design dir 50
 Percent trucks in design lan 95
 Operational speed (kph) 100
Traffic Capacity
 Traffic Capacity Cap Not enforced
Axle Configuration
 Average axle width (m) 2.59
 Tandem axle spacing (m) 1.31
 Dual tire spacing (mm) 305
 Quad axle spacing (m) 1.25
 Tire pressure (kPa) 827.4
 Tridem axle spacing (m) 1.25
Lateral Wander
 Design lane width (m) 3.7
 Mean wheel location (mm) 460
 Traffic wander standard dev 254
Wheelbase
 Average spacing of long axli 5.49
 Average spacing of medium 4.57
 Percent trucks with long axli 61
 Percent trucks with medium 22
 Percent trucks with short ax 17
 Average spacing of short ax 3.66
Identifiers
 Approver
 Date approved 01/01/2011
 Author AASHTOWare
 Date created 01/01/2011
Traffic Capacity Cap
 The average standard deviation of the lateral traffic wander. The recommended default value is 254 mm...

Figure 21: Pavement ME Design traffic inputs

Once all data are inserted, the simulation can run and a PDF report is obtained. There is also the possibility to develop a .xlm file as well as keep all intermediate analysis files to see, for example, how many ESAL the pavement has sustained.

4 RESEARCH PLAN

The following paragraphs will present the objectives, materials, procedures and machineries related to the analysis of the mixtures of interest.

4.1 Objectives

This research aimed to further improve knowledge on the innovative DVR-modified and the more common SBS-modified HMA, used for the construction of a field test section located in East Lansing, not far from the university and the Civil Engineering Department's Advanced Asphalt Characterization Lab (AACL).

The questions raised on the mixtures during the planning of this dissertation were:

- a. Is permanent deformation resistances of DVR-modified mixtures any better, worse or at the same level of SBS-modified ones?
- b. If permanent deformation resistances are at the same level for all mixtures in all conditions, is it because of the materials or because of Michigan climate does not allow permanent deformation to fully develop?
- c. Is moisture damage relevant at all?
- d. Is it possible to evaluate cracking resistance using SCB tests and are results of several models satisfying in terms of accuracy?

Hints for problems a. and b. can be found in the evaluation of E^* mastercurves and FN tests results (permanent strain curves), but in this dissertation the most valuable answer is given by the reports of *Pavement ME Design* because it not only puts together the results mentioned before but also implements the reliable MEPD principles: it's not just a bunch of scattered and unbound results but a cohesive and thorough analysis of a mixture.

The answer of question c. can be found by varying the climate station in the software inputs: the one chosen for the first part of the analysis is in Illinois (the closest to Michigan), while the one chosen for the answer to this question is in Arizona.

Question d. is given by analyzing the results of SCB tests with two different models, one developed at MSU and the other at Illinois' Department of Transportation, and to improve the level of the analysis an advanced characterization of tested samples' Ligament Area has been developed to be implemented in the MSU model.

A summary of the objectives and the processes followed for the developing of this dissertation is in *Figure 22*. It's clear from it that the actual discussion of the permanent deformation results starts after the implementation of the tests' data on the software.

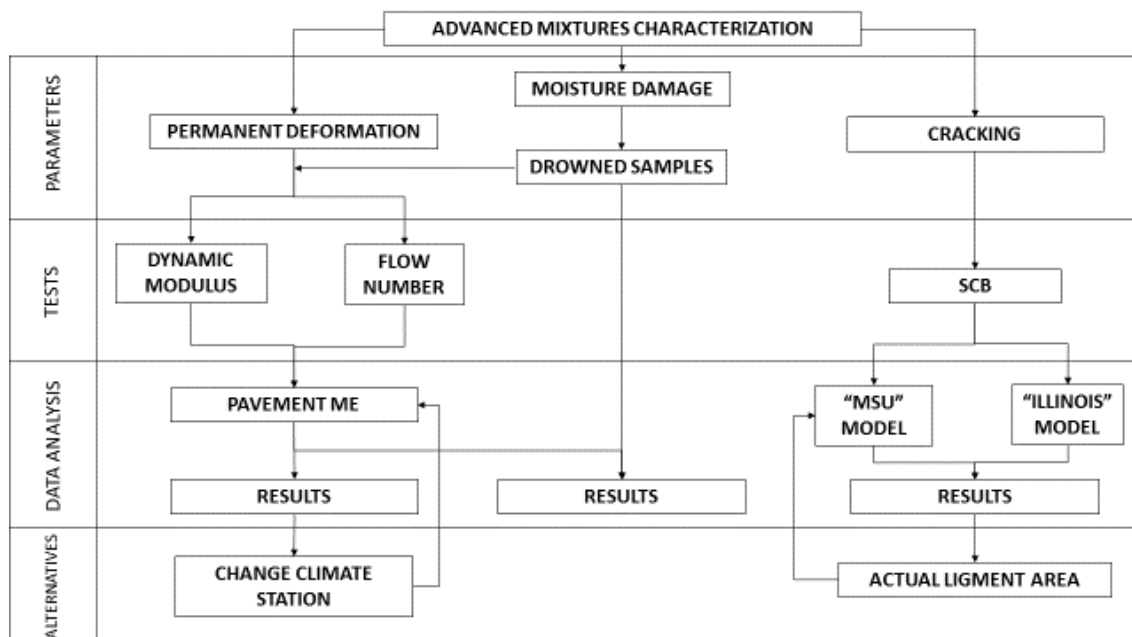


Figure 22: Processes' Flow Chart

4.2 Standard and advanced mixtures characterization

4.2.1 Dynamic Modulus and Flow Number

In MSU's AACL the samples, produced using the standard Superpave procedures explained in detail in Par. 4.3 have been tested for complex modulus ($|E^*|$) and permanent deformation (Flow Number FN) with the local AMPT to determine the data needed for the MEPD model to develop the rutting analysis on the design pavements.

The Mechanistic-Empirical Design for permanent deformation has been carried out using the *AASHTOWare Pavement ME Design* software, in which the M-E model is implemented.

4.2.2 Moisture damage evaluation

A more advanced study of these mixtures was due to further improve the database related to these innovative materials and complete their characterization. This more accurate analysis has been developed by taking into account moisture damage, a critical concern for all those countries that keep a high level of humidity or heavy and constant rainfalls throughout the year. Besides, if in winter air temperature keeps going over and under 0 °C, freeze-thaw cycles develop and could lead to worse outcomes in mechanical characteristics of HMAs. The weather conditions stated above are more than common in the northern part of the United States, and affect Michigan as well.

That's why a simulation of "extreme" moisture exposure to some asphalt samples has been chosen for this dissertation, submerging them into water for a long amount of time, while keeping other samples out of the water and comparing results after testing their mechanical characteristics.

Yu *et al.*²¹ measured stiffness through ITS tests of various HMA samples before and after being soaked in water and sustaining a freeze-thaw cycle to evaluate their moisture susceptibility, while Liu *et al.*²² studied the effects on SBS-modified asphalt mixture under dry and wet conditions, focusing in particular on binder-aggregate adhesion parameters like work of adhesion and work of debonding, and evaluating also the use of particular additives.

Results of both studies showed a fall in mechanical properties, more noticeable in the first one since it involved also freeze - thaw cycles.

The effects of this "extreme" level of moisture damage have been analyzed after submerging in water some of the samples produced and let them rest for 40 days. In this way, water could have penetrated every air void available in the sample and damaged the mixture, representing some sort of "extreme long-term moisture exposition" for the HMA, and rather than using Indirect Tensile Strength (ITS) test (AASHTO T 283), the effects were seen as a difference in mechanical properties between drowned samples and dry ones ($|E^*|$ and Flow Number tests).

4.2.3 *Resistance to Cracking and Actual Ligament Area determination*

Another parameter needed for a better understanding of the mixtures studied was resistance to cracking: using Semi-Circular Bending tests the currently ongoing MSU SCB results' database has been expanded and important factors like Ligament Area, Fracture Energy (G_f) and Flexibility Index have been determined through two different models: the Kutay's research group developed model and the University of Illinois' I-FIT model.

Moreover, since the SCB tests' factors previously noted usually present a very high variability, the actual ligament area of each SCB tested sample was modeled by filming

²¹ Huayang Yu and others, 'Workability and Mechanical Property Characterization of Asphalt Rubber Mixtures Modified with Various Warm Mix Asphalt Additives', *Construction and Building Materials*, 175 (2018), 392–401 <<https://doi.org/10.1016/j.conbuildmat.2018.04.218>>.

²² Xiang Liu and others, 'Effect of Material Composition on Antistripping Performance of SBS Modified Asphalt Mixture under Dry and Wet Conditions', *Journal of Adhesion Science and Technology*, 4243 (2018), 1–14 <<https://doi.org/10.1080/01694243.2018.1426973>>.

the broken half while rotating on a platform and uploading the video on a photogrammetry software (*3DF Zephyr*, from 3DFlow). As a result, a realistic 3D-modeled representation of the cracked surface of the sample was uploaded to *Autodesk Netfabb* software to be scaled so that the actual value of the ligament area could be found.

This value was used instead of $\text{Area} = \text{Length} \times \text{Thickness}$ to evaluate the changes in the results' variability and if this assumption could prove useful for further research.

4.3 Materials

In this paragraph, a detailed analysis of the materials used in this research will be dealt with. As suggested in the previous Chapter, we focused mostly on the asphalt mixtures' characteristics and performances rather than the bitumen and the aggregates as parts of our asphalt samples.

4.3.1 Binders

The modified binders, even though not necessary for the samples production, have been recreated to evaluate some of the properties listed in the previous chapter.

The modification process followed similar steps for both binders, starting from heating the cans of binder up to 163°C and placing it under the high shear mixer (HSM) set at 5000 rotations per minute (RPM).

For the HS-modified bitumen: the specified amount of SBS (2%) was prepared and blended into the hot bitumen for 30 minutes. Once finished, the material was placed under a low shear mixer (1000 RPM) for two hours, monitoring the temperature being in the range of 165-180°C.

For the DVR-modified bitumen: the specified amount of SBS (2%) and DVR (7%) was doubled (resulting in 4% SBS and 14% DVR), prepared and blended into two different cans of hot bitumen for 30 minutes. Once finished, the two cans were mixed together so that the resulting binder had the requested percentage of additives and placed under a low shear mixer (1000 RPM) for two hours, monitoring the temperature being in the range of 165-180°C. In addition to that, during the last half hour, the cross-linker was added (0.4%) with a syringe.



Figure 23: High-speed mixer



Figure 24: Low-speed mixer

4.3.2 Aggregates

Unfortunately, no information was provided for the aggregates' lithological characteristics, and only a visual analysis could be developed after an ignition test: the

aggregates' shape is round, smooth and with almost no angles or faces at all, making it very unlikely to develop some shear force once mixed with bitumen and compacted.

The reason for this particular shape could be found in the source of most of Michigan aggregates: due to the strong presence of water in the country (lakes, rivers...), most of them are fluvial ones, strongly worn out by water and with poor mechanical characteristics. Moreover, aggregate suppliers usually avoid giving particular information about their sources.

4.3.3 *Mixtures*

The mixtures, as stated in Chapter 1, were those used in the construction of a field test road section: that's why there was no need to prepare the mixtures since a lot of spare material was available in the MSU lab. The aggregates gradation, G_{mm} , G_{mb} , bitumen percentage and all information needed are available in the Job Mix Formulas (JMF) at the end of this dissertation.

The objective of this part of the research at MSU was to produce two sets of 6 asphalt samples for each mixture (hereto referred as to 3E1 DVR, 4E1 DVR, 3E1 HS and 4E1 HS), with the following characteristics:

- a. Three 100mm-diameter samples for $|E^*|$ determination,
- b. Three 100mm-diameter samples for $|E^*|$ determination after 40 days in water,
- c. Eight semi-circular samples for SCB testing.

4.4 Volumetric Characterization

4.4.1 *Samples' G_{mm} and mass determination*

The mixtures, ready-to-use and divided into 5-gallon metal buckets, have been heated up until they could be removed from the buckets (around 130°C) and divided into smaller parts on large oven trays (*Figure 25*).



Figure 25: Loose mixtures

A small part of this material was used to produce two samples of loose material, to get the G_{mm} of each mixture gathering the mass of the mold filled with loose material in air and in water (using pycnometers or an air pump to eliminate the air in the samples). The average of the two G_{mm} s was taken (AASHTO T 209).

Afterwards, the required amount of material needed for each of the four mixtures was determined using the following equation ²³:

$$Mass = \left[\frac{100 - (Va_t + F)}{100} \right] \cdot G_{mm} \cdot 176.7147 \cdot H \quad (20)$$

where:

Mass = estimated mass of mixture to prepare a test specimen to the target air voids

Va_t = target air void content for the test specimen, percent by volume

G_{mm} = maximum specific gravity of the mixture

H = height of the gyratory specimen, 180 mm

F = air void adjustment factor, 1

4.4.2 Samples compaction, cutting and air void content determination

²³ AASHTO PP 60-14, 'Standard Practice for Preparation of Cylindrical Performance Test Specimens Using the Superpave Gyratory Compactor', 14.August (2014).

The value of the mass found in the previous paragraph has been adjusted through the production of one or more “test” specimens to evaluate the correct air void content until an acceptable one.

The samples used for the tests were cored and cut from those produced with a Superpave Gyrotory Compactor G1 according to AASHTO T 312. In particular, SCB specimens’ characteristic preparation followed the AASHTO TP 124 specification.

For all samples, the material was put in the oven at 145 °C for two hours, then put inside the preheated mold and then put back in the oven for other two hours. The compaction was made by selecting the maximum height of 180 mm, in a way that after the coring (using a cylindrical drill with 100 mm diameter) a 15 mm slice could be cut from the head and the tail of the E*/FN specimens using the laboratory saw.

For the SCB samples instead no coring was needed, but a different cutting procedure was developed: the asphalt cylinder as it comes out of the SGC has been sliced perpendicularly to the axis right in the middle, and then sliced again to obtain two cylinders with a height of 50 mm, then cut along the diameter to obtain four semi-circular specimens. A notch of 10 mm was then made in the middle of it, where the cracking would start.

No compaction curve was calculated since none was needed for this dissertation.



Figure 26: Superpave Gyrotory Compactor (SGC)



Figure 27: E*/FN samples

The target air void content was, according to previous specifications, 7% (+/- 0.5%). The procedure for the determination of the air void content followed AASHTO T 269 specifications: the 150 mm and SCB samples were first dried with an Instron CoreDry and then weighted (A). After that the sample was weighted in water (B) and weighted with dry surface (C). The temperature of the water T was also taken into account to find water density ρ_w as:

$$\rho_w = 0.00532 \cdot T^2 + 0.00759 \cdot T + 1000.25205 \quad (21)$$

The equations for finding G_{mb} , and the final air void content v_a are:

$$G_{mb} = \frac{A}{C - B} \cdot \rho_w \quad (22)$$

$$v_a = \frac{G_{mm} - G_{mb}}{G_{mm}} \cdot 100 \quad (23)$$

Air voids content results for all mixtures are in attachments. Samples with an air void content outside the limits were rejected.

4.4.3 Sieve analysis

For all the mixtures a standard sieve analysis (AASHTO T 27) was carried out using a Humboldt Motorized Sieve Shaker to evaluate the difference between the actual aggregate gradation and the one stated on the official JMFs. Detailed results, as well as the passing curves, are in Attachments section; neither DVR nor SBS samples' sieve analyses were significantly different from the specifications.

4.4.4 Binder content determination: Ignition Test

Following AASHTO T 308, each mixture's binder content has been evaluated through an Ignition Test using a NCAT Asphalt Content Furnace.



Figure 28: NCAT Asphalt Content Furnace

Around 2 kg of loose mixtures were put in the metal baskets previously weighted (B). The combined weight of the basket and the asphalt was then noted (A) and then the basket was put inside the hot furnace. The electronic scale automatically stopped the experiment when it couldn't register any changes in the weight, meaning that all the bitumen had burnt.

After carefully removing and cooling the hot basket in air, the weight of the remaining aggregate and the basket was noted (C).

The mass of burnt binder M_b and the relative percentage P_b could then be found as:

$$M_b = (B - A) - (C - A) \quad (24)$$

$$P_b = \frac{M_b}{C - A} \quad (25)$$

Results show that a slightly higher binder content has been used during construction, maybe to facilitate the workability.

4.4.5 SCB samples geometry

All the samples' ligament thicknesses and lengths have been measured twice starting from both ends, taking the average of the two values.



Figure 29: SCB samples ready for testing

4.5 Complex Modulus E^*

4.5.1 Overview

One of the most useful tools to analyze the viscoelastic behavior of an asphalt mixture, through the cyclic testing of a sample, is the complex modulus. This parameter is related to the complex form of cyclic one-dimensional loading

$$\sigma^* = \sigma_0 e^{i\omega t} \quad (26)$$

and resulting strain

$$\varepsilon^* = \varepsilon_0 e^{i(\omega t - \varphi)} \quad (27)$$

The resulting equation for the complex modulus will be:

$$\frac{\sigma^*}{\varepsilon^*} = E^*(i\omega) = \left(\frac{\sigma_0}{\varepsilon_0}\right) e^{i\varphi} = E_1 + iE_2 \quad (28)$$

where σ_0 and ε_0 are the stress and strain amplitudes and ω is the angular speed.

The real part of the complex modulus E_1 is the elastic modulus while the imaginary one E_2 is the viscous modulus, which is equal to 0 for elastic material since $\varphi = 0$. This parameter represents of how much out of phase will the strain be with the stress, and it will be needed for asphalt mixtures evaluation with MEPD software.

4.5.2 Testing samples for Complex Modulus

Each asphalt sample has been tested for Complex Modulus E^* following AASHTO T 342 (2012) specifications, at three different temperatures (4 °C, 20 °C, 40 °C) and six loading frequencies (25 Hz, 10 Hz, 5 Hz, 1 Hz, 0.5 Hz, 0.1 Hz) using an AMPT, which applies to the sample a sinusoidal axial compressive stress. Both the stress and the resulting axial strain are measured and used to determine two parameters: dynamic modulus and phase angle.

Conditioning time of samples and AMPT's testing chamber varies from temperature to temperature: an entire night is needed before testing samples at -10 °C, while just one hour is sufficient for testing samples at 20 °C. The test is executed from the lowest to the highest temperature and from the highest to the lowest frequency.

4.5.3 $|E^*|$ Mastercurves development

To describe the viscoelastic behavior of an asphalt sample as a function of temperature and loading time, a mastercurve needs to be developed. As described thoroughly by Kim²⁴ and AASHTO PP 61 specifications, data collected from the AMPT at various temperatures can be shifted, using the Time Temperature Superposition principle (TTS), to the time of loading or frequency: by doing so various curves align to form a mastercurve. Each shift factor $a(T)$ defines the shift for each temperature: time must be divided by this parameter to get a reduced time relative to one specific temperature, while frequency needs to be multiplied for these parameters to obtain reduced frequency ξ .

$$\xi = f \cdot a(T) \quad (29)$$

Each mastercurve can be developed thorough one reference temperature T_0 to which all other data are shifted. At that temperature the relative shift factor $a(T_0) = 1$. This procedure makes possible to derive values of stiffness for each combination of temperature or frequency.

The sigmoidal function selected to fit the E^* test data (from -18°C to 55°C temperatures) is:

$$\log(|E^*|) = \delta + \frac{\alpha}{1 + e^{\beta - \gamma \log(\xi)}} \quad (30)$$

²⁴ Y. Richard Kim, 'Complex Modulus Characterization of Asphalt Concrete', in *Modeling of Asphalt Concrete* (McGraw-Hill Professional, 2009).

where $|E^*|$ is the dynamic modulus, ξ the reduced frequency, δ the minimum modulus value, α the span of modulus values and β, γ are shape parameters. γ represents the steepness of the function while β the position of the turning point on the horizontal.

The reason of the choice of a sigmoidal function resides in the observation of the mix behavior: the function approaches asymptotically to the maximum stiffness of the mix for its higher values at lower temperatures. For high temperatures instead, the most dominant parameter is the aggregate influence: that's why the function approaches a limiting value depending on the aggregate gradation. Therefore, this function is useful to describe the asphalt mixture behavior in the entire range of temperatures analyzed.

For a detailed explanation of the data analysis procedure see chapter 5 *Data Analysis*.

4.6 Flow Number

Another parameter recommended by the National Cooperative Highway Research Program (NCHRP)'s Superpave project is Flow Number (FN), which is most useful in determine asphalt mixtures' rutting behavior. Permanent deformation data, as well as Complex Modulus, is needed for the determination of several parameters which are then put as input for MEPD advanced asphalt characterization.

By cyclically loading a specimen until collapse (after conditioning it at 45 °C for 3 hours), various points on the axial strain – number of cycles graph are developed. These data are fitted using a model that gives a good determination of the three stages of permanent deformation: primary stage or consolidation, secondary stage or creep at constant rate and tertiary stage or flow. Flow Number is the number of cycles corresponding at the beginning of the tertiary flow.

The equation of the model is as follows:

$$\varepsilon_p(N) = \varepsilon_{rz} 10^{\beta_1 k_1} T^{\beta_2 k_2} N^{\beta_3 k_3} \quad (31)$$

where $\varepsilon_p(N)$ is the permanent strain after N cycles, N is the number of loading cycles, T is target temperature, k_1, k_2 and k_3 are MEPD regression parameters, β_1, β_2 and β_3 are test's regression coefficients and ε_{rz} is the resilient strain determined by the following equation:

$$\varepsilon_{rz} = \frac{1}{|E^*|} (\sigma_1 - 2\mu\sigma_3) \quad (32)$$

where $|E^*|$ is the complex modulus, σ_1 is the vertical stress and σ_3 is the confining stress.

4.6.1 Using Time Temperature Superposition for faster Repeated Load Permanent Deformation tests

Khosravifar *et al.* studied 27 different asphalt mixtures to evaluate the possibility to apply TTS principle also for Repeated Load Permanent Deformation tests (RLPD), and more specifically with the objective of reducing the testing time necessary to fully characterize asphalt permanent deformation²⁵.

The TTS principle has been proven right for the viscoelastic region in studies from Goodrich²⁶ and Kim and Lee²⁷: asphalt are “thermorheologically simple” in that region, and remain that way beyond that point when approaching failure^{28 29}. Further studies on TTS were used to develop several advanced models to understand the behavior of asphalt mixtures.

Khosravifar *et al.* focused their attention on the secondary stage of the permanent deformation curve, using the most typical power law:

$$\varepsilon_p = AN^B \quad (33)$$

where ε_p is the permanent strain, N the number of loading cycles, A and B the intercept and slope of the model. This power law plots a line on a log-log graph, and the idea for shifting the asphalt response is based on the concept that one cycle at a certain loading time is equal to multiple cycles at the same loading time at a different temperature.

It means that it is possible to translate any loading time or temperature to its equivalent and “reduced” number of cycles for a test that is set at 20 °C and 0.1 seconds, dividing the number of cycles for a shift factor as it’s done for the viscoelastic region.

Results of that study confirmed that the initial theory was correct and that TTS principle is valid also in the viscoplastic domain of RLPD tests, giving us the possibility

²⁵ Sadaf Khosravifar and others, ‘Application of Time – Temperature Superposition to Develop Master Curves of Cumulative Plastic Strain in Repeated Load Permanent Deformation Tests’, 8436.December 2017 (2015) <<https://doi.org/10.1080/10298436.2014.937810>>.

²⁶ J.L. Goodrich, ‘Asphaltic Binder Rheology, Asphalt Concrete Rheology and Asphalt Concrete Mix Properties (with Discussion)’, *Journal of the Association of Asphalt Paving Technologists*, 60 (1991), 80–120.

²⁷ Y. Richard Kim and Y. C. Lee, ‘Interrelationships among Stiffnesses of Asphalt-Aggregate Mixtures (with Discussion)’, *Journal of the Association of Asphalt Paving Technologists*, 64.

²⁸ R. A. Schapery, ‘Nonlinear Viscoelastic and Viscoplastic Constitutive Equations with Growing Damage’, *International Journal of Fracture*, 1999, 33–66.

²⁹ G.R: et al. Chehab, ‘Time–temperature Superposition Principle for Asphalt Concrete with Growing Damage in Tension State’, *Journal of the Association of Asphalt Paving Technologists*, 2002, 559–93.

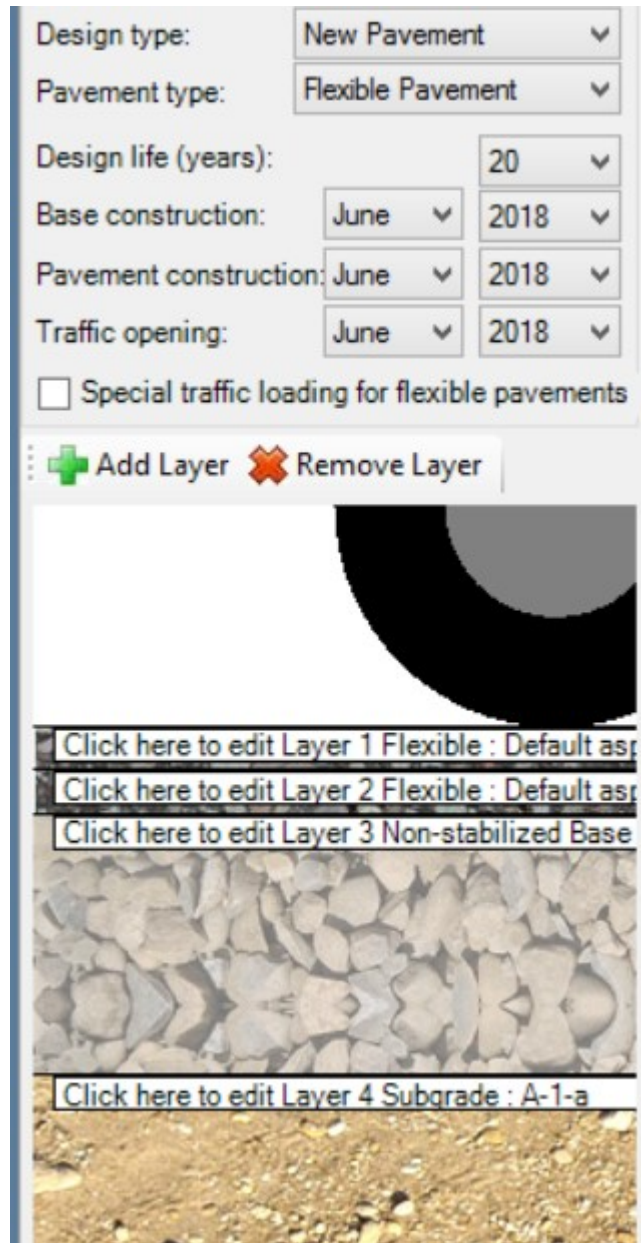
to avoid most time-consuming tests at different temperatures necessary to characterize asphalt mixtures response to permanent deformation.

4.7 Pavement ME Design data implementation and design simulation

The software used for the permanent deformation prediction has been presented in the previous chapter: here the data implementation process will be shown.

First of all the design pavements are new, flexible, expected to last for 20 years and all construction and traffic opening have been set to June 2018. The layers have been organized like this:

- Layer 1 and 2: Flexible asphalt layer, 50 mm thick with binder and dynamic modulus input levels set to 1. All other parameters set as default.
- Layer 3: Non-stabilized Base, all parameters default.
- Layer 4; Subgrade, type A-1-a.



d.

Figure 30: Pavement ME Design project layers, detail

The beta factors are put as inputs in Project Specific Calibration, while Dynamic Modulus inputs for the first layer (4E1) and the second (3E1) are taken from E* results. It was decided to add a new set of results of dynamic modulus at 54 °C, derived from the shift factors. The reason is that the software could have some problem calculating permanent deformation at low temperatures.

The reference climate station, as said before, was taken in Illinois for the first analysis, and in Arizona for the second part of it. Simulations using the Arizona



Figure 31: Reference climate stations – Illinois

The traffic was not set as default: the reason is that these mixtures were not meant to be studied in a “realistic traffic” environment but at their “end of life”, evaluated in 3 million ESALs: in fact –E1 mixtures’ composition (3E1 and 4E1) is very similar to the –E3 ones, and these are meant to last for 3 million ESALs.

Manually varying the traffic in the software (basically turning all traffic in just one category of vehicles, single axle, 8000 kg, no growth factor) a satisfying 3.15 million ESALs was reached.

After running the simulations, PDF reports were produced,

4.8 Intermediate-temperature IL-SCB testing

4.8.1 Introduction

Illinois Department of transportation (IDOT) and University of Illinois at Urbana-Champaign, in December 2015, issued a report on testing protocols of reclaimed asphalt pavements (RAP) and recycled asphalt shingles (RAS)³⁰.

One of the fracture tests methods used was developed using semi-circular bending (SCB) specimens, because of its lower cost of implementation and easier specimen preparation. This method (Intermediate-temperature IL-SCB testing) has been also proposed as an AASHTO specification in 2016 and was published in the same year³¹.

IDOT selected a testing temperature of 25 °C and a loading displacement rate of 50 mm/min for the whole process to develop a practical and reliable method of testing

³⁰ Imad L Al-qadi and others, *Testing Protocols to Ensure Performance of High Asphalt Binder Replacement Mixes Using RAP and RAS*, 2015.

³¹ Hasan Ozer and others, ‘Development of the Fracture-Based Flexibility Index for Asphalt Concrete Cracking Potential Using Modified Semi-Circle Bending Test Parameters’, *Construction and Building Materials*, 115 (2016), 390–401 <<https://doi.org/10.1016/j.conbuildmat.2016.03.144>>.

asphalt mixtures' cracking resistance: in fact it was shown that at lower temperatures the reliability of the test was too low.

Since fracture energy (the area under the load-displacement curve) was not sufficient to distinguish between different asphalt mixtures, the research team underlined the need to find a new parameter to characterize a mixture's cracking behavior: fracture energy, in fact, is a function of both peak load and ductility, defined as the maximum displacement. If the peak load is high, the low ductility in the post-peak region could determine the same fracture energy of a more ductile material.

4.8.2 Flexibility Index determination

This new parameter had to take into account also the “shape” of the load-displacement curve: that's why both the tangential slope at the inflection point after peak load and the critical displacement were considered.

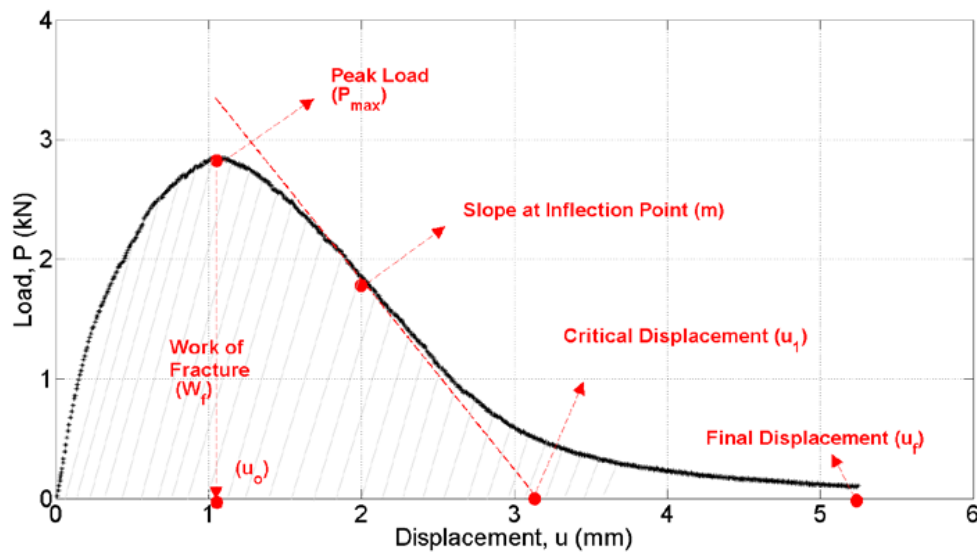


Figure 32: Load-Displacement curve for SCB tests

Critical displacement value was determined by intersecting the tangential slope with the displacement axis. This parameter, along with the slope, reflect the ability of the mixture to resist crack propagation.

Eventually, Flexibility Index was determined as the fracture energy G_f divided by the absolute value of post-peak slope m and multiplied for a factor $A = 0.01$.

$$FI = A \times \frac{G_f}{|m|} \quad (34)$$

Thresholds determination for acceptable FI values are currently undergoing.

4.8.3 *I-FIT software and MSU-developed MATLAB model*

IDOT researchers developed a software that implemented the method mentioned above, called *I-FIT* (ver. 1.1).

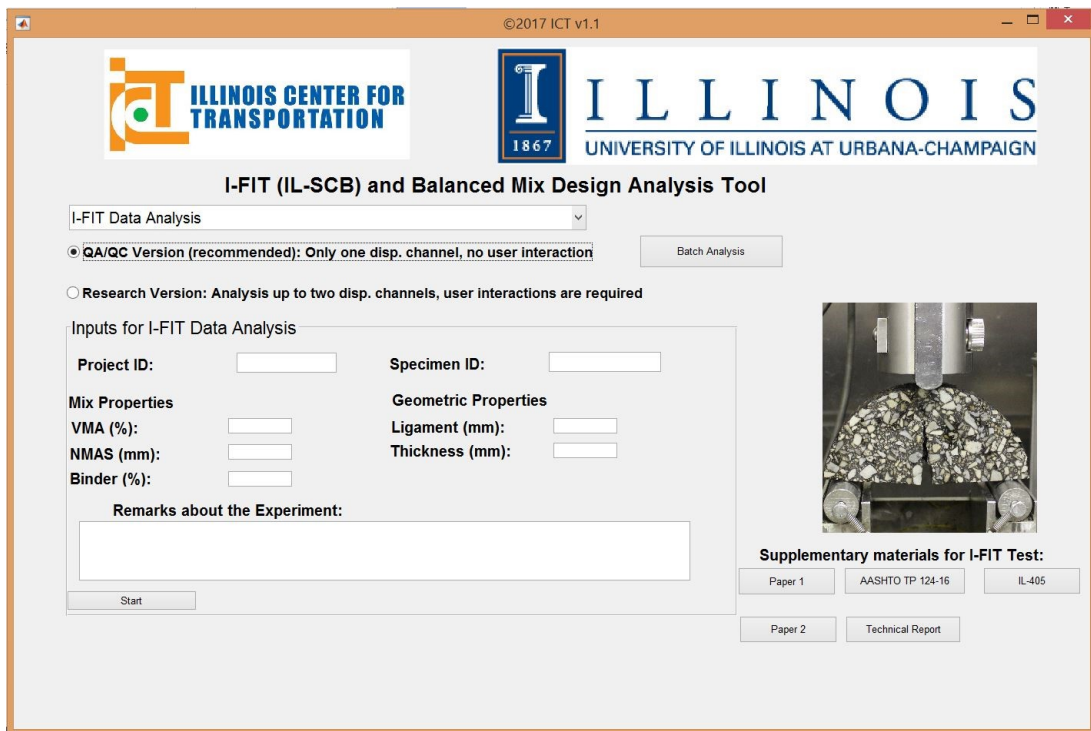


Figure 33: *I-FIT* interface

I-FIT, once the user fills the blank spaces with information collected from the mixtures and uploads the IL-SCB test data, automatically creates a report with all the results and a graphic representation of the Load – Displacement curve and its intercept.

The way of showing results, unfortunately, is a little bit less practical than expected: the .xls output copies all the Load – Displacement data previously uploaded and doesn't highlight very well the most useful results like FI or Fracture Energy, and the .txt output is not well formatted. Moreover, the input data file has to be formatted exactly as the software wants, causing some issues and delays in data analysis.

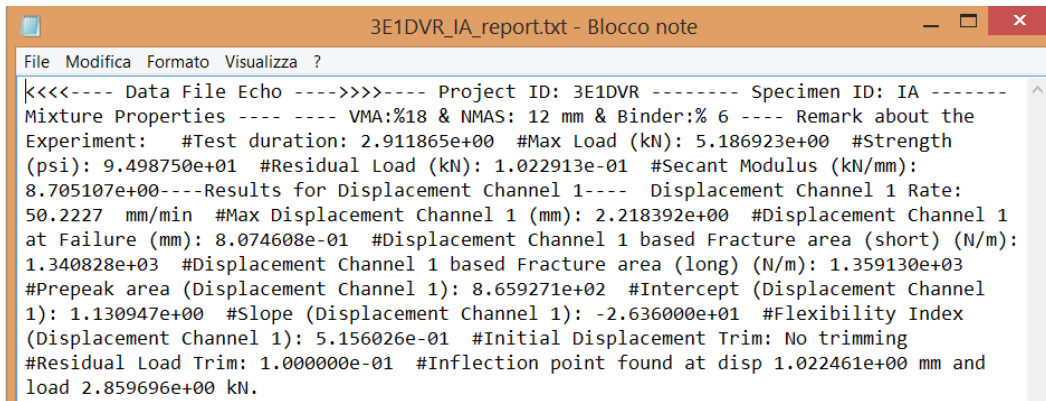


Figure 34: I-FIT report example

MSU researchers developed a new *MATLAB* based model, that processes data in the same way of *I-FIT* but trying to avoid the issues of the Illinois’ software. Although working on the same equations, this has a much more “user friendly” results output.

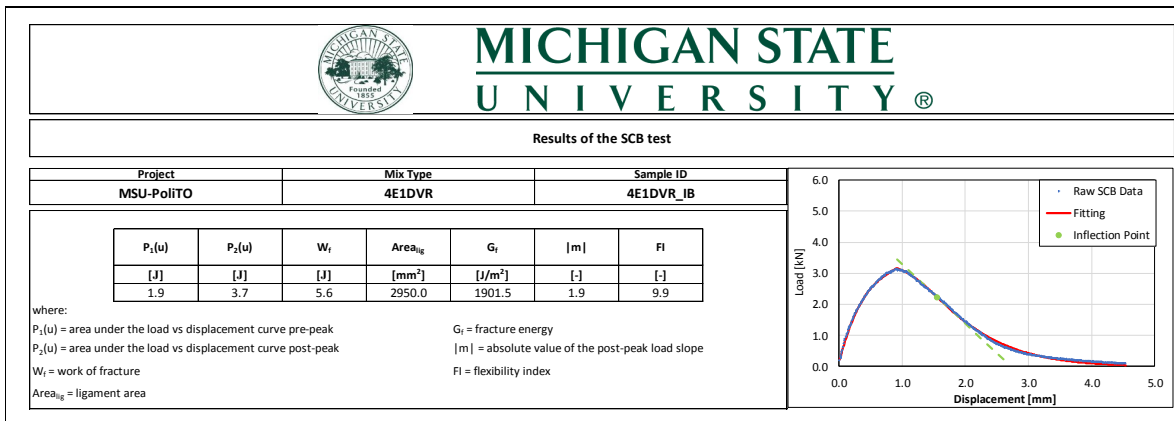


Figure 35: MSU model report example

As we can see from *Figure 35* every result needed, along with a visual representation of the Load – Displacement curve, comes out in a clear .xls file.

4.8.4 SCB test procedure

The test described in AASHTO TP 124 is used to determine the fracture energy (G_f) and post peak slope of semicircular specimens of asphalt mixtures at an intermediate temperature (25 °C). These parameters are then used to calculate the Flexibility Index (FI), a new parameter that predict the resistance to fracture, one of the steps in asphalt evaluation.

Fracture energy indicates a mixture’s resistance to cracking damage: higher fracture energy means resistance to greater stresses. However, this parameter should not be directly used in structural design and analysis but as a base for crack models.

FI helps the designers in the identification of brittle mixes, prone to premature cracking, and the range of acceptance varies according to environmental conditions, nominal maximum aggregate size, asphalt PG, air voids etc.

An asphalt sample, compacted with a Superpave Gyratory Compactor G1 following AASHTO T 312 standards, is trimmed and cut in half to form two semicircular-shaped specimens following AASHTO TP 124 standards.

On their straight edges a notch is sawn, which will be used as a reference when putting the specimen under the testing machine, consisting in a closed-loop axial loading device, a load measuring device, a bend test fixture, specimen deformation measurement devices, and a control and data acquisition system.

The load is applied along the vertical radius, which will be measured along Load Line Displacement (LLD) during the whole test. At first, a load of 0.1 ± 0.01 kN is applied with a loading rate of 0.05 kN/s, and after that the test continues with LLD set at a constant rate of 50 mm/min.

The parameters obtained are:

- Work of Fracture (W_f), calculated as the area under the load/LLD curve (found by numerical integration). To do so, both load and displacement data are divided in two curves described by a fitting equation: for points prior to peak load a polynomial equation with a degree of three is sufficient (P_1), while for post-peak an exponential-based function is needed (P_2):

$$P_1(u) = c_1 \times u^3 + c_2 \times u^2 + c_3 \times u + c_4 \quad (35)$$

$$P_2(u) = \sum_{i=1}^n d_i \times \exp \left[- \left(\frac{u - e_i}{f_i} \right)^2 \right] \quad (36)$$

where c , d , e , f , are polynomial coefficients and n is the number of exponential terms.

Work of fracture can be calculated using an integral equation:

$$W_f = \int_0^{u_0} P_1(u) du + \int_{u_0}^{u_{final}} P_2(u) du \quad (37)$$

where u_{final} is the displacement at 0.1 kN

- Fracture Energy (G_f), calculated by dividing W_f by the ligament area (A_{lig}) of the specimen,
- Post-peak slope (m), the slope of the tangential curve drawn at the inflection point on the load-displacement curve after the peak load,

- Flexibility Index (FI), calculated from the parameters found before as

$$FI = \frac{G_f}{|m|} \cdot A \quad (38)$$

where $A = 0.01$.

4.8.4.1 Considerations on Ligament Area

The Ligament Area parameter (A_{lig}), necessary for the whole procedure described before, for AASHTO TP 124, is taken as the thickness of the specimen times the length of the line starting from the top of the notch and reaching the farthest end on the other side (basically, the radius of the specimen minus the length of the notch).

Looking at one of the two halves of a tested specimen, however, one can see how the test does not follow a straight line when breaking through the sample, resulting in two very rough surfaces full of holes and elevations due to the aggregates matrix (the force applied is way lower than the one needed to break the aggregates).



Figure 36: Tested SCB sample

One of the issues that could affect the high variability of the SCB testing results could be right this gap between the “nominal” Ligament Area and the “actual” one. That’s why the next step of this research was to find the actual value of the Ligament Area through photogrammetry: analyzing several frames of a sample filmed from various

angles, a software can extrapolate a certain amount of points that are used to create a 3D surface. Once this model is scaled to the right dimensions (we know the actual length and thickness), this new unscaled 3D surface is used to calculate the Actual Ligament Area, run again the tests with this new value and then compare the results to see if their variability was lower or not.

4.8.4.2 *Actual Ligament Area characterization: Creating the Mesh*

Each tested half-sample was inserted in a rubber support almost as high as the radius of the initial specimen, in a way that, as we can see in the picture, only the Ligament Area emerged from it. The support was also covered in plain-colored paper to maximize the precision of the virtual points acquisition.



Figure 37: Sample ready for Actual Ligament Area determination

The whole system was then placed onto a rotating platform, and the specimen was filmed while rotating on the platform using an iPhone 6S (1080p, 30 fps) fixed onto a support for a minute, to get various shots from all angles.

Each video was uploaded to *3DF Zephyr Free* and processed to extract all the frames needed to proceed and, later, extracting the key points necessary to build the first step of the model, the “Sparse Points Cloud”.

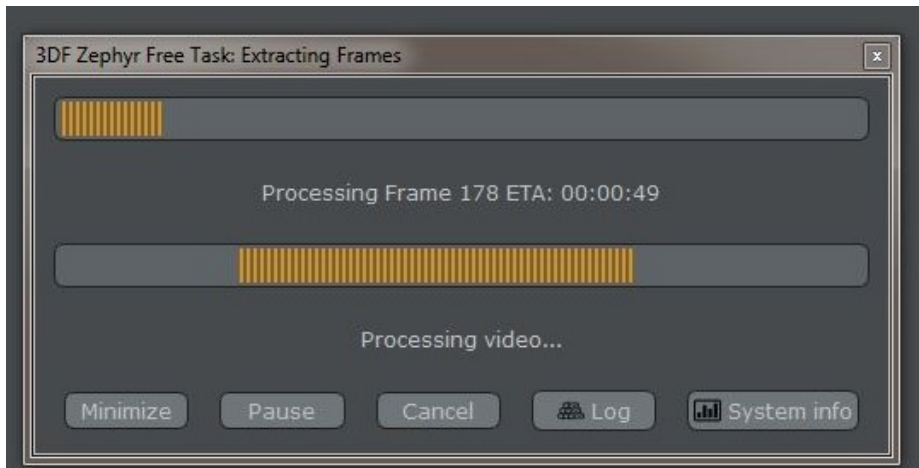


Figure 38: Importing video data on 3DF Zephyr Free

The result was a sparse 3D cloud of points, still very different from the original sample, with its length and thickness not on the plane XY and surrounded by a lot of unnecessary “blank” area that needed to be cut.

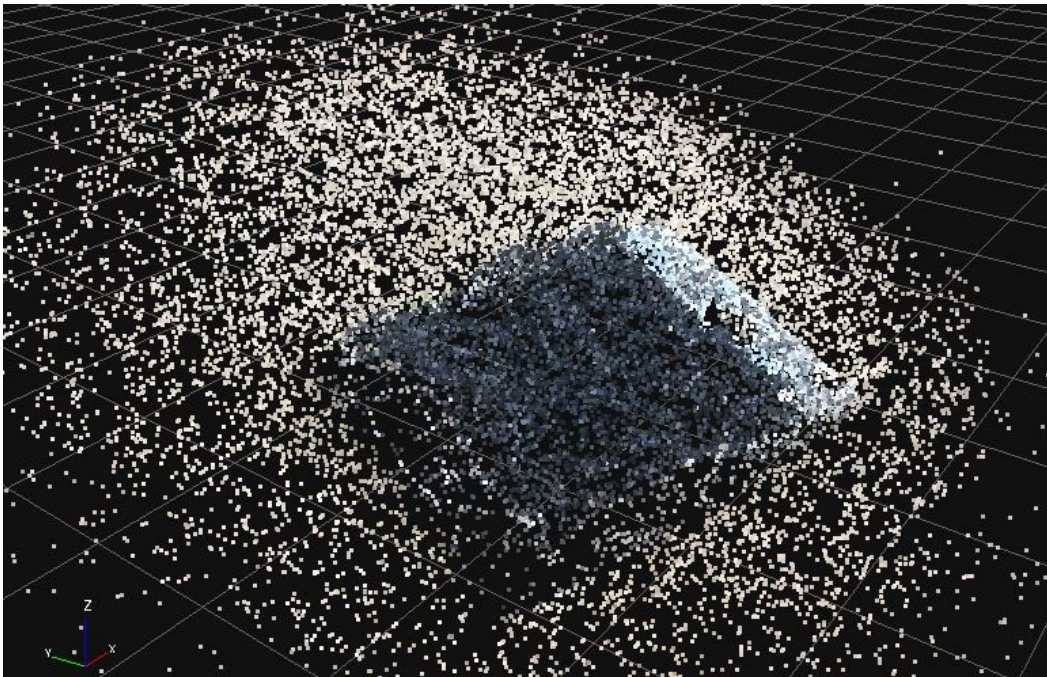


Figure 39: Sparse point cloud

The first thing to do was to rotate and move the cloud to align as best as we could the length and thickness of the specimen with the two virtual axes X and Y, and then the software created the “Dense Points Cloud”, a more detailed representation of the specimen.



Figure 40: Dense point cloud

The last step for the creation of the mesh was to manually cut the points cloud, carefully considering only the Ligament Area we need and eliminating all the surrounding representation of the paper and the specimen's other faces. After doing so, the mesh and the final textured mesh were created and ready for the area calculation.

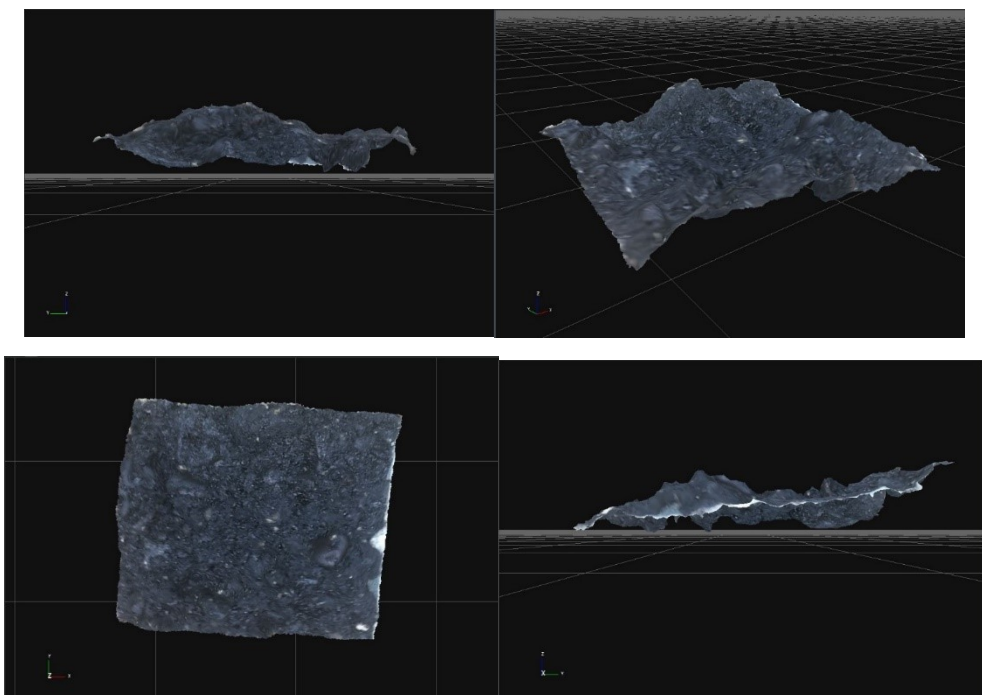


Figure 41: Actual Ligament Area, different views

4.8.4.3 Actual Ligament Area characterization: Calculating the value

The 3D textured surface mesh representing the actual Ligament Area of the specimen was uploaded to *Autodesk Netfabb Standard 2017*. First of all, the texture needed to be shifted and rotated, and later one of the two dimensions needed to be scaled to the real dimension.

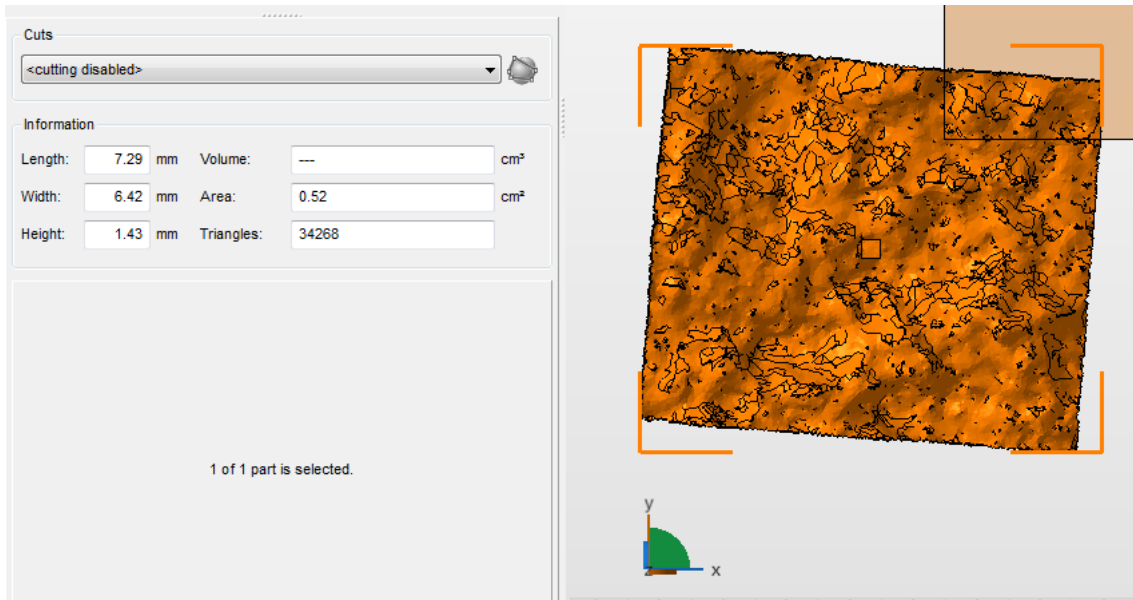


Figure 42: Netfabb mesh implementation

Eventually, the software automatically calculated the Actual Ligament Area of the actual representation of the tested half-specimen. As we can see from the example, this value was quite different from the one suggested by AASHTO TP 124, since $\text{Length} \times \text{Width}$ gives 31.80 cm^2 as a result.

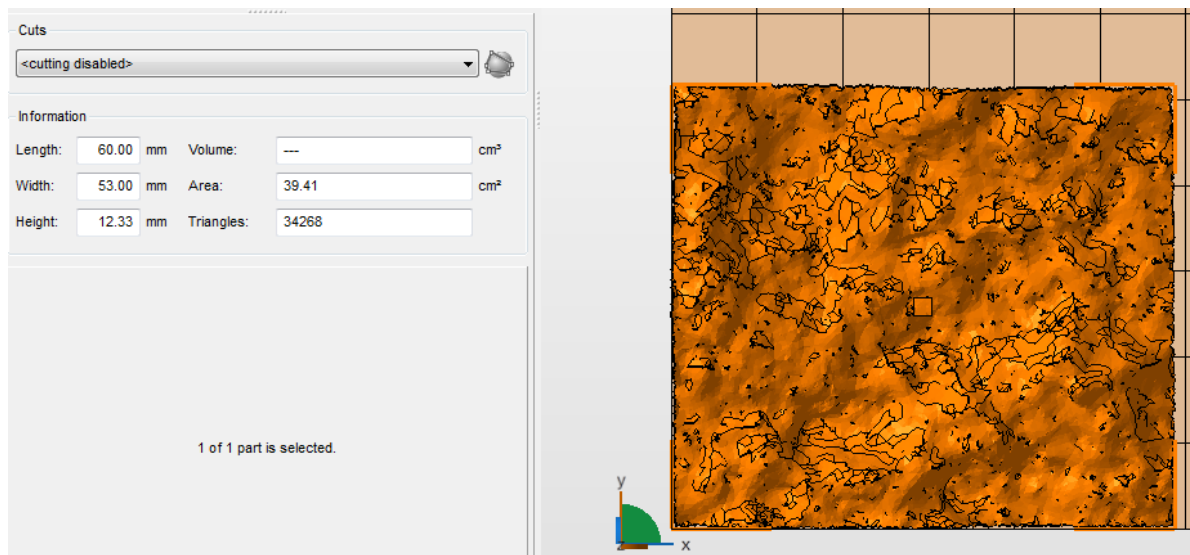


Figure 43: Mesh scaled and rotated

For each specimen, the average A_{lig} values for the two halves have been considered for the data analysis. Blank values mean discarded specimens.

Sample ID				Area	Average	Sample ID				Area	Average
3E1DVR	IA	X	3949	3945	4E1DVR	IA	X	3510	3453		
3E1DVR	IA	Y	3940		4E1DVR	IA	Y	3395			
3E1DVR	IB	X	3941	3967	4E1DVR	IB	X	4028	3951		
3E1DVR	IB	Y	3992		4E1DVR	IB	Y	3873			
3E1DVR	IIA	X	3765	3743	4E1DVR	IIA	X	3729	3764		
3E1DVR	IIA	Y	3720		4E1DVR	IIA	Y	3798			
3E1DVR	IIB	X	3719	3767	4E1DVR	IIB	X	4189	4332		
3E1DVR	IIB	Y	3814		4E1DVR	IIB	Y	4475			
Sample ID				Area	Average	Sample ID				Area	Average
3E1HS	IA	X	3851	3861	4E1HS	IA	X	3986	3967		
3E1HS	IA	Y	3871		4E1HS	IA	Y	3948			
3E1HS	IB	X			4E1HS	IB	X	3607	3673		
3E1HS	IB	Y			4E1HS	IB	Y	3738			
3E1HS	IIA	X	3515	3577	4E1HS	IIA	X				
3E1HS	IIA	Y	3639		4E1HS	IIA	Y				
3E1HS	IIB	X			4E1HS	IIB	X	3598	3657		
3E1HS	IIB	Y			4E1HS	IIB	Y	3716			

Figure 44: ALA calculated values

4.8.4.4 SCB data implementation and results

Data from SCB tests (load and displacement every 0.01 seconds) were uploaded on ICT's software (*I-FIT*) and MSU's *MATLAB* model. The latter let the user choose if he wants to use the calculated Actual Ligament Area, while *I-FIT* forces the user to calculate the area as Length \times Thickness ("Standard" Ligament Area).

All the information needed for filling the “Mix Properties” blank spaces on *I-FIT* (*VMA (%)*, *NMAS (mm)* and *Binder (%)*) are stated on JMFs.

Eventually, three sets of results were submitted:

- MSU’s *MATLAB* model with “Standard” Ligament Area
- MSU’s *MATLAB* model with 3D modeled Ligament Area
- IDOT’s *I-FIT* software with “Standard” Ligament Area

5 DATA ANALYSIS AND RESULTS

This chapter aims to present and discuss the results obtained through all the different steps of the advanced characterization of the asphalt mixtures carried out for this research. The data analysis proceeding will match that of chapter *Research Plan*, starting from basic characterization of mixtures and reaching the results of the most advanced tests. Moreover, only the most important results will be shown in this chapter for the sake of brevity and comprehension, along with comments. For every detailed graph, table and overall output found during this research, see *Appendix*, where the same steps will be followed.

The first paragraph will deal with the most basic characterization of mixtures, including Gmm characterization, binder content and sieve analyses. Once the samples were compacted, air voids content determination has been carried out. Due to the particular shape of SCB samples, accurate measurements on all samples have been made to evaluate differences from the optimum.

A description and a discussion on Dynamic Modulus and Flow Number results will follow, while the various steps of the meticulous SCB tests and ligament area 3D reconstruction will be detailed in Paragraph 5.4.

In the end, all the data for E^* and FN found will be merged and used as input for the mechanistic-empirical analyses on *PavementME*.

5.1 Volumetric and geometric characterization

5.1.1 Gmm determination

In *Table 1*, detailed results of the Gmm characterization of samples for Dynamic modulus and Flow number tests are shown. Good consistency has been found between results, except for 4E1 HS which showed a slightly lesser value than the others. For each mixtures, two samples of loose mixtures have been analyzed, and details are in *Appendix*.

Table 1: Gmm calculation

Gmm	
3E1 DVR	2.485
4E1 DVR	2.451
3E1 HS	2.481
4E1 HS	2.304

5.1.2 Binder content

As stated in *Research Plan* ca. 2 kg of asphalt, preheated to make it loose and workable has been inserted in the NCAT Furnace's special baskets after noting its weight when loose (B) and when combined with the baskets (A).

The temperature reached by the furnace had quickly burnt the bitumen, and after cooling the sample the last weight (baskets + aggregates) was taken (C).

The electronic scale automatically stopped the experiment when it couldn't register any changes in the weight, meaning that all the bitumen had burnt. Through (27) and (28) the percentage of the bitumen for each mixture has been discovered.

Table 2: Binder content

3E1 DVR							
A	B	C	Mass HMA	Mass Agg	Mass AC	Pb	JMF
[g]	[g]	[g]	[g]	[g]	[g]	[%]	[%]
3506.8	5666.0	5545.1	2159.2	2038.3	120.9	5.93%	5.16%
					Delta	0.77%	

4E1 DVR							
A	B	C	Mass HMA	Mass Agg	Mass AC	Pb	JMF
[g]	[g]	[g]	[g]	[g]	[g]	[%]	[%]
3511.5	4999.9	4911.4	1488.4	1399.9	88.5	6.32%	5.45%
					Delta	0.87%	

3E1 HS							
A	B	C	Mass HMA	Mass Agg	Mass AC	Pb	JMF
[g]	[g]	[g]	[g]	[g]	[g]	[%]	[%]
3408.2	5591.0	5479.5	2182.8	2071.3	111.5	5.38%	5.16%
					Delta	0.22%	

4E1 HS							
A	B	C	Mass HMA	Mass Agg	Mass AC	Pb	JMF
[g]	[g]	[g]	[g]	[g]	[g]	[%]	[%]
3510.2	5481.9	5372.5	1971.7	1862.3	109.4	5.87%	5.45%
					Delta	0.42%	

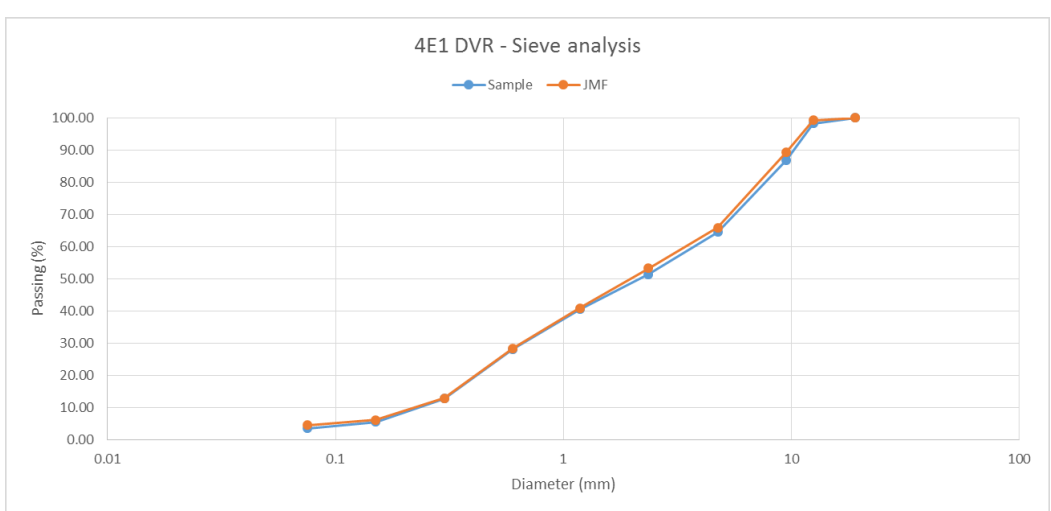
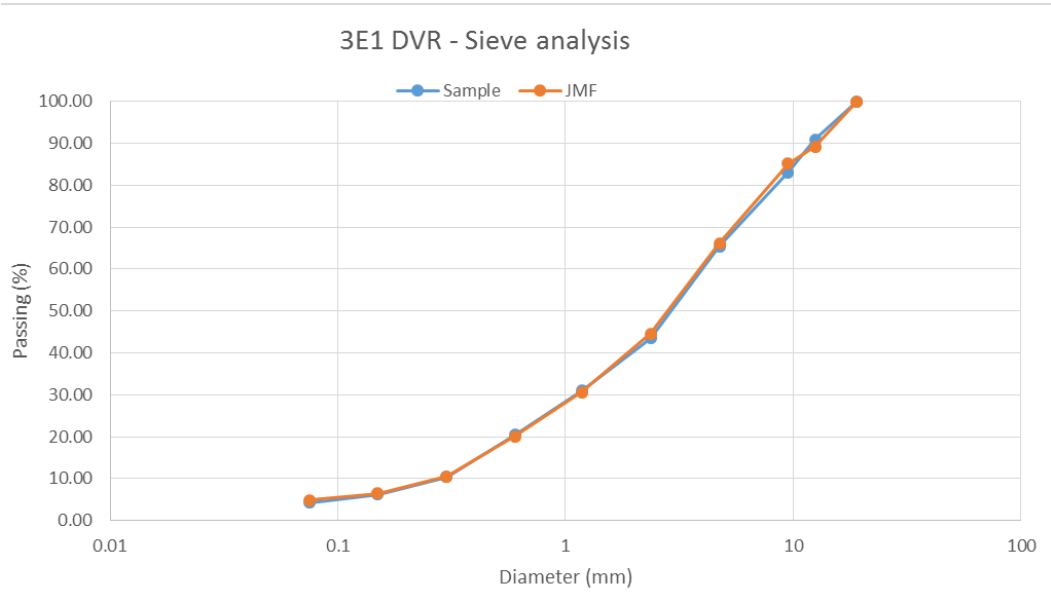
Results show that a slightly higher binder content has been used during construction, maybe to facilitate the workability especially for DVR modified bitumens

5.1.3 Sieve analysis

The graphs in this paragraph show the sieve analysis of the mixtures after the ignition test, and how those differ from Job Mix Formulas: deltas from JMFs are very small, except for 4E1 HS.

The sieve column used is (in mm): 19, 12.5, 9.5, 4.75, 2.36, 1.18, 0.6, 0.3, 0.15, 0.075. MDOT specifications do not require upper/lower granular size limits as other countries do.

Detailed tables for passing and retained percentages are found in *Appendix*.



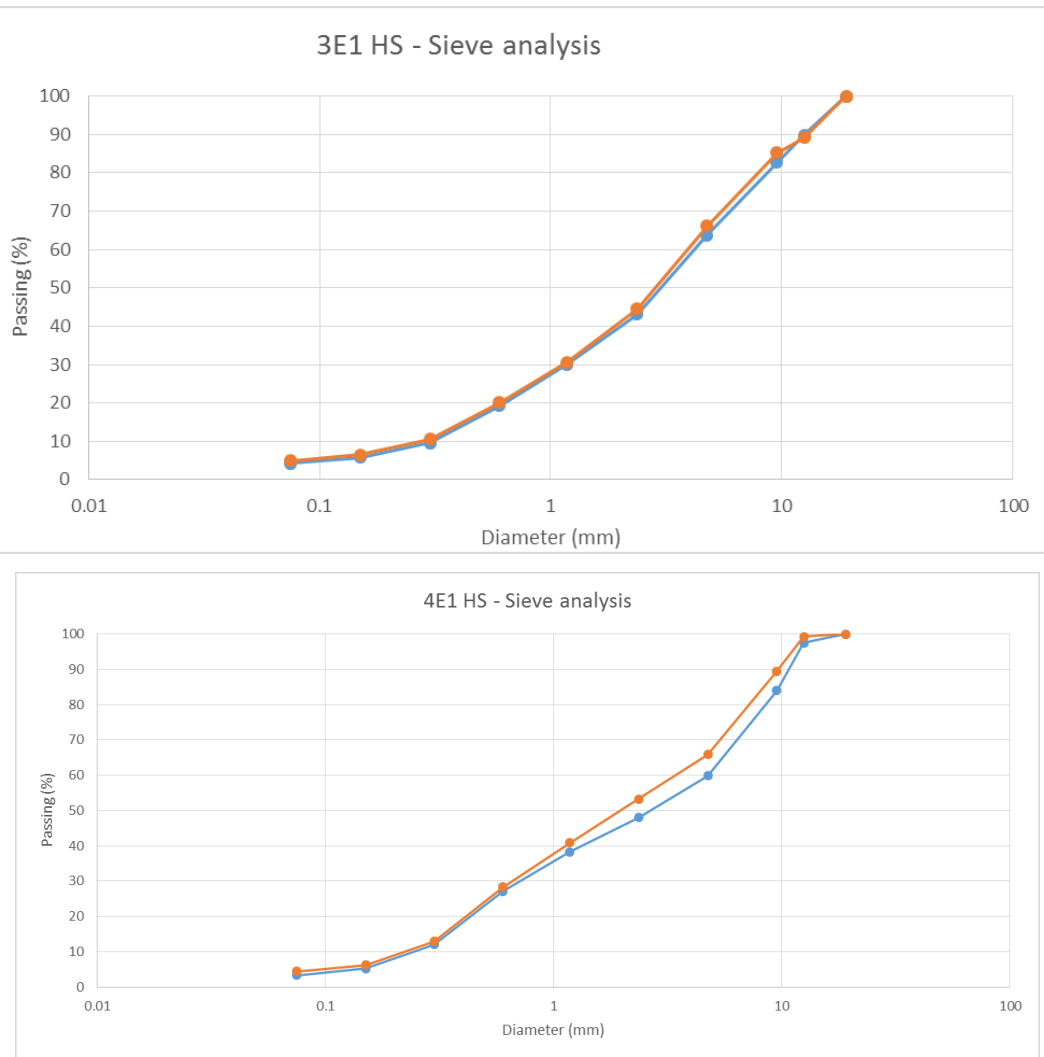


Figure 45: Sieve Analyses

5.1.4 SCB geometric characterization

In the following tables, samples measurements for SCB testing are shown. The length and thicknesses refer to the middle zone of the sample where the notch is located and where the cracking will start.

Target thickness and length should be 50 and 60 mm, however due to the poor cutting equipment measurements showed a small percentage of error. This error, however, is relatively small for length measurements, as only in one sample out of 32 reaches 5%, while is slightly higher for thickness measurements and in three samples even reaches 10%.

Since no electronic devices could be used during samples cutting to measure them, and since the saw used was very “low-tech” (minimal user safety measures and handmade locks), these results were the best that could be achieved.

Table 3: SCB samples' geometry

3E1 DVR SCB Geometry							
ID	Thickness A	Thickness B	Thickness Av	Length A	Length B	Length Av	Area
[-]	[mm]	[mm]	[mm]	[mm]	[mm]	[mm]	[mm ²]
IA	55	54	55	57	57	57	3107
IB	52	53	53	59	60	60	3124
IIA	50	51	51	59	58	59	2954
IIB	49	49	49	59	59	59	2891
IIIA	50	52	51	60	60	60	3060
IIIB	49	49	49	60	59	60	2916
IVA	52	52	52	58	58	58	3016
IVB	51	50	51	59	59	59	2980

4E1 DVR SCB Geometry							
ID	Thickness A	Thickness B	Thickness Av	Length A	Length B	Length Av	Area
[-]	[mm]	[mm]	[mm]	[mm]	[mm]	[mm]	[mm ²]
IA	49	48	49	59	59	59	2862
IB	49	50	50	58	59	59	2896
IIA	52	53	53	59	58	59	3071
IIB	53	54	54	59	60	60	3183
IIIA	53	54	54	61	60	61	3237
IIIB	56	55	56	57	59	58	3219
IVA	52	51	52	59	59	59	3039
IVB	49	50	50	57	58	58	2846

4E1 HS SCB Geometry							
ID	Thickness A	Thickness B	Thickness Av	Length A	Length B	Length Av	Area
[-]	[mm]	[mm]	[mm]	[mm]	[mm]	[mm]	[mm ²]
IA	52.0	51.0	51.5	59	58	58.5	3012.75
IB	51.0	51.0	51.0	60	59	59.5	3034.5
IIB	49.0	51.0	50.0	60	59	59.5	2975
IIIA	55.0	56.0	55.5	58	57	57.5	3191.25
IIIB	55.0	52.0	53.5	59	59	59.0	3156.5
IVA	51.0	52.0	51.5	58	59	58.5	3012.75
IVB	52.0	51.0	51.5	59	58	58.5	3012.75

3E1 HS SCB Geometry							
ID	Thickness A	Thickness B	Thickness Av	Length A	Length B	Length Av	Area
[-]	[mm]	[mm]	[mm]	[mm]	[mm]	[mm]	[mm ²]
IA	52.0	51.0	51.5	58	58	58.0	2987
IIA	50.0	50.0	50.0	59	59	59.0	2950
IIB	51.0	51.0	51.0	58	59	58.5	2983.5
IIIA	52.0	51.0	51.5	59	59	59.0	3038.5
IIIB	54.0	54.0	54.0	58	58	58.0	3132
IVA	52.0	50.0	51.0	60	59	59.5	3034.5
IVB	53.0	53.0	53.0	59	58	58.5	3100.5

5.1.5 Air voids content

In the following tables a summary of air voids content for each sample, both for E*/FN tests and SCB. Detailed process of air voids determination (A = sample weight in air, B = sample weight in water, C = SSD weight) is in *Appendix*. For E* and FN samples, blue cells represent drowned samples. For SCB samples, roman numbers represent full disc and roman numbers plus A or B represent each half of the disc.

Table 4: E* and FN samples' air void content

	Air voids content [%], E* and FN tests			
	3E1 DVR	4E1 DVR	3E1 HS	4E1 HS
I	6.6	6.8	7.3	6.8
II	6.9	6.8	7.2	6.8
III	6.9	6.6	7.0	6.7
IV	6.7	7.1	6.9	6.7
V	6.6	7.3	7.0	6.7
VI	7.0	7.3	6.6	6.7
AVG	6.8	7.0	7.0	6.7

Table 5: SCB samples' air void content

	Air voids content [%], SCB tests			
	3E1 DVR	4E1 DVR	3E1 HS	4E1 HS
IA	6.5	6.8	7.6	6.8
IB	6.5	6.6		7.3
IIA	7.1	7.5	7.3	
IIB	6.5	6.9	7.3	6.9
IIIA	7.3	6.8	7.3	6.7
IIIB	7.1	6.4	6.8	6.8
IVA	7.2	7.0	7.3	7.2
IVB	7.7	7.5	7.5	7.1
AVG	7.0	7.0	7.3	7.0

5.2 Dynamic Modulus |E*|

All Shift factors and Dynamic Modulus coefficients are found with the model shown in Chapter 4, using Excel solver to vary these coefficients while minimizing |E*| mastercurves fit error after incorporating AMPT data and are summarized in the following table:

Table 6: Dynamic Modulus fit and Shift factors coefficients

		3E1 DVR		3E1 HS		4E1 DVR		4E1 HS	
		DRY	WET	DRY	WET	DRY	WET	DRY	WET
Dynamic	δ	0.227	-0.041	-0.004	-0.039	-0.055	-0.061	-0.018	-0.313
Modulus	α	4.314	4.540	4.500	4.596	4.503	4.526	4.521	4.913
fit	β	1.321	1.412	1.386	1.489	1.424	1.642	1.335	1.388
coefficients	γ	0.349	0.361	0.366	0.341	0.351	0.279	0.342	0.320
Shift factors	a1	0.00132	0.00151	0.00057	-0.00045	0.00076	0.00080	0.00099	0.00114
coefficients	a2	-0.186	-0.193	-0.148	-0.101	-0.161	-0.177	-0.168	-0.176

“Drowned” or “Wet” refer to samples conditioned 40 days in water, while “Dry” refers to unconditioned samples.

In the following figures, comparisons of E* mastercurves between the different mixtures are shown. The comparisons have been made between all samples of a certain mixture and taking the average of the value.

The aim of the comparisons was to highlight the differences between the mixtures of interest: DVR samples vs. HS ones, or DRY samples vs. WET ones. Results showed results very similar between 3E1 DVR and HS mixtures, while 4E1 DVR performed quite better (E* is 4 times higher at lowest frequency but tend to be equal to its HS counterpart at highest frequencies).

DVR mixtures don't show a visible trend when comparing DRY and WET asphalt samples: 3E1 performs better in DRY state but 4E1 WET samples show the best results overall. Both HS mixtures, by the way, perform better when in WET state.

All things considered, moisture damage does not seem to affect the mixtures, and more advanced moisture damage tests (like Indirect Tensile Strength) are needed to complete the evaluation.

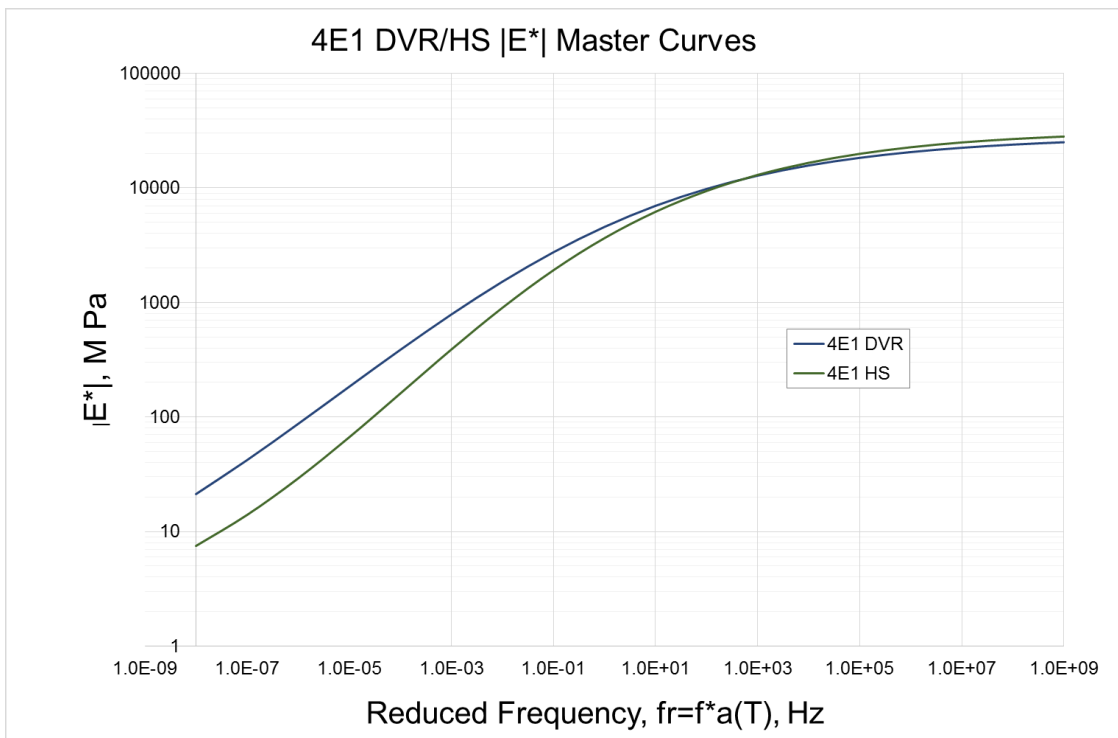
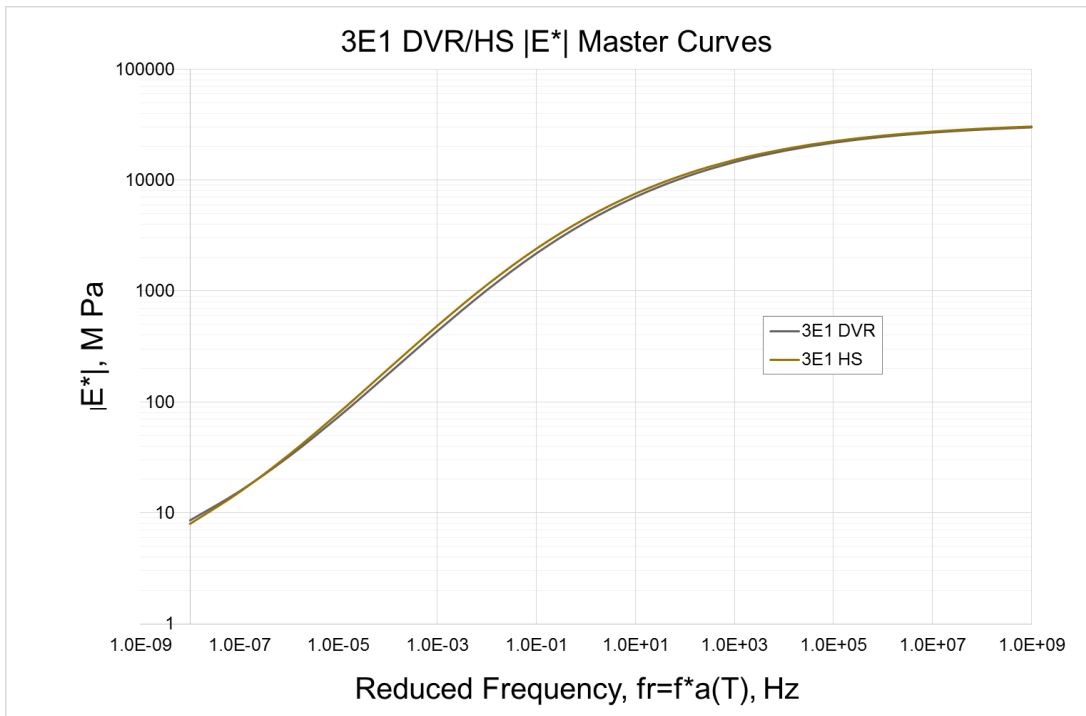


Figure 46: 3E1 and 4E1 E^* mastercurves comparisons

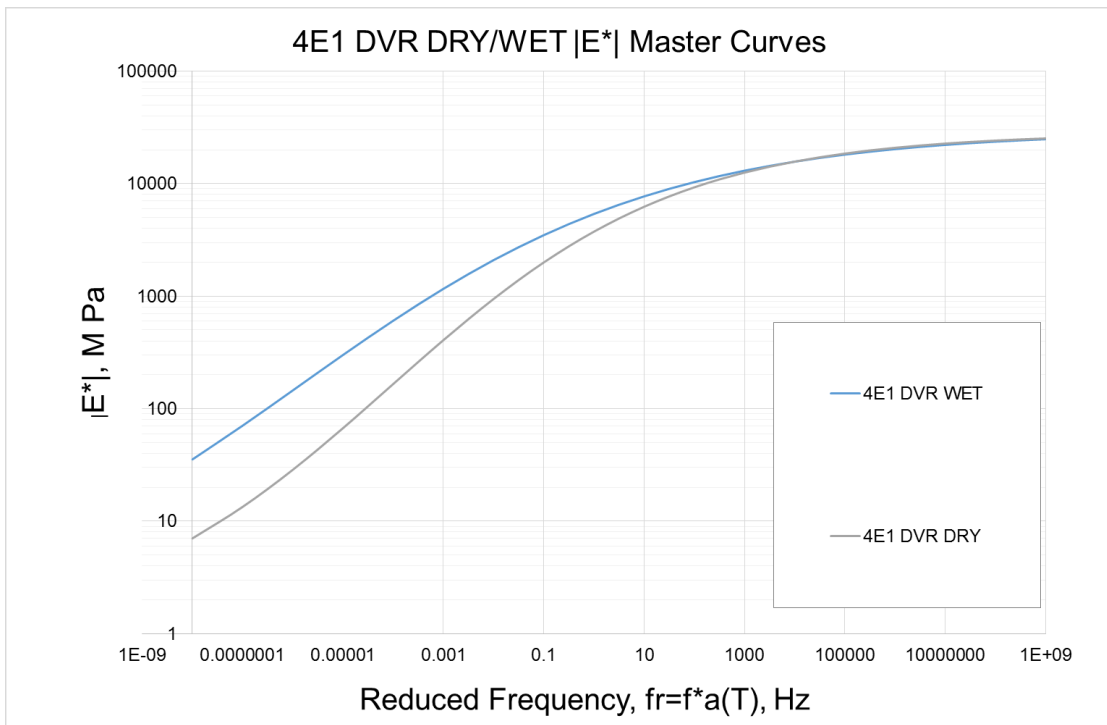
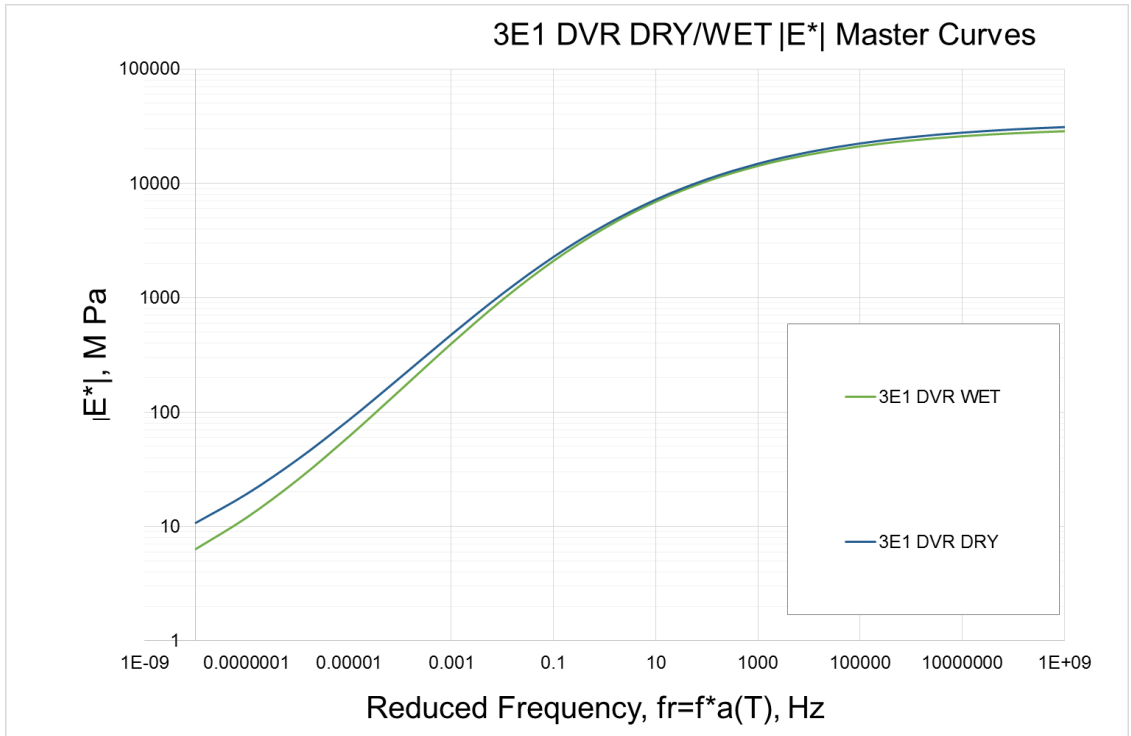


Figure 47: 3E1 and 4E1 DVR DRY/WET E^ mastercurves comparisons*

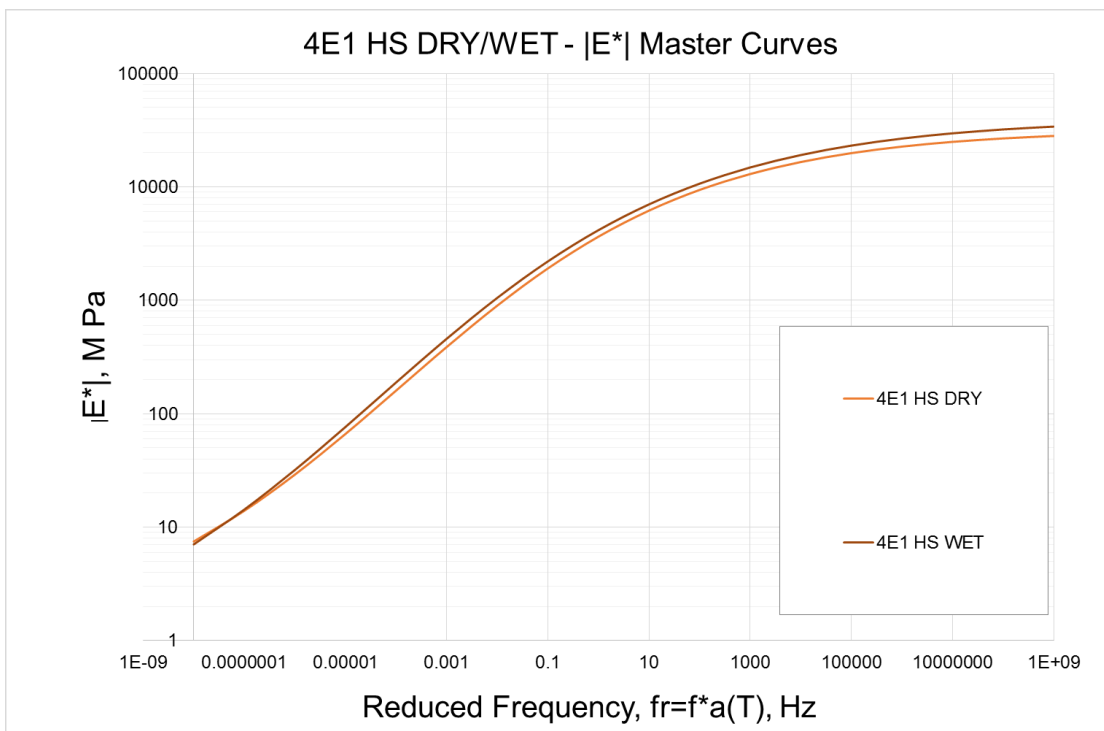
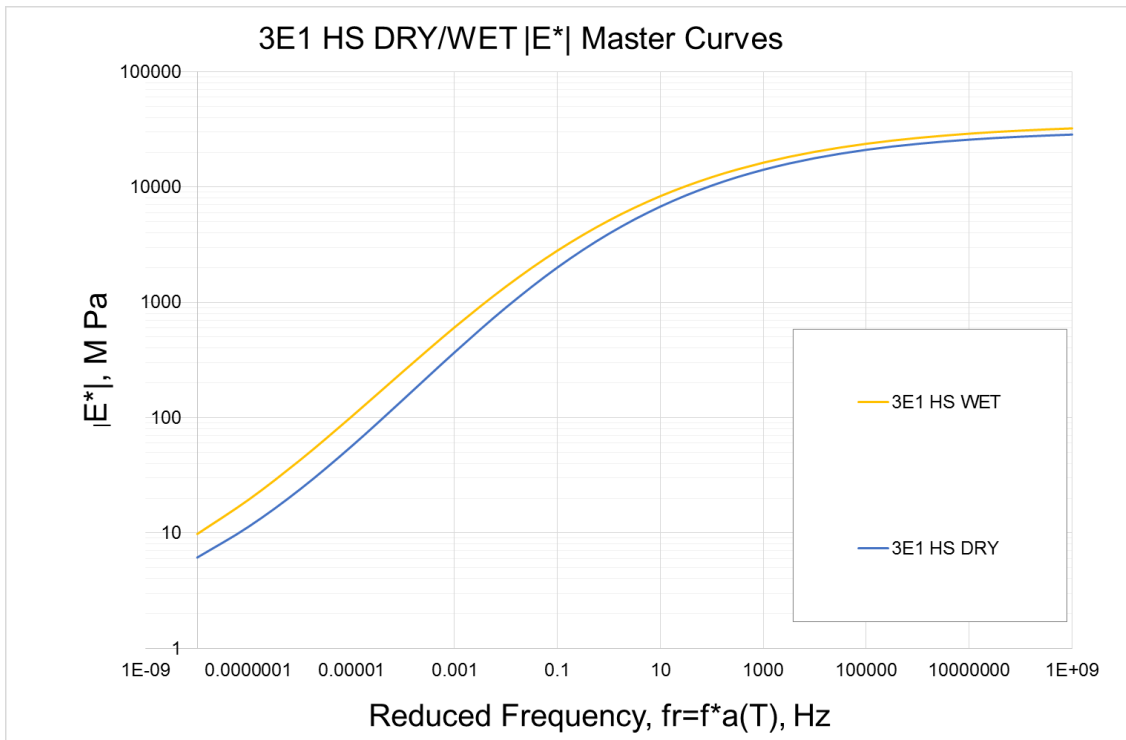


Figure 48: 3E1 and 4E1 HS DRY/WET E^* mastercurves comparisons

All mastercurves are presented in detail, along with AMPT data for each sample for each mixture, in *Appendix*. “Drowned” or “Wet” refer to samples conditioned 40 days in water, while “Dry” refers to unconditioned samples.

Blank values mean obvious data outliers, while red values mean data outside Data Quality Statistics Requirements:

Data Quality Statistic	Limit
Deformation drift	In direction of applied load
Peak-to-peak strain	75 to 125 μ strain for unconfined tests 85 to 115 μ strain for confined tests
Load standard error	10%
Deformation standard error	10%
Deformation uniformity	30%
Phase uniformity	3%

Figure 49: E^* Data Quality Statistics Requirements

5.3 Flow Number tests

Data from AMPT are inserted into the Excel model, along with shift factors coefficients and $|E^*|$ sigmoid taken from $|E^*|$ mastercurves determination.

Resilient strain ε_{rz} is found as

$$\varepsilon_{rz} = \frac{1}{|E^*|} (\sigma_1 - 2\mu\sigma_3) \quad (1)$$

where the two sigma are the vertical and confining stress.

Plastic strain is determined from the equation already seen in *Research Plan*:

$$\varepsilon_p = \varepsilon_{rz} 10^{\beta_1 k_1} T^{\beta_2 k_2} N^{\beta_3 k_3} \quad (2)$$

k_1 , k_2 and k_3 are taken as -3.4488, 1.5606 and 0.4791 respectively, as stated in the MEPD Guide. Regression coefficients (Beta factors) number 1 and 3 are found using the Excel solver and minimizing the error between predicted and actual plastic strain while number 2 is always set to 1.

In the following figures, several comparisons of permanent deformation results between the different mixtures are shown. The comparison have been made between all samples of a certain mixture and taking the average of the value.

The aim of the comparisons, as for E^* , was to highlight the differences between the mixtures of interest: DVR samples vs. HS ones, or DRY samples vs. WET ones.

The graphs, in a Log-Log scale, show that little or no difference are found between DVR or HS mixtures: 3E1 DVR performed a little better than its HS counterpart, while both 4E1 mixtures performed almost in the same way. We can say that both kinds of

mixtures do not show particular differences and DVR modification can be used instead of HS and benefit of its reduced costs.

HS mixtures do not show particularly valuable differences between the DRY and WET state, and only 4E1 DVR seems to perform better in the DRY state. However, 3E1 DVR seemed to perform better when WET. In the end, a common trend seems nowhere to be found.

As said in the previous paragraph, more advanced moisture damage tests are needed to complete the characterization of the mixtures when moisture penetrates them.

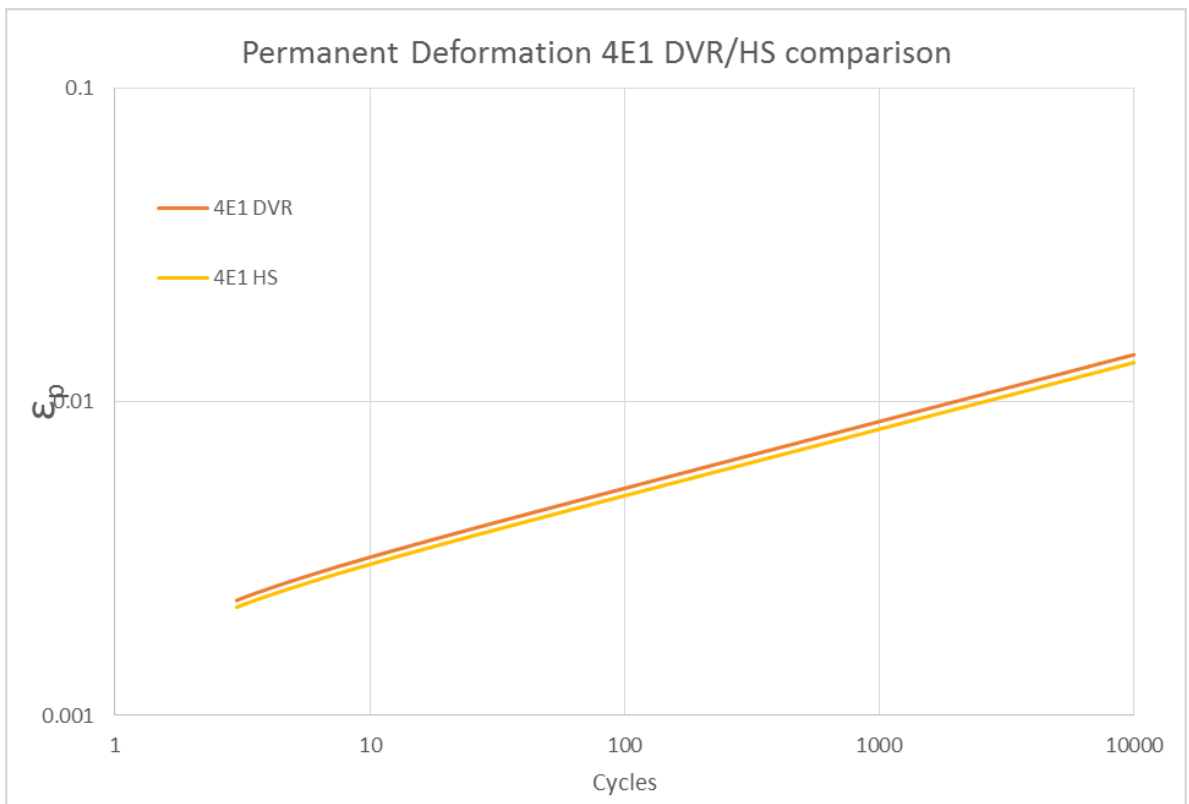
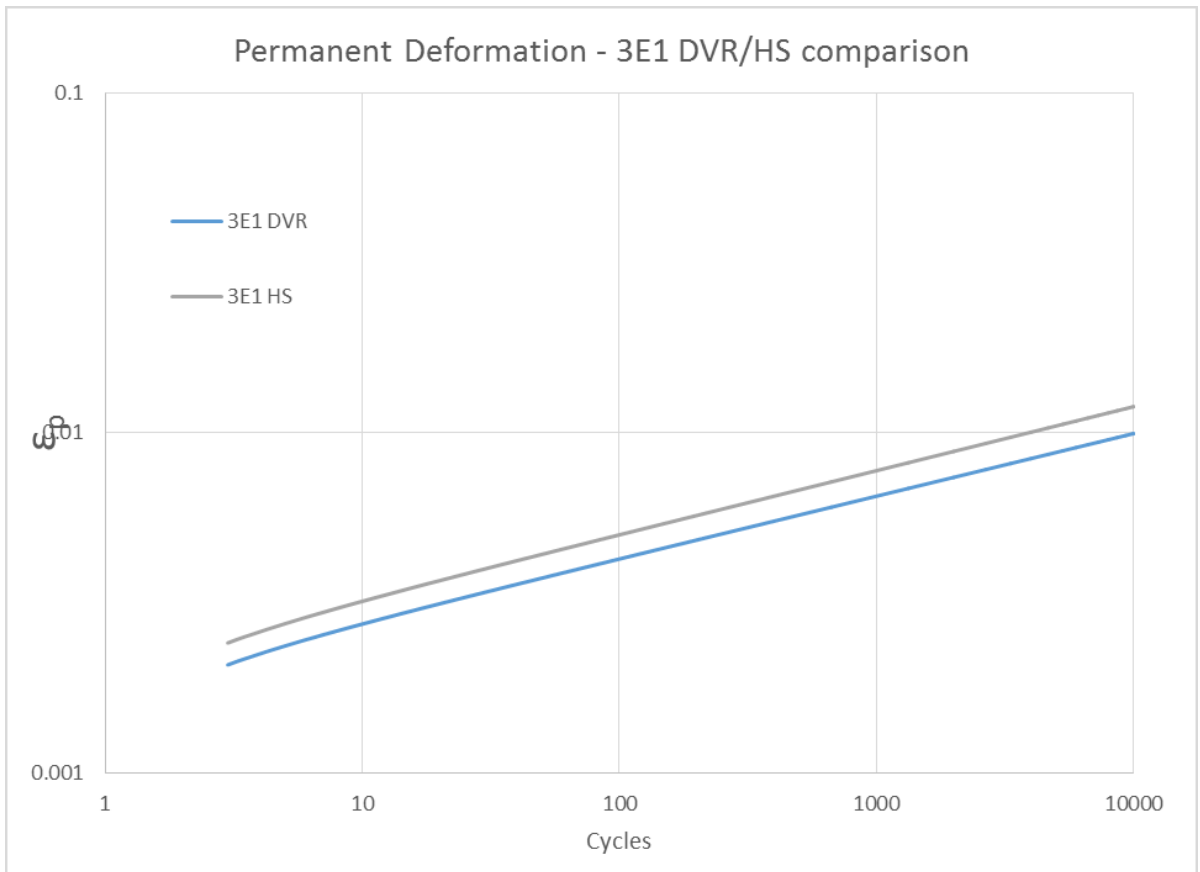


Figure 50: Permanent Deformation comparisons for 3E1 and 4E1 mixtures

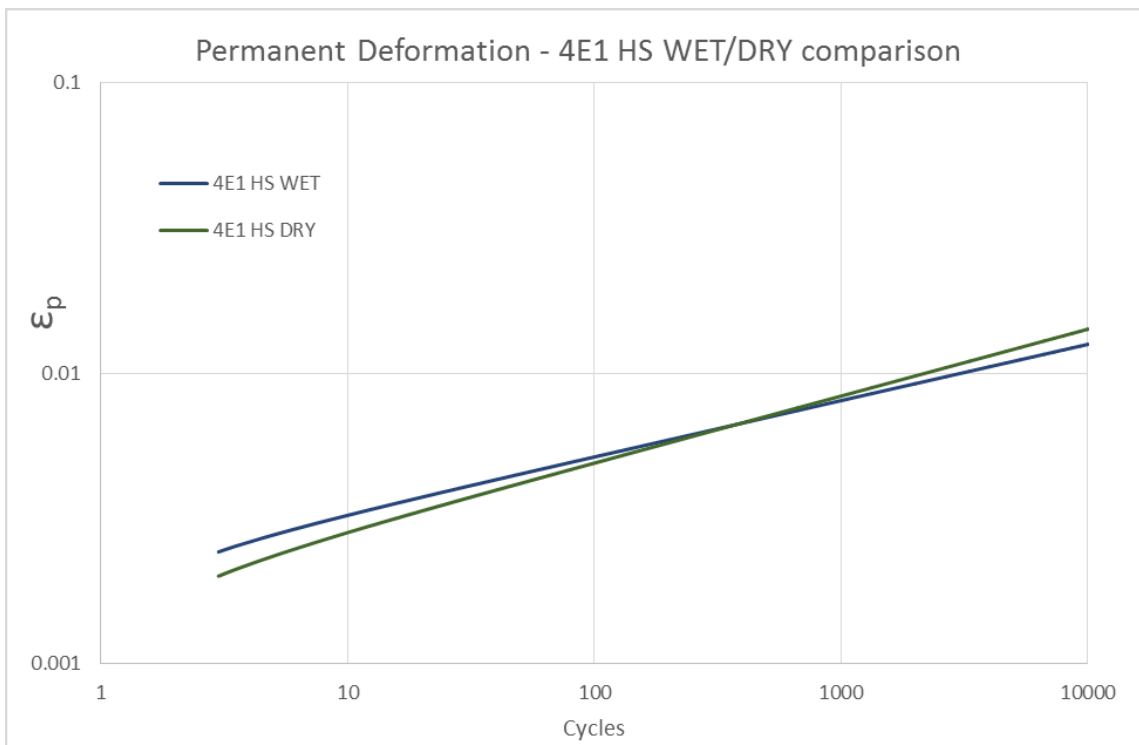
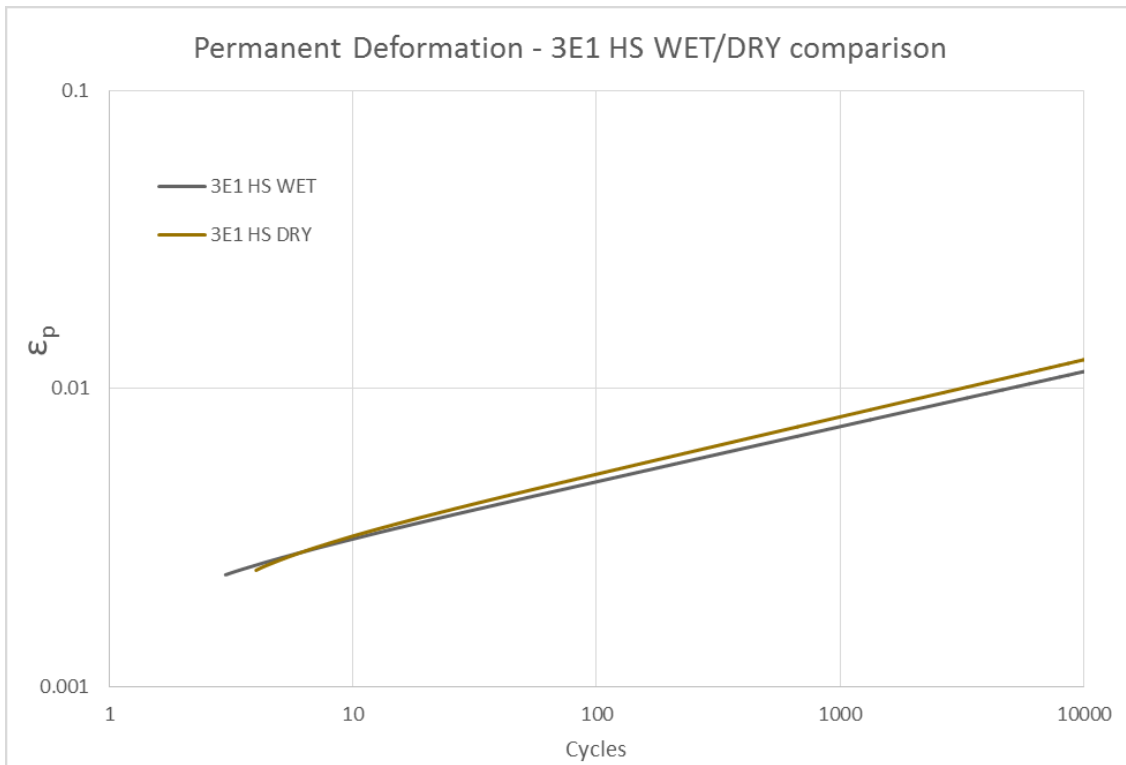


Figure 51: Permanent Deformation comparisons for 3E1 HS and 4E1 HS mixtures

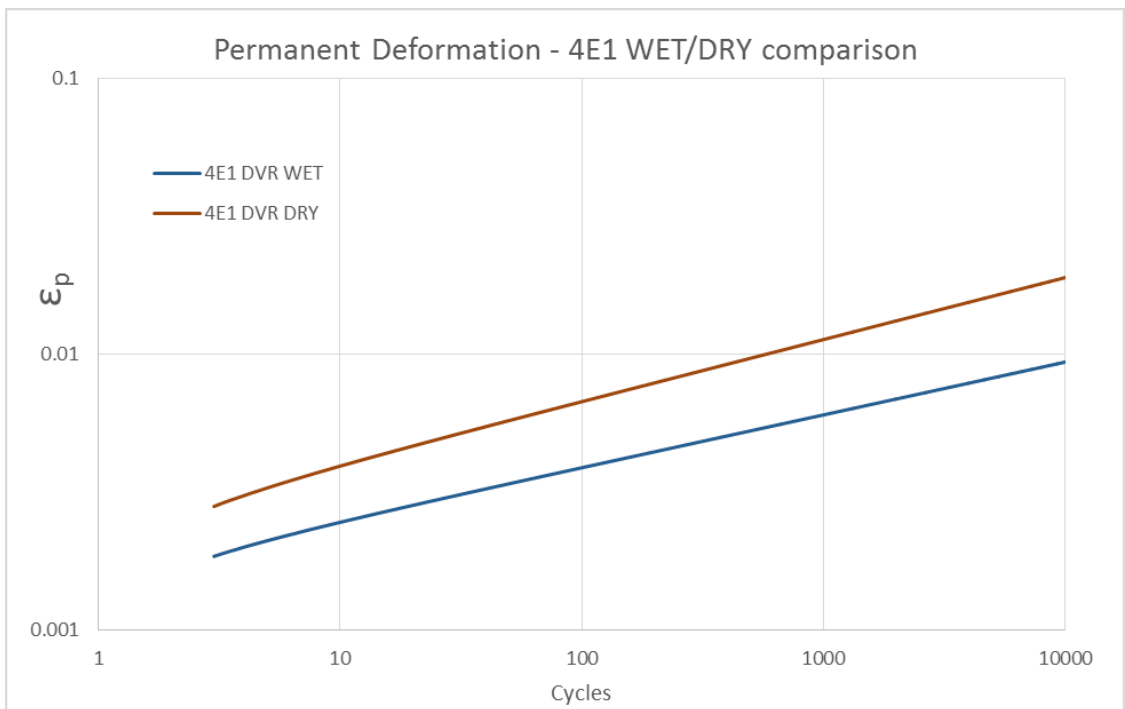
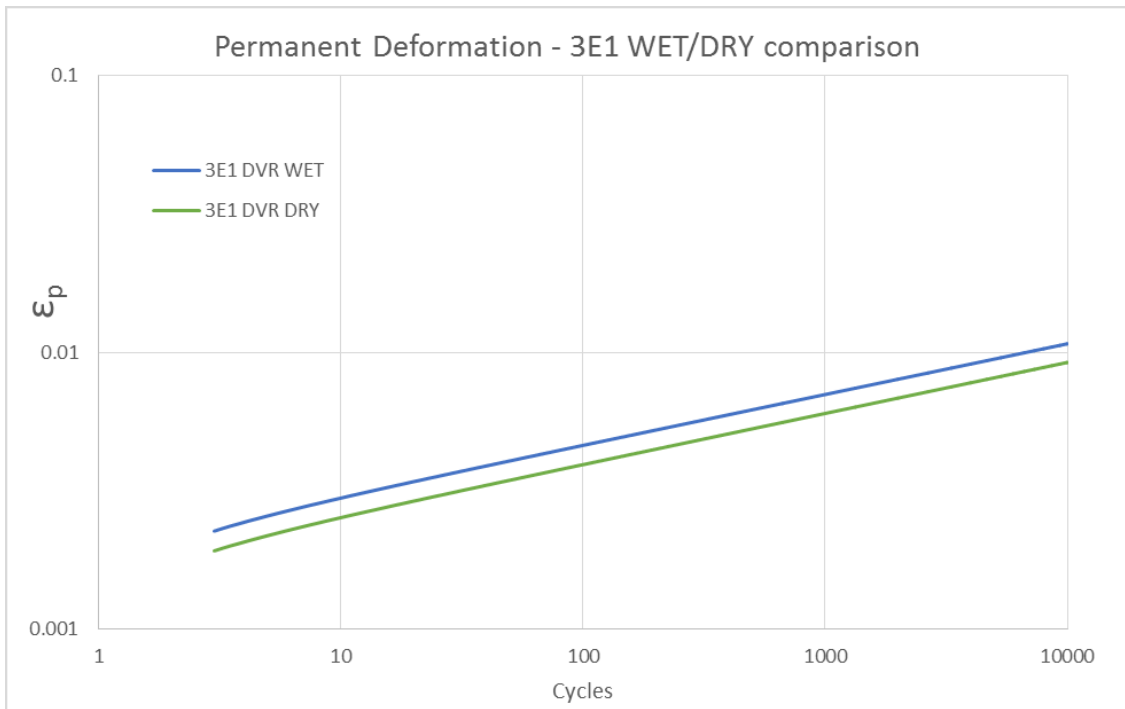


Figure 52: Permanent Deformation comparisons for 3E1 DVR and 4E1 DVR mixtures

A summary of the regression coefficients, used as inputs for *Pavement ME Design* is in the following table:

Table 7: Beta factors summary

	3E1 DVR						4E1 DVR					
	1	2	3	4	5	6	1	2	3	4	5	6
Beta 1	0.735	0.738	0.715	0.765	0.880	0.843	0.743	0.772	0.828	0.808	0.811	0.805
Beta 2	1.000	1.000	1.000	1.000	1.000	1.000	1.000	1.000	1.000	1.000	1.000	1.000
Beta 3	0.368	0.385	0.367	0.397	0.399	0.414	0.433	0.348	0.388	0.455	0.482	0.466
	3E1 HS						4E1 HS					
	1	2	3	4	5	6	1	2	3	4	5	6
Beta 1	0.867	0.876	0.891	0.830	0.853	0.830	0.760	0.779	0.755	0.860	0.799	0.821
Beta 2	1.000	1.000	1.000	1.000	1.000	1.000	1.000	1.000	1.000	1.000	1.000	1.000
Beta 3	0.371	0.388	0.397	0.412	0.417	0.366	0.421	0.416	0.368	0.502	0.458	0.486

See *Appendix* for detailed graphs showing the evolution of plastic strain after N cycles for each sample.

5.4 PavementME Design data implementations and projects

As stated many times before, the data gathered in the previous tests were used as inputs in *AASHTOWare’s PavementME Design*, a software that implements the Mechanistic-Empirical principles for the design of new and rehabilitated pavements.

The pavement structure has already been discussed in the previous chapter, putting in the upper asphalt layer information of 4E1 mixture and in the lower one information of 3E1 mixture, while traffic data was manually adjusted to reach about 3 million ESALs (3,469,880) at the end of the design life (20 years), as in the following *Figure 53*:

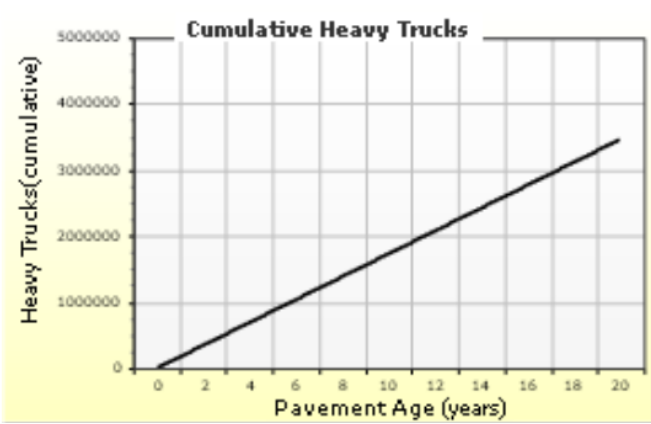


Figure 53: Total ESALs during pavement's design life

For climate data, the climate station chosen for the first evaluation was in Illinois, the closest to Michigan, while for the second analysis, where a much warmer environment was needed, the Arizona station was taken in consideration. In the following *Figure 54*, the Illinois' station air temperature data is shown.

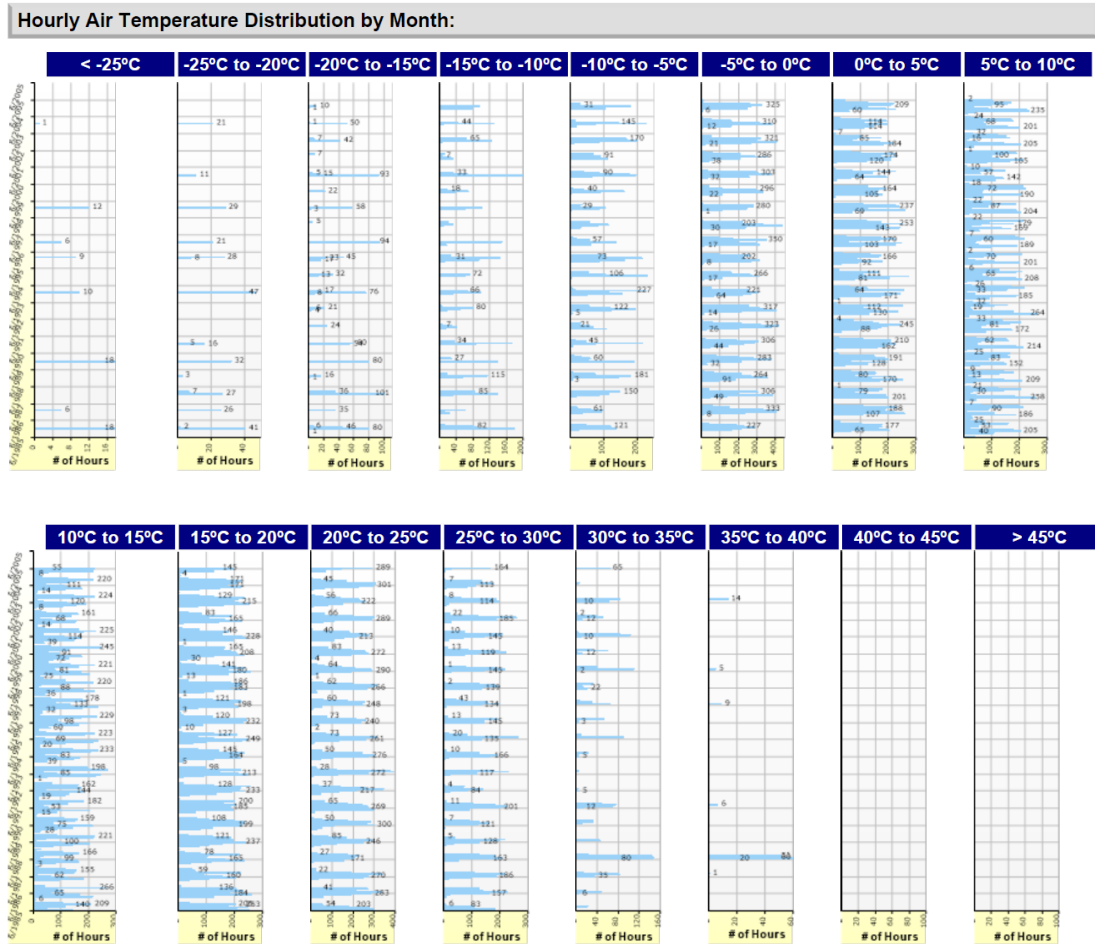


Figure 54: Illinois' air temperature

Dynamic modulus and Flow Number input level is set to 1, the most accurate: this level gives the user the chance to manually paste beta factors from FN tests and E* data for each layer for each temperature and frequency. An example is in *Figure 55*:

Asphalt Dynamic Modulus (Input Level: 1)						
T (°C)	0.1 Hz	0.5 Hz	1 Hz	5 Hz	10 Hz	25 Hz
4	7460.975	9662.075	10645.11	12938.31	13909.18	15158.85
20	2182.390	3396.854	4034.761	5768.805	6612.425	7799.688
40	346.4330	635.5048	816.1570	1411.257	1757.958	2312.455
54	111.2022	209.8510	275.4344	510.5598	659.7852	915.4088

Figure 55: Asphalt Dynamic Modulus input

Once all these data are inserted, the software begins with the pavement design and produces a .PDF as output. Other than permanent deformation, IRI, thermal and fatigue cracking were evaluated but for this dissertation, however, only permanent deformation outputs are taken into account since the other analyses have been run with Input Level 3 (no data inserted).

In the end, as the objectives stated in *Research Plan*, the simulations made have been:

- a. DVR mixture, in DRY state, Illinois climate station;
- b. HS mixture, in DRY state, Illinois climate station;
- c. DVR mixture, in WET state, Illinois climate station;
- d. HS mixture, in WET state, Illinois climate station;
- e. DVR mixture, in DRY state, Arizona climate station;
- f. HS mixture, in DRY state, Arizona climate station.

In this way three comparisons could be made:

- (1) DVR mixtures in both states (a. and c.) vs. HS mixtures in both states (b. and d.), Illinois climate station;
- (2) Both mixtures in DRY state (a. and b.) vs. both mixtures in WET state (C. and D.), Illinois climate station;
- (3) Both mixtures in DRY state (a. and b.), Illinois climate station vs. both mixtures in DRY state (e. and f.), Arizona climate station.

(1) gives the answer to whether the DVR+SBS modification could be used as a valid substitution or even better than the usual HS (only SBS), allowing the manufacturer to reduce the costs and the environmental impact inserting 7% rubber from end-of-life tires into the bitumen.

(2) deals with the problem of moisture damage: are the mixtures susceptible to high levels of moisture damage? If so, the WET performance results should be very lower than the DRY ones.

(3) in a certain way completes the answer given by (1): since the temperatures in Illinois (close to Michigan) are not so high throughout the year, repeating the analysis using the climate of a much more warm place will develop more permanent deformation, since it's the main point of these analysis?

5.4.1 Comparison (1) and (2): DVR vs. HS and DRY vs. WET

Distress Prediction Summary			Distress Prediction Summary		
Distress Type	Distress @ Specified Reliability		Distress Type	Distress @ Specified Reliability	
	Target	Predicted		Target	Predicted
Terminal IRI (m/km)	2.70	2.97	Terminal IRI (m/km)	2.70	3.04
Permanent deformation - total pavement (mm)	19.00	5.86	Permanent deformation - total pavement (mm)	19.00	6.50
AC bottom-up fatigue cracking (percent)	25.00	100.00	AC bottom-up fatigue cracking (percent)	25.00	100.00
AC thermal cracking (m/km)	189.40	40.97	AC thermal cracking (m/km)	189.40	40.97
AC top-down fatigue cracking (m/km)	378.80	1360.16	AC top-down fatigue cracking (m/km)	378.80	2256.01
Permanent deformation - AC only (mm)	6.00	0.28	Permanent deformation - AC only (mm)	6.00	0.46

Figure 56: DVR DRY (left) and HS DRY (right) design's distress report

Distress Prediction Summary			Distress Prediction Summary		
Distress Type	Distress @ Specified Reliability		Distress Type	Distress @ Specified Reliability	
	Target	Predicted		Target	Predicted
Terminal IRI (m/km)	2.70	2.96	Terminal IRI (m/km)	2.70	2.95
Permanent deformation - total pavement (mm)	19.00	5.73	Permanent deformation - total pavement (mm)	19.00	5.74
AC bottom-up fatigue cracking (percent)	25.00	100.00	AC bottom-up fatigue cracking (percent)	25.00	100.00
AC thermal cracking (m/km)	189.40	40.97	AC thermal cracking (m/km)	189.40	40.97
AC top-down fatigue cracking (m/km)	378.80	1281.77	AC top-down fatigue cracking (m/km)	378.80	1224.65
Permanent deformation - AC only (mm)	6.00	0.18	Permanent deformation - AC only (mm)	6.00	0.22

Figure 57: DVR WET (left) and HS WET (right) design's distress report

Figure 56 and 57 show the detail of the distresses' reports of the pavement designs made with the DVR and HS combination of materials in the DRY state, while 58 and 59 in the WET one. As said before, the only distress taken into consideration in this dissertation is permanent deformation, that's why results of Terminal IRI, AC bottom-up and top-down fatigue or thermal cracking are not discussed here.

Talking about the comparison between the two different materials (1), it can be seen that the predicted value of permanent deformation for the total pavement is always far from the target one (19 mm), and if in the WET case the two mixtures react almost in the same way, DVR DRY performs slightly better than HS DRY. Instead, focusing on moisture damage comparison, the WET mixtures react with less permanent deformation than the others. However, in all cases listed above, the distance from the target value is so high and the difference between the predicted values are so little (sometimes less than a tenth of mm in 20 years) that it's like we're analyzing the same material over and over.

5.4.2 Comparison (3): Illinois vs. Arizona climate station

Distress Prediction Summary			Distress Prediction Summary		
Distress Type	Distress @ Specified Reliability		Distress Type	Distress @ Specified Reliability	
	Target	Predicted		Target	Predicted
Terminal IRI (m/km)	2.70	2.70	Terminal IRI (m/km)	2.70	2.78
Permanent deformation - total pavement (mm)	19.00	4.62	Permanent deformation - total pavement (mm)	19.00	5.11
AC bottom-up fatigue cracking (percent)	25.00	100.00	AC bottom-up fatigue cracking (percent)	25.00	100.00
AC thermal cracking (m/km)	189.40	40.97	AC thermal cracking (m/km)	189.40	40.97
AC top-down fatigue cracking (m/km)	378.80	1436.33	AC top-down fatigue cracking (m/km)	378.80	2365.85
Permanent deformation - AC only (mm)	6.00	0.50	Permanent deformation - AC only (mm)	6.00	0.78

Figure 58: DVR DRY (left) and HS DRY (right), Arizona design's distress report

After moving the climate station in a much warmer environment (about 10 °C more than the Illinois counterpart and 14 times less annual freeze-thaw cycles) and repeating the analysis in the same conditions, it can be seen in *Figure 58* that if the total permanent deformation is decreased of about 1 mm, the asphalt layer permanent deformation fraction is overall increased, and almost doubled for both materials. As said before, though, we are talking about tenths of millimeters and the predicted value is still far from reached.

5.5 IL-SCB tests

The summarized database of results for the different IL-SCB tests is shown in the following tables.

Tables 8-10 summarize the most important results (Fracture Energy, Flexibility Index, Slope) for each method used and all the relative inputs, *Figures 59 and 60* compare the different results for Fracture Energy and Flexibility Index for each material, while *Figures 61-63* compare the relation between Slope and Fracture Energy for each sample.

This test, since its results were widely analyzed using two different models and an advanced and innovative determination of the Ligament Area through photogrammetric reconstruction, has been used to try to give the material a cracking resistance parameter in its characterization, even if in a less accurate way than it was done with permanent deformation and without using the ME software.

Using the *I-FIT* software or the MSU-developed models give similar results for Fracture Energy and Flexibility Index, while the 3D modelled Ligament Area gives slightly lower values both for both parameters, since the area on which the cracking develops gets bigger.

Fracture Energy doesn't change much from 4E1 DVR to 4E1 HS, while the 3E1 DVR mixture gives a value 40% lesser than its HS counterpart. Flexibility Index results, instead, are very similar between 3E1 HS, 4E1 DVR and 4E1 HS, while are even six times lower for the 3E1 DVR mixture.

Unfortunately, looking at the relation between slope (m) and Ligament Area, it's not possible to see a direct relation since results are all scattered: sometimes increasing Ligament Area increases slope too, but sometimes we can see a huge drop like for 3E1 HS samples. This, along with the skyrocketing values of standard deviation and coefficient of variation of the results, confirms that SCB tests, even "upgraded" with the

introduction of the Flexibility Index, remain highly not reliable and accurate and should be not used as the only input to characterize an asphalt material. More tests, however, are needed to confirm this statement.

Eventually, detailed results (for each sample and for each of the three methods used) are shown in Appendix.

Table 8: SCB results summary - Standard MSU model

STANDARD MSU MODEL	3E1DVR						4E1DVR						3E1HS			4E1HS			
	3E1DVR_I/A	3E1DVR_I/B	3E1DVR_I/A	3E1DVR_I/B	3E1DVR_I/A	3E1DVR_I/B	4E1DVR_I/A	4E1DVR_I/B	4E1DVR_I/A	4E1DVR_I/B	4E1DVR_I/A	4E1DVR_I/B	3E1HS_I/A	3E1HS_I/A	3E1HS_I/A	4E1HS_I/A	4E1HS_I/B	4E1HS_I/B	
Specimen ID	MSU_PolITO																		
Project ⁽¹⁾	55	53	51	49	59	59	49	59	59	59	59	54	60	52	58	59	59	59	
Thickness, t [mm]	57	60	59	59	59	59	59	59	59	59	59	60	60	58	58	59	59	60	
Length, l [mm]	57	60	59	59	59	59	59	59	59	59	59	60	60	58	58	59	59	60	
Delta from optimum A_{lig} [%]	6.27%	7.80%	2.00%	2.00%	2.00%	2.00%	2.00%	0.00%	6.00%	6.00%	9.83%	2.24%	2.24%	0.00%	0.00%	14.00%	3.73%	1.69%	
Work of Fracture [J]	4.3	3.9	3.7	3.5	3.5	3.5	4.4	5.6	5.4	5.4	5.7	6.6	6.6	5.5	5.5	5.9	5.6	4.9	
Ligament Area, A_{lig} [mm ²]	3135.0	3180.0	3009.0	2891.0	2891.0	2891.0	2891.0	2950.0	3127.0	3127.0	3240.0	3016.0	2950.0	2950.0	3363.0	3060.0	3000.0	3000.0	
Fracture Energy, G_f [J/m ²]	1357.7	1214.5	1231.4	1202.0	1202.0	1202.0	1530.7	1901.5	1735.1	1735.1	1745.8	2199.7	1864.0	1864.0	1748.2	1833.2	1833.2	1626.0	
Slope, m [kN/mm]	20.4	14.4	12.6	14.8	14.8	14.8	3.2	1.9	2.7	2.7	3.1	2.3	5.3	5.3	3.6	1.9	1.9	2.9	
Flexibility Index	0.7	0.8	1.0	0.8	0.8	0.8	4.8	9.9	6.4	6.4	5.5	9.8	9.8	3.5	3.5	4.9	9.6	5.5	
Method of data processing ⁽²⁾	MSU	MSU																	
Sample availability ⁽⁴⁾	Y	Y	Y	Y	Y	Y	Y	Y	Y	Y	Y	Y	Y	Y	Y	Y	Y	Y	Y
AVG Fracture Energy, G_f [J/m ²]	1251.43						1728.27						2031.87			1735.78			
STDEV Fracture Energy, G_f [J/m ²]	71.88						152.12						237.40			104.13			
CV Fracture Energy, G_f [%]	5.7%						8.8%						11.7%			6.0%			
AVG Flexibility Index	0.83						6.67						6.64			6.67			
STDEV Flexibility Index	0.13						2.26						4.41			2.53			
CV Flexibility Index	15.6%						33.9%						66.4%			37.9%			

Table 9: SCB results summary - Actual Ligament Area

LIGAMENT AREA 3D-MODELED	3E1DVR						4E1DVR						3E1HS		4E1HS			
	Specimen ID	3E1DVR_IA	3E1DVR_IB	3E1DVR_IJA	3E1DVR_IIB	3E1DVR_IIB	4E1DVR_IA	4E1DVR_IB	4E1DVR_IJA	4E1DVR_IIB	4E1DVR_IIB	4E1DVR_IIB	3E1HS_IA	3E1HS_IJA	3E1HS_IJA	4E1HS_IA	4E1HS_IB	4E1HS_IIB
Project ⁽¹⁾	MSU_PolITO	MSU_PolITO	MSU_PolITO	MSU_PolITO	MSU_PolITO	MSU_PolITO	MSU_PolITO	MSU_PolITO	MSU_PolITO	MSU_PolITO	MSU_PolITO	MSU_PolITO	MSU_PolITO	MSU_PolITO	MSU_PolITO	MSU_PolITO	MSU_PolITO	MSU_PolITO
Thickness, t [mm]	55	53	51	49	59	49	50	59	53	54	60	52	50	50	51	51	50	50
Length, l [mm]	57	60	59	59	59	59	59	59	59	60	60	58	59	59	59	60	60	60
Delta from optimum A_{lig} [%]	33.73%	34.47%	26.88%	27.69%	27.69%	17.05%	33.93%	27.59%	27.59%	46.85%	46.85%	30.88%	21.25%	21.25%	34.47%	24.51%	24.51%	23.97%
Work of Fracture [J]	4.3	3.9	3.7	3.5	3.5	4.4	5.6	5.4	5.4	5.7	5.7	6.6	5.5	5.5	5.9	5.6	5.6	4.9
Ligament Area, A_{lig} [mm ²]	3945.0	3967.0	3743.0	3767.0	3767.0	3453.0	3951.0	3764.0	3764.0	4332.0	4332.0	3861.0	3577.0	3577.0	3967.0	3673.0	3673.0	3657.0
Fracture Energy, G_f [J/m ²]	1079.0	973.6	989.9	922.5	922.5	1281.5	1419.8	1441.5	1441.5	1305.7	1305.7	1718.3	1537.3	1537.3	1482.0	1527.2	1527.2	1333.9
Slope, m [kN/mm]	20.4	14.4	12.6	14.8	14.8	3.2	1.9	2.7	2.7	3.1	3.1	2.3	5.3	5.3	3.6	1.9	1.9	2.9
Flexibility Index	0.5	0.7	0.8	0.6	0.6	4.0	7.4	5.3	5.3	4.1	4.1	7.6	2.9	2.9	4.2	8.0	8.0	4.5
Method of data processing ⁽³⁾	MSU	MSU	MSU	MSU	MSU	MSU	MSU	MSU	MSU	MSU	MSU	MSU	MSU	MSU	MSU	MSU	MSU	MSU
Sample availability ⁽⁴⁾	Y	Y	Y	Y	Y	Y	Y	Y	Y	Y	Y	Y	Y	Y	Y	Y	Y	Y
AVG Fracture Energy, G_f [J/m ²]	991.25						1362.12						1627.79		1447.70			
STDEV Fracture Energy, G_f [J/m ²]	65.15						80.19						128.02		101.13			
CV Fracture Energy, G_f [%]	6.6%						5.9%						7.9%		7.0%			
AVG Flexibility Index	0.65						5.22						5.27		5.56			
STDEV Flexibility Index	0.11						1.56						3.33		2.10			
CV Flexibility Index	16.5%						29.9%						63.3%		37.7%			

Table 10: SCB results summary - I-FIT

I-FIT MODEL	3E1DVR						4E1DVR						3E1HS		4E1HS		
	Specimen ID	3E1DVR_1A	3E1DVR_1B	3E1DVR_1IA	3E1DVR_1IB	3E1DVR_1IB	4E1DVR_1A	4E1DVR_1B	4E1DVR_1IA	4E1DVR_1IB	4E1DVR_1IB	3E1HS_1A	3E1HS_1IA	3E1HS_1IA	4E1HS_1A	4E1HS_1B	4E1HS_1IB
Project ⁽¹⁾	MSU_PolITO	MSU_PolITO	MSU_PolITO	MSU_PolITO	MSU_PolITO	MSU_PolITO	MSU_PolITO	MSU_PolITO	MSU_PolITO	MSU_PolITO	MSU_PolITO	MSU_PolITO	MSU_PolITO	MSU_PolITO	MSU_PolITO	MSU_PolITO	
Thickness, t [mm]	55	53	51	49	49	49	50	50	53	54	52	50	50	51	51	50	
Length, l [mm]	57	60	59	59	59	59	59	59	59	60	58	59	59	59	60	60	
Delta from optimum A_{lig} [%]	6.27%	7.80%	2.00%	2.00%	2.00%	2.00%	0.00%	6.00%	9.83%	2.24%	0.00%	14.00%	3.73%	1.69%			
Ligament Area, A_{lig} [mm ²]	3135.0	3180.0	3009.0	2891.0	2891.0	2891.0	2950.0	3127.0	3240.0	3016.0	2950.0	3363.0	3060.0	3000.0			
Fracture Energy, G_f [J/m ²]	1359.2	1236.7	1256.1	1287.1	1287.1	1546.0	1959.9	1764.7	1773.9	2234.3	1886.1	2154.3	1889.5	1680.9			
Slope, m [kN/mm]	26.4	12.1	12.6	15.1	15.1	3.0	1.8	2.7	3.0	2.3	5.0	3.5	1.8	3.3			
Flexibility Index	0.5	1.0	1.0	0.9	0.9	5.2	10.7	6.5	5.9	9.8	3.7	6.1	10.3	5.1			
Method of data processing ⁽³⁾	ILLI	ILLI	ILLI	ILLI	ILLI	ILLI	ILLI	ILLI	ILLI	ILLI	ILLI	ILLI	ILLI	ILLI	ILLI	ILLI	
Sample availability ⁽⁴⁾	Y	Y	Y	Y	Y	Y	Y	Y	Y	Y	Y	Y	Y	Y	Y	Y	
AVG Fracture Energy, G_f [J/m ²]	1284.76						1761.12						2060.20		1908.24		
STDEV Fracture Energy, G_f [J/m ²]	53.77						169.29						246.17		237.26		
CV Fracture Energy, G_f [%]	4.2%						9.6%						11.9%		12.4%		
AVG Flexibility Index	0.85						7.06						6.79		7.14		
STDEV Flexibility Index	0.23						2.46						4.31		2.76		
CV Flexibility Index	27.1%						34.8%						63.5%		38.7%		

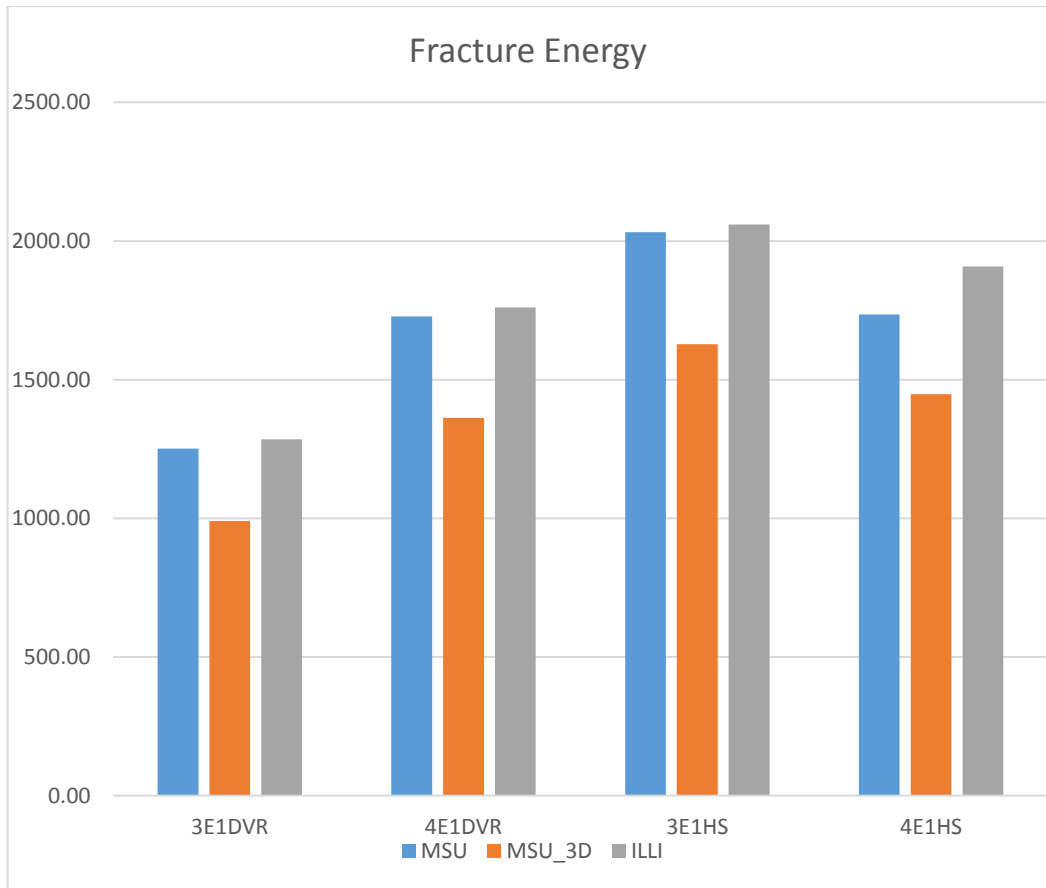


Figure 59: Fracture Energy average for each SCB data analysis model

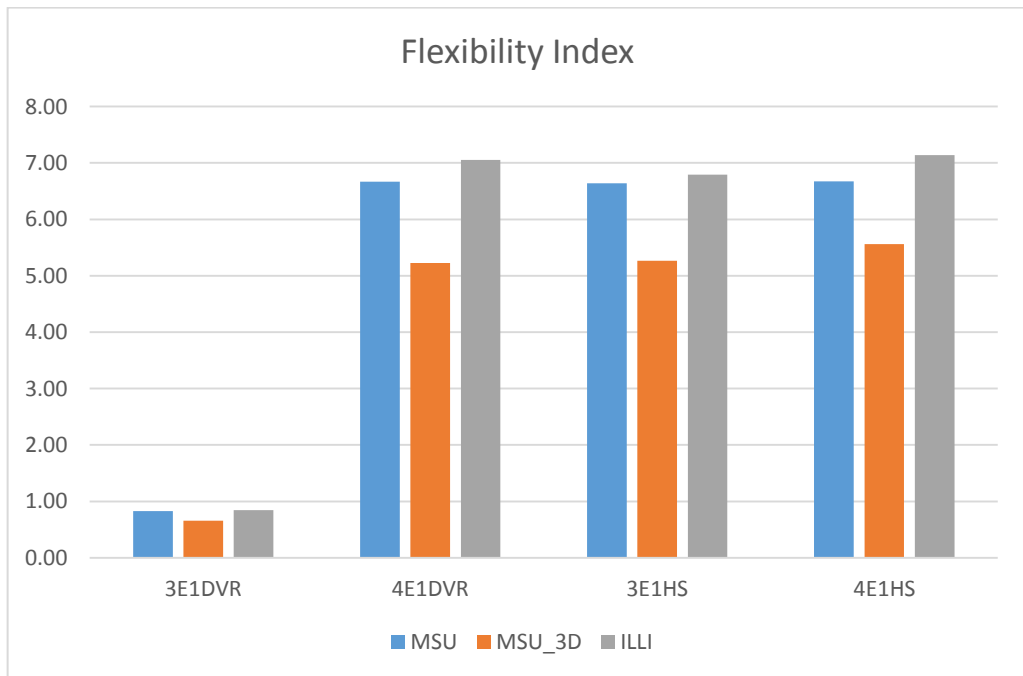


Figure 60: Flexibility Index average for each SCB data analysis model

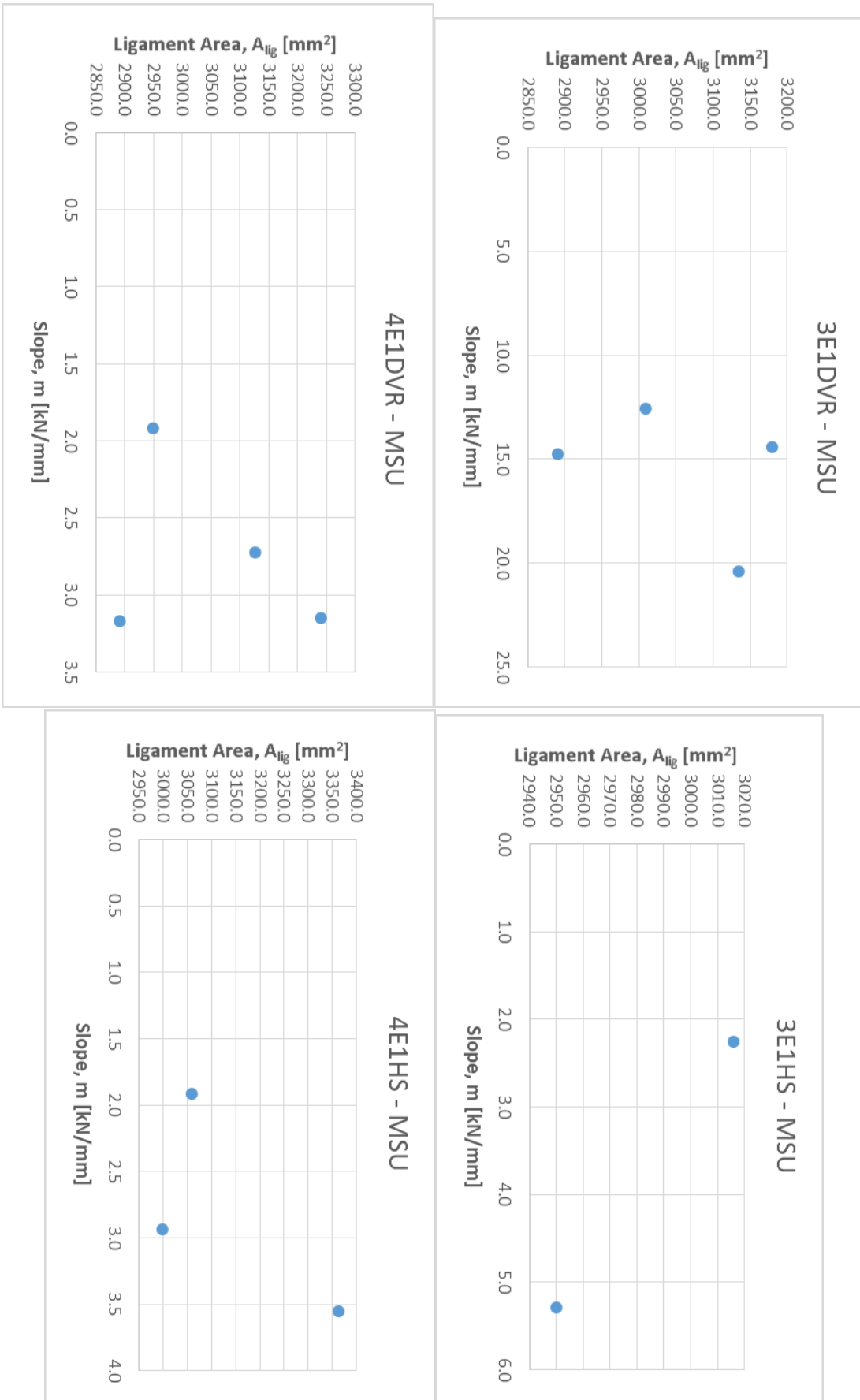


Figure 61: Slope vs. Ligament Area, MSU model

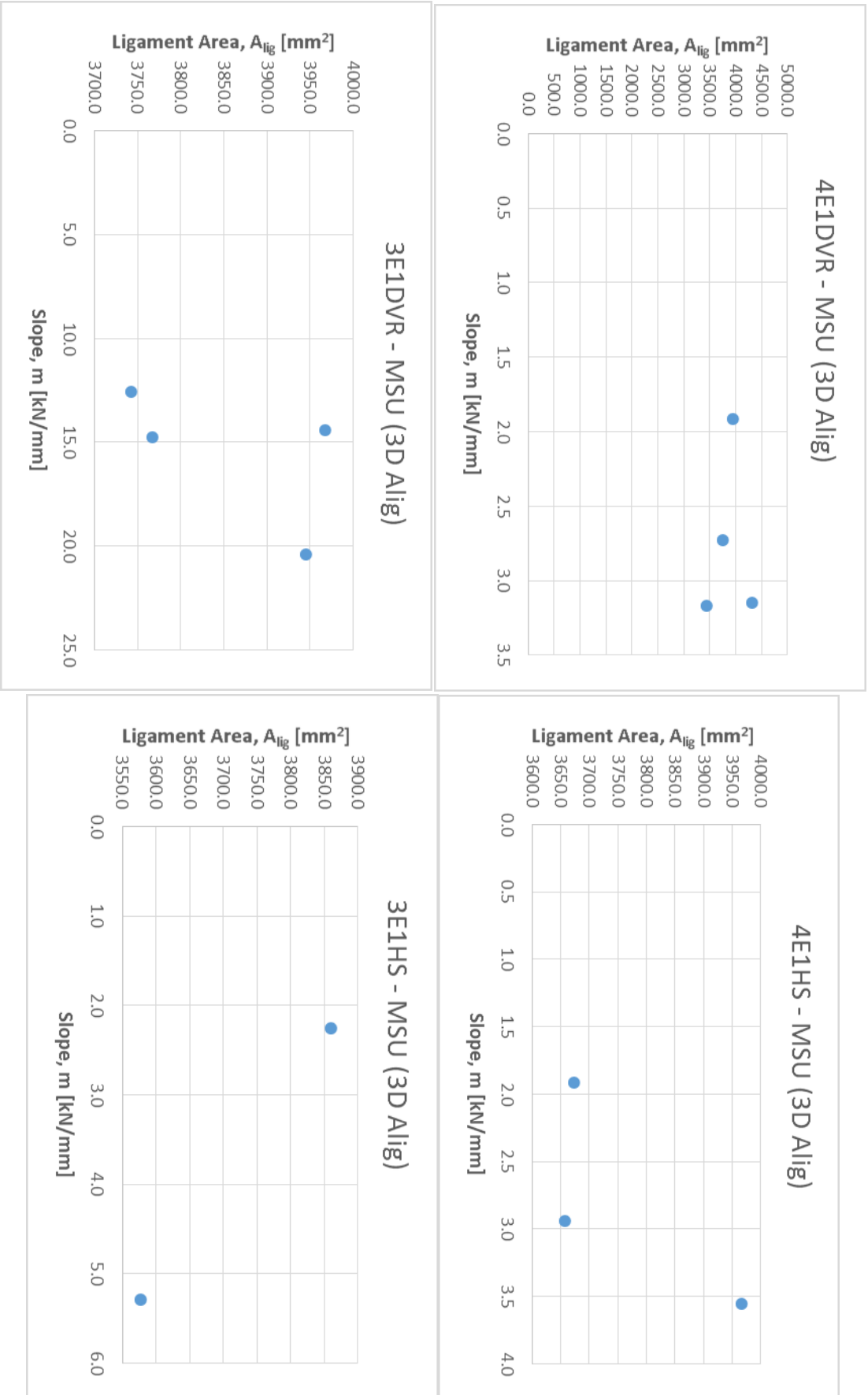


Figure 62: Slope vs. Ligament Area, MSU model with 3D analysis

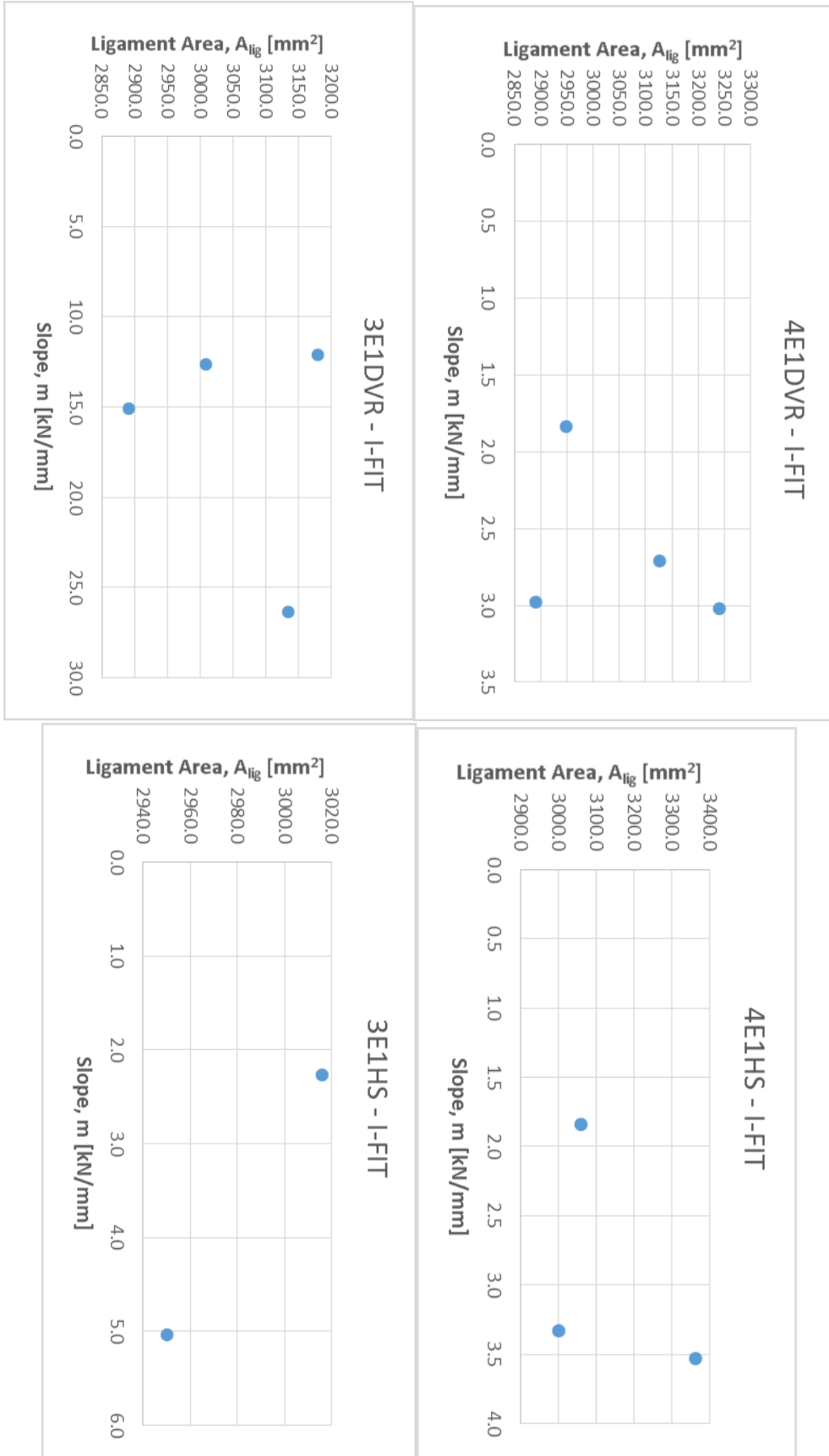


Figure 63: Slope vs. Ligament Area, IFIT model

6 CONCLUSIONS AND FUTURE RESEARCH

After the whole process of testing, data gathering, data analysis and comparison of results developed in the last chapter some conclusions can be made about the three aspects of mixtures' advanced characterization stated in the objectives of this dissertation.

First of all, the main aspect taken into consideration for this dissertation was to define if it would be possible to use DVR+SBS modified binders instead of only SBS ones to cut on costs and environmental impact: the results show that asphalt mixtures developed with these innovative modified binders react with no or little differences to permanent deformation and, if future fatigue cracking tests will confirm the results, they can be used widely for the construction of new flexible pavements with all the improvements stated before.

Changing the climate station to a much warmer environment like Arizona has not changed much in the results: a slight increase of permanent deformation has been noted in the asphalt layers, but only of tenths of millimeters, and still far from the predicted strain for 20 years of design life.

Results of DVR and HS samples left in water for 40 days have not shown many differences from the unconditioned ones: looking at the ME software reports and at the AMPT tests they all seem the same mixture (respectively DVR or HS) over and over. More advanced moisture damage characterization and tests (like Indirect Tensile Strength) are due to better evaluate this parameter.

SCB results have confirmed that this kind of test cannot be used as the only one for the characterization of an asphalt mixture: in the Ligament Area – Slope graphs the results are scattered, coefficients of variation and errors are too high and no trend is visible for the results to be reliable. A more advanced characterization of the Ligament Area through photogrammetry does not help and results keep a low reliability.

All things considered, the characterization of these innovative mixtures is far from completed: more data on Dynamic Modulus, Flow Number and moisture damage are needed, and thermal cracking and fatigue cracking have not been taken at all into account in this dissertation.

A new research, that would run parallel to this one, could start from collecting data for the characterization of cracking resistance of the mixtures with Push-Pull and Indirect Tensile Strength tests, merging the E^* and FN data already gathered and

running again pavement simulations, this time putting some more “Input level 1” and refining the analysis more and more.

A second dissertation could be developed on the initial objective of this one: developing at Politecnico di Torino the same tests on the same mixtures produced using the DVR-modified binders but also high-quality aggregates and to evaluate the differences on the results.

Acknowledgments

Ai miei genitori, che non hanno mai smesso di credere in me.

A Lara, presente e futuro.

Ad Anna e Luca, famiglia.

Agli amici di Firenze, la cui determinazione e dedizione a fare ciò che amano mi hanno ispirato più di quanto loro credano.

Ad Anna e Andrea del Gruppo 5, per ogni difficoltà affrontata insieme con una risata anche alle 3 di notte.

To the research team at MSU for their warm welcome and pleasant stay.

Agli amici del primo anno persi di vista e a quelli con cui ho seguito l'ultima lezione, a chiunque mi abbia lasciato qualcosa nel mio cammino in questi anni al Politecnico.

Bibliography and sites visited

- AASHTO PP 60-14, 'Standard Practice for Preparation of Cylindrical Performance Test Specimens Using the Superpave Gyratory Compactor', 14 (2014)
- Al-qadi, Imad L, Hasan Ozer, John Lambros, Ahmad El Khatib, Punit Singhvi, Tamim Khan, and others, *Testing Protocols to Ensure Performance of High Asphalt Binder Replacement Mixes Using RAP and RAS*, 2015
- Bahia, H., and R Davis, 'Effect of Crumb Rubber Modifiers (CRMs) on Performance Related Properties of Asphalt Binders', *AAPT 1994*, 1994
- Bessert, Christopher J., 'Michigan Highways: Introduction', 2017
<<http://www.michiganhighways.org/introduction.html>> [accessed 24 October 2017]
- Bredberg, K., 'Sulphur-Utilizing Microorganisms in Biotechnological Applications—Rubber Recycling and Vanadium Reduction' (Lund University, 2003)
- Chehab, G.R: et al., 'Time–temperature Superposition Principle for Asphalt Concrete with Growing Damage in Tension State', *Journal of the Association of Asphalt Paving Technologists*, 2002, 559–93
- Goodrich, J.L., 'Asphaltic Binder Rheology, Asphalt Concrete Rheology and Asphalt Concrete Mix Properties (with Discussion)', *Journal of the Association of Asphalt Paving Technologists*, 60 (1991), 80–120
- Heitzman, M., 'Design and Construction of Asphalt Paving Materials with Crumb Rubber Modifier', *Transportation Research Record*, 1992
- Khosravifar, Sadaf, Intikhab Haider, Zahra Afsharikia, and Charles W Schwartz, 'Application of Time – Temperature Superposition to Develop Master Curves of Cumulative Plastic Strain in Repeated Load Permanent Deformation Tests', 8436 (2015)
<<https://doi.org/10.1080/10298436.2014.937810>>
- Kim, Y. Richard, 'Complex Modulus Characterization of Asphalt Concrete', in *Modeling of Asphalt Concrete* (McGraw-Hill Professional, 2009)
- Kim, Y. Richard, and Y. C. Lee, 'Interrelationships among Stiffnesses of Asphalt-Aggregate Mixtures (with Discussion)', *Journal of the Association of Asphalt Paving Technologists*, 64
- Kocak, S., & Kutay, M. E., 'Combined Effect of SBS and Devulcanized Rubber (DVR) Modification on Performance Grade and Fatigue Cracking Resistance of Asphalt Binders', in *8th RILEM International Conference on Mechanisms of Cracking and Debonding in Pavements* (Springer Netherlands, 2016), pp. 269–74
- Lanotte, Michele, and M Emin Kutay, *Evaluation of De-Vulcanized Rubber (DVR) Modified Hot Mix Asphalt (HMA) Pavement*, 2017
- Liu, Xiang, Xiaolong Zou, Xiaolong Yang, and Zhengwei Zhang, 'Effect of Material Composition on Antistripping Performance of SBS Modified Asphalt Mixture under Dry and Wet Conditions', *Journal of Adhesion Science and Technology*, 4243 (2018), 1–14
<<https://doi.org/10.1080/01694243.2018.1426973>>
- 'Michigan Average Climate Data', 2018
<<https://www.usclimatedata.com/climate/michigan/united-states/3192#>> [accessed 21 March 2018]
- Okuda, M., and Y. Hatano, 'Japanese Patent Application 62,121,741', 1987
- Ozdemir, U., Hibner, D., Kutay, M. E., and Lanotte, M., 'Image Processing Techniques For

- Determination Of Aggregate Embedment Depth In Chip Seals', in *96th Transportation Research Board Annual Meeting* (Washington, D.C., 2017)
- Ozer, Hasan, Imad L Al-qadi, John Lambros, Ahmad El-khatib, Punit Singhvi, and Berangere Doll, 'Development of the Fracture-Based Flexibility Index for Asphalt Concrete Cracking Potential Using Modified Semi-Circle Bending Test Parameters', *Construction and Building Materials*, 115 (2016), 390–401
<<https://doi.org/10.1016/j.conbuildmat.2016.03.144>>
- Ozturk, H.I. and Kutay, M.E., 'Effect of Foamed Binder Characteristics on Warm Mix Asphalt (WMA) Performance', in *Proceedings of 93rd Annual Transportation Research Board Conference* (Washington, D.C., 2014)
- 'Percentage of Roads in Good or Fair Condition on the Paved Federal Aid System | Michigan - Open Performance' <midashboard.michigan.gov/Infrastructure-Dashboard/Percentage-of-Roads-in-Good-or-Fair-Condition-on-t/wzdb-93qv> [accessed 24 October 2017]
- Presti, Davide Lo, 'Recycled Tyre Rubber Modified Bitumens for Road Asphalt Mixtures : A Literature Review Q', *Construction and Building Materials*, 49 (2013), 863–81
<<https://doi.org/10.1016/j.conbuildmat.2013.09.007>>
- Sato, S., 'DeVulcanization of Polyisoprene Rubbers by Wood Rot Fungi' (Prague, Czech Republic, 2003) <<https://www.imc.cas.cz/sympo/42micros/poster1.htm#P09>>
- Schapery, R. A., 'Nonlinear Viscoelastic and Viscoplastic Constitutive Equations with Growing Damage', *International Journal of Fracture*, 1999, 33–66
- Total Michigan Mileage*, 2017
- Tzoganakis, C., and M. Meysami, 'Thermo-mechanical Devulcanization of Tire Rubber Crumb with Supercritical CO₂: Devulcanized Rubber Properties', *IPR*, 2009
- Yoder, E. J., and M. W. Witczak, *Principles of Pavement Design* (John Wiley & Sons, 1975)
- Yu, Huayang, Zhen Leng, Zejiao Dong, Zhifei Tan, Feng Guo, and Jinhai Yan, 'Workability and Mechanical Property Characterization of Asphalt Rubber Mixtures Modified with Various Warm Mix Asphalt Additives', *Construction and Building Materials*, 175 (2018), 392–401 <<https://doi.org/10.1016/j.conbuildmat.2018.04.218>>
- Zanetti, M C, S Fiore, B Ruffino, E Santagata, D Dalmazzo, and M Lanotte, 'Characterization of Crumb Rubber from End-of-Life Tyres for Paving Applications', *Waste Management*, 45 (2015), 161–70 <<https://doi.org/10.1016/j.wasman.2015.05.003>>

APPENDIX

Gmm determination

3E1 DVR			
Sample A		Sample B	
Mold Empty in Air [gr]	2112.7	Mold Empty in Air [gr]	2006.5
Mold Filled in Air [gr]	4146.2	Mold Filled in Air [gr]	4486.1
Mold + Mixture in Water [gr]	2567	Mold + Mixture in Water [gr]	2765
Mold Empty in Water [gr]	1352.3	Mold Empty in Water [gr]	1282.5
Mass of sample in air [gr]	2033.5	Mass of sample in air [gr]	2479.6
Mass of water displaced by sample [gr]	1214.7	Mass of water displaced by sample [gr]	1482.5
Theoretical max. specific gravity, Gmm:	2.484	Theoretical max. specific gravity, Gmm:	2.487

4E1 DVR			
Sample A		Sample B	
Mold Empty in Air [gr]	2112.7	Mold Empty in Air [gr]	2006.5
Mold Filled in Air [gr]	3706.8	Mold Filled in Air [gr]	3637.7
Mold + Mixture in Water [gr]	2294.1	Mold + Mixture in Water [gr]	2250.1
Mold Empty in Water [gr]	1352.3	Mold Empty in Water [gr]	1282.5
Mass of sample in air [gr]	1594.1	Mass of sample in air [gr]	1631.2
Mass of water displaced by sample [gr]	941.8	Mass of water displaced by sample [gr]	967.6
Theoretical max. specific gravity, Gmm:	2.444	Theoretical max. specific gravity, Gmm:	2.458

3E1HS			
Sample A		Sample B	
Mold Empty in Air [gr]	2112.4	Mold Empty in Air [gr]	2006.6
Mold Filled in Air [gr]	3801	Mold Filled in Air [gr]	3543
Mold + Mixture in Water [gr]	2362.6	Mold + Mixture in Water [gr]	2197.5
Mold Empty in Water [gr]	1352.3	Mold Empty in Water [gr]	1282.5
Mass of sample in air [gr]	1688.6	Mass of sample in air [gr]	1536.4
Mass of water displaced by sample [gr]	1010.3	Mass of water displaced by sample [gr]	915
Theoretical max. specific gravity, Gmm:	2.489	Theoretical max. specific gravity, Gmm:	2.472

4E1HS			
Sample A		Sample B	
Mold Empty in Air [gr]	2112.8	Mold Empty in Air [gr]	2007.8
Mold Filled in Air [gr]	3836.2	Mold Filled in Air [gr]	3877.1
Mold + Mixture in Water [gr]	2328	Mold + Mixture in Water [gr]	2340.4
Mold Empty in Water [gr]	1352.3	Mold Empty in Water [gr]	1282.5
Mass of sample in air [gr]	1723.4	Mass of sample in air [gr]	1869.3
Mass of water displaced by sample [gr]	975.7	Mass of water displaced by sample [gr]	1057.9
Theoretical max. specific gravity, Gmm:	2.305	Theoretical max. specific gravity, Gmm:	2.304

Sieve analyses after ignition test

3E1 DVR					
Sieve	Retained	Retained _{prog}	Retained _{prog}	Passing _{prog}	JMF_Passing _{prog}
(mm)	(g)	(g)	(%)	(%)	(%)
19	0	0	0	100.00	100
12.5	183.8	183.8	9.07	90.93	89.2
9.5	158.6	342.4	16.89	83.11	85.2
4.75	358	700.4	34.56	65.44	66.1
2.36	444.9	1145.3	56.51	43.49	44.6
1.18	254.2	1399.5	69.05	30.95	30.6
0.6	212.6	1612.1	79.54	20.46	20.1
0.3	203.8	1815.9	89.59	10.41	10.5
0.15	85.8	1901.7	93.83	6.17	6.5
0.075	39.2	1940.9	95.76	4.24	4.9
Bottom+washed	85.9	2026.8	100.00	0.00	0
Total	2026.8	2026.8			

4E1 DVR					
Sieve	Retained	Retained _{prog}	Retained _{prog}	Passing _{prog}	JMF_Passing _{prog}
(mm)	(g)	(g)	(%)	(%)	(%)
19	0	0	0	100.00	100
12.5	23.1	23.1	1.66	98.34	99.3
9.5	159.1	182.2	13.11	86.89	89.4
4.75	310.9	493.1	35.49	64.51	65.9
2.36	181.6	674.7	48.56	51.44	53.3
1.18	150.5	825.2	59.40	40.60	40.9
0.6	172.2	997.4	71.79	28.21	28.4
0.3	214.2	1211.6	87.21	12.79	12.9
0.15	101.1	1312.7	94.49	5.51	6.2
0.075	27.3	1340	96.45	3.55	4.5
Bottom	49.3	1389.3	100.00	0.00	0
Total	1389.3	1389.3	-	-	

3E1 HS					
Sieve	Retained	Retained _{prog}	Retained _{prog}	Passing _{prog}	JMF Passing _{prog}
(mm)	(g)	(g)	(%)	(%)	(%)
19	0	0	0	100	100
12.5	206.1	206.1	10.10	89.90	89.2
9.5	145.6	351.7	17.23	82.77	85.2
4.75	388.7	740.4	36.27	63.73	66.1
2.36	421.9	1162.3	56.93	43.07	44.6
1.18	266	1428.3	69.96	30.04	30.6
0.6	218.9	1647.2	80.68	19.32	20.1
0.3	200.1	1847.3	90.48	9.52	10.5
0.15	74.8	1922.1	94.15	5.85	6.5
0.075	34	1956.1	95.81	4.19	4.9
Bottom	85.5	2041.6	100.00	0.00	0
Total	2041.6	2041.6			

4E1 HS					
Sieve	Retained	Retained _{prog}	Retained _{prog}	Passing _{prog}	JMF Passing _{prog}
(mm)	(g)	(g)	(%)	(%)	(%)
19	0	0	0	100	100
12.5	47.1	47.1	2.54	97.46	99.3
9.5	251.4	298.5	16.08	83.92	89.4
4.75	446.6	745.1	40.13	59.87	65.9
2.36	219.2	964.3	51.93	48.07	53.3
1.18	181.6	1145.9	61.71	38.29	40.9
0.6	207.3	1353.2	72.88	27.12	28.4
0.3	279.2	1632.4	87.91	12.09	12.9
0.15	127.1	1759.5	94.76	5.24	6.2
0.075	36	1795.5	96.70	3.30	4.5
Bottom	61.3	1856.8	100.00	0.00	
Total	1856.8	1856.8	-	-	

Air voids content – E and FN samples*

3E1 DVR								
ID	A	B	C	T	ρ_w	Gmb	Gmm	v@Nmax
[-]	[g]	[g]	[g]	[°C]	[kg/m ³]	[kg/m ³]	[kg/m ³]	[%]
II	2815.0	1613.0	2822.9	21.1	998.0	2322	2485	6.6
III	2828.0	1615.0	2834.4	21.1	998.0	2315	2485	6.9
IV	2830.0	1616.5	2837.3	21.1	998.0	2314	2485	6.9
V	2835.5	1642.6	2863.2	21.1	998.0	2318	2485	6.7
VI	2811.0	1614.7	2823.1	20.9	998.1	2322	2485	6.6
VII	2860.7	1636.9	2871.9	21.4	998.0	2312	2485	7.0

4E1 DVR								
ID	A	B	C	T	ρ_w	Gmb	Gmm	v@Nmax
[-]	[g]	[g]	[g]	[°C]	[kg/m ³]	[kg/m ³]	[kg/m ³]	[%]
I	2821.0	1600.1	2832.5	20.8	998.1	2285	2451	6.8
II	2817.6	1598.2	2829.1	21.1	998.0	2285	2451	6.8
III	2778.2	1577.6	2788.4	21.1	998.0	2290	2451	6.6
IV	2786.2	1576.4	2797.4	21.3	998.0	2277	2451	7.1
V	2806.8	1586.4	2819.1	21.3	998.0	2272	2451	7.3
VI	2779.0	1570.8	2791.0	21.1	998.0	2273	2451	7.3

3E1 HS								
ID	A	B	C	T	ρ_w	Gmb	Gmm	v@Nmax
[-]	[g]	[g]	[g]	[°C]	[kg/m ³]	[kg/m ³]	[kg/m ³]	[%]
I	2796.2	1593.1	2806.1	20.9	998.1	2301	2481	7.3
II	2789.9	1596.0	2805.3	21	998.1	2303	2481	7.2
III	2799.8	1602.1	2813.5	21	998.1	2307	2481	7.0
IV	2811.7	1604.0	2818.7	20.9	998.1	2310	2481	6.9
V	2847.7	1626.9	2858.5	20.9	998.1	2308	2481	7.0
VI	2847.4	1629.0	2855.0	21.1	998.0	2318	2481	6.6

4E1 HS								
ID	A	B	C	T	ρ_w	Gmb	Gmm	v@Nmax
[-]	[g]	[g]	[g]	[°C]	[kg/m ³]	[kg/m ³]	[kg/m ³]	[%]
I	2756.3	1570.0	2763.1	21	998.1	2306	2475	6.8
II	2809.0	1597.6	2813.0	20.9	998.1	2307	2475	6.8
III	2753.6	1570.9	2760.5	21.2	998.0	2310	2475	6.7
IV	2771.7	1582.0	2780.0	20.8	998.1	2309	2475	6.7
V	2796.8	1598.5	2807.7	21	998.1	2308	2475	6.7
VI	2783.8	1589.0	2792.8	20.8	998.1	2308	2475	6.7

Air voids content – SCB samples

4E1 DVR SCB										
ID	A	B	C	T	ρ_w	Gmb	Gmm	$v@N_{max}$		
-I-	[g]	[g]	[g]	[°C]	[kg/m ³]	[kg/m ³]	[kg/m ³]	[%]		
I	1974.2	1121.0	1985.0	20.7	998.1	2281	2451	6.9		
II	2129.5	1206.0	2140.5	20.8	998.1	2274	2451	7.2		
IA	956.4	541.0	959.1	20.7	998.1	2283	2451	6.8		
IB	983.1	557.5	986.3	20.8	998.1	2288	2451	6.6		
IIA	1022.3	576.0	1026.0	20.8	998.1	2267	2451	7.5		
IIIB	1070.3	605.0	1073.4	20.8	998.1	2281	2451	6.9		
III	2214.4	1259.0	2225.0	20.9	998.1	2288	2451	6.7		
IV	2019.5	1143.6	2030.0	20.8	998.1	2274	2451	7.2		
IIIA	1076.0	609.0	1079.3	20.9	998.1	2284	2451	6.8		
IIIB	1098.4	625.3	1103.0	21	998.1	2295	2451	6.4		
IVA	1015.8	575.2	1020.0	21	998.1	2279	2451	7.0		
IVB	967.6	545.8	971.8	21	998.1	2267	2451	7.5		

3E1 HS										
ID	A	B	C	T	ρ_w	Gmb	Gmm	$v@N_{max}$		
-I-	[g]	[g]	[g]	[°C]	[kg/m ³]	[kg/m ³]	[kg/m ³]	[%]		
I	2049.7	1176.8	2064.1	20.4	998.2	2306	2481	7.1		
II	2031.0	1166.5	2047.7	20.5	998.2	2301	2481	7.3		
IA	1013.0	577.0	1018.0	20.6	998.2	2293	2481	7.6		
IB					1000.3		2481			
IIA	991.0	566.7	996.7	20.4	998.2	2300	2481	7.3		
IIIB	1004.5	575.9	1012.0	20.5	998.2	2299	2481	7.3		
III	2138.7	1230.0	2156.5	20.6	998.2	2304	2481	7.1		
IV	2094.8	1203.0	2114.0	20.8	998.1	2295	2481	7.5		
IIIA	1035.6	591.0	1040.3	20.8	998.1	2301	2481	7.3		
IIIB	1063.9	610.0	1069.3	20.8	998.1	2312	2481	6.8		
IVA	1010.1	577.7	1016.0	20.8	998.1	2300	2481	7.3		
IVB	1046.4	601.1	1056.3	20.8	998.1	2294	2481	7.5		

3E1 DVR SCB										
ID	A	B	C	T	ρ_w	Gmb	Gmm	$v@N_{max}$		
-I-	[g]	[g]	[g]	[°C]	[kg/m ³]	[kg/m ³]	[kg/m ³]	[%]		
I	2162.0	1246.8	2175.0	21.2	998.0	2325	2485	6.5		
II	2007.9	1161.8	2026.3	21.2	998.0	2318	2485	6.7		
IA	1060.3	609.5	1064.9	21	998.1	2324	2485	6.5		
IB	1061.3	610.0	1065.8	21	998.1	2324	2485	6.5		
IIA	976.1	558.6	980.6	21	998.1	2309	2485	7.1		
IIIB	994.2	572.2	999.1	21	998.1	2324	2485	6.5		
III	2010.7	1152.9	2022.0	20.4	998.2	2309	2485	7.1		
IV	2061.7	1180.0	2073.9	20.4	998.2	2302	2485	7.4		
IIIA	1010.1	575.8	1013.5	20.8	998.1	2303	2485	7.3		
IIIB	964.7	550.3	967.5	20.9	998.1	2308	2485	7.1		
IVA	1018.0	580.5	1021.3	20.7	998.1	2305	2485	7.2		
IVB	1006.6	571.4	1009.5	20.8	998.1	2293	2485	7.7		

4E1 HS										
ID	A	B	C	T	ρ_w	Gmb	Gmm	$v@N_{max}$		
-I-	[g]	[g]	[g]	[°C]	[kg/m ³]	[kg/m ³]	[kg/m ³]	[%]		
I	2071.5	1178.3	2076.5	20.4	998.2	2302	2475	7.0		
II	2056.4	1167.4	2062.2	20.5	998.2	2294	2475	7.3		
IA	1023.0	584.0	1026.7	20.5	998.2	2307	2475	6.8		
IB	1011.5	575.0	1015.0	20.5	998.2	2295	2475	7.3		
IIIB	997.2	568.1	999.9	20.7	998.1	2305	2475	6.9		
III	2197.3	1256.0	2205.3	20.8	998.1	2310	2475	6.7		
IV	2085.2	1187.6	2093.0	20.8	998.1	2299	2475	7.1		
IIIA	1092.5	623.9	1096.3	20.8	998.1	2308	2475	6.7		
IIIB	1065.0	608.0	1068.7	20.8	998.1	2307	2475	6.8		
IVA	1021.0	579.4	1023.0	20.8	998.1	2297	2475	7.2		
IVB	1027.0	584.0	1030.0	20.8	998.1	2298	2475	7.1		

*E** tests: AMPT data for 3E1 DVR DROWNED samples

Replicate 1													Replicate 2													Replicate 3												
40°C													20°C													40°C												
Frequency													Frequency													Frequency												
25 Hz	10 Hz	5 Hz	1 Hz	0.5 Hz	0.1 Hz	25 Hz	10 Hz	5 Hz	1 Hz	0.5 Hz	0.1 Hz	25 Hz	10 Hz	5 Hz	1 Hz	0.5 Hz	0.1 Hz	25 Hz	10 Hz	5 Hz	1 Hz	0.5 Hz	0.1 Hz															
Dynamic modulus (MPa)	19232	17557	16306	13554	12348	9766	9326	7858	6847	4785	4074	2676	8111	6759	5833	3988	3367	2141	12248	10870	9899	7842	7050	5338														
Phase angle (Degrees)	7.94	8.79	9.52	11.54	12.65	15.49	17.26	19.1	20.42	23.76	24.81	27.63	18.26	20.26	21.69	25.27	26.27	29.09	11.74	12.75	13.53	15.61	16.53	19														
Average temperature (°C)	4	4	4	3.9	3.9	3.7	19.9	20	0.1	0.2	0.2	0.2	19.6	19.7	19.6	19.8	19.9	19.9	19.8	19.9	19.9	19.8	19.8	19.8														
Average confining pressure (kPa)	0.4	0.4	0.4	0.4	0.4	0.4	0.2	0.1	0.2	0.2	0.2	0.2	0.2	0.1	0.2	0.2	0.2	0.2	0.2	0.2	0.2	0.2	0.2	0.1														
Average micro-strain	57	64	71	85	94	102	91	94	96	96	97	97	91	94	95	96	97	97	88	86	86	97	98	99														
Load drift (%)	-0.3	0.3	0.5	0	0	0	-0.1	0.5	0.6	0	0	0	-0.2	0.4	0.6	0	0	0	-0.2	0.4	0.6	0.1	0.1	0														
Load standard error (%)	3.6	1.2	0.9	0.4	0.3	0.3	3.5	1.5	1	0.5	0.3	0.2	3.3	1.7	0.9	0.5	0.3	0.2	3.5	1.2	0.8	0.5	0.5	0.3														
Average deformation drift (%)	-23.6	-26.2	-28.3	-41.2	-42.4	-73.4	-102.5	-115.6	-112.1	-133.8	-122.2	-138.9	-119.2	-140.5	-137.4	-164.9	-148.1	-174.6	-39.5	-43.7	-41.3	-53.2	-49.4	-71.6														
Average deformation standard error (%)	4.4	2.2	1.5	1.2	1	1.3	3.6	2.9	2.3	2	1.6	2.2	3.8	3.3	2.6	2.3	1.8	3.1	3.5	1.9	1.5	1.4	1.4	1.6														
Deformation uniformity (%)	14.5	12	10.3	8.5	6.7	5	3.7	3	2.7	2.2	1.9	1.5	19.2	19.3	19.2	18.6	18.7	18.5	9.6	10.1	10.3	11.1	11.4	12.3														
Phase uniformity (Degrees)	0.3	0.3	0.2	0.3	0.3	0.4	0.5	0.4	0.5	0.7	0.7	0.9	0.3	0.4	0.5	0.5	0.5	0.7	0.8	0.9	0.9	1	1.1	1.2														
40°C													20°C													40°C												
Frequency													Frequency													Frequency												
25 Hz	10 Hz	5 Hz	1 Hz	0.5 Hz	0.1 Hz	25 Hz	10 Hz	5 Hz	1 Hz	0.5 Hz	0.1 Hz	25 Hz	10 Hz	5 Hz	1 Hz	0.5 Hz	0.1 Hz	25 Hz	10 Hz	5 Hz	1 Hz	0.5 Hz	0.1 Hz															
Dynamic modulus (MPa)	3213	2416	1915	1076	844.3	461.7	3273	2416	1915	1076	844.3	2793	2075	1640	905.2	711	388	5013	4115	3564	2428	2107	1379															
Phase angle (Degrees)	29.5	30.58	31.11	31.92	31.24	40.1	30.48	31.61	32.05	32.52	31.66	30.33	31.98	32.61	33.05	32.52	31.66	30.33	21.9	23.24	23.94	26.21	26.54	28.15														
Average temperature (°C)	40	40	40.1	40.2	40.3	40.1	40	40	40	40.1	40.2	40.1	40	40	40.1	40.1	40.2	40.1	39.9	39.9	39.9	39.9	39.9	39.9														
Average confining pressure (kPa)	0	0	0	0	0	0	0	0	0	0	0	0	0	0	0	0	0	0	0	0	0	0	0	0														
Average micro-strain	86	86	91	95	96	99	84	85	85	90	95	96	84	85	85	90	95	99	92	90	92	92	94	93														
Load drift (%)	0.1	0.4	0.9	0.1	0	0	0.1	0.4	0.4	1	0.2	0.1	0.3	0.4	0.4	0.2	0	0.1	-0.3	0.4	0.9	0.1	0.2	0														
Load standard error (%)	4	2.7	1.6	0.7	0.4	0.4	4.2	3	3	1.8	0.8	0.5	3.8	2.5	1.3	0.5	0.5	0.5	3.8	2.5	1.3	0.5	0.5	0.3														
Average deformation drift (%)	-313.6	-258.5	-197.8	-135.1	-100.4	-46.1	-319.8	-260.2	-196.1	-125.5	-92.6	-50.4	-104.3	-118.3	-107.3	-109.5	-101.9	-110.7	4.1	4	2.9	2.5	2.7	3.1														
Average deformation standard error (%)	7.4	6	4.2	2.8	2.9	3.8	7.5	6.1	4.4	2.9	3.1	4.2	6.5	6.4	6.2	6.1	5.7	5.4	6.5	6.4	6.2	6.1	5.7	5.4														
Deformation uniformity (%)	9.2	8.8	8.5	7.9	7.5	5.8	11.3	11.9	12.5	13.7	14.7	16	0.8	0.8	0.7	0.5	0.4	0.3	0.8	0.8	0.7	0.5	0.4	0.1														
Phase uniformity (Degrees)	0.9	1	0.9	0.7	0.6	0.7	0.7	0.7	0.7	0.5	0.4	0.3	0.7	0.7	0.7	0.5	0.4	0.3	0.8	0.8	0.7	0.5	0.4	0.1														

*E** tests: AMPT data for 3E1 HS DRY samples

	Replicate 1										Replicate 2										Replicate 3									
	Frequency										Frequency										Frequency									
	25 Hz	10 Hz	5 Hz	1 Hz	0.5 Hz	0.1 Hz	0.1 Hz	0.5 Hz	1 Hz	5 Hz	25 Hz	10 Hz	5 Hz	1 Hz	0.5 Hz	0.1 Hz	0.1 Hz	0.5 Hz	1 Hz	5 Hz	25 Hz	10 Hz	5 Hz	1 Hz	0.5 Hz	0.1 Hz	0.1 Hz	0.5 Hz	1 Hz	5 Hz
40°C																														
Dynamic modulus (MPa)	16385	14867	13747	11130	10052	7650	16880	15388	14265	11662	10562	8163	16622	15182	14136	11649	10579	8245												
Phase angle (Degrees)	9.31	10.42	11.41	14.16	15.45	18.81	8.65	9.61	10.43	12.82	13.93	16.93	8.38	9.34	10.12	12.37	13.42	16.16												
Average temperature (°C)	4.2	4.2	4.2	4.1	4	3.6	4.3	4.2	4.2	4.1	3.9	3.6	4.4	4.3	4.3	4.2	4.2	3.9	3.5											
Average confining pressure (kPa)	0.3	0.3	0.3	0.3	0.3	0.3	0.3	0.3	0.3	0.3	0.3	0.3	0.3	0.3	0.3	0.3	0.3	0.3	0.3											
Average micro-strain	66	76	84	97	98	99	64	73	81	99	99	101	65	74	81	98	99	101												
Load drift (%)	-0.2	0.3	0.5	0.1	0	0	-0.4	0.3	0.5	0	0	0	-0.4	0.2	0.5	0.1	0	0												
Load standard error (%)	3.6	1.3	0.9	0.4	0.3	0.3	3.9	1.3	0.7	0.4	0.3	0.3	3.5	1.2	1	0.4	0.3	0.3												
Average deformation drift (%)	-33.5	-39.8	-41.6	-64.7	-58.6	-86.3	-27.6	-31.8	-32	-51.8	-46.5	-75.8	-28.6	-29.9	-30.2	-46.9	-41.9	-70.5												
Average deformation standard error (%)	3.4	1.6	1.4	1.4	1.2	1.5	3.9	1.8	1.3	1.3	0.9	1	3.5	1.9	1.6	1.4	1.3	1.5												
Deformation uniformity (%)	4.2	3.6	2.1	0.9	0.5	1.6	36.8	37.1	37.2	37.3	37.2	37.4	32.3	31.9	31.3	30.3	29.7	30.5												
Phase uniformity (Degrees)	0.6	0.5	0.5	0.6	0.6	0.6	0.2	0.1	0	0.2	0.3	0.6	0.4	0.4	0.4	0.5	0.7	0.8	1.2											
20°C																														
Dynamic modulus (MPa)	8248	6826	5649	3861	3189	1919	8820	7389	6390	4399	3703	2341	8700	7269	6278	4348	3676	2353												
Phase angle (Degrees)	19.45	21.59	23.06	26.59	27.52	29.65	17.59	19.49	20.9	24.39	25.38	28.01	17.17	19.06	20.46	23.86	24.9	27.69												
Average temperature (°C)	19.8	19.9	19.9	19.9	19.8	19.9	19.9	19.8	19.8	19.6	19.6	19.9	20	20	20	19.8	19.7	19.9												
Average confining pressure (kPa)	0.2	0	0.2	0	0	0	0	0.1	0.1	0	0	0	0	0	0	0	0	0												
Average micro-strain	90	92	94	95	97	99	91	94	96	96	98	99	92	95	96	96	97	98	98											
Load drift (%)	-0.3	0.4	0.7	0	0.1	0	-0.1	0.3	0.7	0	0.1	0	-0.4	0.3	0.7	0.1	0	0												
Load standard error (%)	3.1	1.6	1.1	0.5	0.3	0.3	3.8	1.6	0.9	0.5	0.3	0.3	4	1.7	0.9	0.5	0.3	0.3												
Average deformation drift (%)	-148	-164.6	-149.7	-153.8	-128.2	-115	-121.6	-132	-122.2	-131.3	-108.9	-96.1	-110	-119.2	-112.4	-125.9	-110.1	-113.9												
Average deformation standard error (%)	4.1	3.9	3	2.4	1.8	2	4.3	3.3	2.5	2.2	1.6	1.8	4.6	3.1	2.4	2.4	1.5	1.7												
Deformation uniformity (%)	2.7	3.7	4.7	6.5	6.9	9.6	19.9	19.4	18.9	18.4	17.8	17.7	28.4	27.7	26.9	26.8	26.4	26.4												
Phase uniformity (Degrees)	0.7	0.9	1	1.2	1.2	1.4	0.1	0.1	0.2	0.1	0.1	0.1	0.6	0.7	0.6	0.6	0.7	0.4												
40°C																														
Dynamic modulus (MPa)	2252	1608	1249	653.7	503.7	274.5	2549	1863	1475	814.3	644.9	365.2	2570	1915	1519	840.4	666.3	367.1												
Phase angle (Degrees)	32.25	32.84	32.58	31.96	30.96	28.86	30.6	31.7	31.67	31.43	30.27	28.21	30.46	31.47	31.83	32.24	31.36	30.14												
Average temperature (°C)	39.6	39.6	39.6	39.7	39.7	39.8	39.6	39.6	39.6	39.7	39.8	39.7	40.1	40.1	40.2	40.2	40.2	40.2												
Average confining pressure (kPa)	-0.1	0	0	0	0	0	-0.1	0.1	0	0	0	0	-0.1	0	0	0	0	0												
Average micro-strain	82	83	95	97	97	97	82	84	89	95	96	98	84	84	89	95	95	98												
Load drift (%)	0.1	0.1	1	0	0.2	0.1	-0.2	1.1	0.9	0.1	0	-0.1	-0.3	0.2	0.9	0.1	0.1	0												
Load standard error (%)	5.1	3.7	2.1	1	1.3	0.6	4.8	3.3	2	0.9	1	0.5	4.5	3	1.9	0.8	0.8	0.4												
Average deformation drift (%)	-287.3	-209.4	-153	-60.4	-44.8	16.9	-281.4	-229.7	-149.1	-75.9	-45.6	17.8	-285.6	-230.6	-172.2	-105.8	-79.2	-41.7												
Average deformation standard error (%)	8.2	6.4	4.4	3.4	4.1	4.4	8.1	7.2	4.2	3.3	3.7	4.4	7.8	6.1	4.2	3.2	3.3	4												
Deformation uniformity (%)	17.4	18	18.3	20.8	20.2	20.5	27.8	27.4	27.1	26.5	26	24.5	21.5	20.5	20.1	20.4	20	19.4												
Phase uniformity (Degrees)	1.1	1	0.9	0.6	0.5	0.6	0.7	0.9	0.9	1.1	1.1	1.1	0.1	0.2	0.3	0.3	0.6	0.8												

*E** tests: AMPT data for 3E1 HS DROWNED samples

		Replicate 1					Replicate 2					Replicate 3							
		Frequency					Frequency					Frequency							
		25 Hz	10 Hz	5 Hz	1 Hz	0.5 Hz	0.1 Hz	25 Hz	10 Hz	5 Hz	1 Hz	0.5 Hz	0.1 Hz	25 Hz	10 Hz	5 Hz	1 Hz	0.5 Hz	0.1 Hz
40°C																			
Dynamic modulus (MPa)		17985	16507	15362	12694	11542	9081	16693	15350	14285	11793	10709	8386						
Phase angle (Degrees)		8.63	9.43	10.11	12.27	13.37	16.16	8.25	9.2	9.96	12.14	13.21	16.03						
Average temperature (°C)		4.3	4.3	4.2	4.1	3.9	3.5	4.2	4.2	4.2	4.1	3.8	3.5						
Average confining pressure (kPa)		0.3	0.2	0.2	0.3	0.3	0.3	0.2	0.2	0.2	0.2	0.2	0.2						
Average micro-strain		60	68	75	91	99	101	65	73	81	98	100	102						
Load drift (%)		-0.6	0.3	0.5	0	0	0	-0.3	0.4	0.6	0	0	0						
Load standard error (%)		3.7	1.3	0.7	0.4	0.3	0.3	3.7	1.1	0.7	0.4	0.3	0.3						
Average deformation drift (%)		-23.7	-27.6	-27.7	-42.6	-41.8	-67.6	-24.7	-28.2	-28	-44.5	-40.9	-65.9						
Average deformation standard error (%)		3.6	1.6	1.1	1.1	0.9	1.1	3.5	1.5	1.1	1.1	0.8	0.9						
Deformation uniformity (%)		30	29.7	29.4	28.9	28.4	27.2	14.8	15.5	15.8	16.2	16.5	16.5						
Phase uniformity (Degrees)		0.2	0.3	0.4	0.6	0.7	1	0.2	0.3	0.3	0.2	0.1	0.2						
20°C																			
Dynamic modulus (MPa)		9689	8229	7199	5104	4356	2942	9073	7676	6693	4719	4020	2616						
Phase angle (Degrees)		16.28	18.06	19.4	22.68	23.77	26.86	16.36	18.18	19.54	23	24.16	27.32						
Average temperature (°C)		20	19.9	19.9	19.6	19.5	19.9	20	20	20	19.8	19.7	19.9						
Average confining pressure (kPa)		0	0	0	0	0	0	0.1	0	0.1	0	0	0						
Average micro-strain		91	94	96	96	98	103	92	99	97	97	98	98						
Load drift (%)		-0.3	0.4	0.7	0	0.1	0	-0.2	0.4	0.6	0	0	0						
Load standard error (%)		3.7	1.5	0.9	0.5	0.3	0.3	3.7	1.6	1.1	0.5	0.2	0.3						
Average deformation drift (%)		-99.4	-109.4	-105.1	-123.7	-110.3	-144.1	-100.8	-112.8	-105.9	-127.1	-110.5	-120.4						
Average deformation standard error (%)		3.9	2.8	2.2	1.9	1.5	3	4	2.7	2.2	1.9	1.3	1.7						
Deformation uniformity (%)		25.6	23.8	21.7	20.7	20	20.1	24.9	25.2	25.1	24.3	24	23.3						
Phase uniformity (Degrees)		0.3	0.5	0.7	0.9	0.9	0.7	0.1	0.1	0.2	0.3	0.4	0.6						
40°C																			
Dynamic modulus (MPa)		2951	2216	1772	1006	805.5	446.5	2690	2011	1599	891.6	706.4	388.2						
Phase angle (Degrees)		29.62	30.67	31	31.56	30.76	30.01	29.99	31.19	31.66	32.35	31.63	30.59						
Average temperature (°C)		40	40	40	40.1	40.2	40.1	39.8	39.8	39.9	39.9	40	39.8						
Average confining pressure (kPa)		0	0	0	0	0	0	0	0	0	0	0	0						
Average micro-strain		85	85	90	94	95	97	83	84	90	94	95	98						
Load drift (%)		0.1	0.5	1.1	0.1	0	0	-0.2	0.5	0.9	0.1	0	0						
Load standard error (%)		4.7	3.1	1.8	0.7	0.7	0.4	4.7	3.3	2	0.8	0.8	0.4						
Average deformation drift (%)		-294.4	-233.2	-174.9	-107.7	-75	-44.1	-295.3	-243.2	-183.7	-115.4	-84.4	-41.5						
Average deformation standard error (%)		7.8	6.1	4.1	3	3.1	4.4	7.7	6.3	4.3	2.9	3.1	3.8						
Deformation uniformity (%)		17.9	18.4	18.7	19.6	19.7	20.1	7.7	8.3	9	9.8	10.3	10.4						
Phase uniformity (Degrees)		0.7	0.4	0.2	0.4	0.6	0.9	0.7	0.7	0.7	0.7	0.6	0.5						

*E** tests: AMPT data for 4E1 DVR DROWNED samples

Replicate 1																		
	Frequency					Frequency					Frequency							
	25 Hz	10 Hz	5 Hz	1 Hz	0.5 Hz	25 Hz	10 Hz	5 Hz	1 Hz	0.5 Hz	0.1 Hz	0.1 Hz						
40°C																		
Dynamic modulus (MPa)	16182	14813	13773	11420	10436	8340	15035	14053	13281	11514	10744	9048	16705	15608	14667	12685	11783	9973
Phase angle (Degrees)	8.63	9.41	10.07	11.91	12.78	15.08	7.36	7.88	8.28	9.48	10.07	11.67	6.44	7.3	7.71	8.81	9.45	10.9
Average temperature (°C)	4.3	4.2	4.2	4	3.6	3.3	4.4	4.4	4.3	4.2	3.9	3.3	4.3	4.3	4.2	4.1	3.8	3.4
Average confining pressure (kPa)	0	0	0	0	0.1	0.1	0.1	0.1	0.1	0.1	0.1	0.1	0.2	0.2	0.2	0.2	0.2	0.2
Average micro-strain	67	76	84	99	99	101	72	80	87	97	98	101	65	72	78	91	99	102
Load drift (%)	-0.4	0.2	0.5	0	0	0	-0.5	0.2	0.5	0	0	0	-0.4	0.2	0.5	0	0	0
Load standard error (%)	3.8	1.2	0.9	0.4	0.3	0.3	4	1.3	0.9	0.4	0.4	0.3	4.2	1.3	0.7	0.4	0.3	0.3
Average deformation standard error (%)	-25	-26.8	-26	-37.2	-32.6	-57.9	-15.9	-17.4	-15.9	-19.5	-14.9	-32.1	-16.5	-15.3	-14.1	-17.4	-14.5	-22.6
Deformation uniformity (%)	3.7	1.5	1.3	1.1	0.9	1.2	3.5	1.9	1.6	1.3	1.2	1.3	4.4	2.1	1.5	1.1	0.8	0.7
Phase uniformity (Degrees)	16.5	16	15.7	15.4	15.1	15.4	34.8	34	33.2	32	31.1	29.6	6.3	3.6	2.2	2.6	3.4	3.9
	0.5	0.5	0.5	0.6	0.6	0.7	0.3	0.4	0.5	0.5	0.5	0.6	0.8	0.2	0.1	0.2	0.2	0.2
Replicate 2																		
20°C																		
Dynamic modulus (MPa)	8471	7143	6210	4418	3782	2538	8821	7728	6953	5365	4752	3505	9568	8434	7630	6002	5382	4055
Phase angle (Degrees)	16.36	17.88	19.11	22.21	23.26	26.11	13.09	14.16	15.02	17.1	18.06	20.48	12.22	13.11	13.87	15.72	16.55	18.77
Average temperature (°C)	20	20	20	20	19.9	19.9	20	19.9	19.8	19.5	19.3	19.6	19.9	19.8	19.8	19.6	19.5	19.7
Average confining pressure (kPa)	0	0	0	0	0	0	0.3	0	0	0	0	0	0	0	0.1	0	0	0
Average micro-strain	95	96	97	98	99	99	91	94	97	98	99	99	96	97	98	99	100	100
Load drift (%)	0	0.4	0.7	0	0	0	-0.3	0.3	0.6	0.1	0	0	-0.5	0.2	0.6	0.1	0	0
Load standard error (%)	4.1	1.5	0.8	0.5	0.3	0.3	4.2	1.7	1	0.5	0.2	0.3	4.1	1.5	1	0.4	0.2	0.3
Average deformation standard error (%)	-95.8	-101.3	-97	-119.2	-108.5	-136.7	-50.4	-50.9	-47.3	-55.9	-51.8	-68.1	-42.6	-42.5	-39	-44.3	-38	-53.7
Deformation uniformity (%)	4.7	3	2.3	2.1	1.5	1.8	3.8	2.2	1.9	1.6	1.3	1.3	4	1.9	1.4	1.1	0.9	1.6
Phase uniformity (Degrees)	9.5	11.2	12.7	13.8	15	15.8	27.5	26.1	24.8	23.8	22.8	22.1	7.4	7.6	7.6	7.5	7.1	6.9
	0.1	0.2	0.3	0.4	0.5	0.6	0.8	0.7	0.6	0.4	0.4	0.4	0.4	0.3	0.3	0.2	0.2	0.2
Replicate 3																		
40°C																		
Dynamic modulus (MPa)	2600	1988	1611	946.9	756.7	419.5	3391	2736	2308	1528	1302	819.7	3622	2941	2513	1695	1480	956.2
Phase angle (Degrees)	27.89	29.03	29.58	30.65	30.37	30.61	22.72	24.03	25.01	26.98	27.31	28.84	21.56	22.82	23.71	25.78	26.19	27.79
Average temperature (°C)	39.6	39.5	39.6	39.5	39.5	39.6	39.5	39.4	39.4	39.4	39.4	39.4	39.4	39.4	39.4	39.4	39.4	39.5
Average confining pressure (kPa)	0	0	0	0	0	0	0	0	0	0	0	0	0	0.1	0	0	0	0
Average micro-strain	86	88	91	95	97	100	85	89	92	94	95	96	91	92	94	95	95	94
Load drift (%)	-0.1	0.3	0.9	0.1	0.1	0.3	-0.2	0.3	1	0.1	0	0	-0.1	0.4	0.9	0.1	0.1	0
Load standard error (%)	4.6	3.1	1.9	0.8	0.6	0.3	4.8	3.1	1.7	0.7	0.3	0.3	4.5	2.7	1.6	0.6	0.3	0.2
Average deformation drift (%)	-210.3	-185.1	-144.5	-93.5	-72.3	-45	-155.6	-139.3	-130.7	-112	-97.7	-96.2	-129.2	-120.8	-105.6	-103.7	-93.9	-100.8
Average deformation standard error (%)	6.3	5.3	3.6	2.5	2.4	2.8	6.9	5.9	5.3	4	3.7	3.4	4.9	3.7	2.8	2.1	2	2.4
Deformation uniformity (%)	8	7.8	7.3	6.4	6	5.8	20.5	21.6	21.7	22.6	18.8	17	8.1	7.2	6.3	5.6	4.3	3
Phase uniformity (Degrees)	0.5	0.6	0.7	0.8	0.9	1.1	1.7	1.5	1.3	0.9	0.6	0.7	0.5	0.4	0.2	0.1	0.1	0.3

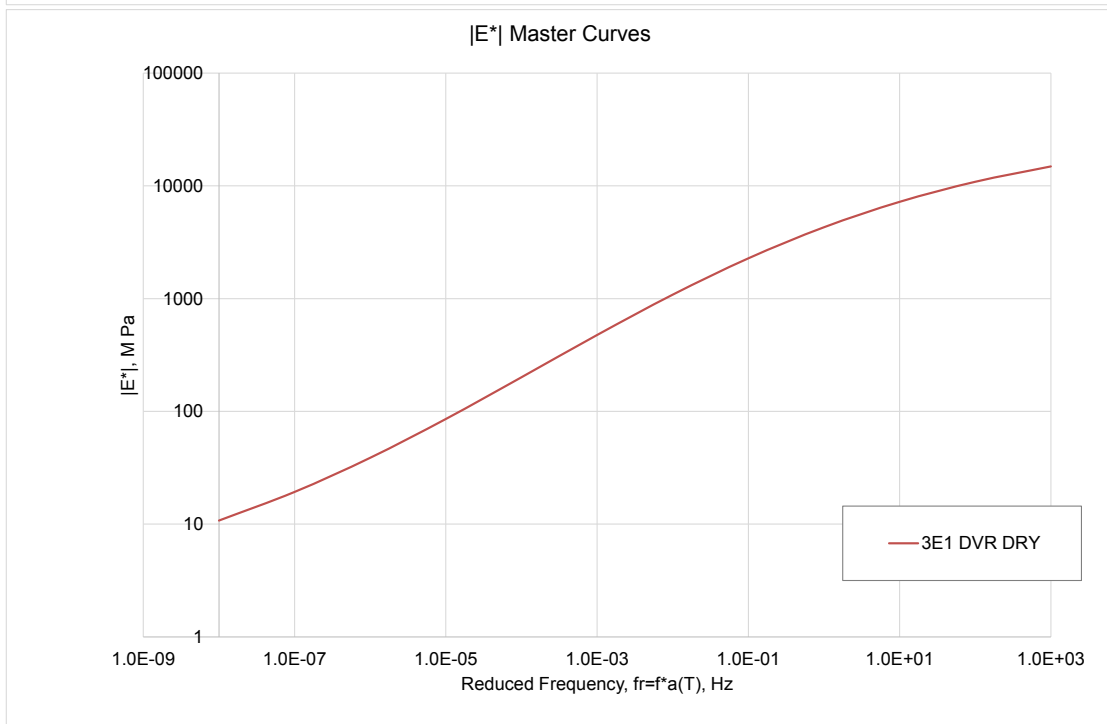
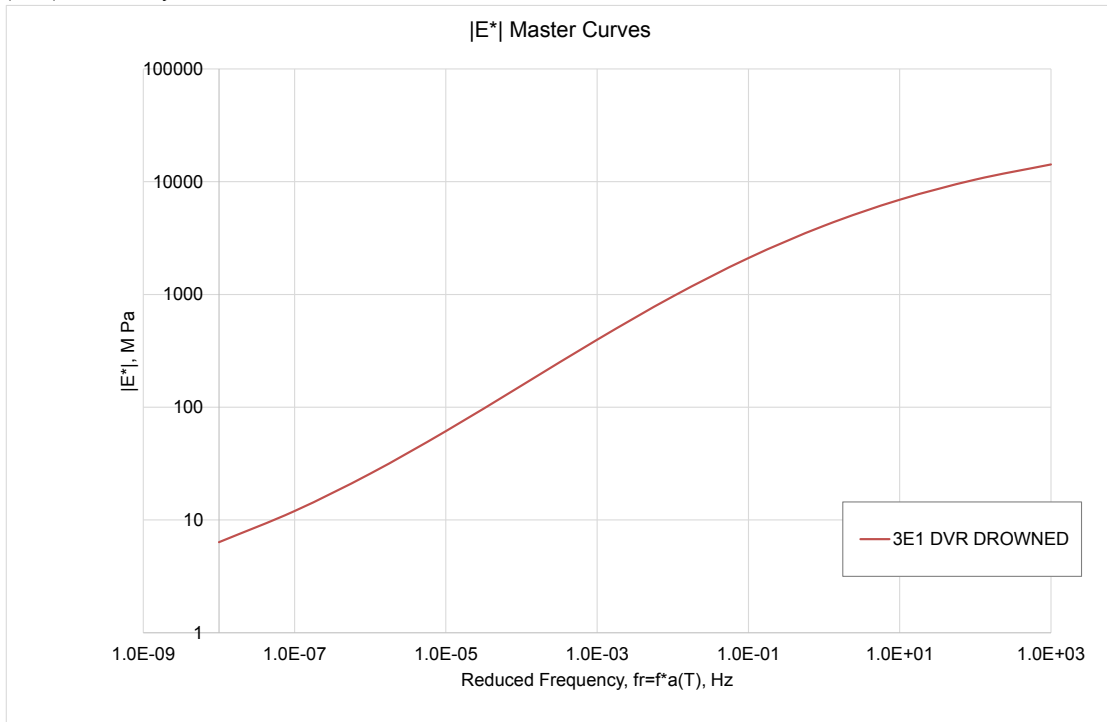
*E** tests: AMPT data for 4E1 HS DRY samples

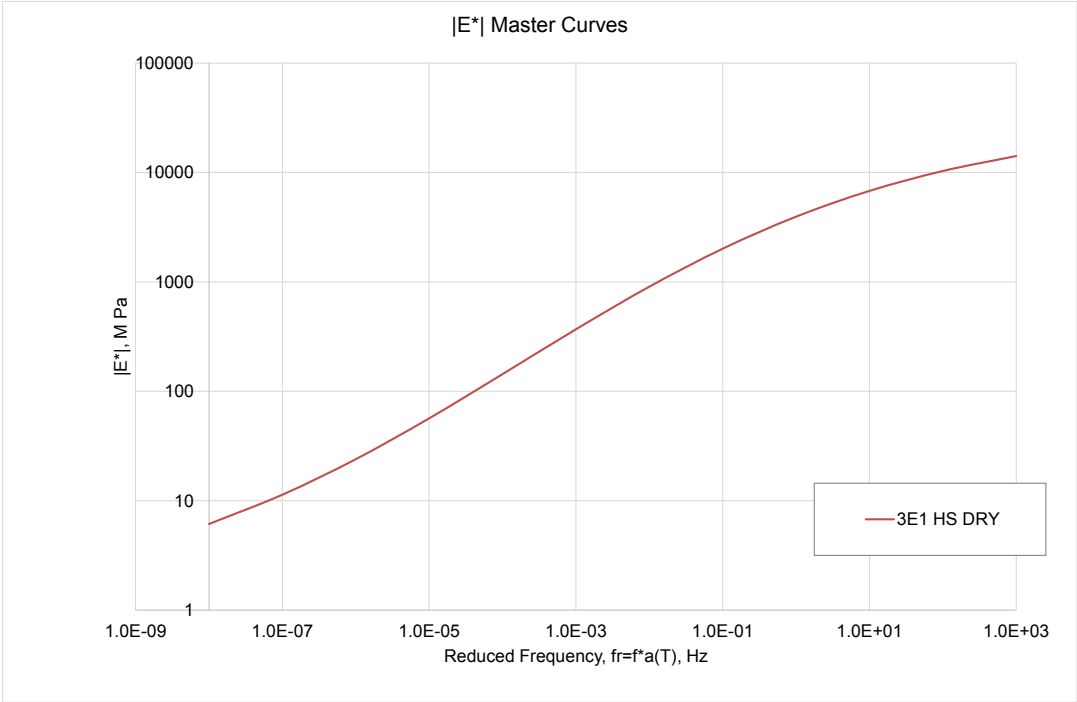
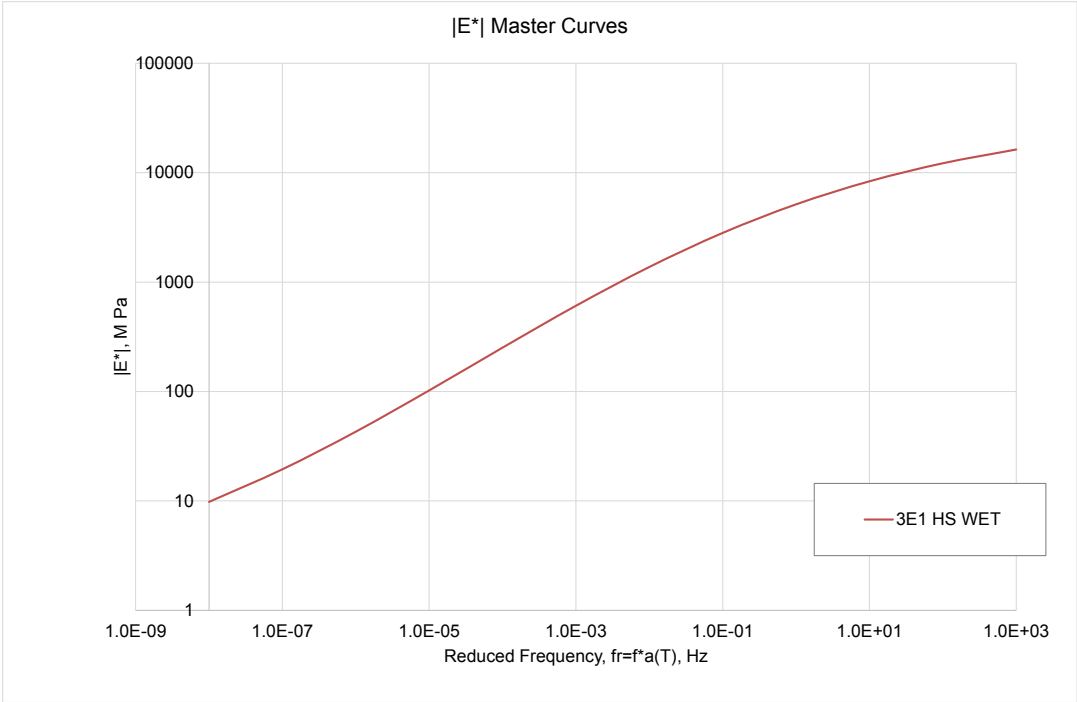
	Replicate 1										Replicate 2										Replicate 3									
	Frequency										Frequency										Frequency									
	25 Hz	10 Hz	5 Hz	1 Hz	0.5 Hz	0.1 Hz	25 Hz	10 Hz	5 Hz	1 Hz	0.5 Hz	0.1 Hz	25 Hz	10 Hz	5 Hz	1 Hz	0.5 Hz	0.1 Hz	25 Hz	10 Hz	5 Hz	1 Hz	0.5 Hz	0.1 Hz						
4°C																														
Dynamic modulus (MPa)	15973	14566	13609	11158	10160	7972	15922	14322	13109	10448	9354	6993	16514	14637	13327	10747	9683	7335	16514	14637	13327	10747	9683	7335						
Phase angle (Degrees)	8.84	9.63	10.38	12.54	13.52	16.24	10.17	11.43	12.5	15.43	16.75	20.3	8.62	10.25	11.62	13.9	14.93	18.47	8.62	10.25	11.62	13.9	14.93	18.47						
Average temperature (°C)	4.4	4.4	4.4	4.4	4.4	4.3	4.3	4.3	4.3	4.3	4.2	4.2	4.4	4.4	4.4	4.4	4.4	4.4	4.4	4.4	4.4	4.4	4.4	4.4						
Average confining pressure (kPa)	0.4	0.4	0.4	0.4	0.4	0.4	0.4	0.4	0.4	0.4	0.4	0.4	0.4	0.4	0.4	0.4	0.4	0.4	0.4	0.4	0.4	0.4	0.4	0.4						
Average micro-strain	68	78	85	99	99	102	68	79	88	98	99	99	66	77	86	99	99	101	66	77	86	99	99	101						
Load drift (%)	-0.3	0.3	0.6	0	0.1	0	-0.1	0.3	0.5	0	0	0	-0.5	0.3	0.6	0	0.1	0	-0.5	0.3	0.6	0	0.1	0						
Load standard error (%)	3.7	1.3	0.7	0.4	0.3	0.3	3.7	1.3	0.8	0.4	0.3	0.3	4.1	1.3	0.7	0.4	0.3	0.3	4.1	1.3	0.7	0.4	0.3	0.3						
Average deformation drift (%)	-29	-30.4	-30.7	-46.3	-4.3	-69.8	-39.9	-48.4	-51.5	-81.6	-78.8	-120.8	-253.4	-91.6	-44.2	-91.2	-99.3	-92.1	-253.4	-91.6	-44.2	-91.2	-99.3	-92.1						
Average deformation standard error (%)	3.9	1.9	1.3	1.2	0.9	1	3.9	2.5	2.1	2.1	1.8	1.9	8.9	3.3	2.6	2.6	4.6	5.6	2.4	8.9	3.3	2.6	2.6	4.6	5.6	2.4				
Deformation uniformity (%)	6.7	5	3.8	2.6	2.4	2.3	22.6	19.5	17.4	15	13.1	10.8	27.1	22.9	20.9	20.8	20.9	20.4	27.1	22.9	20.9	20.8	20.9	20.4						
Phase uniformity (Degrees)	0.3	0.3	0.3	0.3	0.3	0.3	0.1	0.1	0.2	0.1	0.2	0.3	1.4	0.8	0.2	0.2	0.7	0.4	1.4	0.8	0.2	0.2	0.7	0.4						
20°C																														
Dynamic modulus (MPa)	8083	6806	5927	4127	3521	2317	7434	6032	5075	3266	2679	1595	7660	6328	5427	3641	3053	1922	7660	6328	5427	3641	3053	1922						
Phase angle (Degrees)	17.35	19.18	20.52	23.82	24.8	27.29	20.99	23.22	24.87	28.34	29.11	30.85	19.1	21.03	22.38	25.66	26.49	28.52	19.1	21.03	22.38	25.66	26.49	28.52						
Average temperature (°C)	20.1	20.1	20.1	20.1	20.2	20.1	19.9	19.9	19.9	19.9	19.9	19.9	20	20	20.1	20.1	20.2	20.2	20	20	20.1	20.1	20.2	20.2						
Average confining pressure (kPa)	0.1	0.1	0.1	0.1	0.1	0.1	0.1	0.1	0.1	0.1	0.1	0.1	0.1	0.1	0.1	0.1	0.1	0.1	0.1	0.1	0.1	0.1	0.1	0.1						
Average micro-strain	92	94	96	96	97	97	90	93	95	96	97	98	91	94	95	96	97	98	91	94	95	96	97	98						
Load drift (%)	-0.3	0.4	0.8	0.1	0	0	-0.3	0.5	0.7	0.1	0.1	0	-0.3	0.4	0.7	0.1	0	0	-0.3	0.4	0.7	0.1	0	0						
Load standard error (%)	3.4	1.9	1.2	0.5	0.2	0.2	3.1	1.9	1.2	0.5	0.3	0.3	3.3	1.9	1.1	0.5	0.3	0.2	3.3	1.9	1.1	0.5	0.3	0.2						
Average deformation drift (%)	-92.5	-110.5	-107.1	-123.6	-108.3	-110.8	-167.4	-178.4	-176.2	-165.2	-135.2	-113.5	-115.8	-133.2	-124.8	-134.7	-116.5	-116.1	-115.8	-133.2	-124.8	-134.7	-116.5	-116.1						
Average deformation standard error (%)	3.6	3	2.3	1.8	1.5	2	4.2	4.2	4.1	2.6	2.1	2.1	4	3.7	2.9	2.5	2.1	2.3	4	3.7	2.9	2.5	2.1	2.3						
Deformation uniformity (%)	11.7	12.2	12.3	12	12	11.1	7.2	8.2	8.6	8.7	8.9	8.9	16.5	15.3	14.5	14.1	13.6	14.1	16.5	15.3	14.5	14.1	13.6	14.1						
Phase uniformity (Degrees)	0.5	0.5	0.5	0.5	0.5	0.6	0.5	0.5	0.5	0.6	0.7	0.6	0.6	0.6	0.5	0.5	0.5	0.5	0.6	0.6	0.5	0.5	0.5	0.5						
40°C																														
Dynamic modulus (MPa)	2769	2020	1618	908	735.5	412.6	2066	1386	1048	535.9	415.7	226.2	2437	1723	1353	735.5	590.7	333.4	2437	1723	1353	735.5	590.7	333.4						
Phase angle (Degrees)	29.41	31.39	31.69	32.37	31.26	30.1	32.69	35.04	35.11	34.32	32.73	30.09	31.15	33.03	32.96	32.6	31.03	28.92	31.15	33.03	32.96	32.6	31.03	28.92						
Average temperature (°C)	39.8	39.9	39.8	39.8	39.8	39.8	39.8	39.9	39.8	39.8	39.8	39.8	39.8	39.9	39.8	39.9	39.9	39.8	39.8	39.9	39.8	39.9	39.9	39.8						
Average confining pressure (kPa)	-0.1	0	-0.1	0	0	0	0.1	-0.1	0	0	0	0	0.1	0	0	0	0	0	0.1	0	0	0	0	0						
Average micro-strain	94	87	89	96	95	98	106	86	89	99	97	102	94	86	88	96	95	98	94	86	88	96	95	98						
Load drift (%)	-0.1	0.3	1.2	0.6	0.1	0	-0.4	0.2	1.3	0.7	0.2	-0.2	-0.2	0.3	1.2	0.7	0.2	0.2	-0.2	0.3	1.2	0.7	0.2	0.2						
Load standard error (%)	4.7	3.4	1.9	4.1	2.4	0.7	5.1	4.1	2.5	5.9	3.3	0.9	4.9	3.6	2.2	4.7	2.6	0.8	4.9	3.6	2.2	4.7	2.6	0.8						
Average deformation drift (%)	-138.7	-164.3	-124.7	-75.8	-66.1	-44.4	-99.7	-122.4	-79.5	-27.8	-22.5	0.5	-128.2	-152.7	-107.7	-56.9	-48.9	-32	-128.2	-152.7	-107.7	-56.9	-48.9	-32						
Average deformation standard error (%)	5	6.3	4.1	3.8	3.1	3.5	4.8	6	3.9	5.1	3.6	3.4	5.1	6.4	4.2	4.7	3.7	3.8	5.1	6.4	4.2	4.7	3.7	3.8						
Deformation uniformity (%)	2.5	2.6	2.6	2.6	2.6	2.4	8.7	9.3	9.4	9.5	9.5	9.7	6.3	8.1	9.2	11.9	12	13.3	6.3	8.1	9.2	11.9	12	13.3						
Phase uniformity (Degrees)	0.6	0.4	0.3	0.2	0.3	0.4	0.6	0.8	0.9	0.8	0.8	0.7	0.4	0.5	0.5	0.5	0.6	0.8	0.4	0.5	0.5	0.5	0.6	0.8						

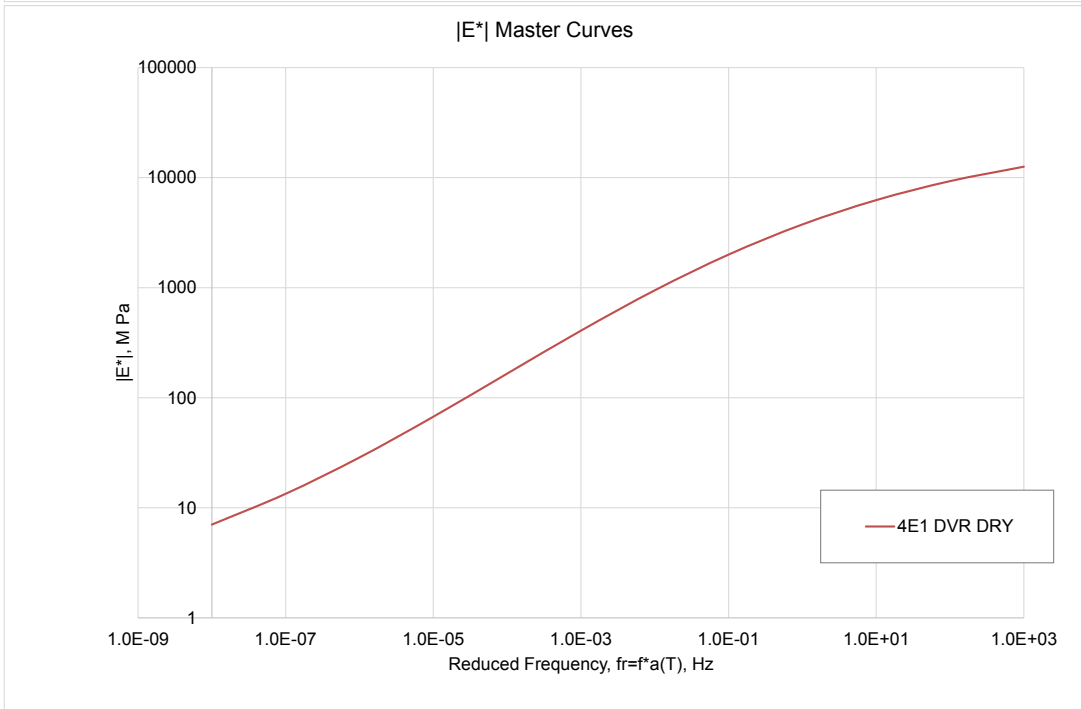
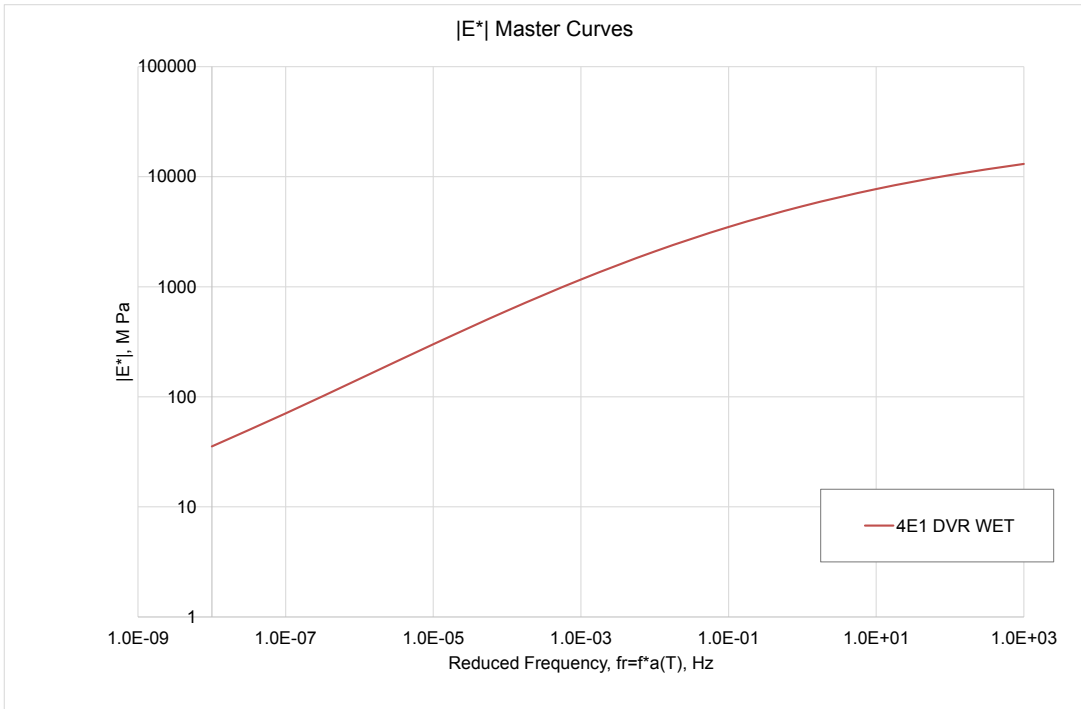
* tests: AMPT data for 4E1 HS DROWNED samples

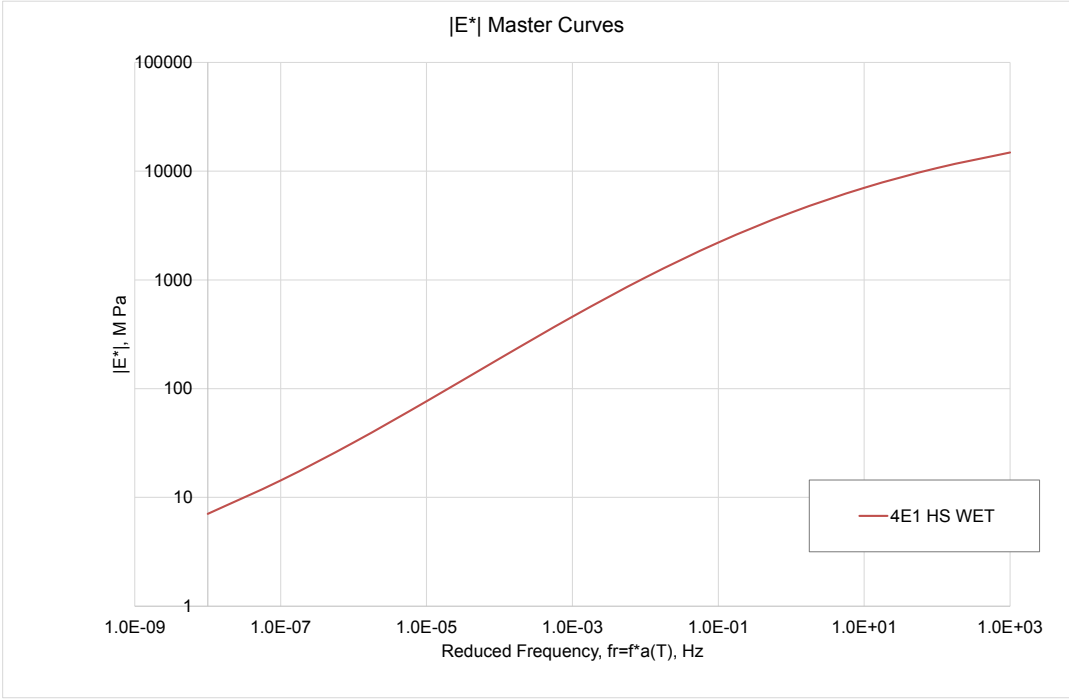
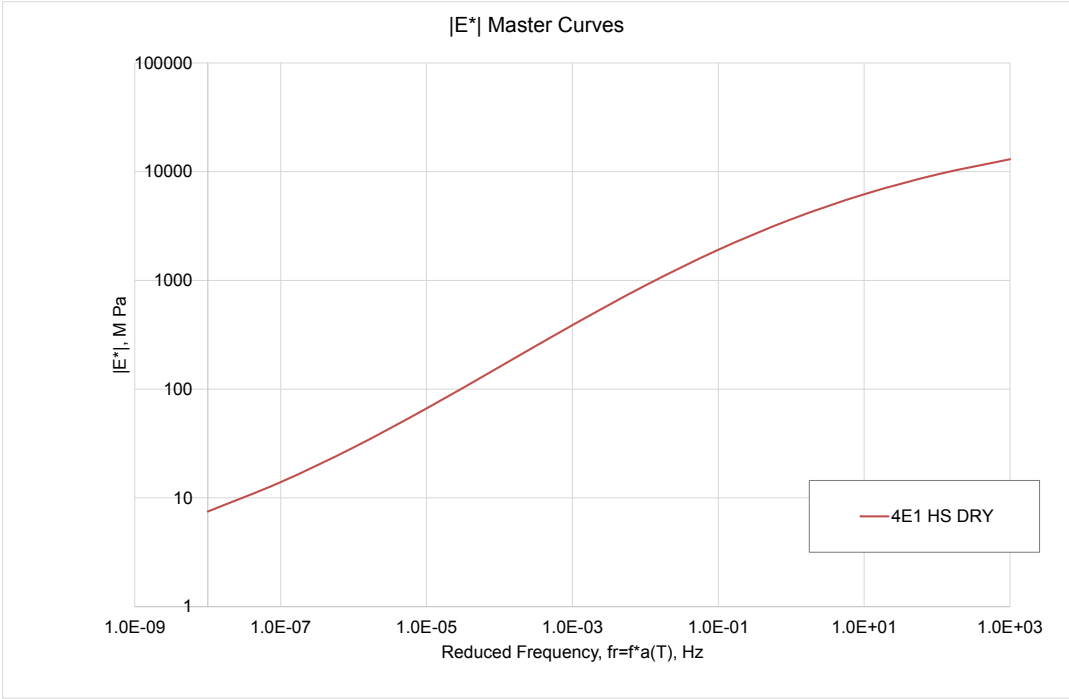
	Replicate 1												Replicate 2												Replicate 3											
	Frequency				Frequency				Frequency				Frequency				Frequency				Frequency															
	25 Hz	10 Hz	5 Hz	1 Hz	0.5 Hz	0.1 Hz	25 Hz	10 Hz	5 Hz	1 Hz	0.5 Hz	0.1 Hz	25 Hz	10 Hz	5 Hz	1 Hz	0.5 Hz	0.1 Hz	25 Hz	10 Hz	5 Hz	1 Hz	0.5 Hz	0.1 Hz												
40°C																																				
Dynamic modulus (MPa)	14577	13090	11966	9657	8585	6532	28155	25264	23079	18694	16814	12953	19361	17298	15703	12639	11317	8777	19361	17298	15703	12639	11317	8777												
Phase angle (Degrees)	10.15	11.21	12.14	14.65	15.83	18.98	27.74	37.14	26.83	34.44	35.48	22.86	7.75	9.75	10.31	12.13	13.27	16.06	7.75	9.75	10.31	12.13	13.27	16.06												
Average temperature (°C)	4.5	4.5	4.5	4.5	4.6	4.8	4.4	4.4	4.4	4.3	4.3	4.3	4.3	4.3	4.3	4.2	4.2	4.1	4.3	4.3	4.3	4.2	4.2	4.1												
Average confining pressure (kPa)	0.4	0.4	0.4	0.4	0.4	0.4	0.5	0.4	0.4	0.4	0.4	0.4	0.4	0.4	0.4	0.4	0.4	0.4	0.4	0.4	0.4	0.4	0.4	0.4												
Average micro-strain	74	86	96	99	99	100	38	45	50	62	69	91	34	65	73	92	100	103	34	65	73	92	100	103												
Load drift (%)	-0.3	0.3	0.5	0	0.1	0	-0.8	0.1	0.5	0	0	0	-0.3	0.2	0.5	0	0	0	-0.3	0.2	0.5	0	0	0												
Load standard error (%)	4.4	1.3	0.7	0.4	0.3	0.3	4.1	1.3	0.9	0.4	0.3	0.3	4.5	1.3	1	0.4	0.3	0.3	4.5	1.3	1	0.4	0.3	0.3												
Average deformation drift (%)	-36.8	-42.8	-45.7	-65.4	-62.5	-101.2	-12.4	-14.4	241.5	99.8	99.5	-529.7	13.5	-20.9	-23.4	-36.4	-36.2	-59.5	13.5	-20.9	-23.4	-36.4	-36.2	-59.5												
Average deformation standard error (%)	4.6	2.4	1.9	1.7	1.8	2	4	3.7	96.3	83.9	83	181.4	5.3	2	1.6	1.5	1.3	1.2	5.3	2	1.6	1.5	1.3	1.2												
Deformation uniformity (%)	11.7	11.5	11.4	10.4	9.2	7.2	73.9	76.4	78.7	81.7	83.4	84.5	13.3	6	6.3	5.5	4.2	3.5	13.3	6	6.3	5.5	4.2	3.5												
Phase uniformity (Degrees)	0.3	0.3	0.3	0.4	0.4	0.5	27.2	39.2	23.5	31.1	30.9	8.5	0.8	0.3	0.2	0.2	0.8	0.8	0.8	0.3	0.2	0.2	0.8	0.8												
20°C																																				
Dynamic modulus (MPa)	6915	5712	4878	3223	2683	1644	8696	7347	6401	4472	3816	2500	8851	7441	6463	4528	3847	2545	8851	7441	6463	4528	3847	2545												
Phase angle (Degrees)	19.55	21.6	23.12	26.8	27.81	30.27	16.82	19.17	20.39	23.55	24.5	27.07	17.1	18.85	20.17	23.41	24.46	27.16	17.1	18.85	20.17	23.41	24.46	27.16												
Average temperature (°C)	19.9	19.9	19.9	19.9	19.8	19.8	20	19.9	19.9	19.9	19.9	19.8	19.8	19.8	19.8	19.8	19.9	19.8	19.8	19.8	19.8	19.8	19.9	19.8												
Average confining pressure (kPa)	0.1	0.1	0.2	0.1	0.1	0.1	0.1	0.2	0.1	0.1	0.2	0.1	0.1	0.1	0.2	0.1	0.1	0.1	0.1	0.1	0.2	0.1	0.1	0.1												
Average micro-strain	92	92	95	96	97	97	91	93	95	95	97	97	91	95	96	97	98	97	91	95	96	97	98	97												
Load drift (%)	-0.4	0.4	0.7	0.1	0.1	0	-0.4	0.3	0.6	0	0	0	-0.5	0.5	0.6	0	0	0	-0.5	0.5	0.6	0	0	0												
Load standard error (%)	3.8	2.1	1.3	0.5	0.3	0.2	3.8	1.6	0.9	0.5	0.3	0.2	3.5	1.6	1.1	0.5	0.3	0.2	3.5	1.6	1.1	0.5	0.3	0.2												
Average deformation drift (%)	-121.9	-144.7	-141.6	-157	-140.2	-142.1	-131.5	-112.7	-106.7	-121.5	-107.6	-118.3	-93.3	-107.6	-103.3	-122.3	-108.6	-125.9	-93.3	-107.6	-103.3	-122.3	-108.6	-125.9												
Average deformation standard error (%)	4.6	3.9	3.2	2.7	2.3	2.5	5.4	3.2	2.5	2.2	1.9	2.1	3.9	2.9	2.3	2	1.6	1.7	3.9	2.9	2.3	2	1.6	1.7												
Deformation uniformity (%)	10.4	8.4	7.1	6.6	5.6	5.4	22.7	22.5	22.6	23.7	23.8	23.4	11.2	10	9.3	8.4	7.7	7.7	11.2	10	9.3	8.4	7.7	7.7												
Phase uniformity (Degrees)	0.3	0.4	0.4	0.5	0.5	0.5	0.7	0.8	0.8	0.9	0.8	1	0.7	0.8	0.9	1	1	1.1	0.7	0.8	0.9	1	1	1.1												
40°C																																				
Dynamic modulus (MPa)	2113	1457	1125	581.9	459.1	248.1	2998	2201	1768	987.5	799.9	446.2	2955	2188	1762	1001	814.6	460.6	2955	2188	1762	1001	814.6	460.6												
Phase angle (Degrees)	32.51	34.85	35.03	35.18	33.6	31.58	29.62	31.53	31.84	32.75	31.72	30.57	29.42	31.25	31.63	32.6	31.67	30.81	29.42	31.25	31.63	32.6	31.67	30.81												
Average temperature (°C)	39.8	39.8	39.8	39.8	39.7	39.7	39.8	39.8	39.8	39.9	39.9	39.8	39.8	39.8	39.8	39.8	39.8	39.8	39.8	39.8	39.8	39.8	39.8	39.8												
Average confining pressure (kPa)	0	0	0	0	0	0	0.1	-0.1	0	0	0	0	-0.1	0	0	0	0	0	-0.1	0	0	0	0	0												
Average micro-strain	94	86	88	97	95	99	92	86	89	95	94	97	90	87	90	95	94	97	90	87	90	95	94	97												
Load drift (%)	-0.6	-0.1	1.3	0.7	0	0	-0.4	0.4	1.1	0.4	0.1	0.1	-0.1	0.5	1.3	0.4	0.1	0	-0.1	0.5	1.3	0.4	0.1	0												
Load standard error (%)	5.4	4.1	2.5	5.6	3	0.8	4.7	3.4	2	3.8	2	0.5	4.7	3.3	1.9	3.7	1.9	0.6	4.7	3.3	1.9	3.7	1.9	0.6												
Average deformation drift (%)	-131.8	-177.2	-125.4	-59.1	-51.1	-31.7	-145.6	-173.9	-130.9	-76.6	-64.1	-40.4	-146.5	-175	-134.7	-85.1	-75.7	-58.3	-146.5	-175	-134.7	-85.1	-75.7	-58.3												
Average deformation standard error (%)	5.2	7.3	4.7	5	3.6	3.8	5.2	6.5	4.2	3.6	3	3.4	5.3	6.2	4.2	3.7	3.1	3.3	5.3	6.2	4.2	3.7	3.1	3.3												
Deformation uniformity (%)	4.7	5.4	5.2	5	4.5	2.9	22.3	23.4	23.3	24.9	24.4	25.5	7.2	8.1	8.9	11	11.8	13.8	7.2	8.1	8.9	11	11.8	13.8												
Phase uniformity (Degrees)	0.2	0.1	0.1	0.5	0.6	0.9	0.6	0.7	0.8	1.6	1.8	2.1	1	1.1	1	0.6	0.5	0.3	1	1.1	1	0.6	0.5	0.3												

$|E^*|$ tests: Dynamic modulus mastercurves

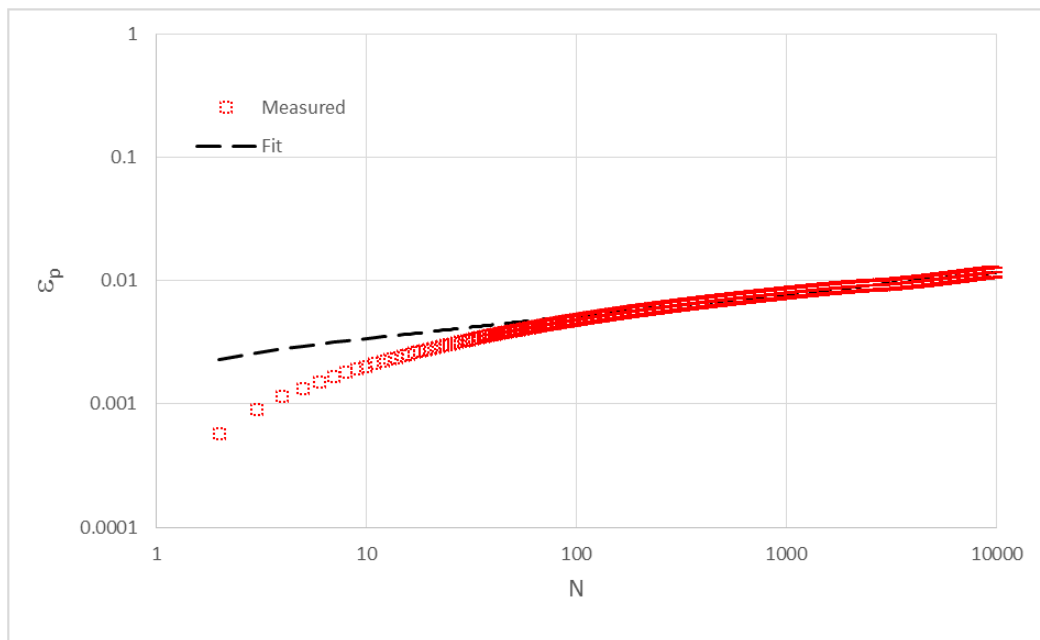
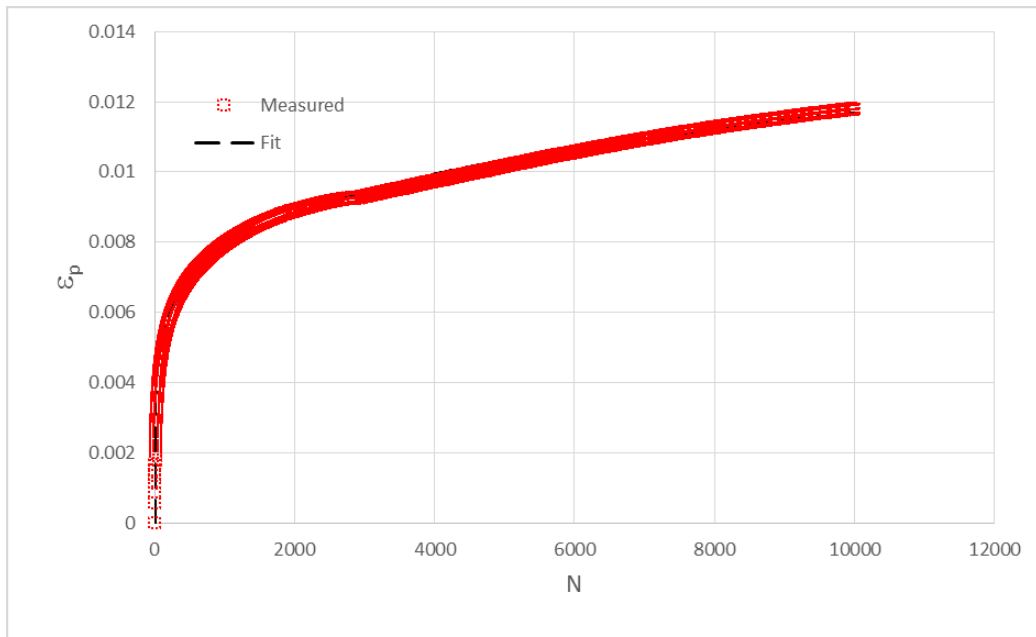




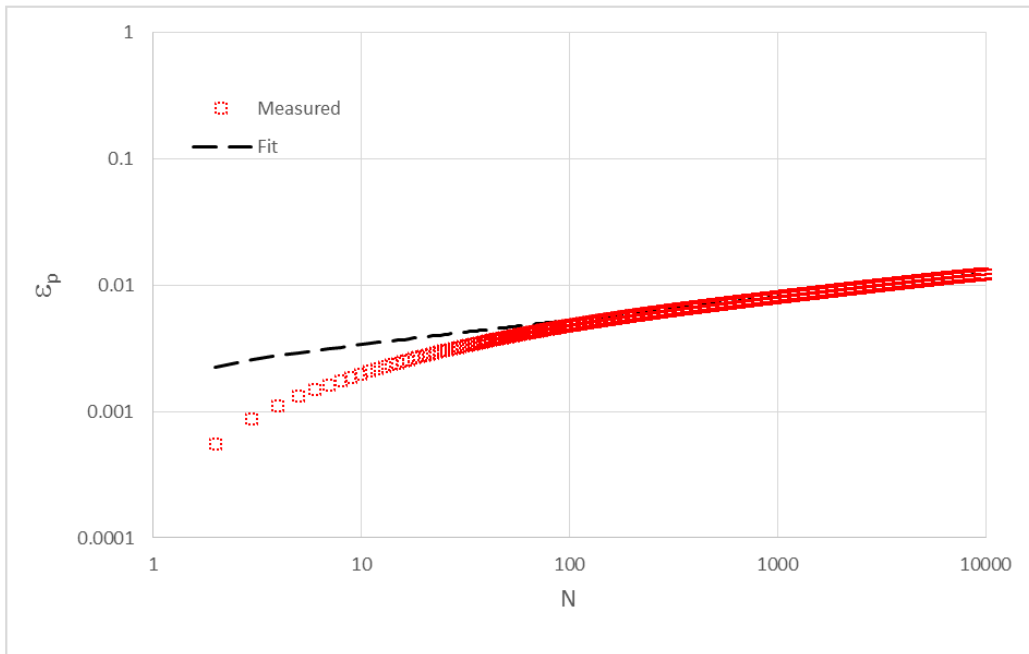
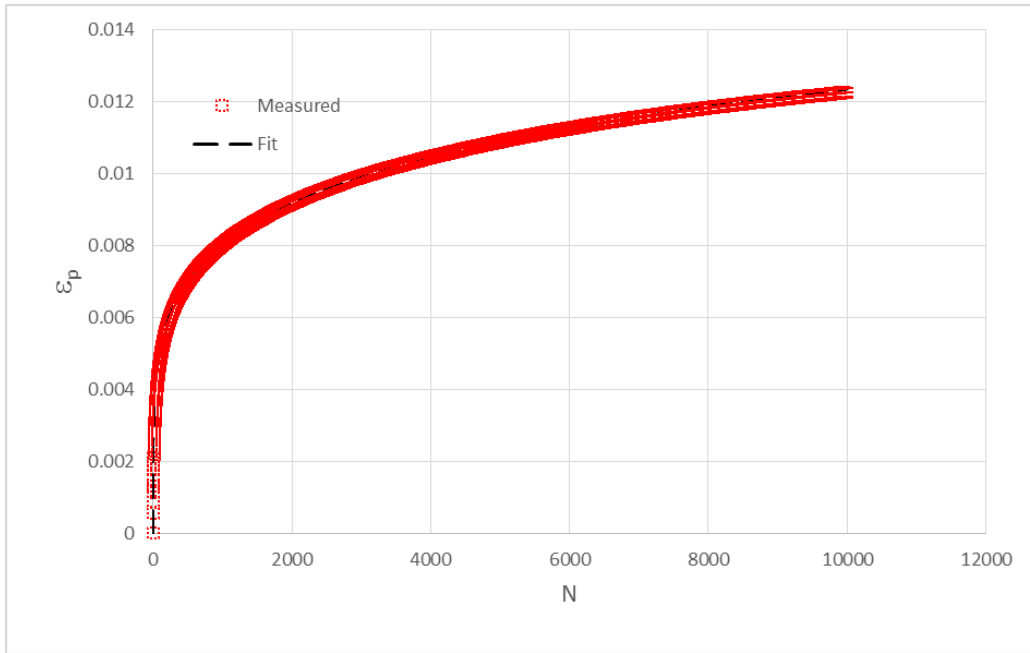




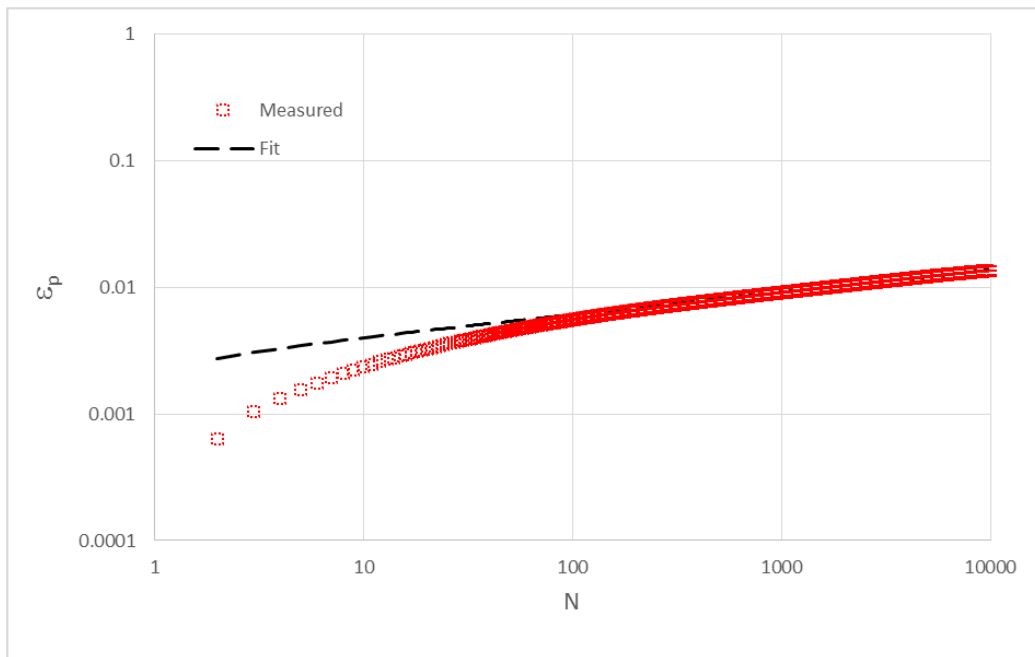
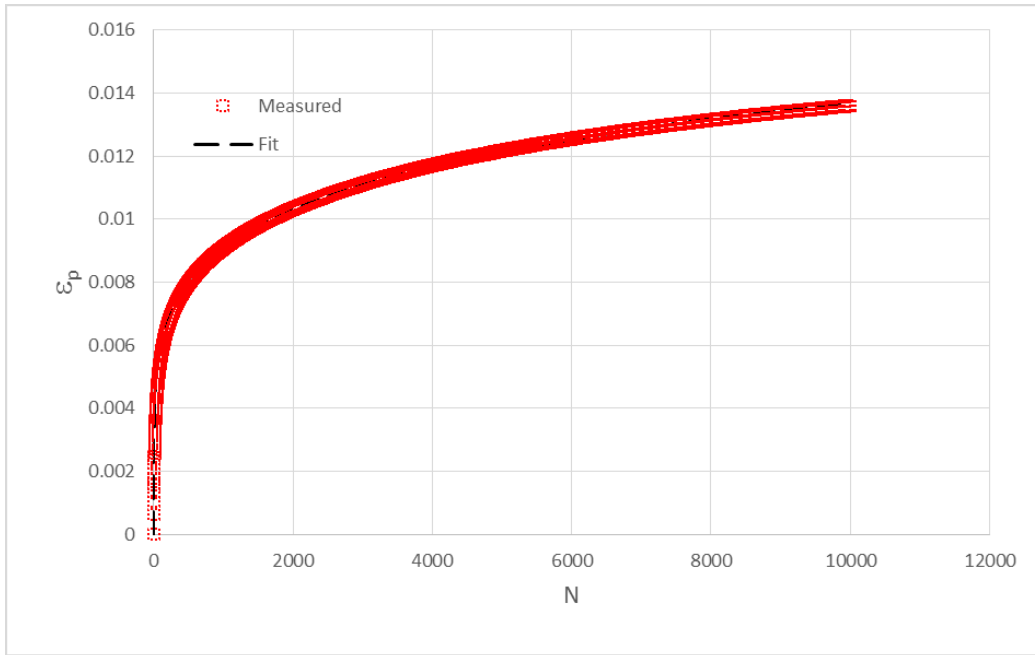
Flow Number tests: Evolution of plastic strain ϵ_p (standard and logarithmic scale) after N cycles



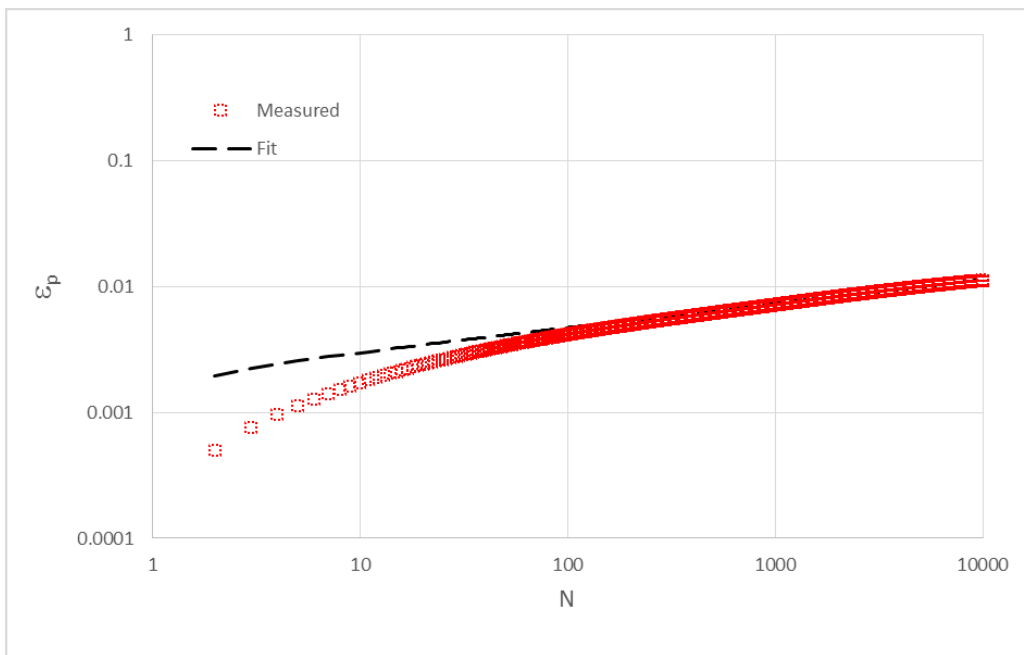
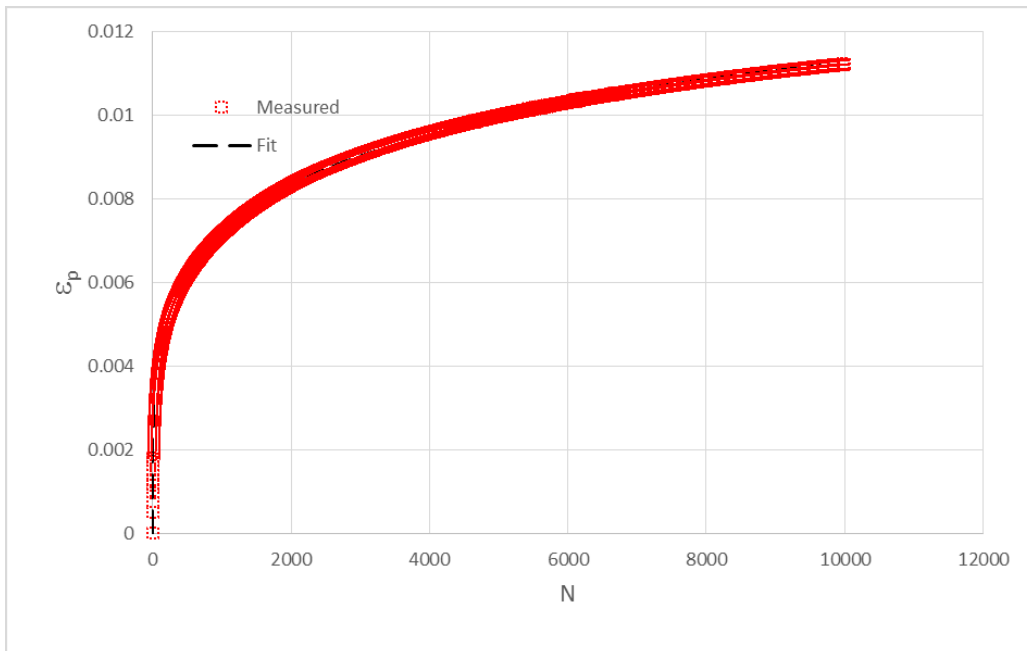
3EI DVR 1



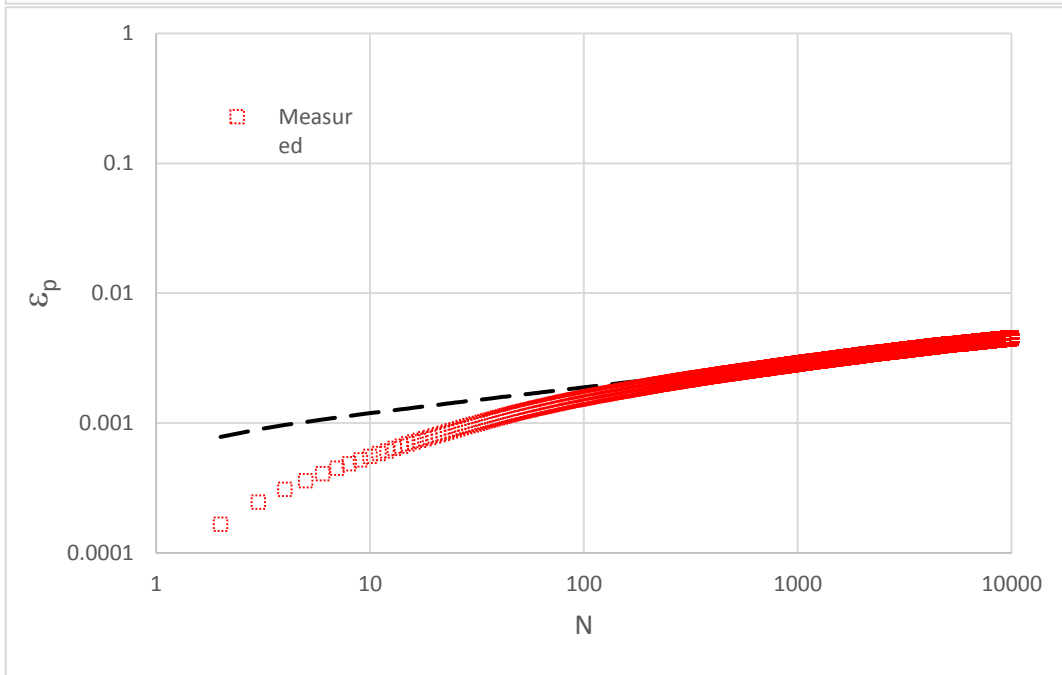
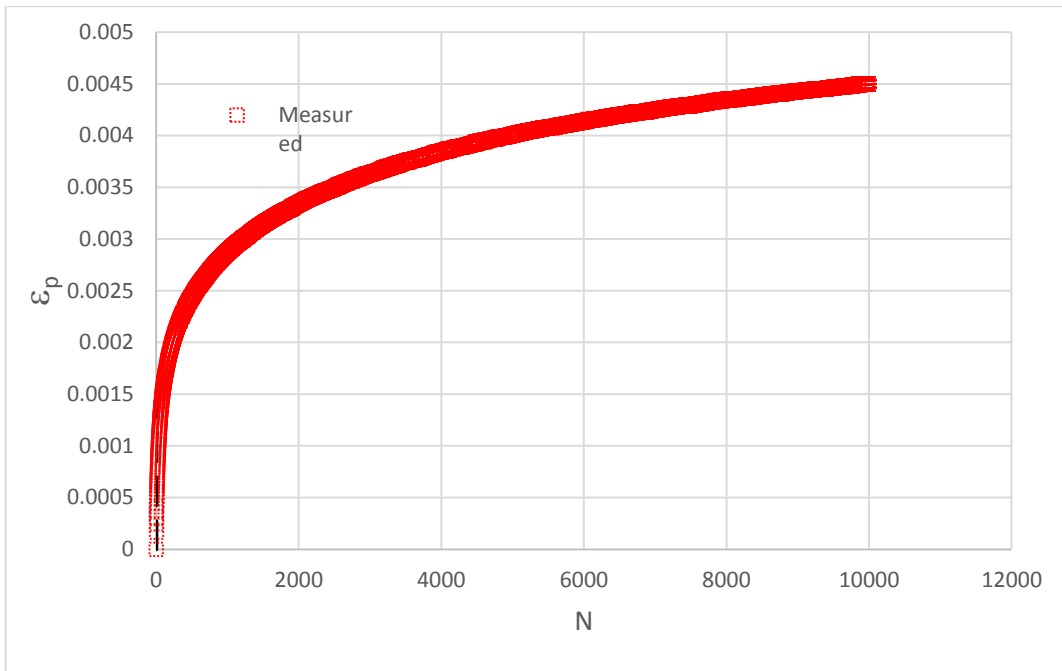
3EI DVR 2



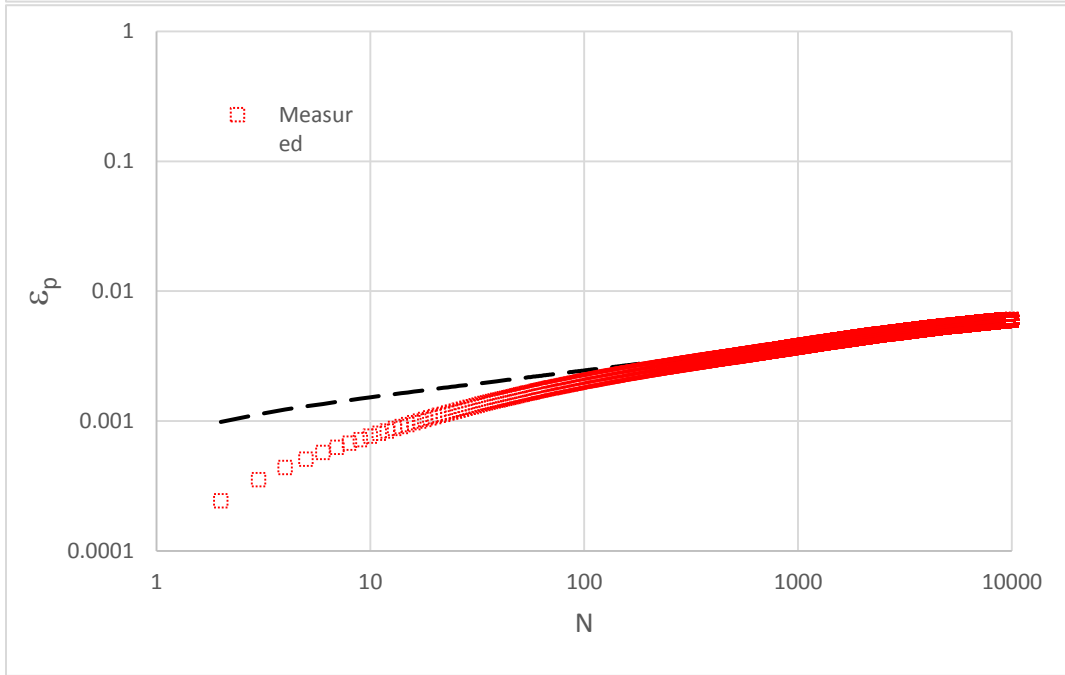
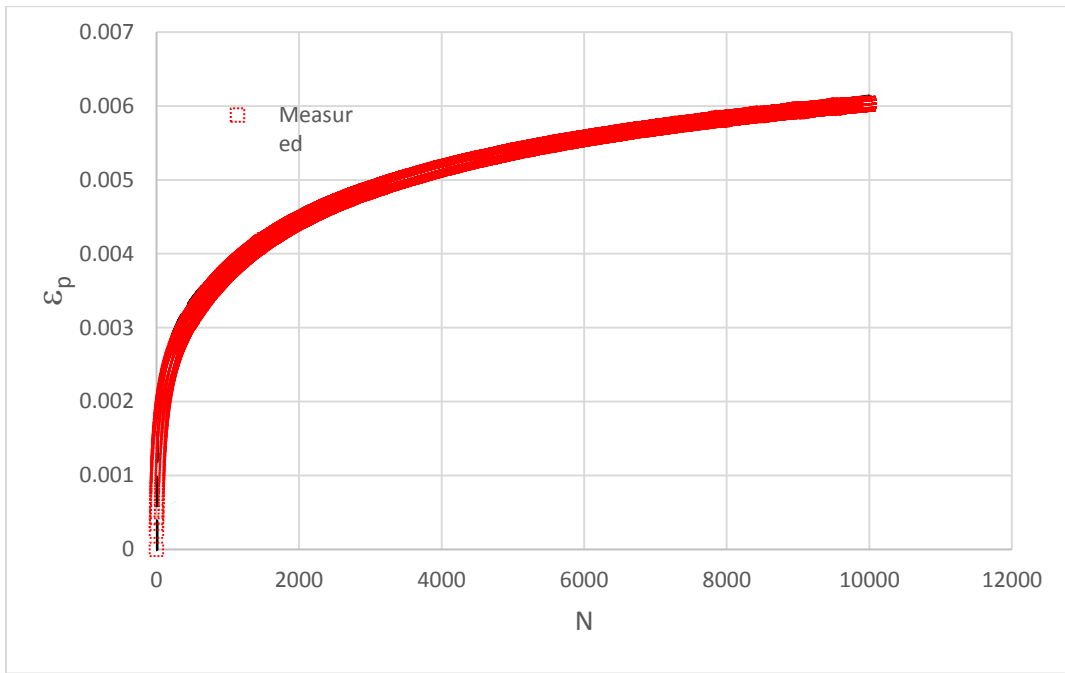
3EI DVR 3



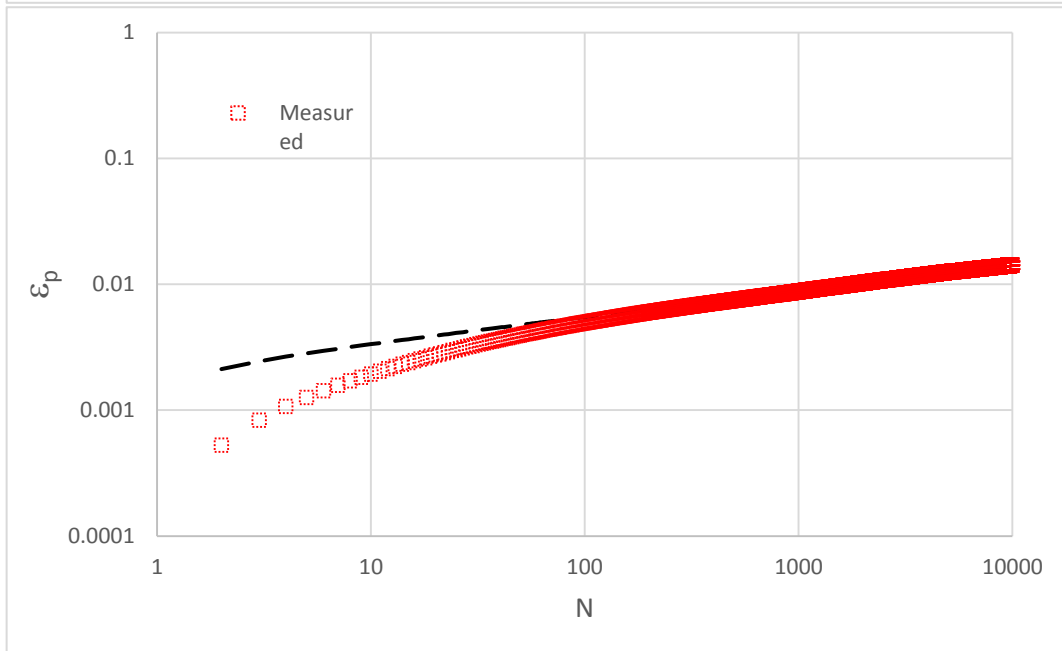
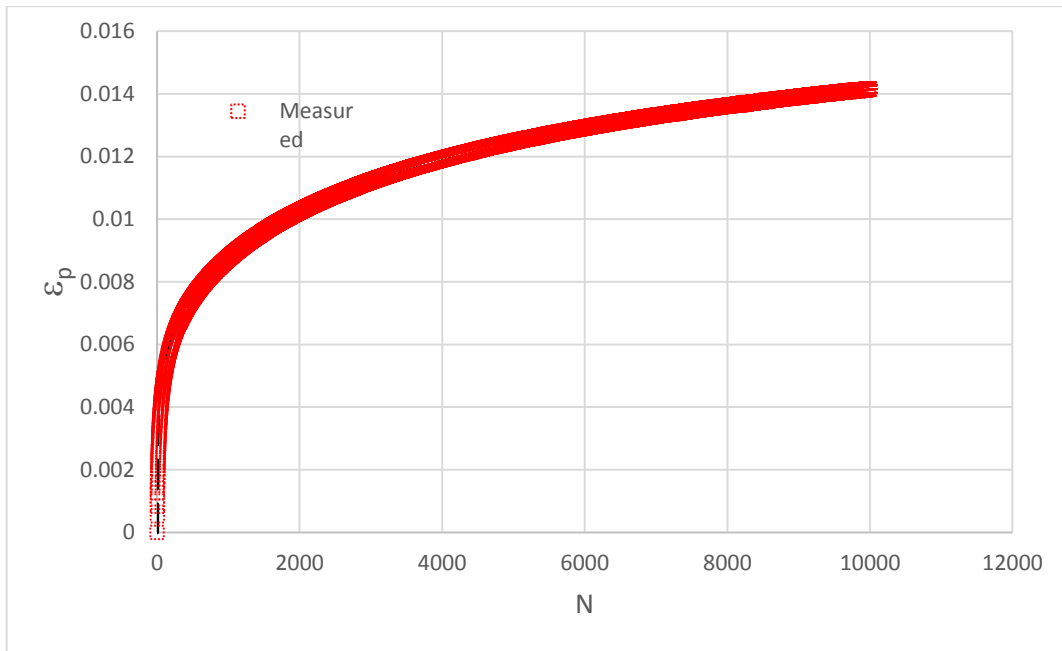
3EI DVR 4



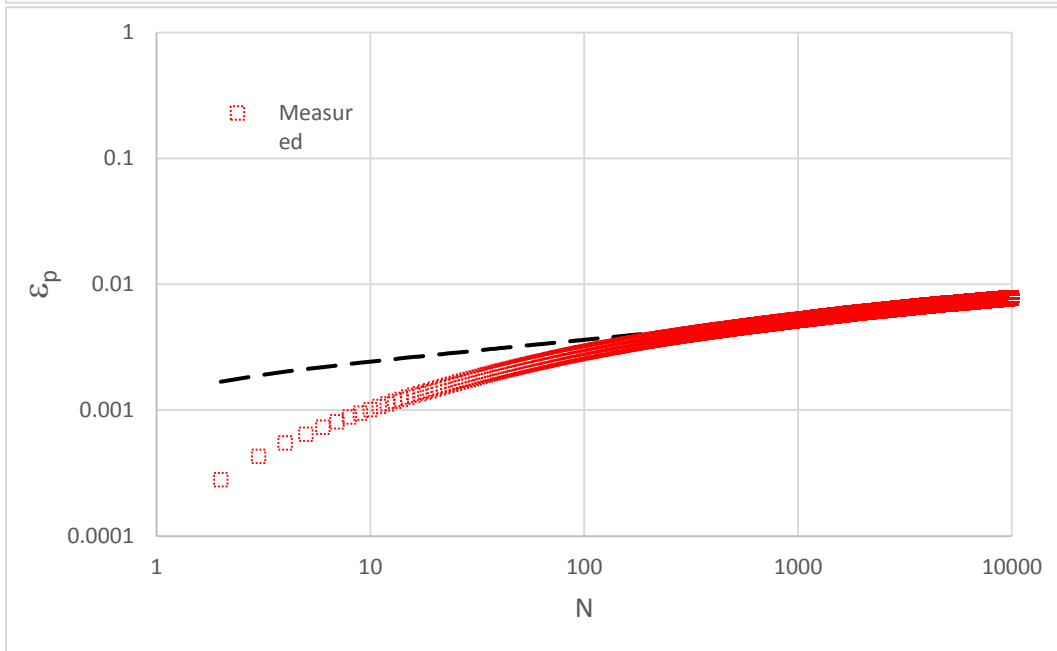
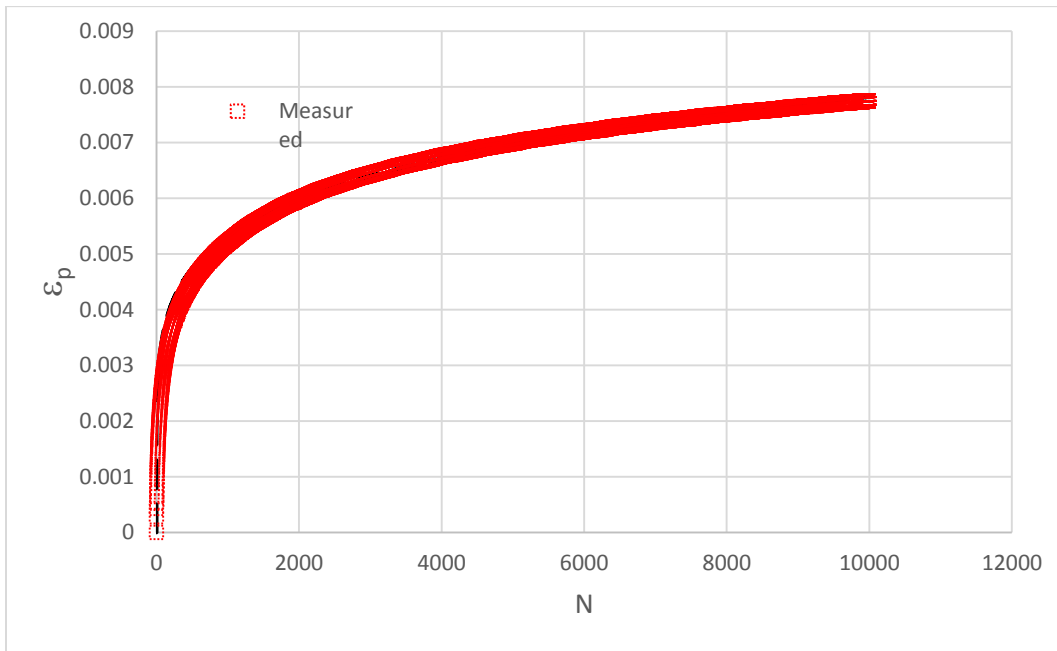
3EI DVR 5



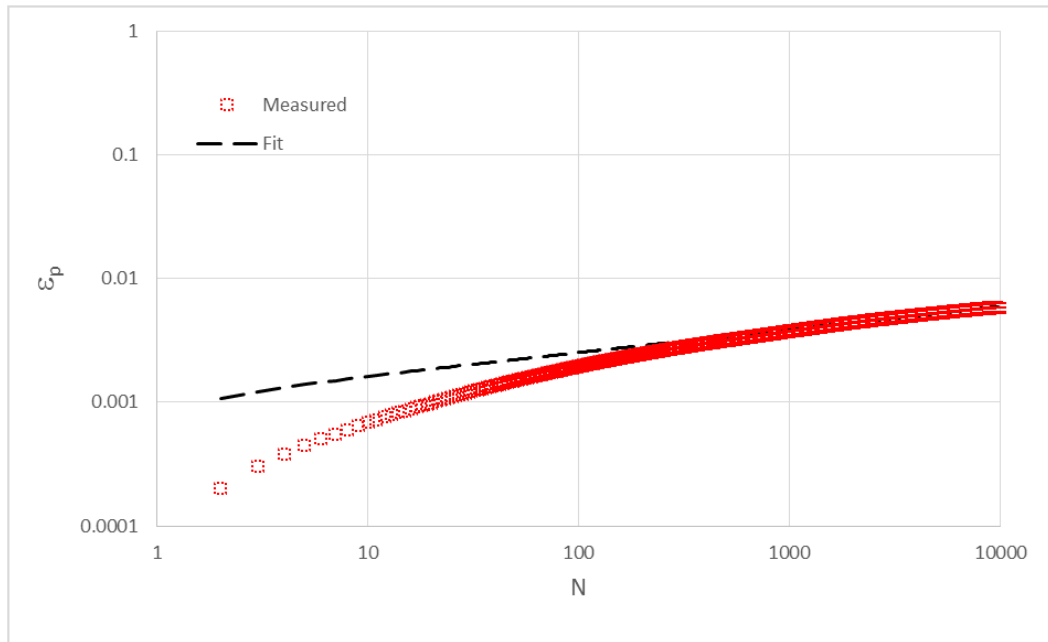
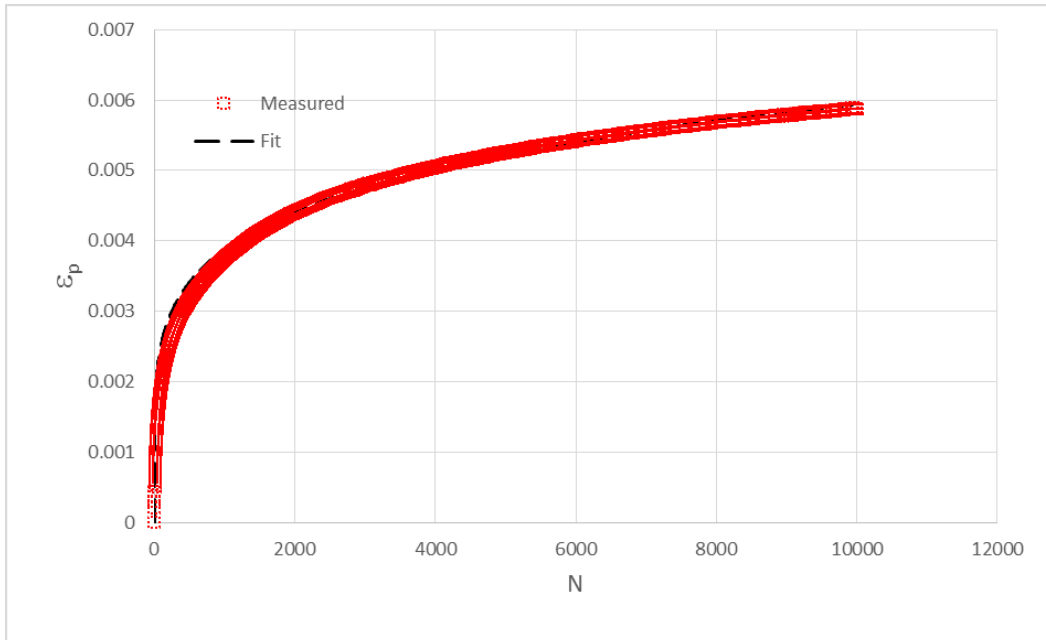
3EI DVR 6



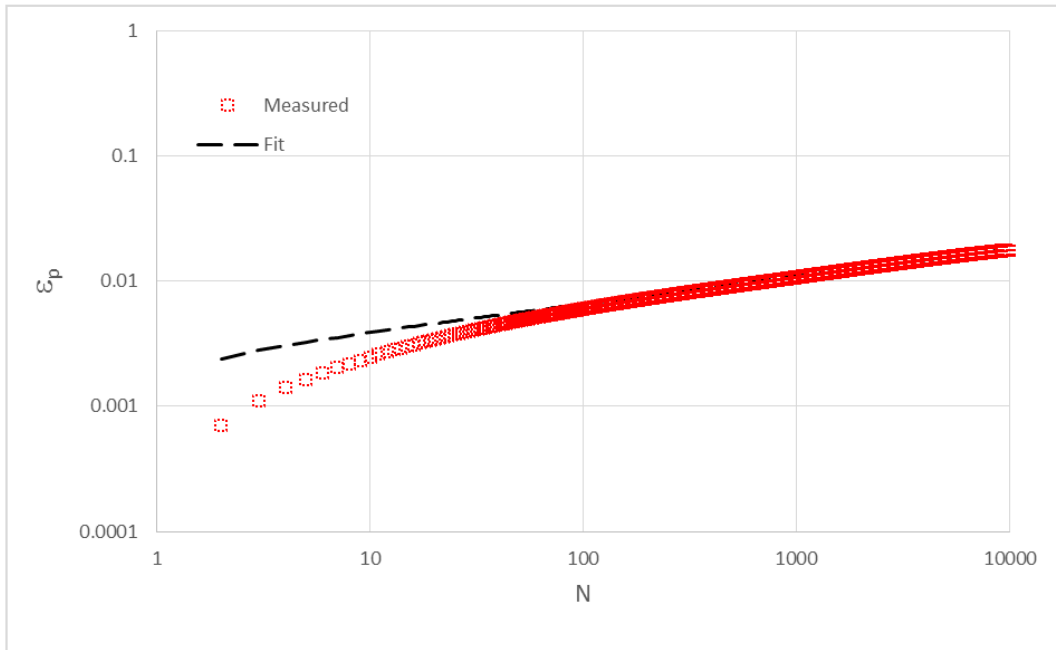
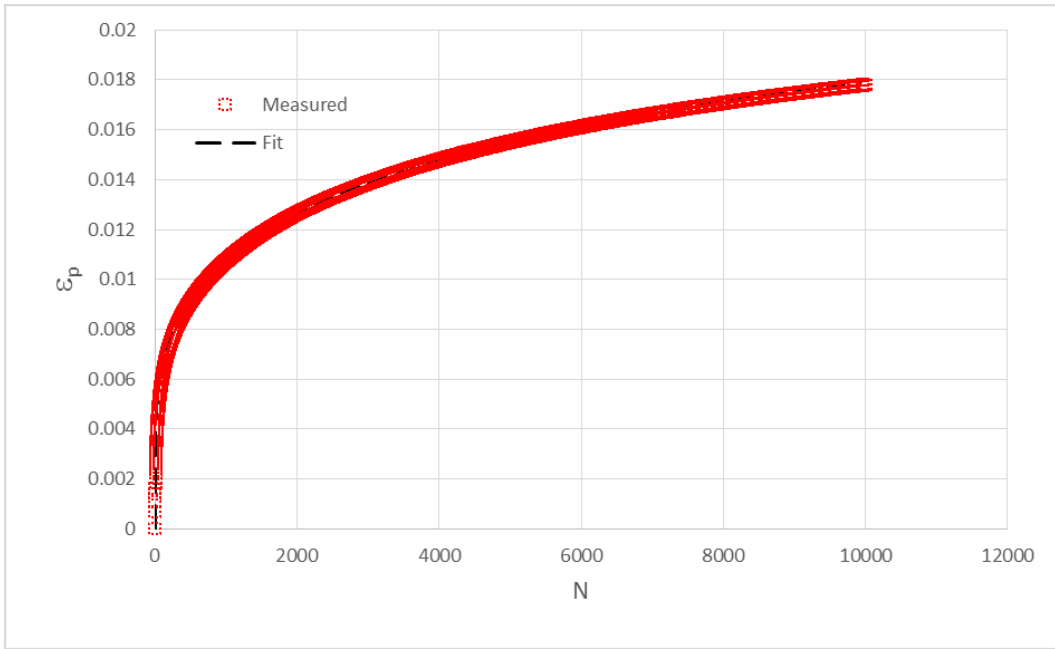
4EI DVR 1



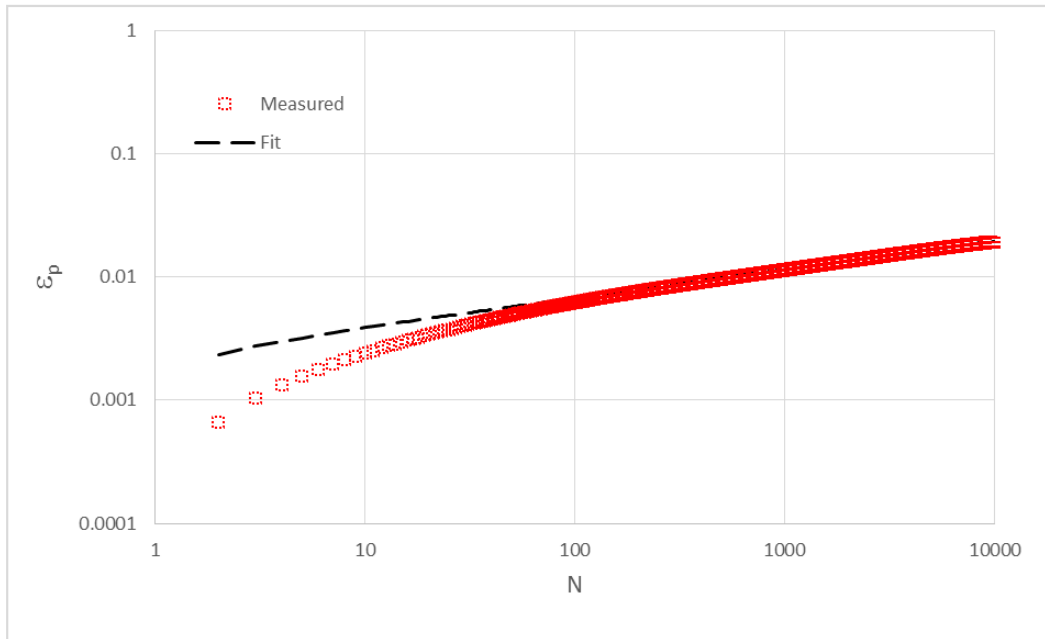
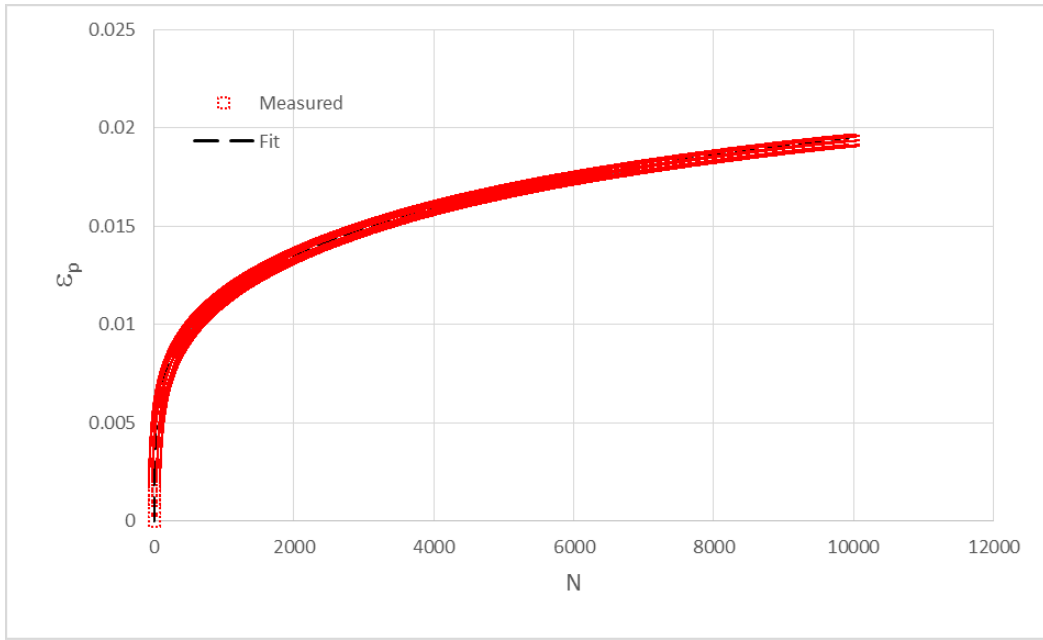
4E1 DVR 2



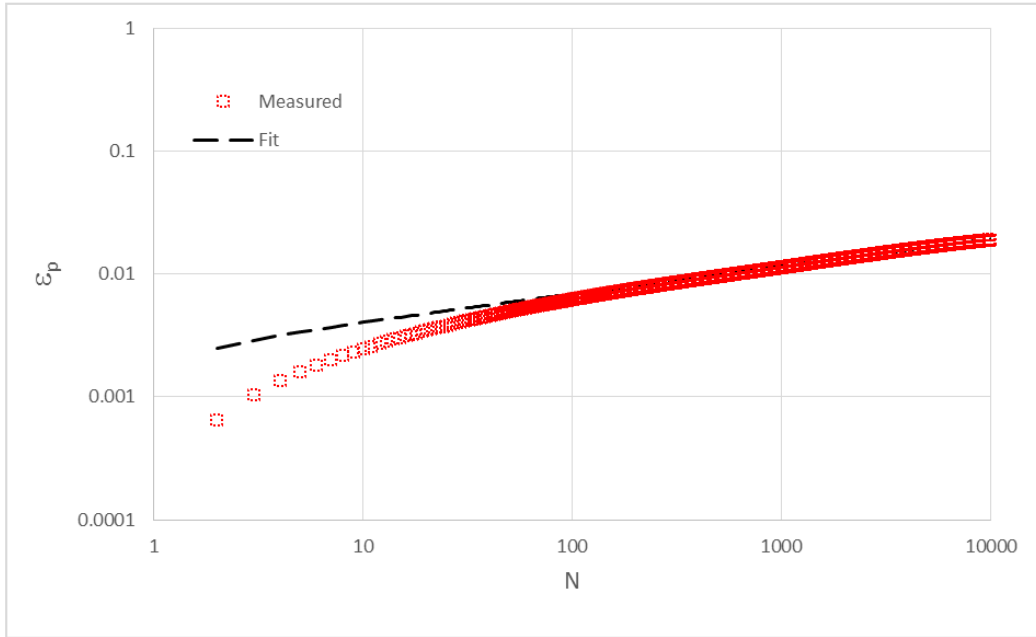
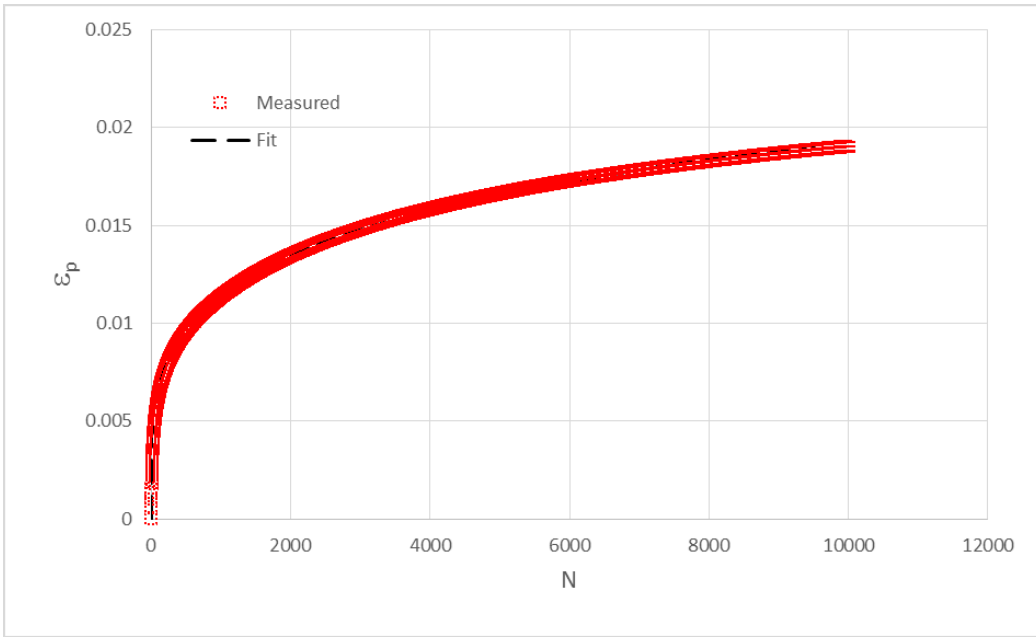
4E1 DVR 3



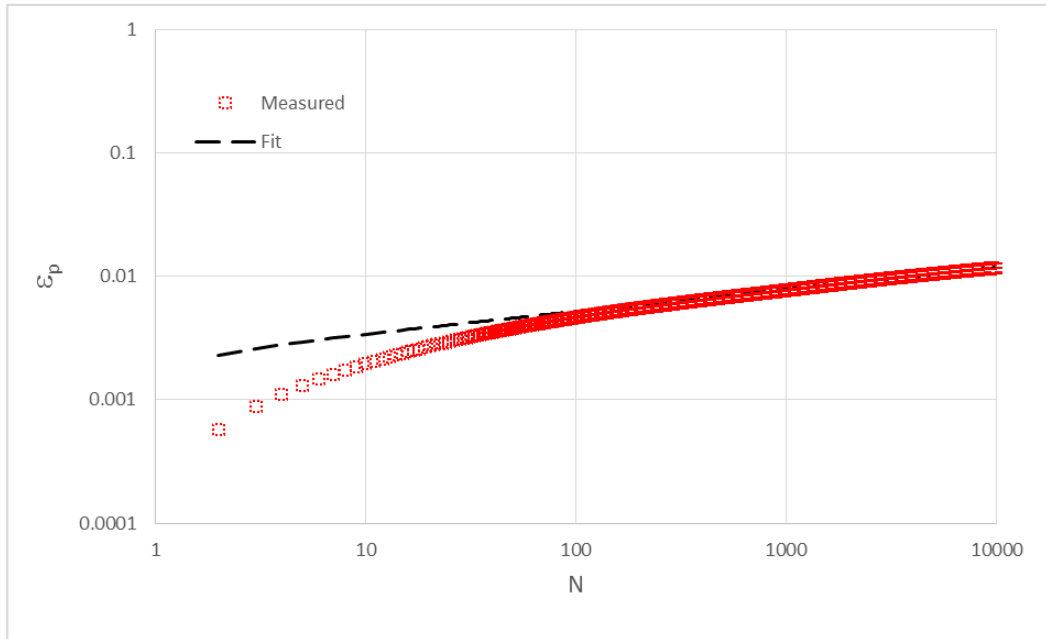
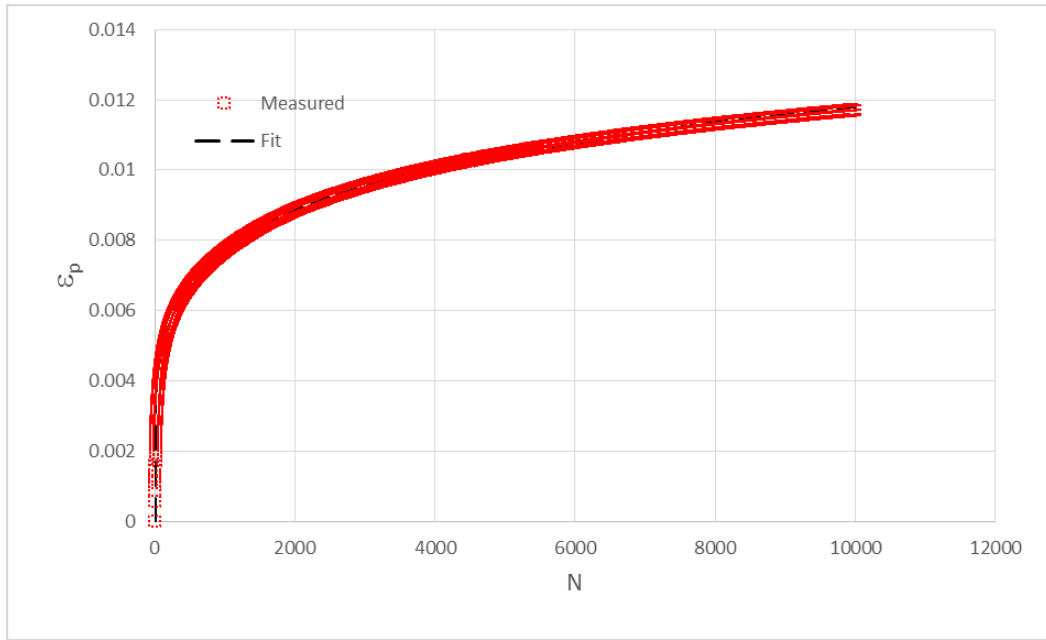
4EI DVR 4



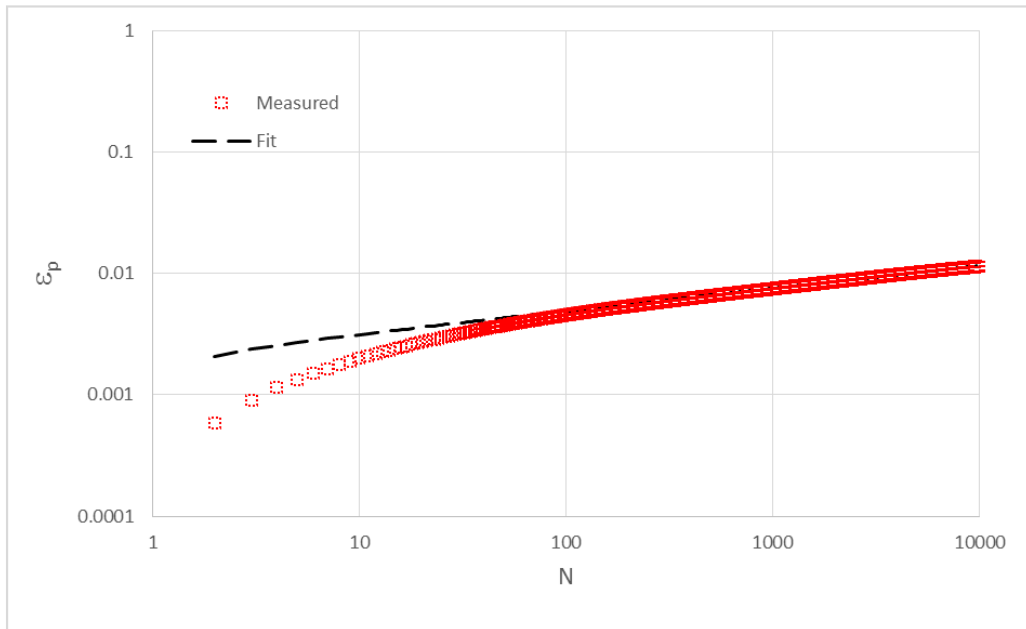
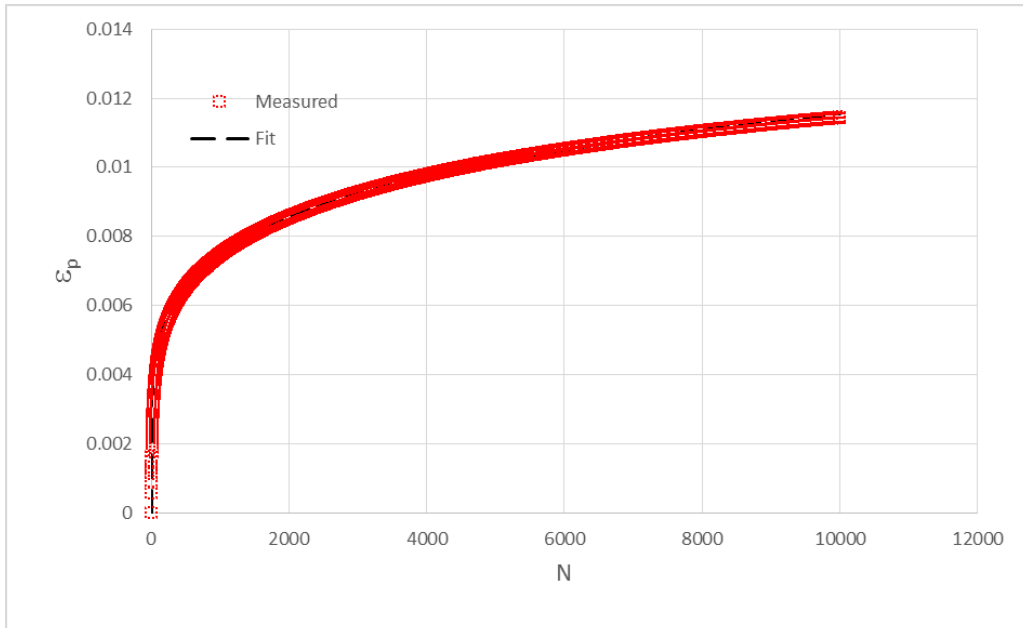
4E1 DVR 5



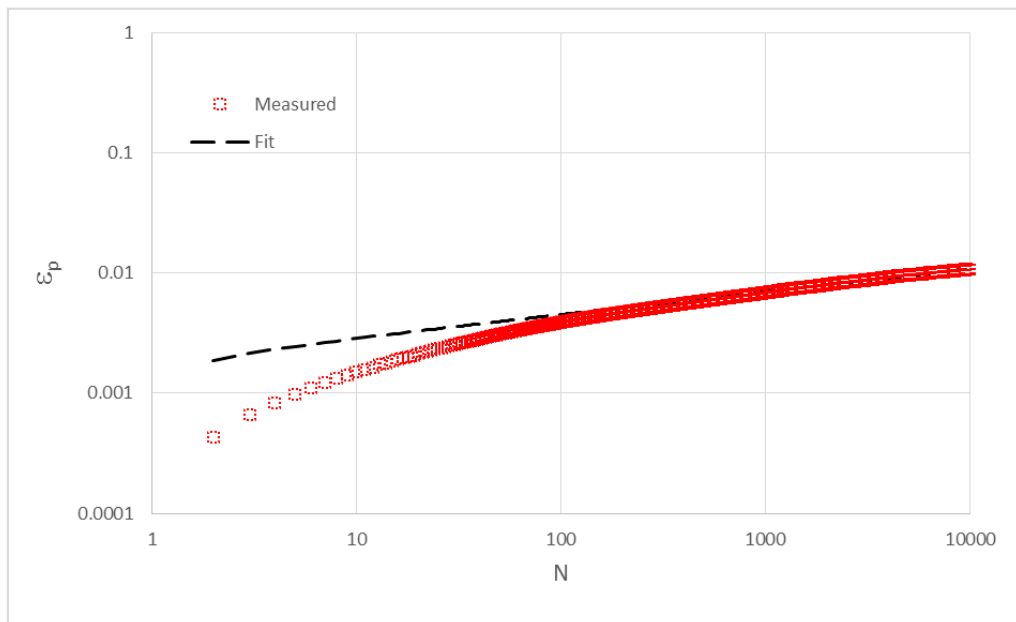
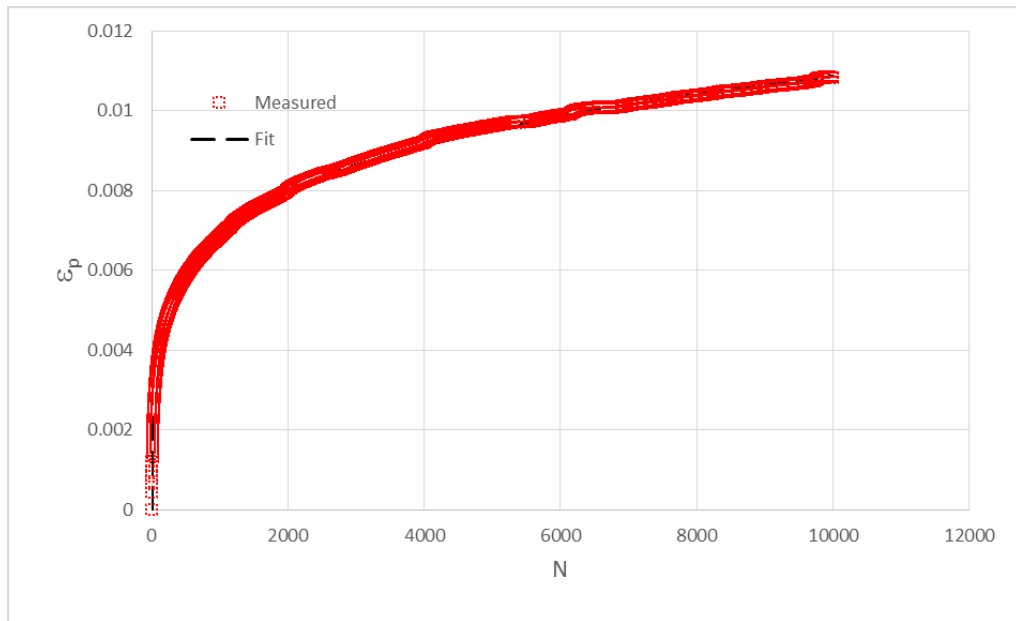
4E1 DVR 6



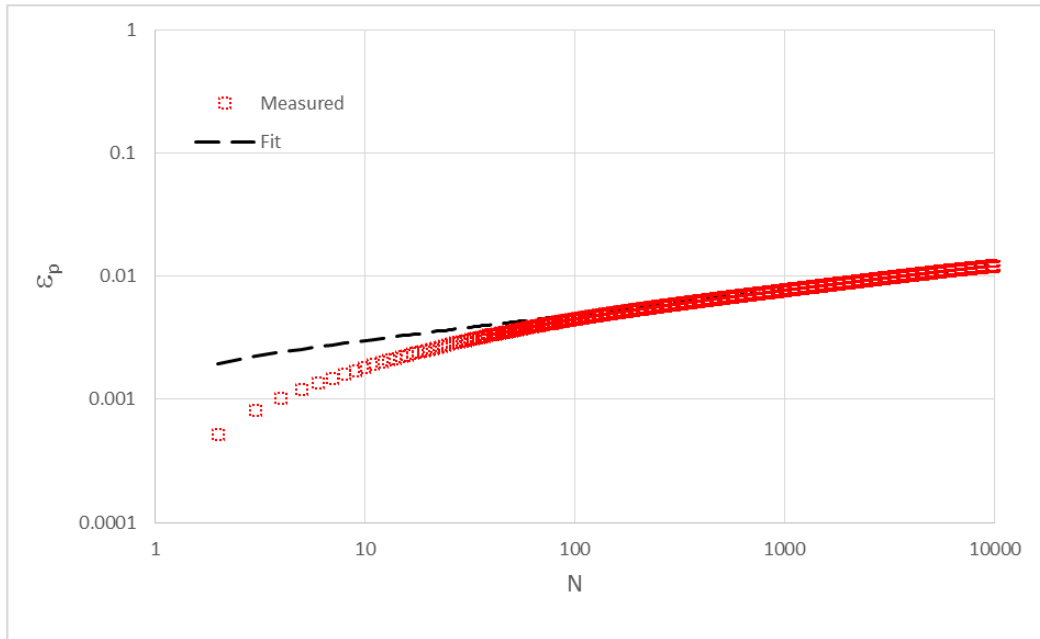
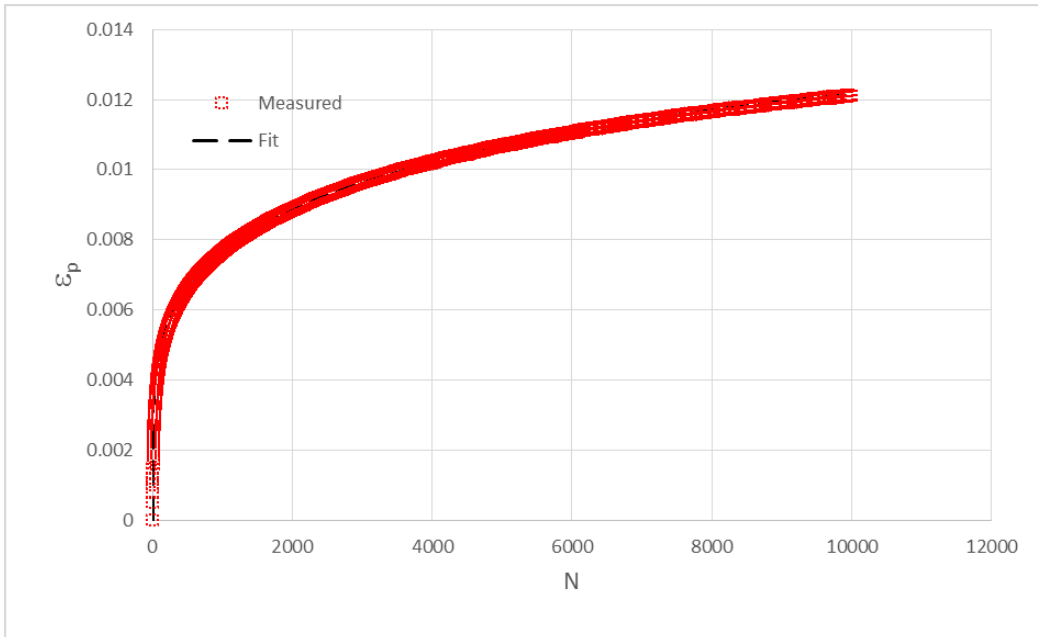
3E1 HS 1



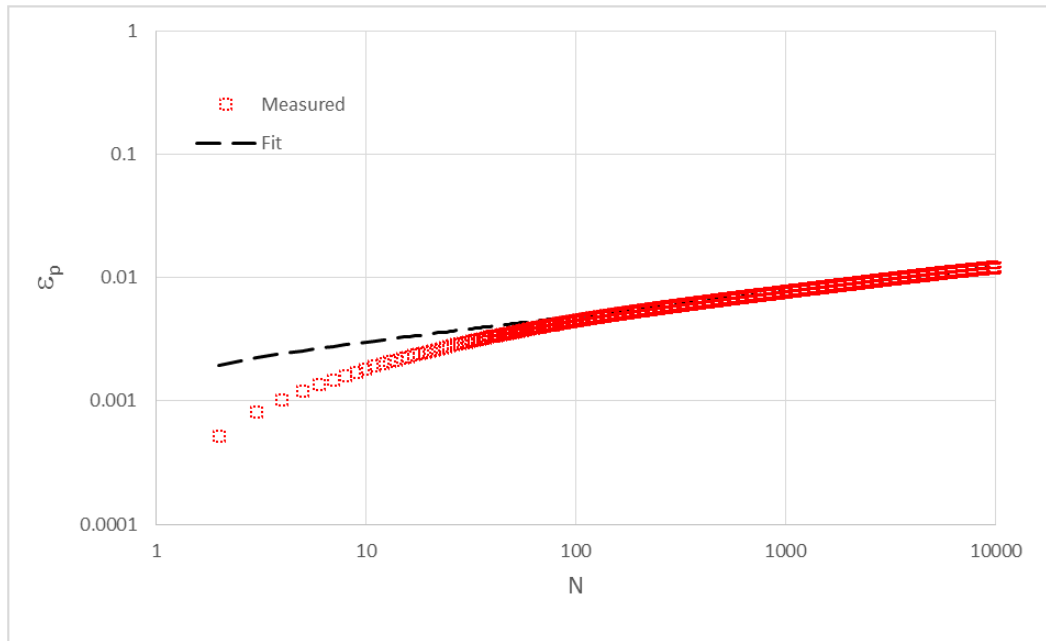
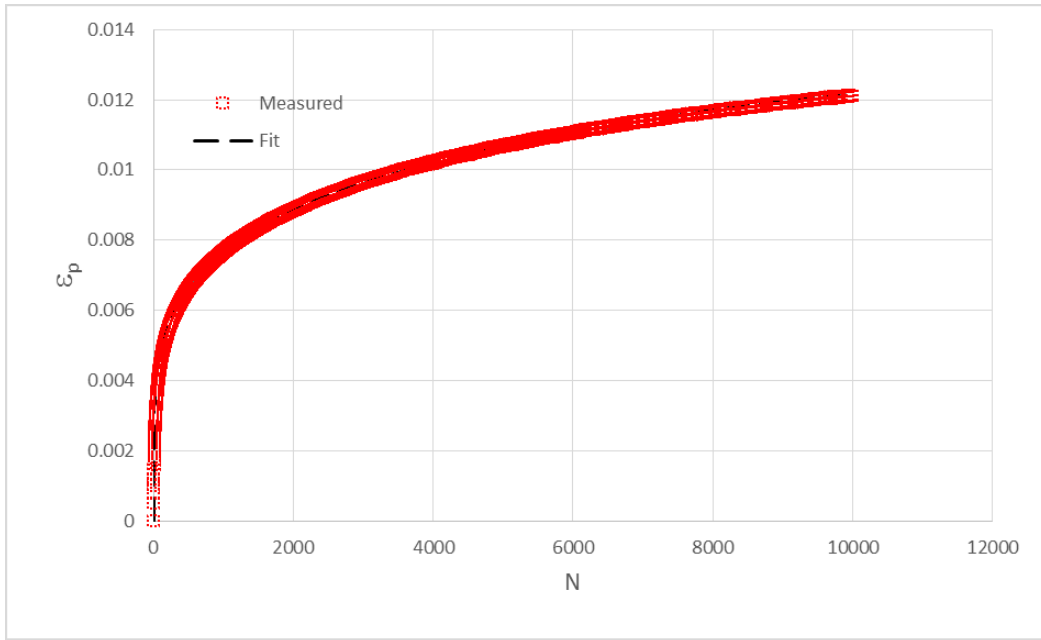
3E1 HS 2



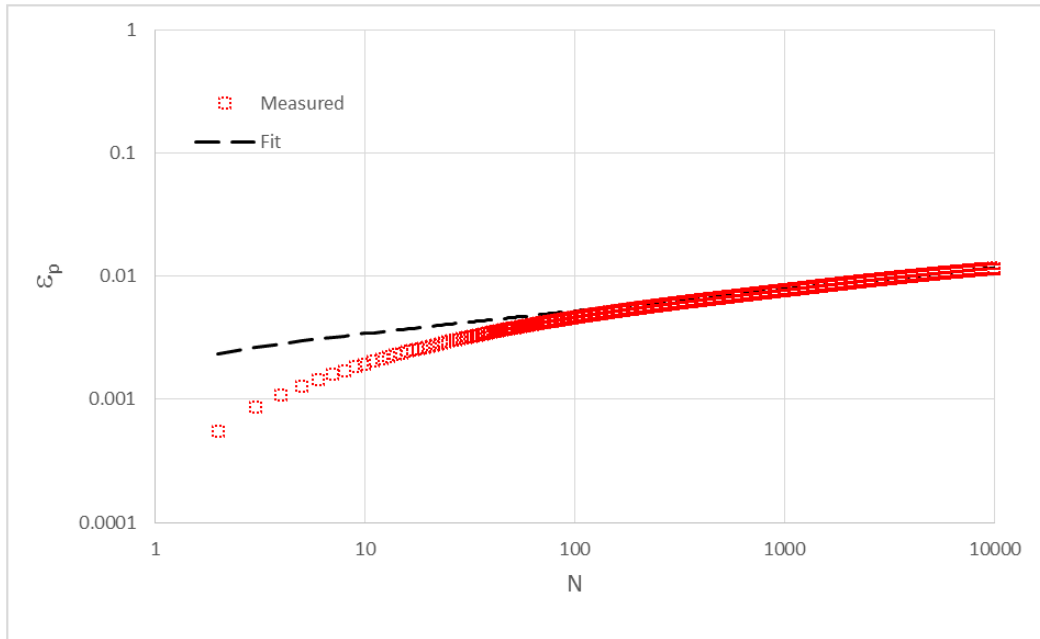
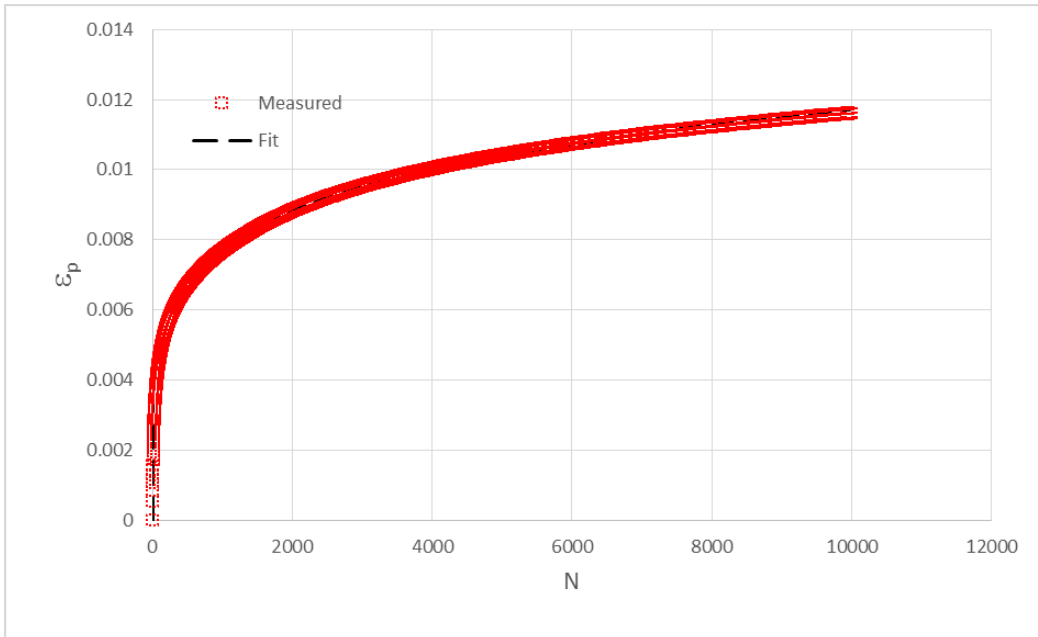
3E1 HS 3



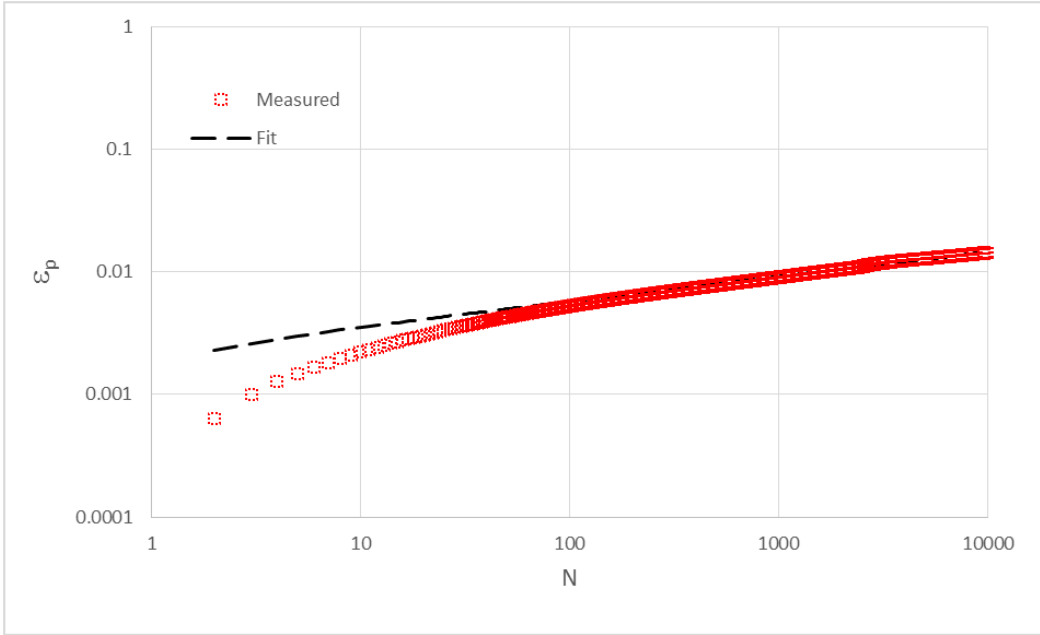
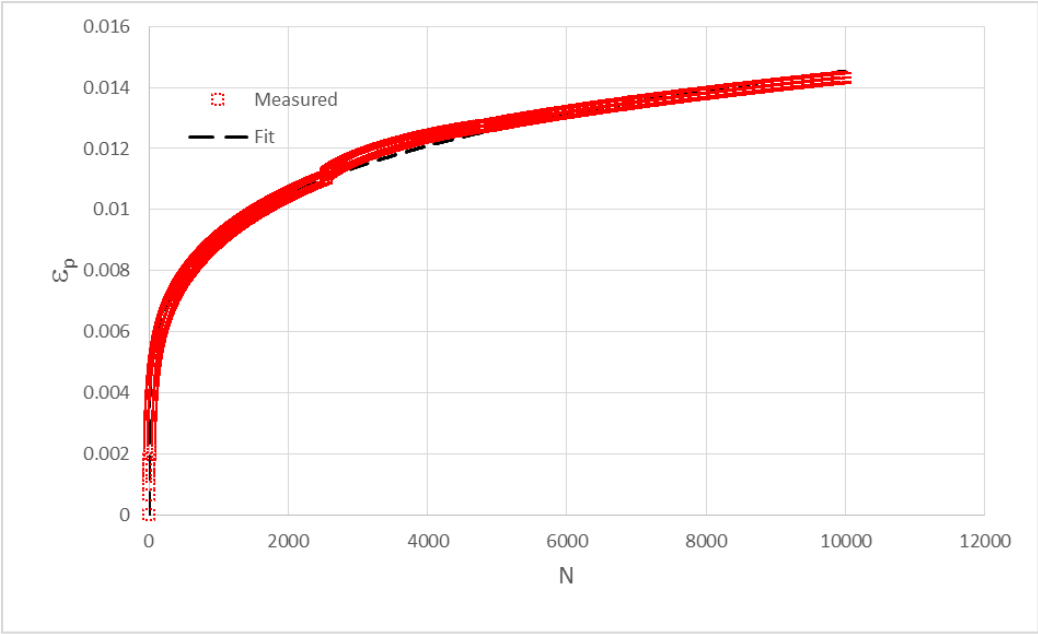
3EI HS 4



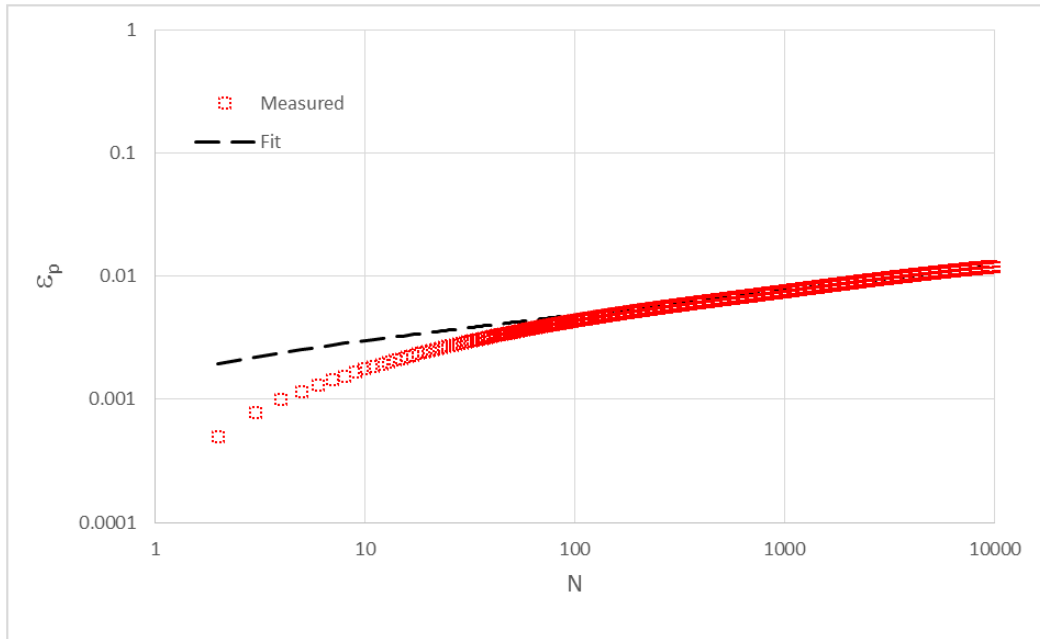
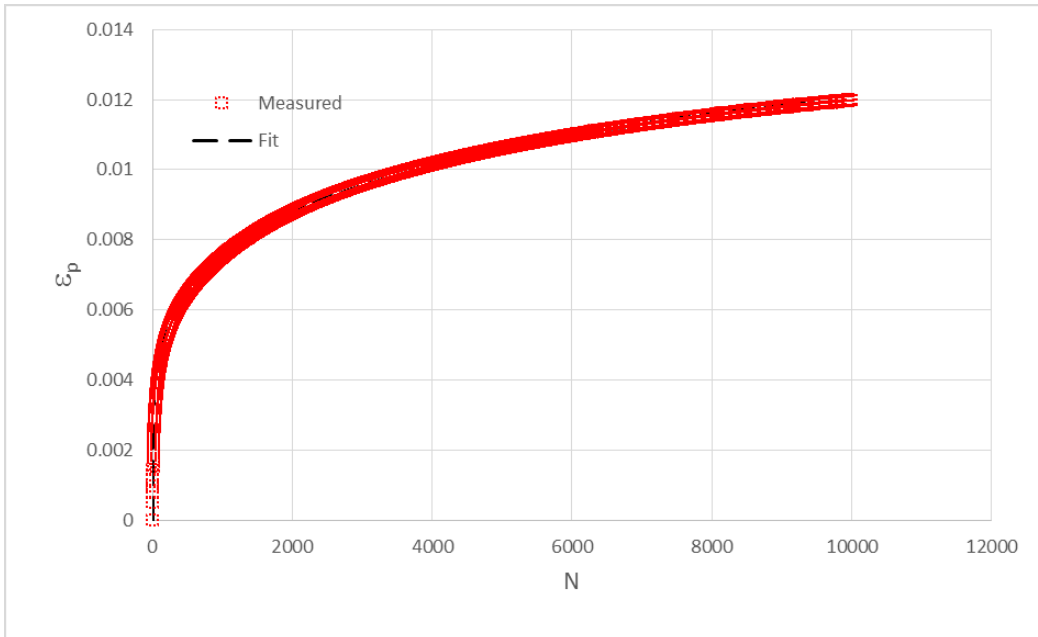
3E1 HS 5



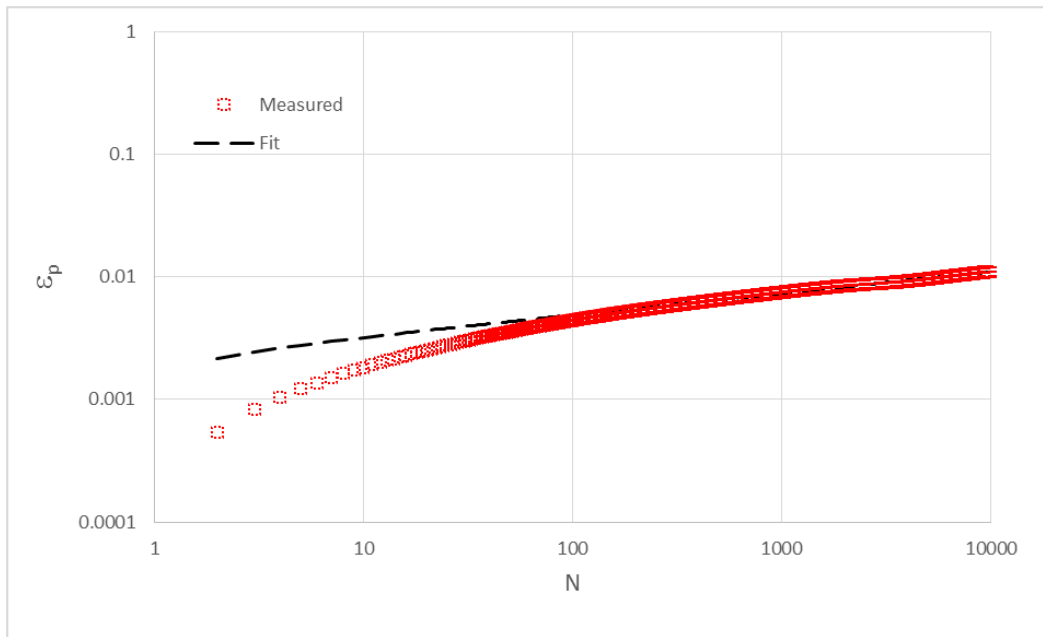
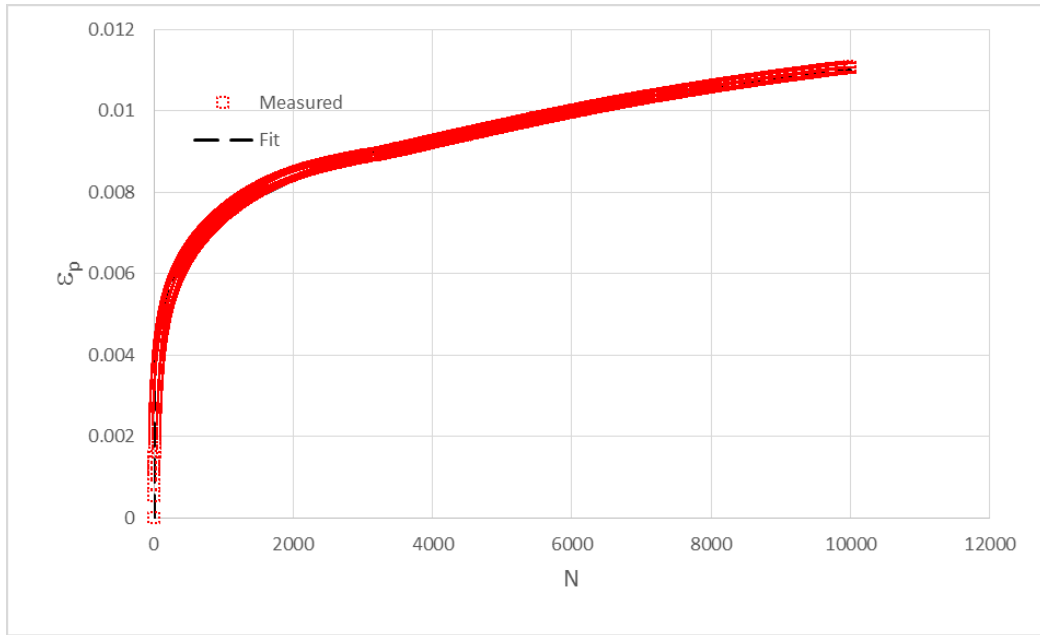
3EI HS 6



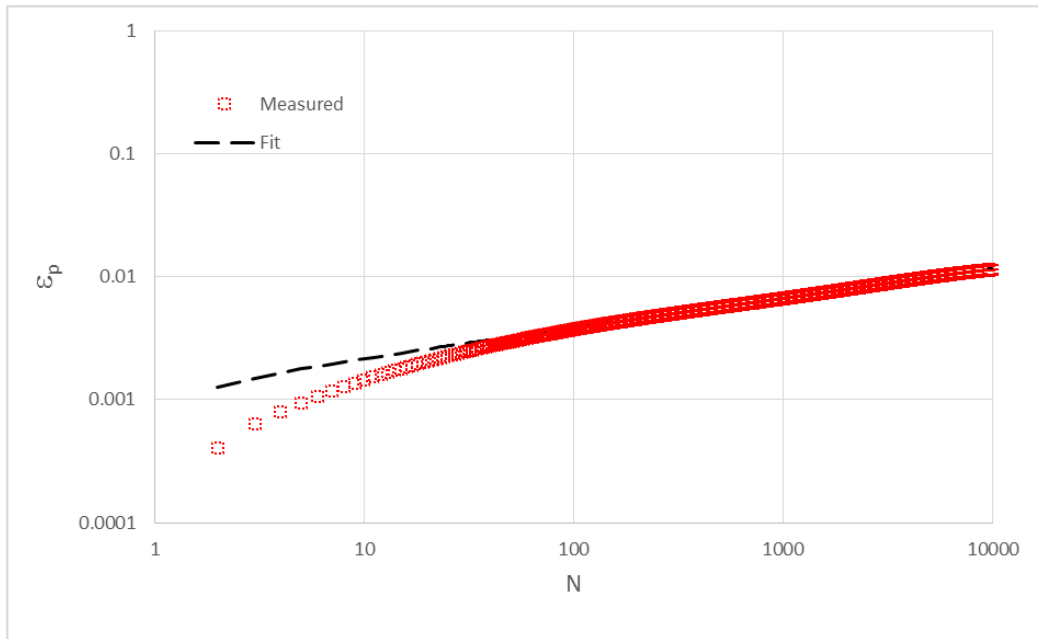
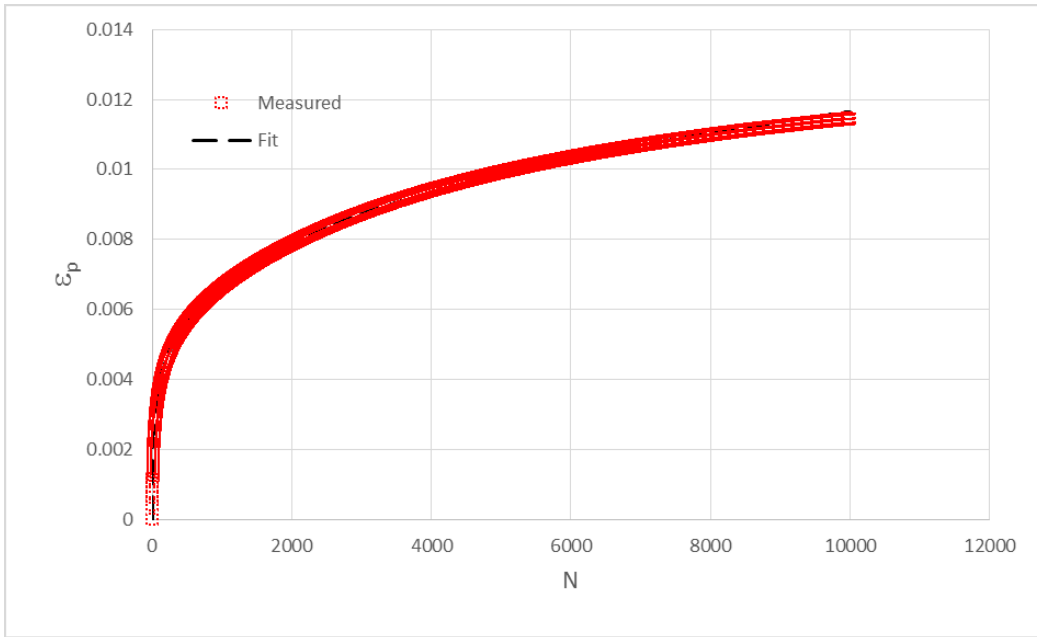
4E1 HS 1



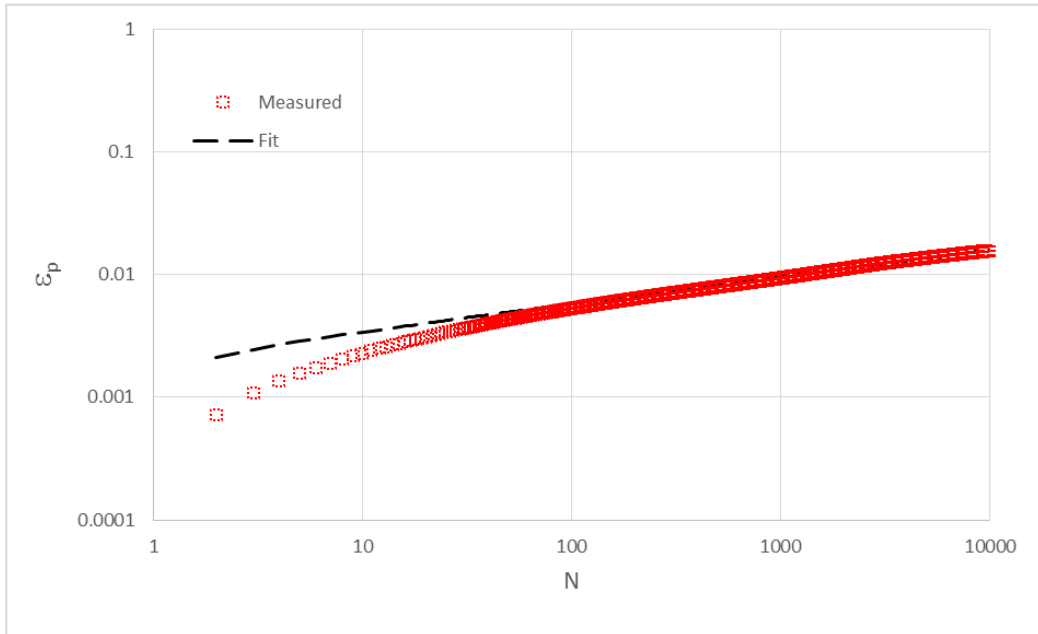
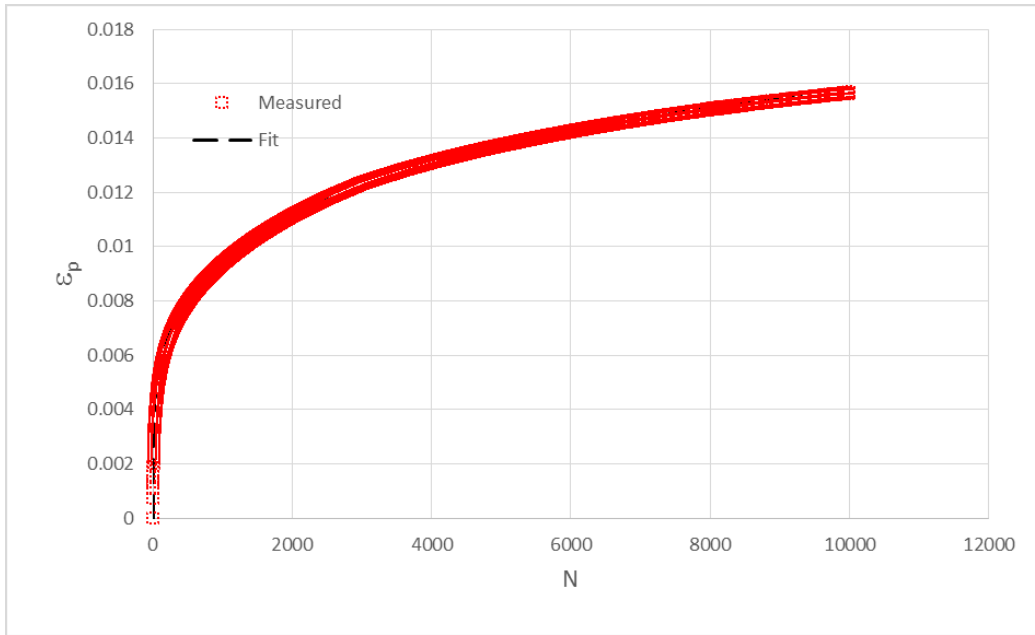
4E1 HS 2



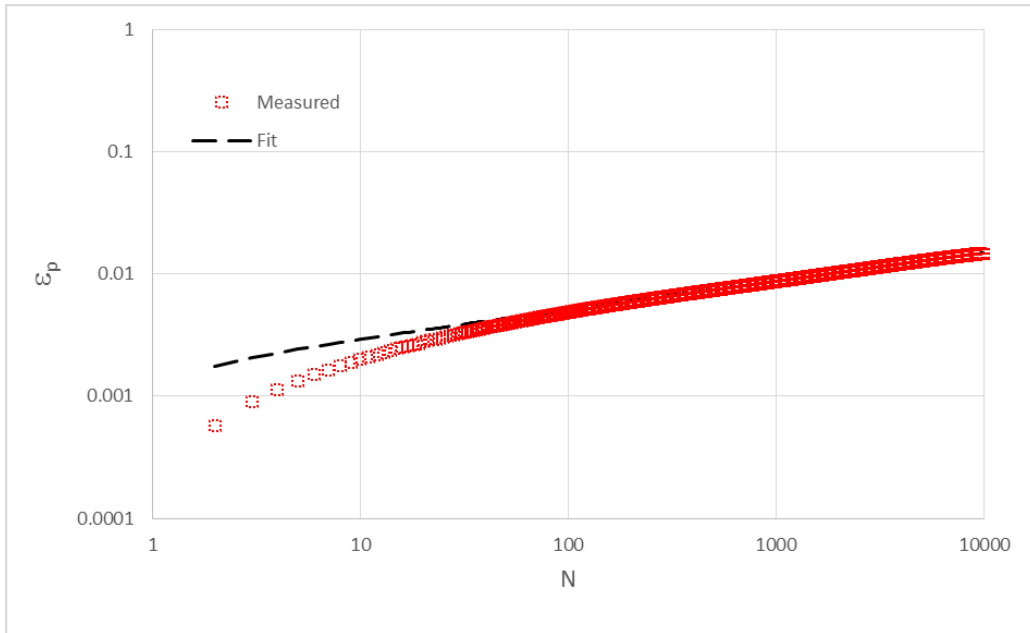
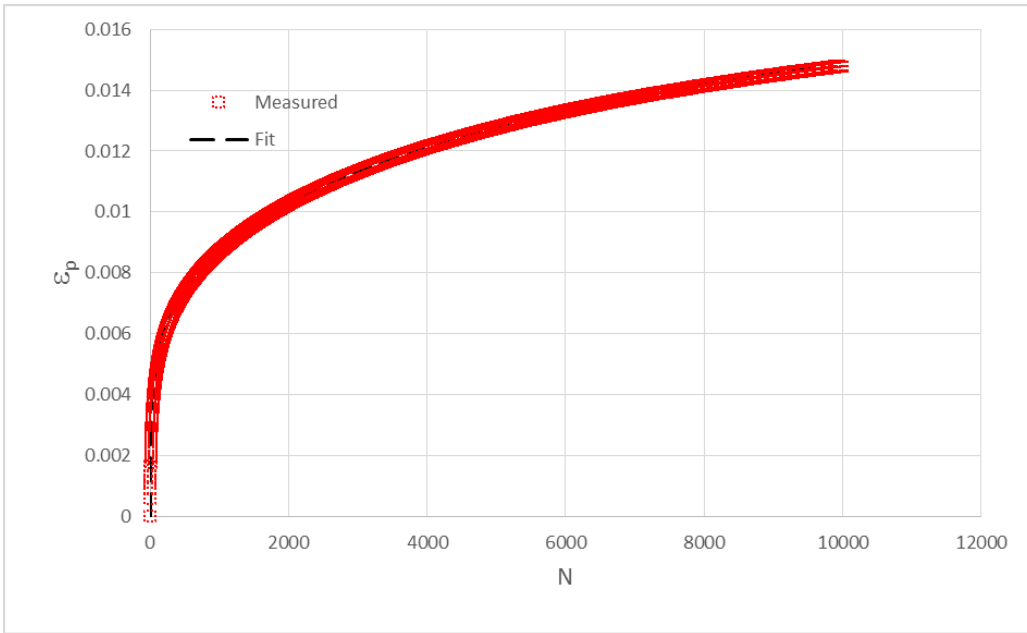
4E1 HS 3



4E1 HS 4



4E1 HS 5



4E1 HS 6

IL-SCB: Standard MSU model results



MICHIGAN STATE UNIVERSITY

Results of the SCB test

Project	Mix Type	Sample ID
MSU_Politto	3E1DVR	3E1DVR_1A

$P_1(u)$	$P_2(u)$	W_f	A_{relig}	G_f	$ m $	FI
[J]	[J]	[J]	[mm ²]	[J/m ²]	[-]	[-]
2.7	1.5	4.3	3135.0	1357.7	20.4	0.7

where:

$P_1(u)$ = area under the load vs displacement curve pre-peak

$P_2(u)$ = area under the load vs displacement curve post-peak

W_f = work of fracture

A_{relig} = ligament area

G_f = fracture energy

$|m|$ = absolute value of the post-peak load slope

FI = flexibility index

where:

$P_1(u)$ = area under the load vs displacement curve pre-peak

$P_2(u)$ = area under the load vs displacement curve post-peak

W_f = work of fracture

A_{relig} = ligament area

G_f = fracture energy

$|m|$ = absolute value of the post-peak load slope

FI = flexibility index

Project	Mix Type	Sample ID
MSU_Politto	3E1DVR	3E1DVR_1B

$P_1(u)$	$P_2(u)$	W_f	A_{relig}	G_f	$ m $	FI
[J]	[J]	[J]	[mm ²]	[J/m ²]	[-]	[-]
2.2	1.7	3.9	3180.0	1214.5	14.4	0.8

where:

$P_1(u)$ = area under the load vs displacement curve pre-peak

$P_2(u)$ = area under the load vs displacement curve post-peak

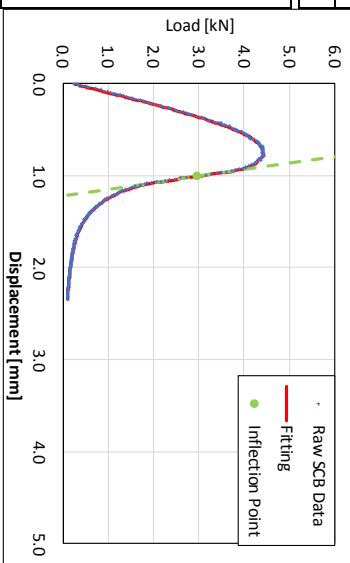
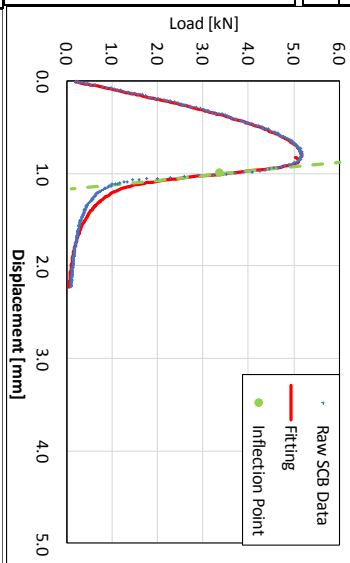
W_f = work of fracture

A_{relig} = ligament area

G_f = fracture energy

$|m|$ = absolute value of the post-peak load slope

FI = flexibility index



Project	Mix Type	Sample ID
MSU_Politto	3E1HS	3E1HS_IIA

$P_1(u)$	$P_2(u)$	W_f	Area _{lig}	G_f	m	FI
[J]	[J]	[J]	[mm ²]	[J/m ²]	[-]	[-]
3.0	2.5	5.5	2950.0	1864.0	5.3	3.5

where:
 $P_1(u)$ = area under the load vs displacement curve pre-peak
 $P_2(u)$ = area under the load vs displacement curve post-peak
 W_f = work of fracture
 Area_{lig} = ligament area
 G_f = fracture energy
 |m| = absolute value of the post-peak load slope
 FI = Flexibility index

Project	Mix Type	Sample ID
MSU_Politto	3E1DVR	3E1DVR_IIA

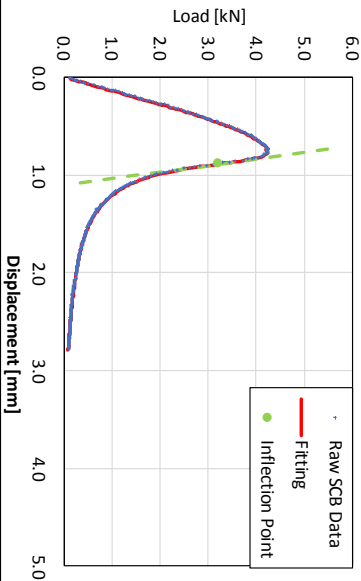
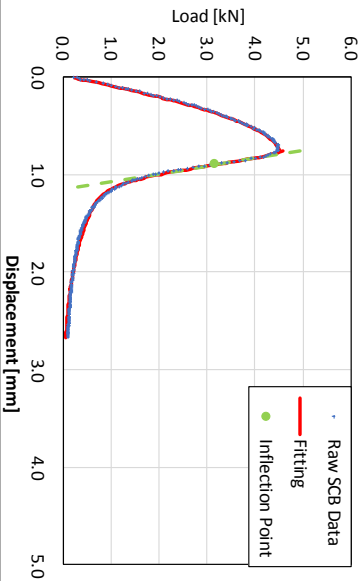
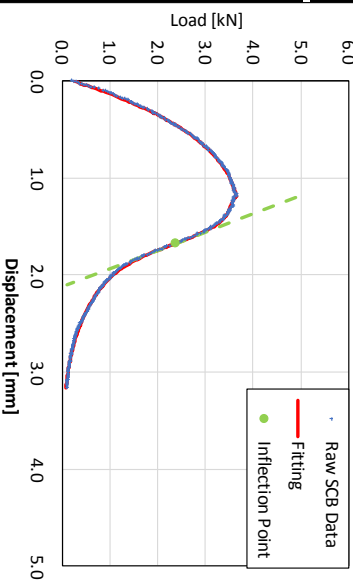
$P_1(u)$	$P_2(u)$	W_f	Area _{lig}	G_f	m	FI
[J]	[J]	[J]	[mm ²]	[J/m ²]	[-]	[-]
2.2	1.5	3.7	3009.0	1231.4	12.6	1.0

where:
 $P_1(u)$ = area under the load vs displacement curve pre-peak
 $P_2(u)$ = area under the load vs displacement curve post-peak
 W_f = work of fracture
 Area_{lig} = ligament area
 G_f = fracture energy
 |m| = absolute value of the post-peak load slope
 FI = flexibility index

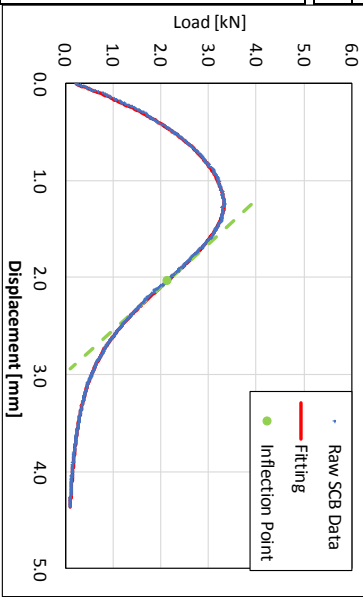
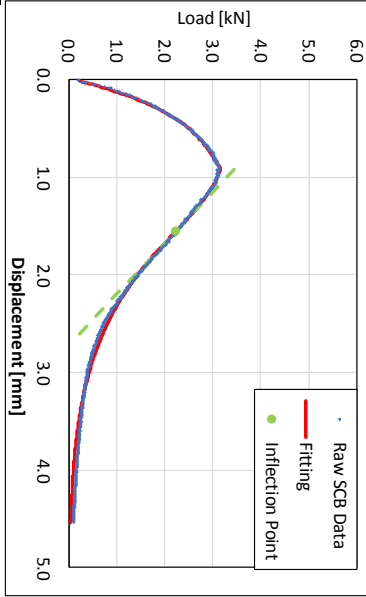
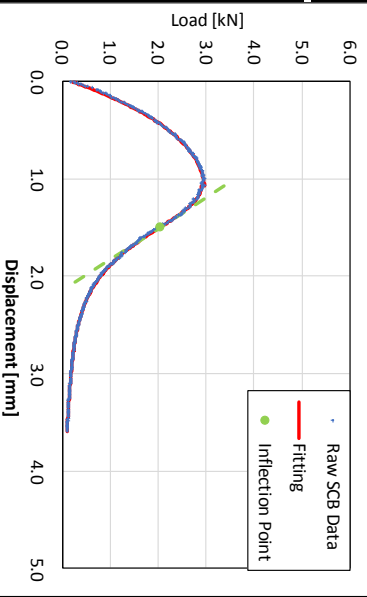
Project	Mix Type	Sample ID
MSU_Politto	3E1DVR	3E1DVR_IIB

$P_1(u)$	$P_2(u)$	W_f	Area _{lig}	G_f	m	FI
[J]	[J]	[J]	[mm ²]	[J/m ²]	[-]	[-]
1.8	1.7	3.5	2891.0	1202.0	14.8	0.8

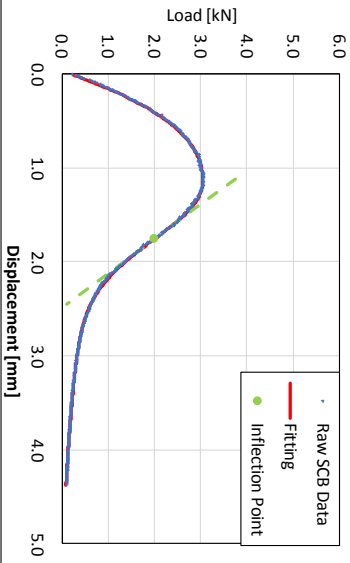
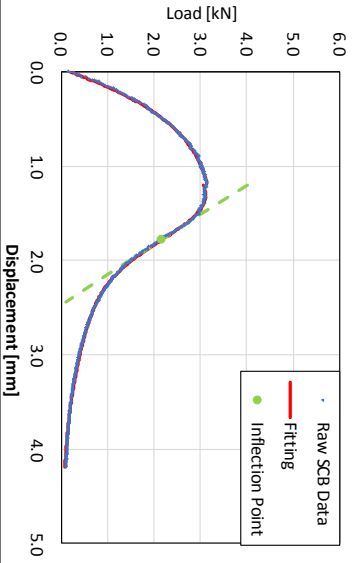
where:
 $P_1(u)$ = area under the load vs displacement curve pre-peak
 $P_2(u)$ = area under the load vs displacement curve post-peak
 W_f = work of fracture
 Area_{lig} = ligament area
 G_f = fracture energy
 |m| = absolute value of the post-peak load slope
 FI = flexibility index



Project	Mix Type	Sample ID																																																															
MSU_Politto	4E1DVR	4E1DVR_1A																																																															
<table border="1"> <thead> <tr> <th>$P_1(u)$</th> <th>$P_2(u)$</th> <th>W_f</th> <th>A_{relig}</th> <th>G_f</th> <th>m</th> <th>FI</th> </tr> </thead> <tbody> <tr> <td>[J]</td> <td>[J]</td> <td>[J]</td> <td>[mm²]</td> <td>[J/m²]</td> <td>[-]</td> <td>[-]</td> </tr> <tr> <td>2.2</td> <td>2.2</td> <td>4.4</td> <td>2891.0</td> <td>1530.7</td> <td>3.2</td> <td>4.8</td> </tr> </tbody> </table> <p>where: $P_1(u)$ = area under the load vs displacement curve pre-peak $P_2(u)$ = area under the load vs displacement curve post-peak W_f = work of fracture A_{relig} = ligament area G_f = fracture energy m = absolute value of the post-peak load slope FI = flexibility index</p>			$P_1(u)$	$P_2(u)$	W_f	A_{relig}	G_f	$ m $	FI	[J]	[J]	[J]	[mm ²]	[J/m ²]	[-]	[-]	2.2	2.2	4.4	2891.0	1530.7	3.2	4.8																																										
$P_1(u)$	$P_2(u)$	W_f	A_{relig}	G_f	$ m $	FI																																																											
[J]	[J]	[J]	[mm ²]	[J/m ²]	[-]	[-]																																																											
2.2	2.2	4.4	2891.0	1530.7	3.2	4.8																																																											
<table border="1"> <thead> <tr> <th>Project</th> <th>Mix Type</th> <th>Sample ID</th> </tr> </thead> <tbody> <tr> <td>MSU_Politto</td> <td>4E1DVR</td> <td>4E1DVR_1B</td> </tr> <tr> <td colspan="3"> <table border="1"> <thead> <tr> <th>$P_1(u)$</th> <th>$P_2(u)$</th> <th>W_f</th> <th>A_{relig}</th> <th>G_f</th> <th>m</th> <th>FI</th> </tr> </thead> <tbody> <tr> <td>[J]</td> <td>[J]</td> <td>[J]</td> <td>[mm²]</td> <td>[J/m²]</td> <td>[-]</td> <td>[-]</td> </tr> <tr> <td>1.9</td> <td>3.7</td> <td>5.6</td> <td>2950.0</td> <td>1901.5</td> <td>1.9</td> <td>9.9</td> </tr> </tbody> </table> <p>where: $P_1(u)$ = area under the load vs displacement curve pre-peak $P_2(u)$ = area under the load vs displacement curve post-peak W_f = work of fracture A_{relig} = ligament area G_f = fracture energy m = absolute value of the post-peak load slope FI = flexibility index</p> </td> </tr> <tr> <td colspan="3"> <table border="1"> <thead> <tr> <th>Project</th> <th>Mix Type</th> <th>Sample ID</th> </tr> </thead> <tbody> <tr> <td>MSU_Politto</td> <td>3E1HS</td> <td>3E1HS_1A</td> </tr> <tr> <td colspan="3"> <table border="1"> <thead> <tr> <th>$P_1(u)$</th> <th>$P_2(u)$</th> <th>W_f</th> <th>A_{relig}</th> <th>G_f</th> <th>m</th> <th>FI</th> </tr> </thead> <tbody> <tr> <td>[J]</td> <td>[J]</td> <td>[J]</td> <td>[mm²]</td> <td>[J/m²]</td> <td>[-]</td> <td>[-]</td> </tr> <tr> <td>2.9</td> <td>3.8</td> <td>6.6</td> <td>3016.0</td> <td>2199.7</td> <td>2.3</td> <td>9.8</td> </tr> </tbody> </table> <p>where: $P_1(u)$ = area under the load vs displacement curve pre-peak $P_2(u)$ = area under the load vs displacement curve post-peak W_f = work of fracture A_{relig} = ligament area G_f = fracture energy m = absolute value of the post-peak load slope FI = flexibility index</p> </td> </tr> </tbody> </table> </td></tr></tbody></table>			Project	Mix Type	Sample ID	MSU_Politto	4E1DVR	4E1DVR_1B	<table border="1"> <thead> <tr> <th>$P_1(u)$</th> <th>$P_2(u)$</th> <th>W_f</th> <th>A_{relig}</th> <th>G_f</th> <th>m</th> <th>FI</th> </tr> </thead> <tbody> <tr> <td>[J]</td> <td>[J]</td> <td>[J]</td> <td>[mm²]</td> <td>[J/m²]</td> <td>[-]</td> <td>[-]</td> </tr> <tr> <td>1.9</td> <td>3.7</td> <td>5.6</td> <td>2950.0</td> <td>1901.5</td> <td>1.9</td> <td>9.9</td> </tr> </tbody> </table> <p>where: $P_1(u)$ = area under the load vs displacement curve pre-peak $P_2(u)$ = area under the load vs displacement curve post-peak W_f = work of fracture A_{relig} = ligament area G_f = fracture energy m = absolute value of the post-peak load slope FI = flexibility index</p>			$P_1(u)$	$P_2(u)$	W_f	A_{relig}	G_f	$ m $	FI	[J]	[J]	[J]	[mm ²]	[J/m ²]	[-]	[-]	1.9	3.7	5.6	2950.0	1901.5	1.9	9.9	<table border="1"> <thead> <tr> <th>Project</th> <th>Mix Type</th> <th>Sample ID</th> </tr> </thead> <tbody> <tr> <td>MSU_Politto</td> <td>3E1HS</td> <td>3E1HS_1A</td> </tr> <tr> <td colspan="3"> <table border="1"> <thead> <tr> <th>$P_1(u)$</th> <th>$P_2(u)$</th> <th>W_f</th> <th>A_{relig}</th> <th>G_f</th> <th>m</th> <th>FI</th> </tr> </thead> <tbody> <tr> <td>[J]</td> <td>[J]</td> <td>[J]</td> <td>[mm²]</td> <td>[J/m²]</td> <td>[-]</td> <td>[-]</td> </tr> <tr> <td>2.9</td> <td>3.8</td> <td>6.6</td> <td>3016.0</td> <td>2199.7</td> <td>2.3</td> <td>9.8</td> </tr> </tbody> </table> <p>where: $P_1(u)$ = area under the load vs displacement curve pre-peak $P_2(u)$ = area under the load vs displacement curve post-peak W_f = work of fracture A_{relig} = ligament area G_f = fracture energy m = absolute value of the post-peak load slope FI = flexibility index</p> </td> </tr> </tbody> </table>			Project	Mix Type	Sample ID	MSU_Politto	3E1HS	3E1HS_1A	<table border="1"> <thead> <tr> <th>$P_1(u)$</th> <th>$P_2(u)$</th> <th>W_f</th> <th>A_{relig}</th> <th>G_f</th> <th>m</th> <th>FI</th> </tr> </thead> <tbody> <tr> <td>[J]</td> <td>[J]</td> <td>[J]</td> <td>[mm²]</td> <td>[J/m²]</td> <td>[-]</td> <td>[-]</td> </tr> <tr> <td>2.9</td> <td>3.8</td> <td>6.6</td> <td>3016.0</td> <td>2199.7</td> <td>2.3</td> <td>9.8</td> </tr> </tbody> </table> <p>where: $P_1(u)$ = area under the load vs displacement curve pre-peak $P_2(u)$ = area under the load vs displacement curve post-peak W_f = work of fracture A_{relig} = ligament area G_f = fracture energy m = absolute value of the post-peak load slope FI = flexibility index</p>			$P_1(u)$	$P_2(u)$	W_f	A_{relig}	G_f	$ m $	FI	[J]	[J]	[J]	[mm ²]	[J/m ²]	[-]	[-]	2.9	3.8	6.6	3016.0	2199.7	2.3	9.8
Project	Mix Type	Sample ID																																																															
MSU_Politto	4E1DVR	4E1DVR_1B																																																															
<table border="1"> <thead> <tr> <th>$P_1(u)$</th> <th>$P_2(u)$</th> <th>W_f</th> <th>A_{relig}</th> <th>G_f</th> <th>m</th> <th>FI</th> </tr> </thead> <tbody> <tr> <td>[J]</td> <td>[J]</td> <td>[J]</td> <td>[mm²]</td> <td>[J/m²]</td> <td>[-]</td> <td>[-]</td> </tr> <tr> <td>1.9</td> <td>3.7</td> <td>5.6</td> <td>2950.0</td> <td>1901.5</td> <td>1.9</td> <td>9.9</td> </tr> </tbody> </table> <p>where: $P_1(u)$ = area under the load vs displacement curve pre-peak $P_2(u)$ = area under the load vs displacement curve post-peak W_f = work of fracture A_{relig} = ligament area G_f = fracture energy m = absolute value of the post-peak load slope FI = flexibility index</p>			$P_1(u)$	$P_2(u)$	W_f	A_{relig}	G_f	$ m $	FI	[J]	[J]	[J]	[mm ²]	[J/m ²]	[-]	[-]	1.9	3.7	5.6	2950.0	1901.5	1.9	9.9																																										
$P_1(u)$	$P_2(u)$	W_f	A_{relig}	G_f	$ m $	FI																																																											
[J]	[J]	[J]	[mm ²]	[J/m ²]	[-]	[-]																																																											
1.9	3.7	5.6	2950.0	1901.5	1.9	9.9																																																											
<table border="1"> <thead> <tr> <th>Project</th> <th>Mix Type</th> <th>Sample ID</th> </tr> </thead> <tbody> <tr> <td>MSU_Politto</td> <td>3E1HS</td> <td>3E1HS_1A</td> </tr> <tr> <td colspan="3"> <table border="1"> <thead> <tr> <th>$P_1(u)$</th> <th>$P_2(u)$</th> <th>W_f</th> <th>A_{relig}</th> <th>G_f</th> <th>m</th> <th>FI</th> </tr> </thead> <tbody> <tr> <td>[J]</td> <td>[J]</td> <td>[J]</td> <td>[mm²]</td> <td>[J/m²]</td> <td>[-]</td> <td>[-]</td> </tr> <tr> <td>2.9</td> <td>3.8</td> <td>6.6</td> <td>3016.0</td> <td>2199.7</td> <td>2.3</td> <td>9.8</td> </tr> </tbody> </table> <p>where: $P_1(u)$ = area under the load vs displacement curve pre-peak $P_2(u)$ = area under the load vs displacement curve post-peak W_f = work of fracture A_{relig} = ligament area G_f = fracture energy m = absolute value of the post-peak load slope FI = flexibility index</p> </td> </tr> </tbody> </table>			Project	Mix Type	Sample ID	MSU_Politto	3E1HS	3E1HS_1A	<table border="1"> <thead> <tr> <th>$P_1(u)$</th> <th>$P_2(u)$</th> <th>W_f</th> <th>A_{relig}</th> <th>G_f</th> <th>m</th> <th>FI</th> </tr> </thead> <tbody> <tr> <td>[J]</td> <td>[J]</td> <td>[J]</td> <td>[mm²]</td> <td>[J/m²]</td> <td>[-]</td> <td>[-]</td> </tr> <tr> <td>2.9</td> <td>3.8</td> <td>6.6</td> <td>3016.0</td> <td>2199.7</td> <td>2.3</td> <td>9.8</td> </tr> </tbody> </table> <p>where: $P_1(u)$ = area under the load vs displacement curve pre-peak $P_2(u)$ = area under the load vs displacement curve post-peak W_f = work of fracture A_{relig} = ligament area G_f = fracture energy m = absolute value of the post-peak load slope FI = flexibility index</p>			$P_1(u)$	$P_2(u)$	W_f	A_{relig}	G_f	$ m $	FI	[J]	[J]	[J]	[mm ²]	[J/m ²]	[-]	[-]	2.9	3.8	6.6	3016.0	2199.7	2.3	9.8																																	
Project	Mix Type	Sample ID																																																															
MSU_Politto	3E1HS	3E1HS_1A																																																															
<table border="1"> <thead> <tr> <th>$P_1(u)$</th> <th>$P_2(u)$</th> <th>W_f</th> <th>A_{relig}</th> <th>G_f</th> <th>m</th> <th>FI</th> </tr> </thead> <tbody> <tr> <td>[J]</td> <td>[J]</td> <td>[J]</td> <td>[mm²]</td> <td>[J/m²]</td> <td>[-]</td> <td>[-]</td> </tr> <tr> <td>2.9</td> <td>3.8</td> <td>6.6</td> <td>3016.0</td> <td>2199.7</td> <td>2.3</td> <td>9.8</td> </tr> </tbody> </table> <p>where: $P_1(u)$ = area under the load vs displacement curve pre-peak $P_2(u)$ = area under the load vs displacement curve post-peak W_f = work of fracture A_{relig} = ligament area G_f = fracture energy m = absolute value of the post-peak load slope FI = flexibility index</p>			$P_1(u)$	$P_2(u)$	W_f	A_{relig}	G_f	$ m $	FI	[J]	[J]	[J]	[mm ²]	[J/m ²]	[-]	[-]	2.9	3.8	6.6	3016.0	2199.7	2.3	9.8																																										
$P_1(u)$	$P_2(u)$	W_f	A_{relig}	G_f	$ m $	FI																																																											
[J]	[J]	[J]	[mm ²]	[J/m ²]	[-]	[-]																																																											
2.9	3.8	6.6	3016.0	2199.7	2.3	9.8																																																											



Project	Mix Type	Sample ID																																	
MSU_Polito	4E1DVR	4E1DVR_IIB																																	
<table border="1"> <thead> <tr> <th>$P_1(u)$</th> <th>$P_2(u)$</th> <th>W_f</th> <th>$Area_{lig}$</th> <th>G_f</th> <th>m</th> <th>FI</th> </tr> </thead> <tbody> <tr> <td>[J]</td> <td>[J]</td> <td>[J]</td> <td>[mm²]</td> <td>[J/m²]</td> <td>[-]</td> <td>[-]</td> </tr> <tr> <td>2.6</td> <td>3.1</td> <td>5.7</td> <td>3240.0</td> <td>1745.8</td> <td>3.1</td> <td>5.5</td> </tr> </tbody> </table>			$P_1(u)$	$P_2(u)$	W_f	$Area_{lig}$	G_f	$ m $	FI	[J]	[J]	[J]	[mm ²]	[J/m ²]	[-]	[-]	2.6	3.1	5.7	3240.0	1745.8	3.1	5.5												
$P_1(u)$	$P_2(u)$	W_f	$Area_{lig}$	G_f	$ m $	FI																													
[J]	[J]	[J]	[mm ²]	[J/m ²]	[-]	[-]																													
2.6	3.1	5.7	3240.0	1745.8	3.1	5.5																													
<p>where:</p> <p>$P_1(u)$ = area under the load vs displacement curve pre-peak</p> <p>$P_2(u)$ = area under the load vs displacement curve post-peak</p> <p>W_f = work of fracture</p> <p>$Area_{lig}$ = ligament area</p> <p>G_f = fracture energy</p> <p>m = absolute value of the post-peak load slope</p> <p>FI = flexibility index</p>																																			
<table border="1"> <thead> <tr> <th>Project</th> <th>Mix Type</th> <th>Sample ID</th> </tr> </thead> <tbody> <tr> <td>MSU_Polito</td> <td>4E1DVR</td> <td>4E1DVR_IIA</td> </tr> <tr> <td colspan="3"> <table border="1"> <thead> <tr> <th>$P_1(u)$</th> <th>$P_2(u)$</th> <th>W_f</th> <th>$Area_{lig}$</th> <th>G_f</th> <th>m</th> <th>FI</th> </tr> </thead> <tbody> <tr> <td>[J]</td> <td>[J]</td> <td>[J]</td> <td>[mm²]</td> <td>[J/m²]</td> <td>[-]</td> <td>[-]</td> </tr> <tr> <td>2.4</td> <td>3.1</td> <td>5.4</td> <td>3127.0</td> <td>1735.1</td> <td>2.7</td> <td>6.4</td> </tr> </tbody> </table> </td> </tr> <tr> <td colspan="3"> <p>where:</p> <p>$P_1(u)$ = area under the load vs displacement curve pre-peak</p> <p>$P_2(u)$ = area under the load vs displacement curve post-peak</p> <p>W_f = work of fracture</p> <p>$Area_{lig}$ = ligament area</p> <p>G_f = fracture energy</p> <p>m = absolute value of the post-peak load slope</p> <p>FI = flexibility index</p> </td> </tr> </tbody> </table>			Project	Mix Type	Sample ID	MSU_Polito	4E1DVR	4E1DVR_IIA	<table border="1"> <thead> <tr> <th>$P_1(u)$</th> <th>$P_2(u)$</th> <th>W_f</th> <th>$Area_{lig}$</th> <th>G_f</th> <th>m</th> <th>FI</th> </tr> </thead> <tbody> <tr> <td>[J]</td> <td>[J]</td> <td>[J]</td> <td>[mm²]</td> <td>[J/m²]</td> <td>[-]</td> <td>[-]</td> </tr> <tr> <td>2.4</td> <td>3.1</td> <td>5.4</td> <td>3127.0</td> <td>1735.1</td> <td>2.7</td> <td>6.4</td> </tr> </tbody> </table>			$P_1(u)$	$P_2(u)$	W_f	$Area_{lig}$	G_f	$ m $	FI	[J]	[J]	[J]	[mm ²]	[J/m ²]	[-]	[-]	2.4	3.1	5.4	3127.0	1735.1	2.7	6.4	<p>where:</p> <p>$P_1(u)$ = area under the load vs displacement curve pre-peak</p> <p>$P_2(u)$ = area under the load vs displacement curve post-peak</p> <p>W_f = work of fracture</p> <p>$Area_{lig}$ = ligament area</p> <p>G_f = fracture energy</p> <p>m = absolute value of the post-peak load slope</p> <p>FI = flexibility index</p>		
Project	Mix Type	Sample ID																																	
MSU_Polito	4E1DVR	4E1DVR_IIA																																	
<table border="1"> <thead> <tr> <th>$P_1(u)$</th> <th>$P_2(u)$</th> <th>W_f</th> <th>$Area_{lig}$</th> <th>G_f</th> <th>m</th> <th>FI</th> </tr> </thead> <tbody> <tr> <td>[J]</td> <td>[J]</td> <td>[J]</td> <td>[mm²]</td> <td>[J/m²]</td> <td>[-]</td> <td>[-]</td> </tr> <tr> <td>2.4</td> <td>3.1</td> <td>5.4</td> <td>3127.0</td> <td>1735.1</td> <td>2.7</td> <td>6.4</td> </tr> </tbody> </table>			$P_1(u)$	$P_2(u)$	W_f	$Area_{lig}$	G_f	$ m $	FI	[J]	[J]	[J]	[mm ²]	[J/m ²]	[-]	[-]	2.4	3.1	5.4	3127.0	1735.1	2.7	6.4												
$P_1(u)$	$P_2(u)$	W_f	$Area_{lig}$	G_f	$ m $	FI																													
[J]	[J]	[J]	[mm ²]	[J/m ²]	[-]	[-]																													
2.4	3.1	5.4	3127.0	1735.1	2.7	6.4																													
<p>where:</p> <p>$P_1(u)$ = area under the load vs displacement curve pre-peak</p> <p>$P_2(u)$ = area under the load vs displacement curve post-peak</p> <p>W_f = work of fracture</p> <p>$Area_{lig}$ = ligament area</p> <p>G_f = fracture energy</p> <p>m = absolute value of the post-peak load slope</p> <p>FI = flexibility index</p>																																			



IL-SCB: 3D-modeled Ligament Area – MSU model results



MICHIGAN STATE UNIVERSITY

Results of the SCB test

Project	Mix Type	Sample ID
MSU_Polito	3E1DVR	3E1DVR_1A

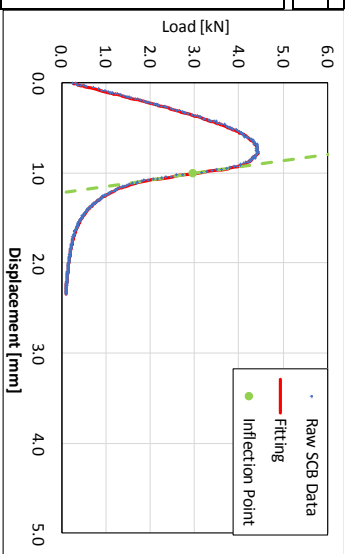
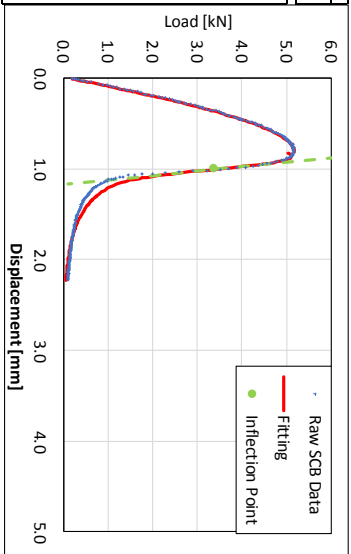
$P_1(u)$ [J]	$P_2(u)$ [J]	W_f [J]	A_{relig} [mm ²]	G_f [J/m ²]	$ m $ [-]	FI
2.7	1.5	4.3	3945.0	1079.0	20.4	0.5

where:
 $P_1(u)$ = area under the load vs displacement curve pre-peak
 $P_2(u)$ = area under the load vs displacement curve post-peak
 W_f = work of fracture
 A_{relig} = ligament area
 G_f = fracture energy
 $|m|$ = absolute value of the post-peak load slope
 FI = flexibility index

Project	Mix Type	Sample ID
MSU_Polito	3E1DVR	3E1DVR_1B

$P_1(u)$ [J]	$P_2(u)$ [J]	W_f [J]	A_{relig} [mm ²]	G_f [J/m ²]	$ m $ [-]	FI
2.2	1.7	3.9	3967.0	973.6	14.4	0.7

where:
 $P_1(u)$ = area under the load vs displacement curve pre-peak
 $P_2(u)$ = area under the load vs displacement curve post-peak
 W_f = work of fracture
 A_{relig} = ligament area
 G_f = fracture energy
 $|m|$ = absolute value of the post-peak load slope
 FI = flexibility index



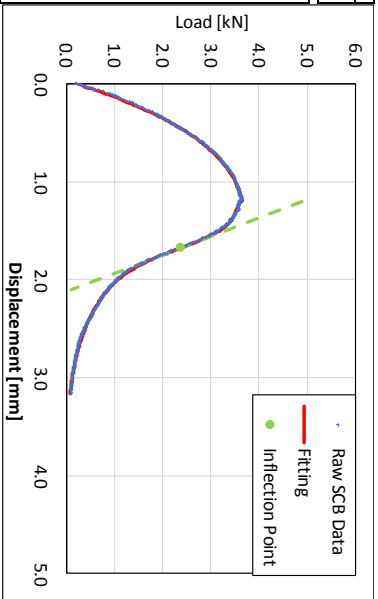
Project	Mix Type	Sample ID
MSU_Politto	3E1DVS	3E1DVS_IIA

$P_1(u)$	$P_2(u)$	W_f	$Area_{lig}$	G_f	$ m $	FI
[J]	[J]	[J]	[mm ²]	[J/m ²]	[-]	[-]
3.0	2.5	5.5	3577.0	1537.3	5.3	2.9

where:

- $P_1(u)$ = area under the load vs displacement curve pre-peak
- $P_2(u)$ = area under the load vs displacement curve post-peak
- W_f = work of fracture
- $Area_{lig}$ = ligament area

G_f = fracture energy
 $|m|$ = absolute value of the post-peak load slope
 FI = flexibility index



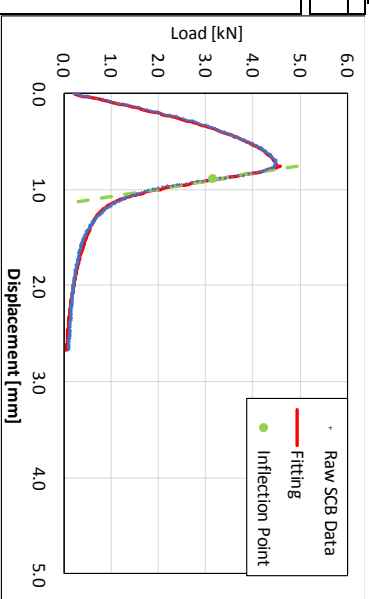
Project	Mix Type	Sample ID
MSU_Politto	3E1DVR	3E1DVR_IIA

$P_1(u)$	$P_2(u)$	W_f	$Area_{lig}$	G_f	$ m $	FI
[J]	[J]	[J]	[mm ²]	[J/m ²]	[-]	[-]
2.2	1.5	3.7	3743.0	989.9	12.6	0.8

where:

- $P_1(u)$ = area under the load vs displacement curve pre-peak
- $P_2(u)$ = area under the load vs displacement curve post-peak
- W_f = work of fracture
- $Area_{lig}$ = ligament area

G_f = fracture energy
 $|m|$ = absolute value of the post-peak load slope
 FI = flexibility index



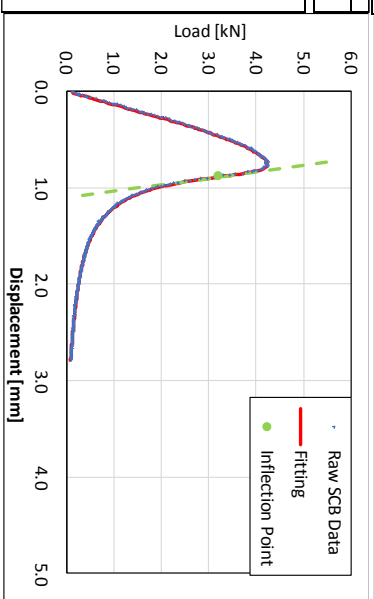
Project	Mix Type	Sample ID
MSU_Politto	3E1DVR	3E1DVR_IIB

$P_1(u)$	$P_2(u)$	W_f	$Area_{lig}$	G_f	$ m $	FI
[J]	[J]	[J]	[mm ²]	[J/m ²]	[-]	[-]
1.8	1.7	3.5	3767.0	922.5	14.8	0.6

where:

- $P_1(u)$ = area under the load vs displacement curve pre-peak
- $P_2(u)$ = area under the load vs displacement curve post-peak
- W_f = work of fracture
- $Area_{lig}$ = ligament area

G_f = fracture energy
 $|m|$ = absolute value of the post-peak load slope
 FI = flexibility index



Project	Mix Type	Sample ID
MSU_Politto	4E1DVR	4E1DVR_1A

$P_1(u)$	$P_2(u)$	W_f	Area _{lig}	G_f	m	FI
[J]	[J]	[J]	[mm ²]	[J/m ²]	[-]	[-]
2.2	2.2	4.4	3453.0	1281.5	3.2	4.0

where:

$P_1(u)$ = area under the load vs displacement curve pre-peak

$P_2(u)$ = area under the load vs displacement curve post-peak

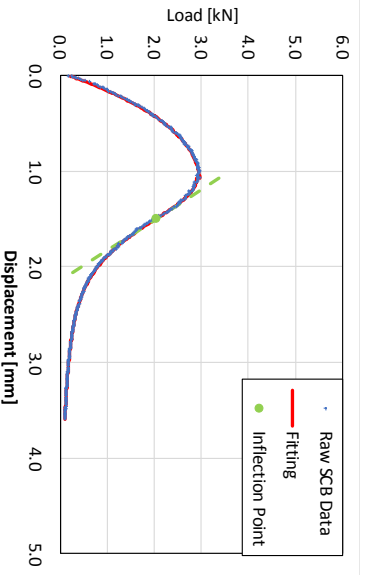
W_f = work of fracture

Area_{lig} = ligament area

G_f = fracture energy

|m| = absolute value of the post-peak load slope

FI = flexibility index



Project	Mix Type	Sample ID
MSU_Politto	4E1DVR	4E1DVR_1B

$P_1(u)$	$P_2(u)$	W_f	Area _{lig}	G_f	m	FI
[J]	[J]	[J]	[mm ²]	[J/m ²]	[-]	[-]
1.9	3.7	5.6	3951.0	1419.8	1.9	7.4

where:

$P_1(u)$ = area under the load vs displacement curve pre-peak

$P_2(u)$ = area under the load vs displacement curve post-peak

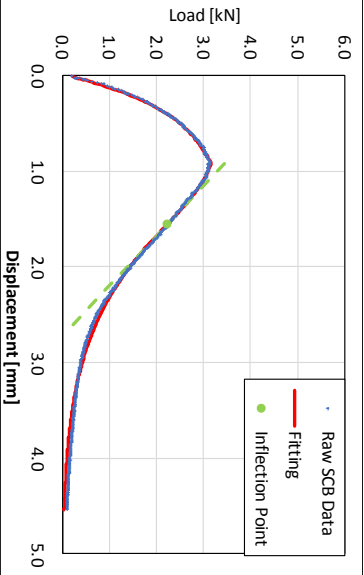
W_f = work of fracture

Area_{lig} = ligament area

G_f = fracture energy

|m| = absolute value of the post-peak load slope

FI = flexibility index



Project	Mix Type	Sample ID
MSU_Politto	3E1HS	3E1HS_1A

$P_1(u)$	$P_2(u)$	W_f	Area _{lig}	G_f	m	FI
[J]	[J]	[J]	[mm ²]	[J/m ²]	[-]	[-]
2.9	3.8	6.6	3861.0	1718.3	2.3	7.6

where:

$P_1(u)$ = area under the load vs displacement curve pre-peak

$P_2(u)$ = area under the load vs displacement curve post-peak

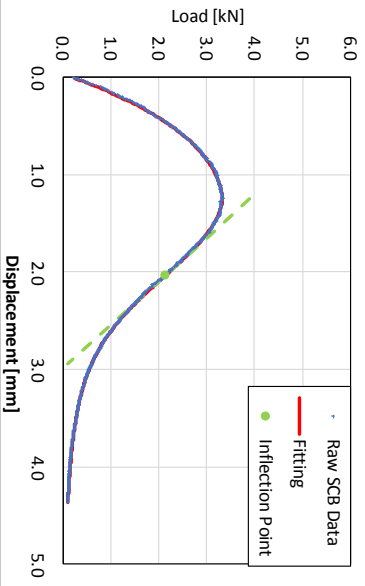
W_f = work of fracture

Area_{lig} = ligament area

G_f = fracture energy

|m| = absolute value of the post-peak load slope

FI = flexibility index

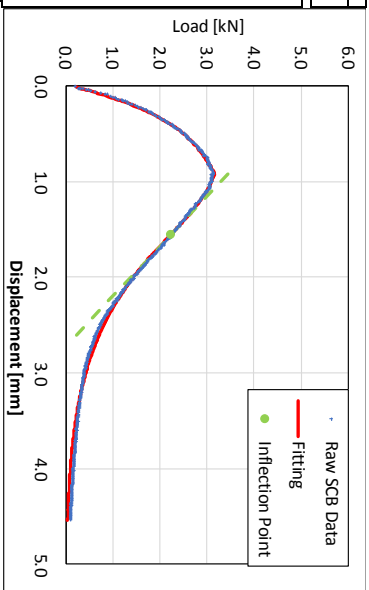


Project	Mix Type	Sample ID
MSU_Politto	4E1HS	4E1HSIB

$P_1(u)$	$P_2(u)$	W_f	$Area_{lig}$	G_f	$ m $	FI
[J]	[J]	[J]	[mm ²]	[J/m ²]	[-]	[-]
1.9	3.7	5.6	3673.0	1527.2	1.9	8.0

where:
 $P_1(u)$ = area under the load vs displacement curve pre-peak
 $P_2(u)$ = area under the load vs displacement curve post-peak
 W_f = work of fracture
 $Area_{lig}$ = ligament area

G_f = fracture energy
 $|m|$ = absolute value of the post-peak load slope
 FI = flexibility index

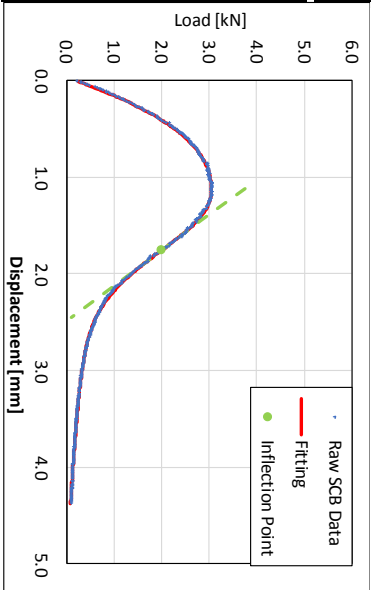


Project	Mix Type	Sample ID
MSU_Politto	4E1DVR	4E1DVR_IIA

$P_1(u)$	$P_2(u)$	W_f	$Area_{lig}$	G_f	$ m $	FI
[J]	[J]	[J]	[mm ²]	[J/m ²]	[-]	[-]
2.4	3.1	5.4	3764.0	1441.5	2.7	5.3

where:
 $P_1(u)$ = area under the load vs displacement curve pre-peak
 $P_2(u)$ = area under the load vs displacement curve post-peak
 W_f = work of fracture
 $Area_{lig}$ = ligament area

G_f = fracture energy
 $|m|$ = absolute value of the post-peak load slope
 FI = flexibility index

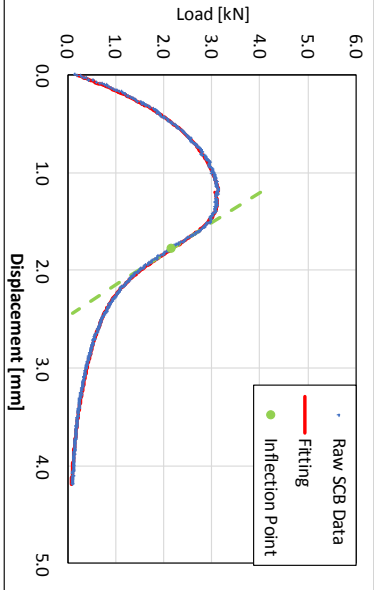


Project	Mix Type	Sample ID
MSU_Politto	4E1DVR	4E1DVR_IIB

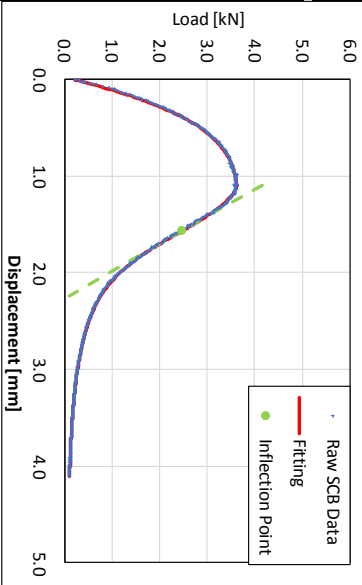
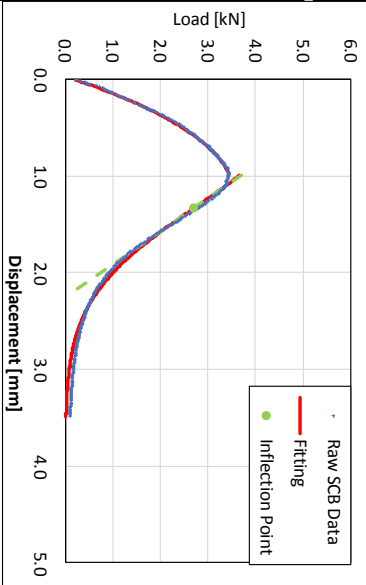
$P_1(u)$	$P_2(u)$	W_f	$Area_{lig}$	G_f	$ m $	FI
[J]	[J]	[J]	[mm ²]	[J/m ²]	[-]	[-]
2.6	3.1	5.7	4332.0	1305.7	3.1	4.1

where:
 $P_1(u)$ = area under the load vs displacement curve pre-peak
 $P_2(u)$ = area under the load vs displacement curve post-peak
 W_f = work of fracture
 $Area_{lig}$ = ligament area

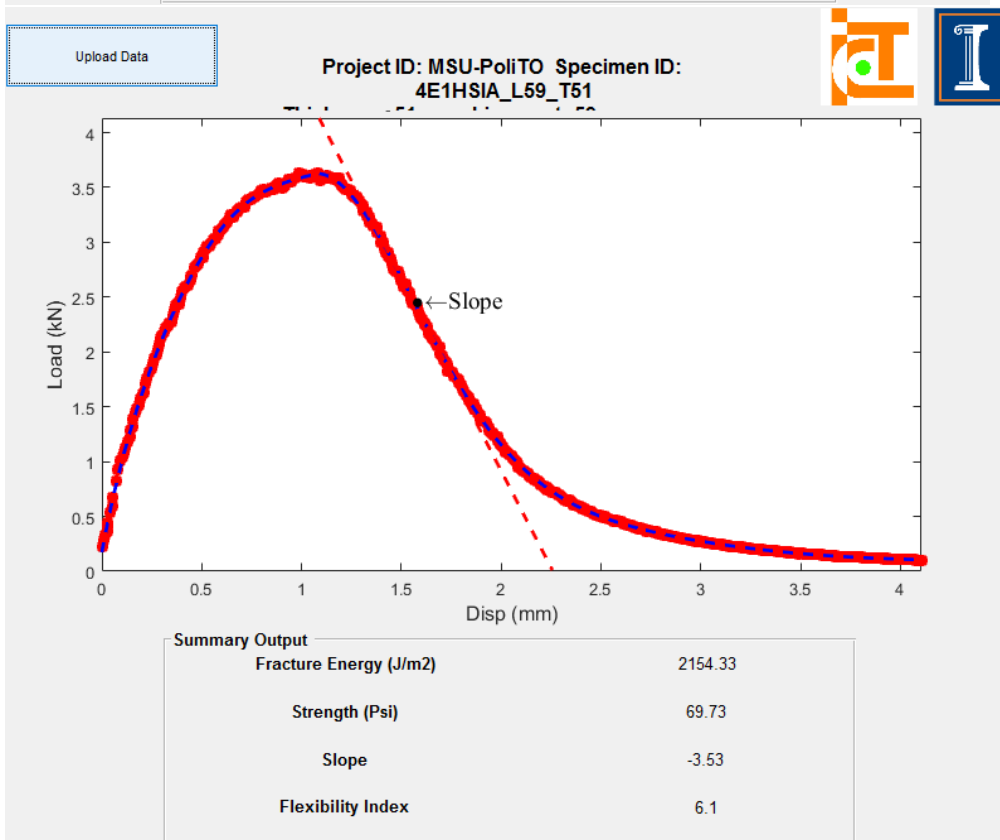
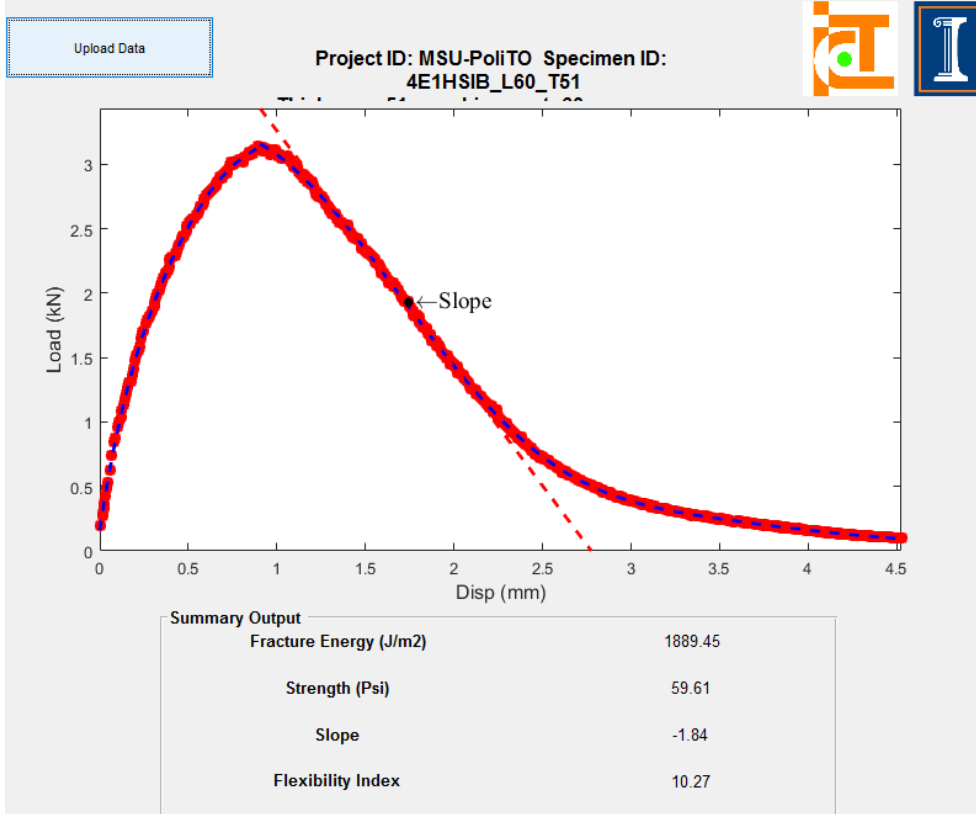
G_f = fracture energy
 $|m|$ = absolute value of the post-peak load slope
 FI = flexibility index

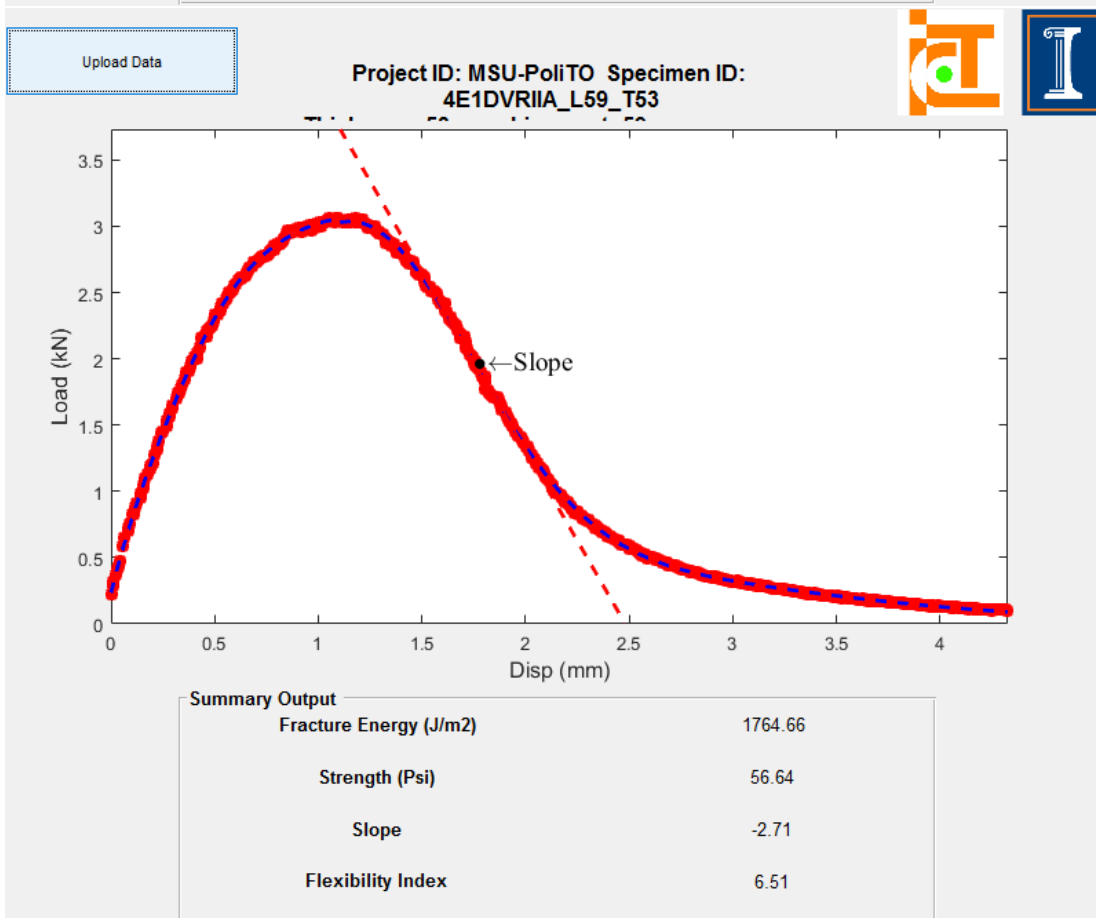
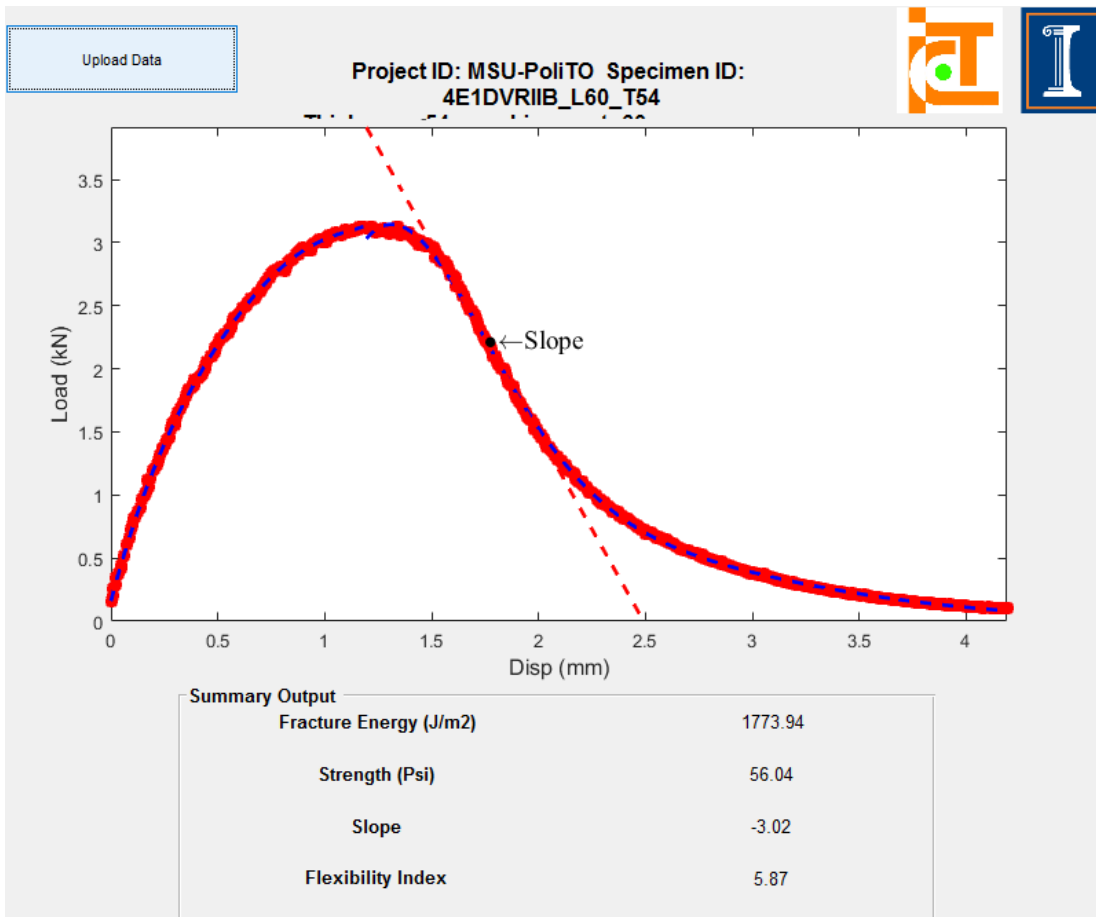


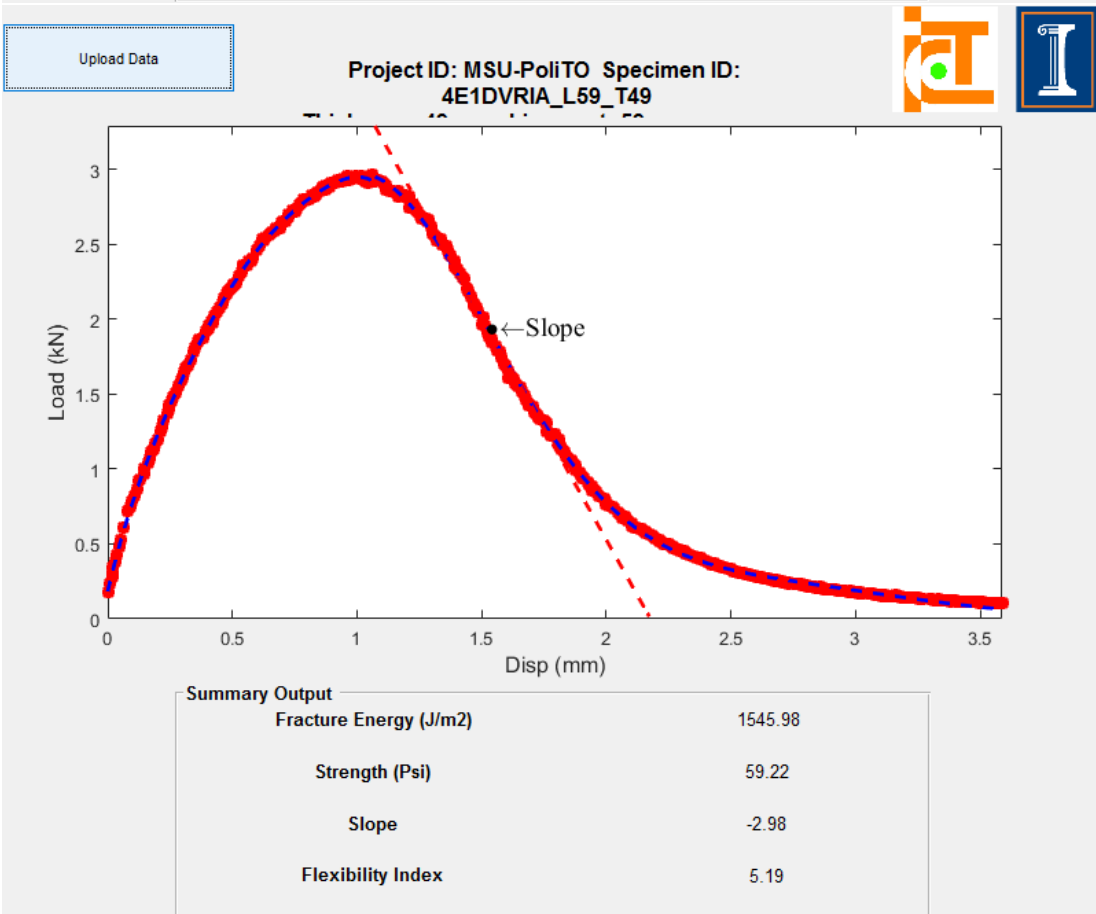
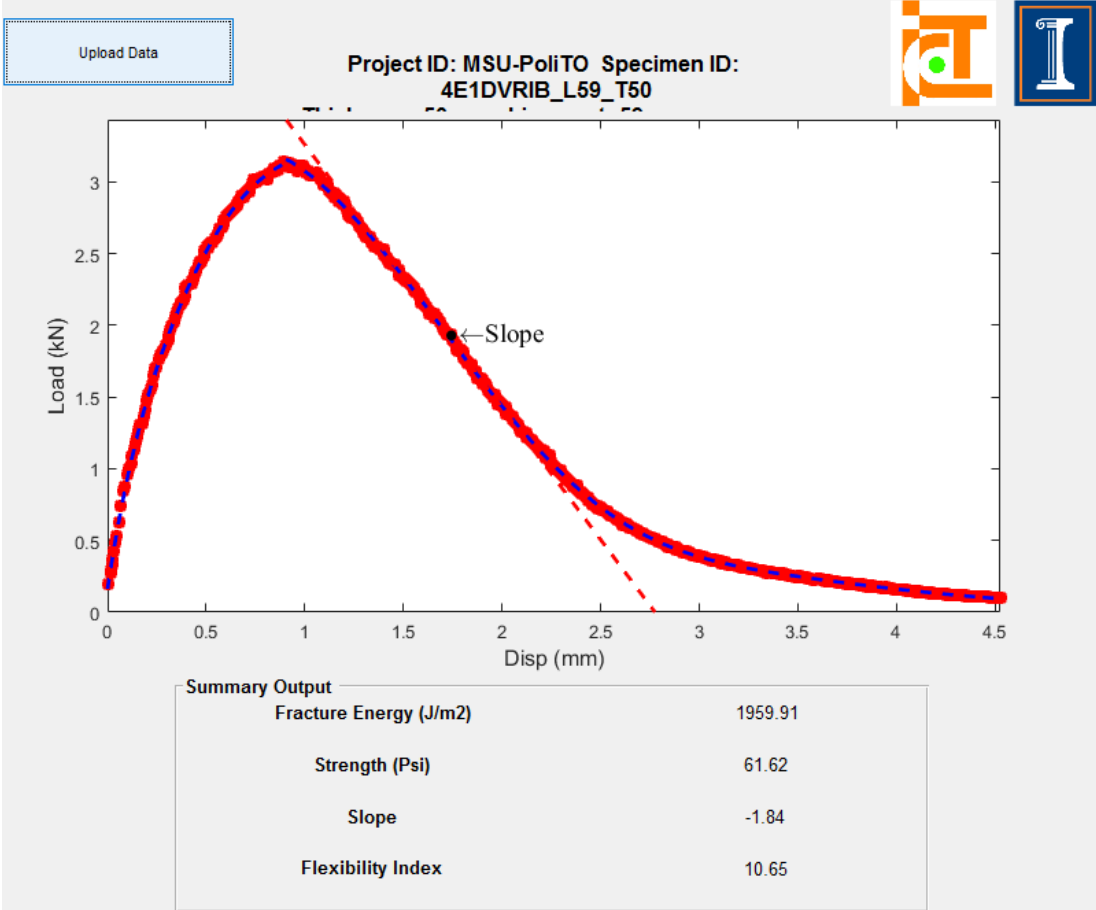
Project	Mix Type	Sample ID																														
MSU_Polito	4E1HS	4E1HS_IIB																														
<table border="1"> <thead> <tr> <th>$P_1(u)$</th> <th>$P_2(u)$</th> <th>W_f</th> <th>$Area_{lig}$</th> <th>G_f</th> <th>m</th> <th>FI</th> </tr> </thead> <tbody> <tr> <td>[J]</td> <td>[J]</td> <td>[J]</td> <td>[mm²]</td> <td>[J/m²]</td> <td>[-]</td> <td>[-]</td> </tr> <tr> <td>2.2</td> <td>2.7</td> <td>4.9</td> <td>3657.0</td> <td>1333.9</td> <td>2.9</td> <td>4.5</td> </tr> </tbody> </table> <p>where: $P_1(u)$ = area under the load vs displacement curve pre-peak $P_2(u)$ = area under the load vs displacement curve post-peak W_f = work of fracture $Area_{lig}$ = ligament area G_f = fracture energy m = absolute value of the post-peak load slope FI = flexibility index</p>			$P_1(u)$	$P_2(u)$	W_f	$Area_{lig}$	G_f	$ m $	FI	[J]	[J]	[J]	[mm ²]	[J/m ²]	[-]	[-]	2.2	2.7	4.9	3657.0	1333.9	2.9	4.5									
$P_1(u)$	$P_2(u)$	W_f	$Area_{lig}$	G_f	$ m $	FI																										
[J]	[J]	[J]	[mm ²]	[J/m ²]	[-]	[-]																										
2.2	2.7	4.9	3657.0	1333.9	2.9	4.5																										
<table border="1"> <thead> <tr> <th>Project</th> <th>Mix Type</th> <th>Sample ID</th> </tr> </thead> <tbody> <tr> <td>MSU_Polito</td> <td>4E1HS</td> <td>4E1HS_IA</td> </tr> <tr> <td colspan="3"> <table border="1"> <thead> <tr> <th>$P_1(u)$</th> <th>$P_2(u)$</th> <th>W_f</th> <th>$Area_{lig}$</th> <th>G_f</th> <th>m</th> <th>FI</th> </tr> </thead> <tbody> <tr> <td>[J]</td> <td>[J]</td> <td>[J]</td> <td>[mm²]</td> <td>[J/m²]</td> <td>[-]</td> <td>[-]</td> </tr> <tr> <td>2.9</td> <td>3.0</td> <td>5.9</td> <td>3967.0</td> <td>1482.0</td> <td>3.6</td> <td>4.2</td> </tr> </tbody> </table> <p>where: $P_1(u)$ = area under the load vs displacement curve pre-peak $P_2(u)$ = area under the load vs displacement curve post-peak W_f = work of fracture $Area_{lig}$ = ligament area G_f = fracture energy m = absolute value of the post-peak load slope FI = flexibility index</p> </td> </tr> </tbody> </table>			Project	Mix Type	Sample ID	MSU_Polito	4E1HS	4E1HS_IA	<table border="1"> <thead> <tr> <th>$P_1(u)$</th> <th>$P_2(u)$</th> <th>W_f</th> <th>$Area_{lig}$</th> <th>G_f</th> <th>m</th> <th>FI</th> </tr> </thead> <tbody> <tr> <td>[J]</td> <td>[J]</td> <td>[J]</td> <td>[mm²]</td> <td>[J/m²]</td> <td>[-]</td> <td>[-]</td> </tr> <tr> <td>2.9</td> <td>3.0</td> <td>5.9</td> <td>3967.0</td> <td>1482.0</td> <td>3.6</td> <td>4.2</td> </tr> </tbody> </table> <p>where: $P_1(u)$ = area under the load vs displacement curve pre-peak $P_2(u)$ = area under the load vs displacement curve post-peak W_f = work of fracture $Area_{lig}$ = ligament area G_f = fracture energy m = absolute value of the post-peak load slope FI = flexibility index</p>			$P_1(u)$	$P_2(u)$	W_f	$Area_{lig}$	G_f	$ m $	FI	[J]	[J]	[J]	[mm ²]	[J/m ²]	[-]	[-]	2.9	3.0	5.9	3967.0	1482.0	3.6	4.2
Project	Mix Type	Sample ID																														
MSU_Polito	4E1HS	4E1HS_IA																														
<table border="1"> <thead> <tr> <th>$P_1(u)$</th> <th>$P_2(u)$</th> <th>W_f</th> <th>$Area_{lig}$</th> <th>G_f</th> <th>m</th> <th>FI</th> </tr> </thead> <tbody> <tr> <td>[J]</td> <td>[J]</td> <td>[J]</td> <td>[mm²]</td> <td>[J/m²]</td> <td>[-]</td> <td>[-]</td> </tr> <tr> <td>2.9</td> <td>3.0</td> <td>5.9</td> <td>3967.0</td> <td>1482.0</td> <td>3.6</td> <td>4.2</td> </tr> </tbody> </table> <p>where: $P_1(u)$ = area under the load vs displacement curve pre-peak $P_2(u)$ = area under the load vs displacement curve post-peak W_f = work of fracture $Area_{lig}$ = ligament area G_f = fracture energy m = absolute value of the post-peak load slope FI = flexibility index</p>			$P_1(u)$	$P_2(u)$	W_f	$Area_{lig}$	G_f	$ m $	FI	[J]	[J]	[J]	[mm ²]	[J/m ²]	[-]	[-]	2.9	3.0	5.9	3967.0	1482.0	3.6	4.2									
$P_1(u)$	$P_2(u)$	W_f	$Area_{lig}$	G_f	$ m $	FI																										
[J]	[J]	[J]	[mm ²]	[J/m ²]	[-]	[-]																										
2.9	3.0	5.9	3967.0	1482.0	3.6	4.2																										

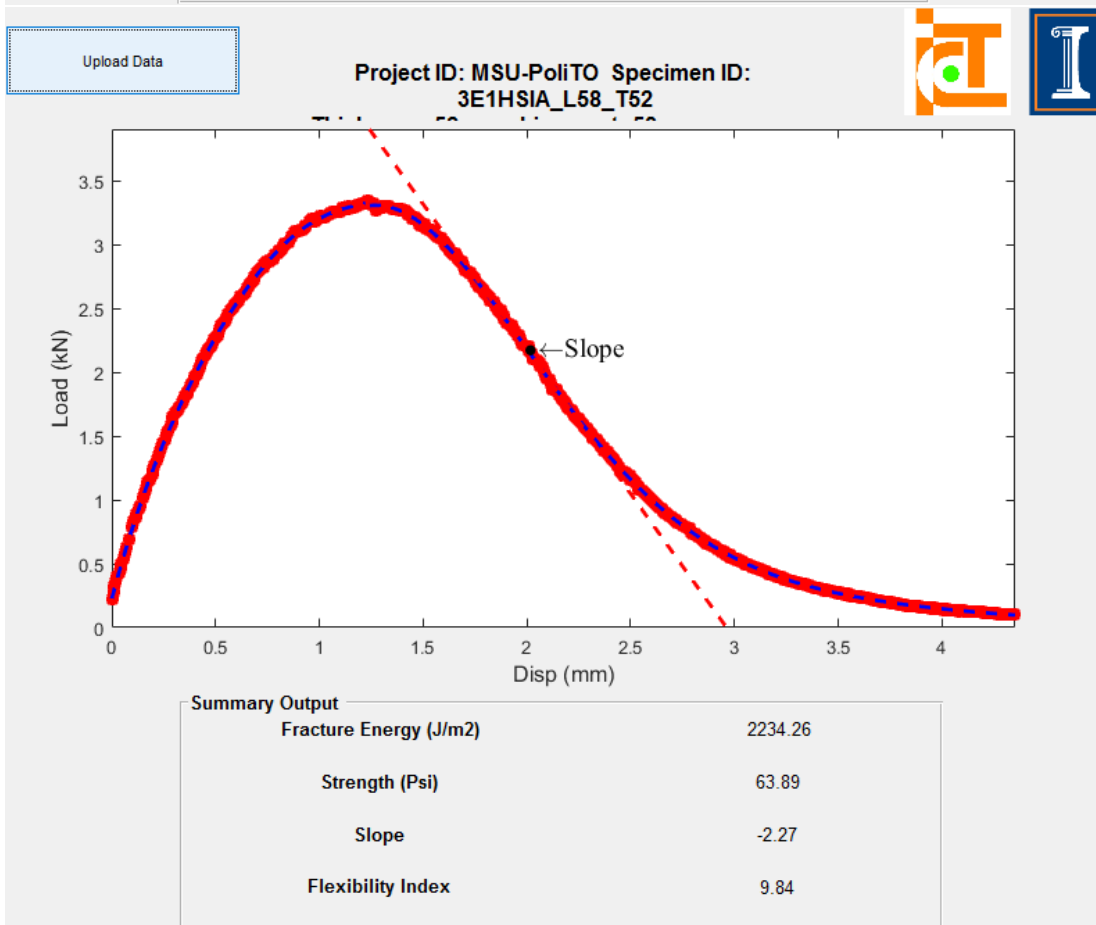
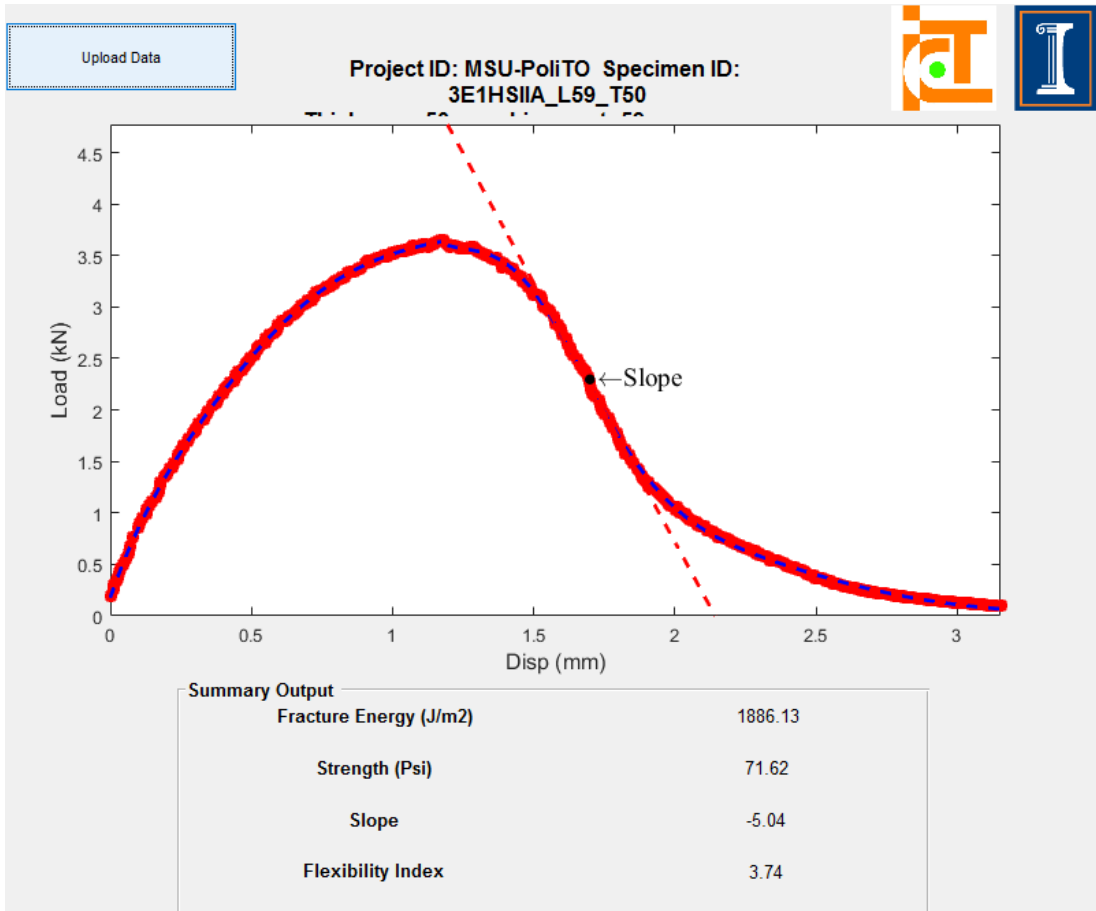


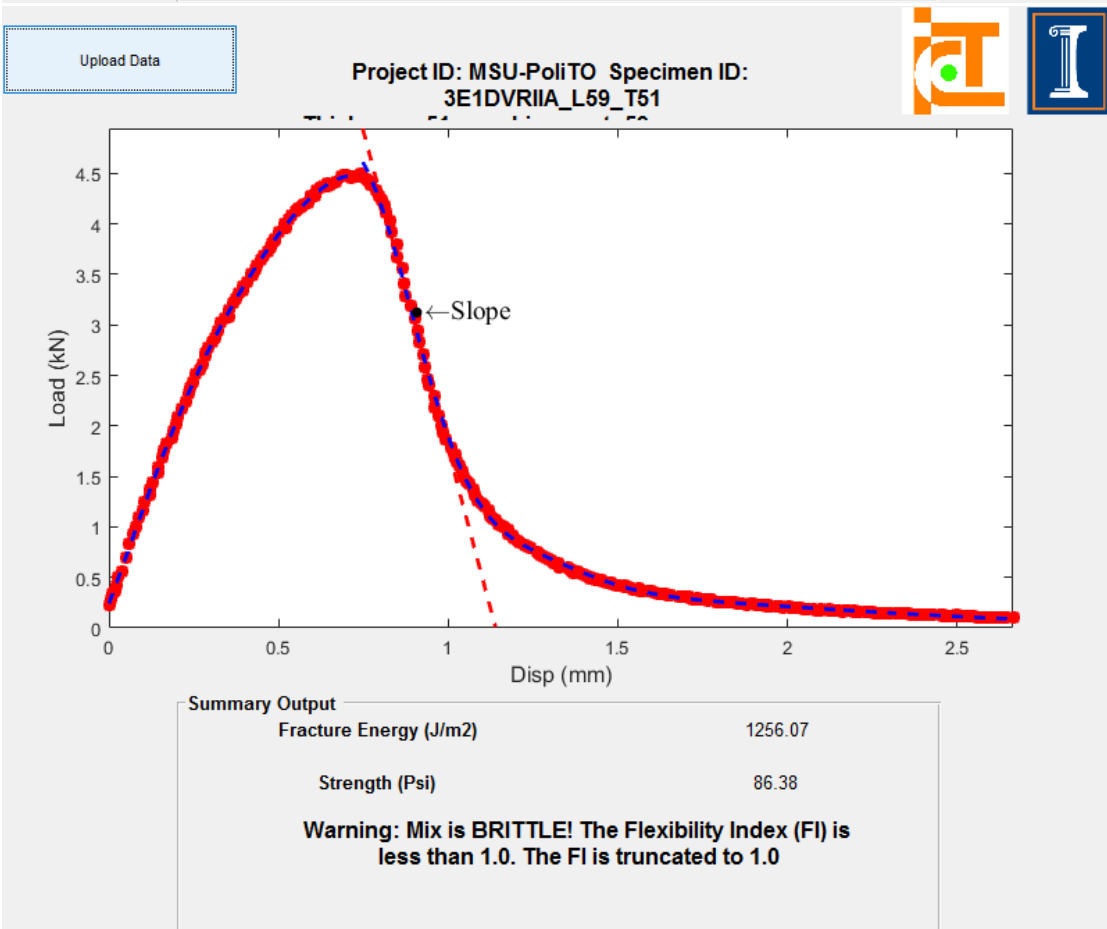
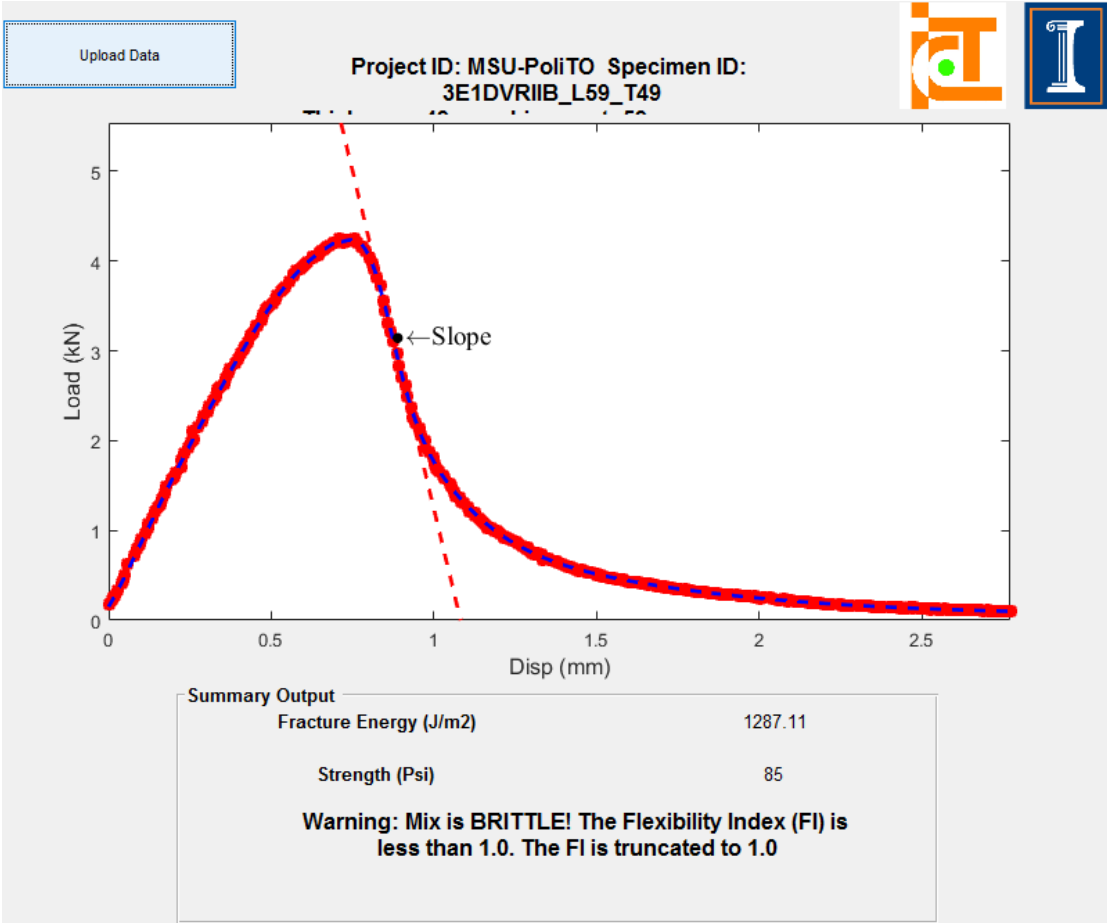
IL-SCB:I-FIT results

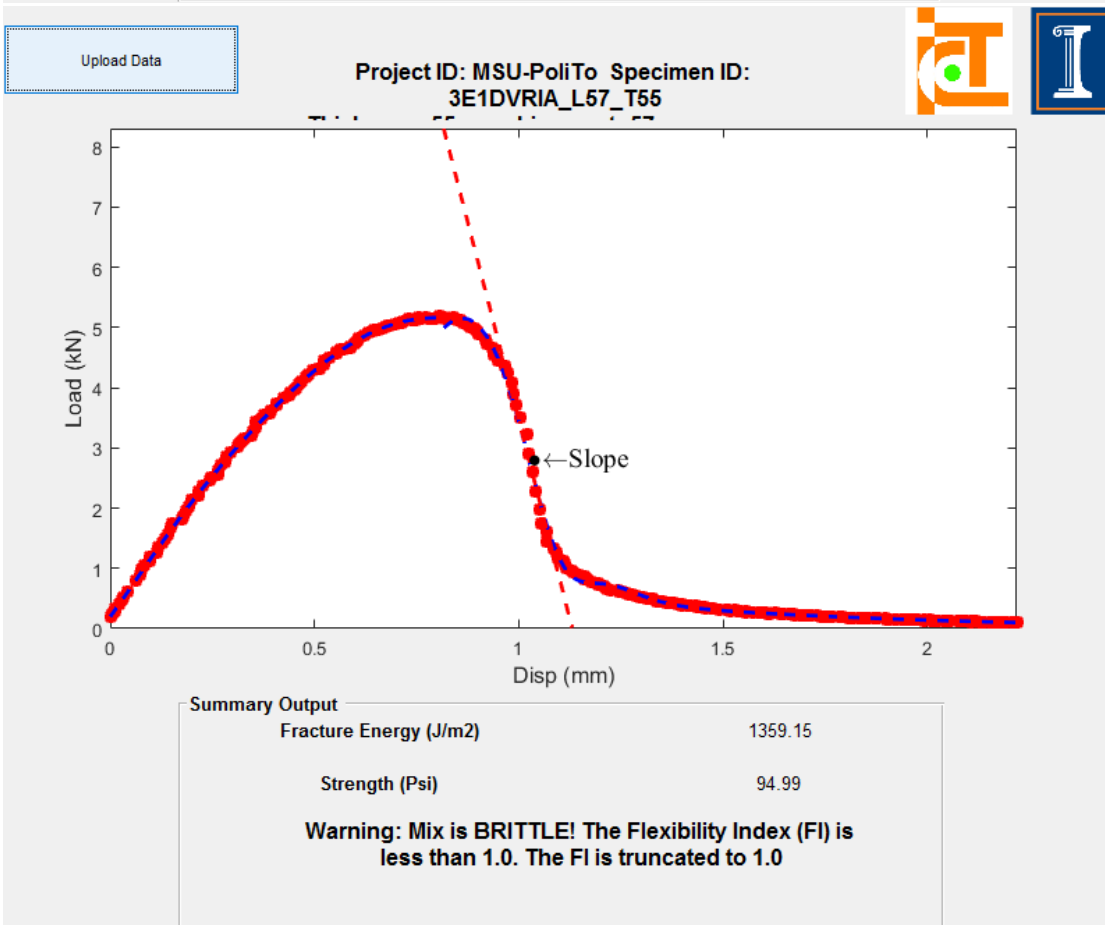
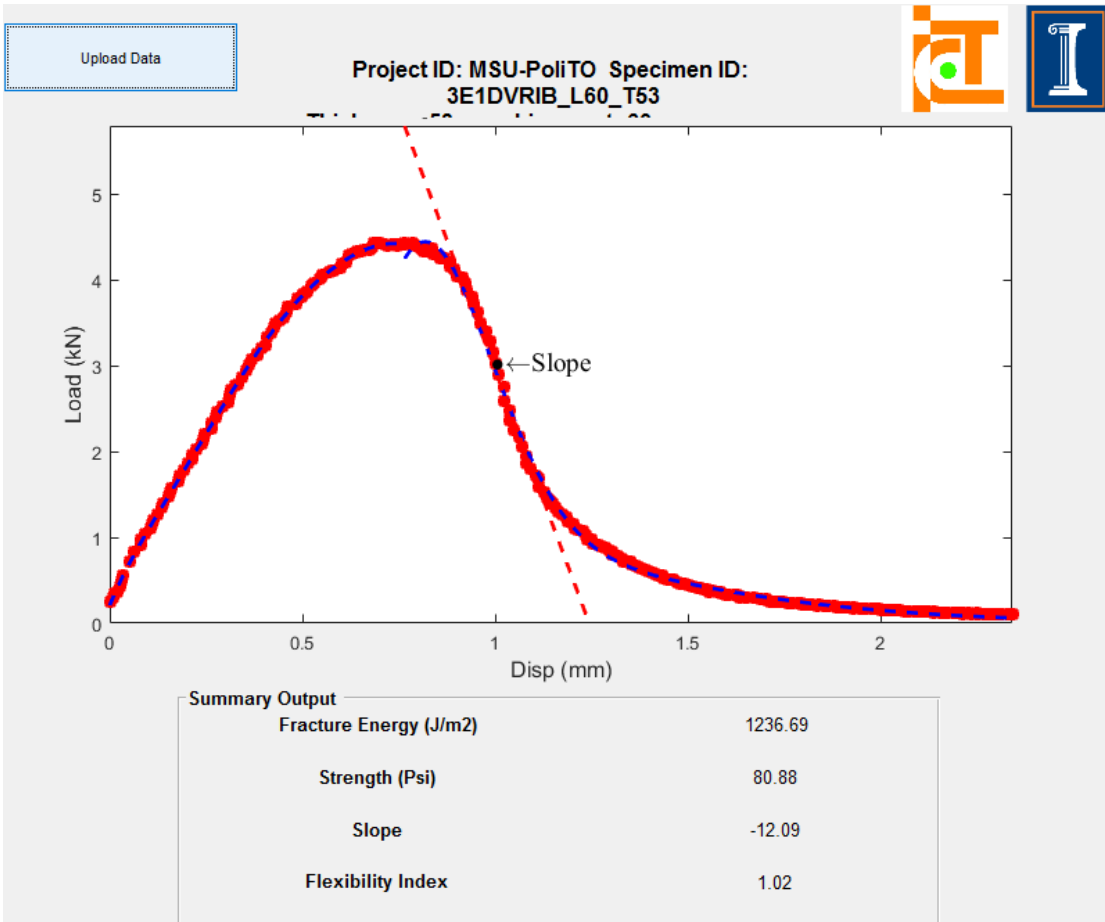






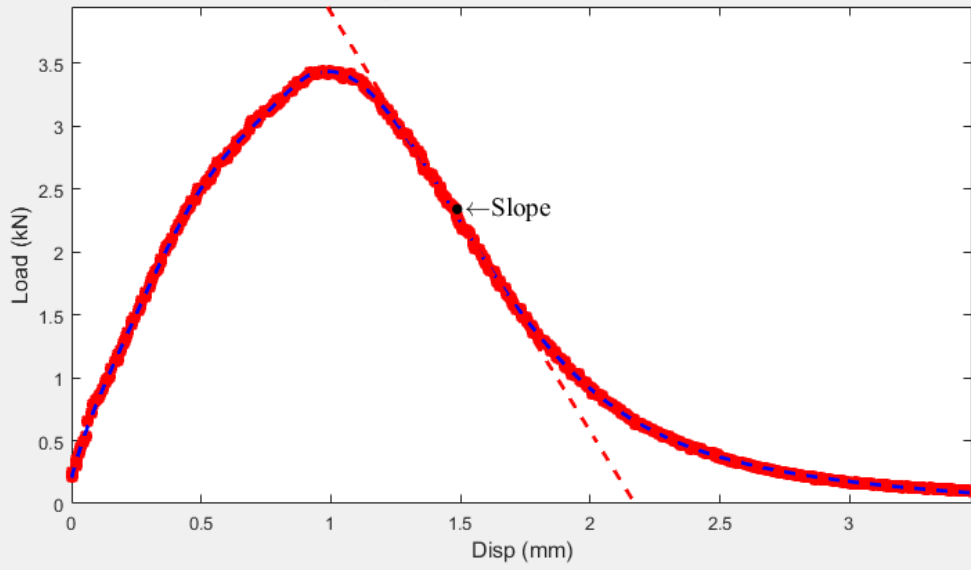






Upload Data

Project ID: MSU-PoliTO Specimen ID:
4E1HSIIB_L60_T50



Summary Output

Fracture Energy (J/m ²)	1680.93
Strength (Psi)	66.46
Slope	-3.33
Flexibility Index	5.05

DVR DRY ILLINOIS Pavement ME Design PDF Output



DVR_DRY_1ESAI



File Name: C:\Users\pc\Documents\Michele\Politecnico\TESI\Pavement ME\DESIGNS\DVR_DRY_1ESAI.dgp

Design Inputs

Design Life: 20 years Base construction: June, 2018 Climate Data: 40, -88.125
 Design Type: FLEXIBLE Pavement construction: June, 2018 Sources (Lat/Lon)
 Traffic opening: June, 2018

Design Structure

Layer type	Material Type	Thickness(mm)
Flexible	Default asphalt concrete	50.0
Flexible	Default asphalt concrete	50.0
NonStabilized	A-1-a	300.0
Subgrade	A-1-a	Semi-infinite

Volumetric at Construction:	
Effective binder content (%)	11.6
Air voids (%)	7.0

Traffic

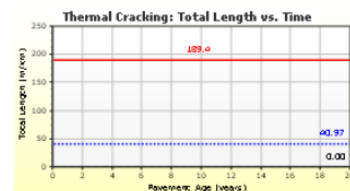
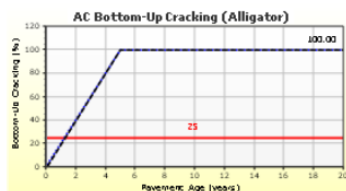
Age (year)	Heavy Trucks (cumulative)
2018 (initial)	1 000
2028 (10 years)	1 734 940
2038 (20 years)	3 469 880

Design Outputs

Distress Prediction Summary

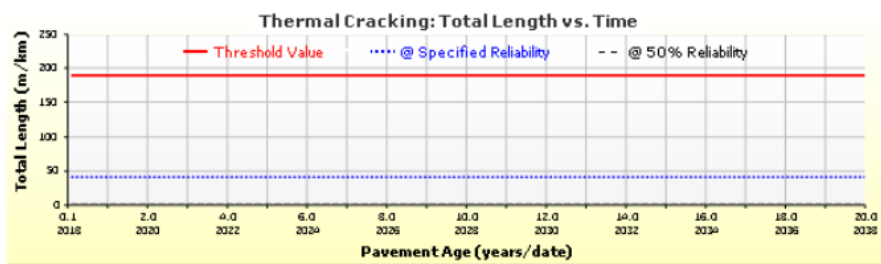
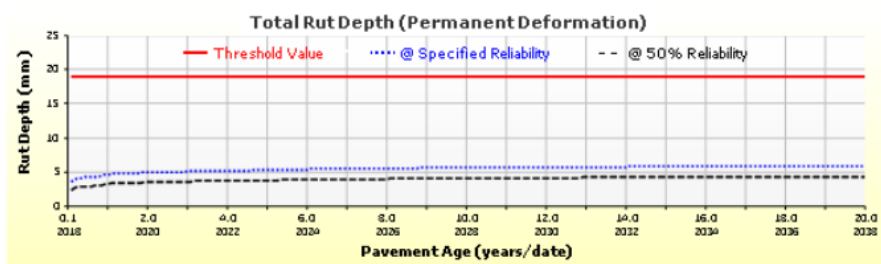
Distress Type	Distress @ Specified Reliability		Reliability (%)		Criterion Satisfied?
	Target	Predicted	Target	Achieved	
Terminal IRI (m/km)	2.70	2.97	90.00	79.61	Fail
Permanent deformation - total pavement (mm)	19.00	5.86	90.00	100.00	Pass
AC bottom-up fatigue cracking (percent)	25.00	100.00	90.00	0.00	Fail
AC thermal cracking (m/km)	189.40	40.97	90.00	100.00	Pass
AC top-down fatigue cracking (m/km)	378.80	1360.16	90.00	18.74	Fail
Permanent deformation - AC only (mm)	6.00	0.28	90.00	100.00	Pass

Distress Charts



— Threshold Value @ Specified Reliability --- @ 50% Reliability

Analysis Output Charts



HS DRY ILLINOIS Pavement ME Design PDF Output



HS_DRY_1ESAL

File Name: C:\Users\pc\Documents\Michele\Politecnico\TESI\Pavement ME\DESIGNS\HS_DRY_1ESAL.dgpx



Design Inputs

Design Life: 20 years Base construction: June, 2018 Climate Data Sources (Lat/Lon): 40, -88.125
 Design Type: FLEXIBLE Pavement construction: June, 2018 Traffic opening: June, 2018

Design Structure

Layer type	Material Type	Thickness(mm)
Flexible	Default asphalt concrete	50.0
Flexible	Default asphalt concrete	50.0
NonStabilized	A-1-a	300.0
Subgrade	A-1-a	Semi-infinite

Volumetric at Construction:	
Effective binder content (%)	11.6
Air voids (%)	7.0

Traffic

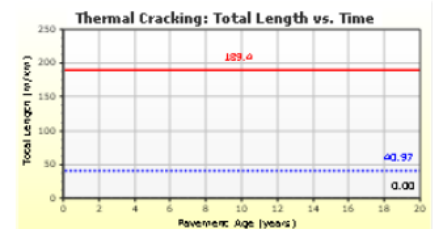
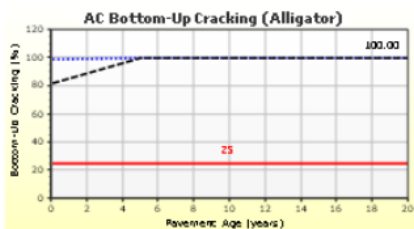
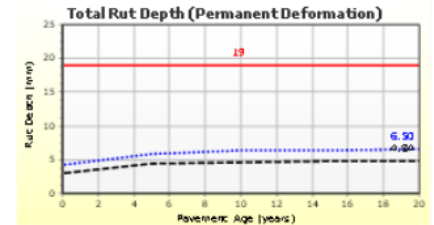
Age (year)	Heavy Trucks (cumulative)
2018 (initial)	4 000
2028 (10 years)	6 939 750
2038 (20 years)	13 879 500

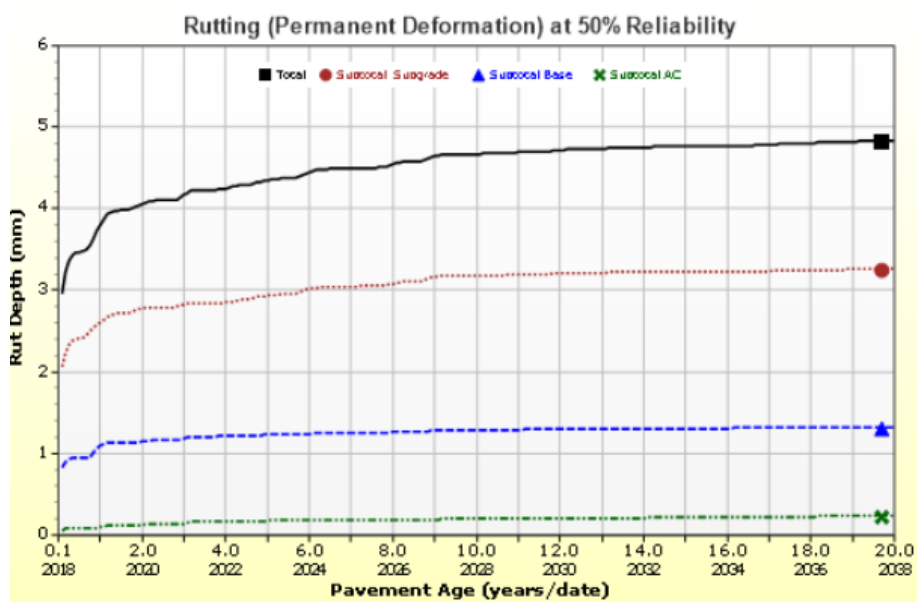
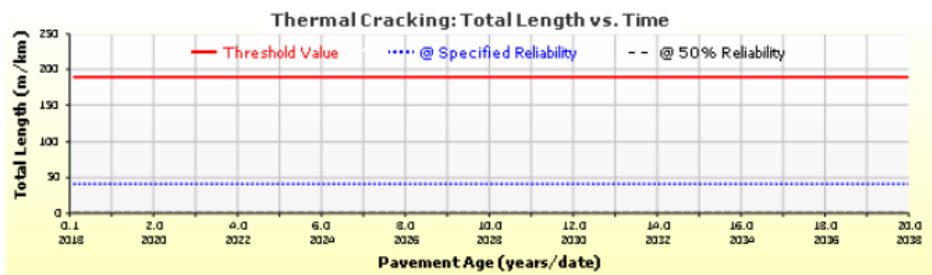
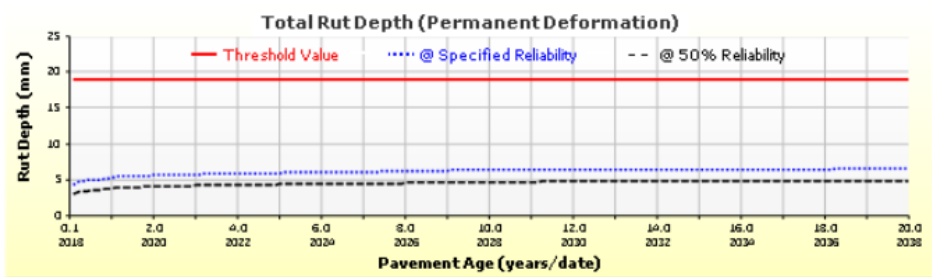
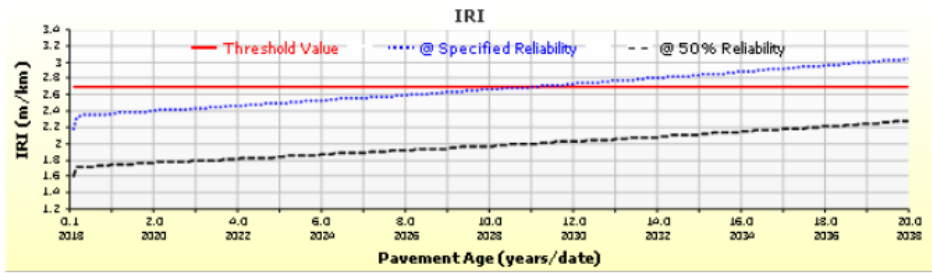
Design Outputs

Distress Prediction Summary

Distress Type	Distress @ Specified Reliability		Reliability (%)		Criterion Satisfied?
	Target	Predicted	Target	Achieved	
Terminal IRI (m/km)	2.70	3.04	90.00	76.12	Fail
Permanent deformation - total pavement (mm)	19.00	6.50	90.00	100.00	Pass
AC bottom-up fatigue cracking (percent)	25.00	100.00	90.00	0.00	Fail
AC thermal cracking (m/km)	189.40	40.97	90.00	100.00	Pass
AC top-down fatigue cracking (m/km)	378.80	2256.01	90.00	0.31	Fail
Permanent deformation - AC only (mm)	6.00	0.46	90.00	100.00	Pass

Distress Charts





DVR WET ILLINOIS Pavement ME Design PDF Output



DVR_WET_1ESAL

File Name: C:\Users\pc\Documents\Michele\Politecnico\TESI\Pavement ME\DESIGNS\DVR_WET_1ESAL.dgpx



Design Inputs

Design Life: 20 years Base construction: June, 2018 Climate Data: 40, -88.125
 Design Type: FLEXIBLE Pavement construction: June, 2018 Sources (Lat/Lon)
 Traffic opening: June, 2018

Design Structure

Layer type	Material Type	Thickness(mm)
Flexible	Default asphalt concrete	50.0
Flexible	Default asphalt concrete	50.0
NonStabilized	A-1-a	300.0
Subgrade	A-1-a	Semi-infinite

Volumetric at Construction:

Effective binder content (%)	11.6
Air voids (%)	7.0

Traffic

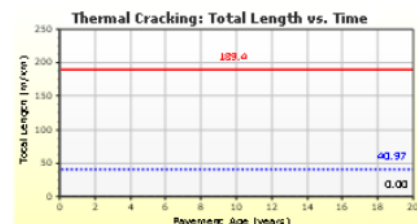
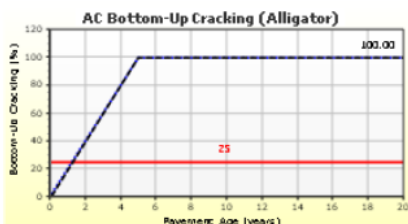
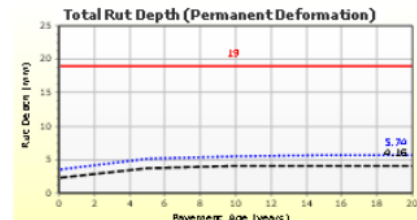
Age (year)	Heavy Trucks (cumulative)
2018 (initial)	1 000
2028 (10 years)	1 734 940
2038 (20 years)	3 469 880

Design Outputs

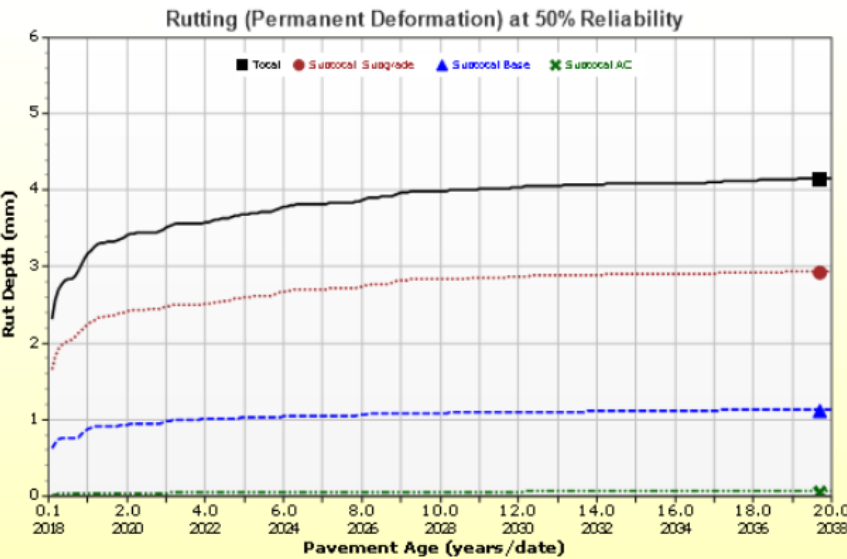
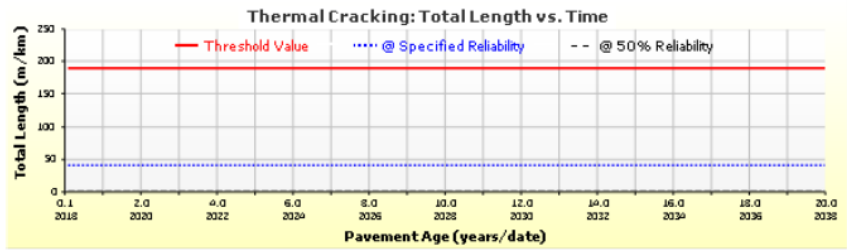
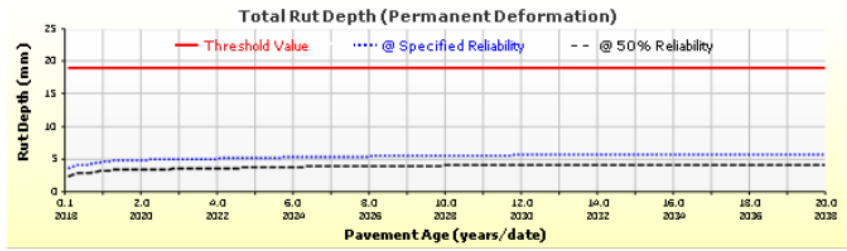
Distress Prediction Summary

Distress Type	Distress @ Specified Reliability		Reliability (%)		Criterion Satisfied?
	Target	Predicted	Target	Achieved	
Terminal IRI (m/km)	2.70	2.96	90.00	80.00	Fail
Permanent deformation - total pavement (mm)	19.00	5.73	90.00	100.00	Pass
AC bottom-up fatigue cracking (percent)	25.00	100.00	90.00	0.00	Fail
AC thermal cracking (m/km)	189.40	40.97	90.00	100.00	Pass
AC top-down fatigue cracking (m/km)	378.80	1281.77	90.00	23.48	Fail
Permanent deformation - AC only (mm)	6.00	0.18	90.00	100.00	Pass

Distress Charts



— Threshold Value @ Specified Reliability - - - @ 50% Reliability



HS WET ILLINOIS Pavement ME Design PDF Output



HS_WET_1ESAL

File Name: C:\Users\pc\Documents\Michele\Politecnico\TESI\Pavement ME\DESIGNS\HS_WET_1ESAL.dgpx



Design Inputs

Design Life: 20 years Base construction: June, 2018 Climate Data: 40, -88.125
 Design Type: FLEXIBLE Pavement construction: June, 2018 Sources (Lat/Lon)
 Traffic opening: June, 2018

Design Structure

Layer type	Material Type	Thickness(mm)
Flexible	Default asphalt concrete	50.0
Flexible	Default asphalt concrete	50.0
NonStabilized	A-1-a	300.0
Subgrade	A-1-a	Semi-infinite

Volumetric at Construction:	
Effective binder content (%)	11.6
Air voids (%)	7.0

Traffic

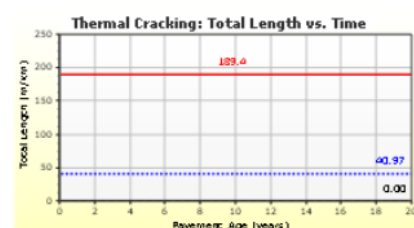
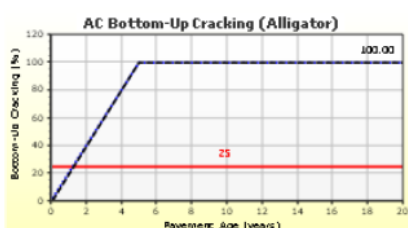
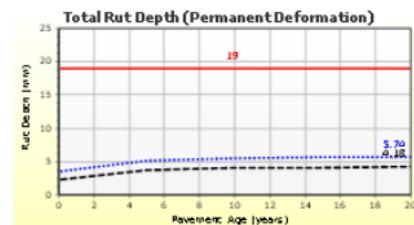
Age (year)	Heavy Trucks (cumulative)
2018 (initial)	1 000
2028 (10 years)	1 734 940
2038 (20 years)	3 469 880

Design Outputs

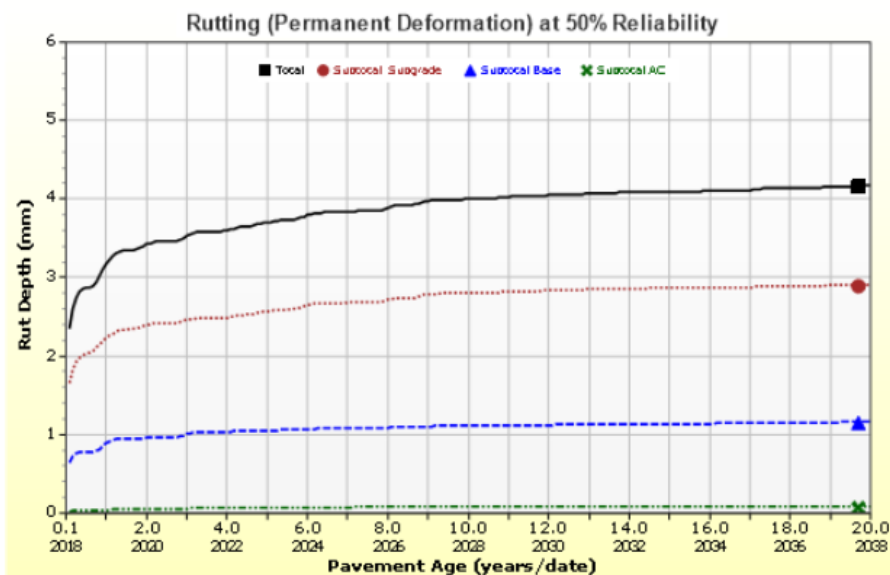
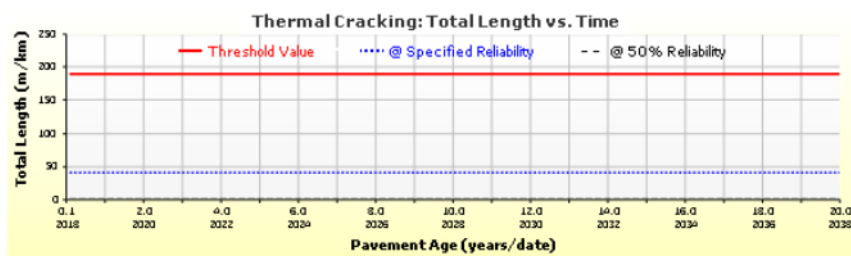
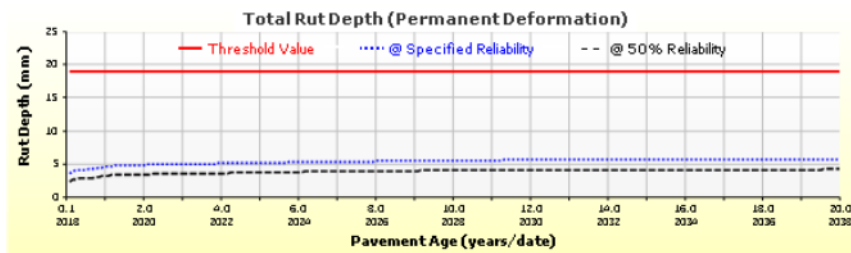
Distress Prediction Summary

Distress Type	Distress @ Specified Reliability		Reliability (%)		Criterion Satisfied?
	Target	Predicted	Target	Achieved	
Terminal IRI (m/km)	2.70	2.95	90.00	80.14	Fail
Permanent deformation - total pavement (mm)	19.00	5.74	90.00	100.00	Pass
AC bottom-up fatigue cracking (percent)	25.00	100.00	90.00	0.00	Fail
AC thermal cracking (m/km)	189.40	40.97	90.00	100.00	Pass
AC top-down fatigue cracking (m/km)	378.80	1224.65	90.00	27.31	Fail
Permanent deformation - AC only (mm)	6.00	0.22	90.00	100.00	Pass

Distress Charts



— Threshold Value @ Specified Reliability - - - @ 50% Reliability



DVR DRY ARIZONA Pavement ME Design PDF Output



DVR_DRY_1ESAL_AZ



File Name: C:\Users\pc\Documents\Michele\Politecnico\TESI\Pavement ME\DESIGNS\DVR_DRY_1ESAL_AZ.dgpx

Design Inputs

Design Life: 20 years Base construction: June, 2018 Climate Data: 33.5, -111.875
 Design Type: FLEXIBLE Pavement construction: June, 2018 Sources (Lat/Lon)
 Traffic opening: June, 2018

Design Structure

Layer type	Material Type	Thickness(mm)
Flexible	Default asphalt concrete	50.0
Flexible	Default asphalt concrete	50.0
NonStabilized	A-1-a	300.0
Subgrade	A-1-a	Semi-infinite

Volumetric at Construction:	
Effective binder content (%)	11.6
Air voids (%)	7.0

Traffic

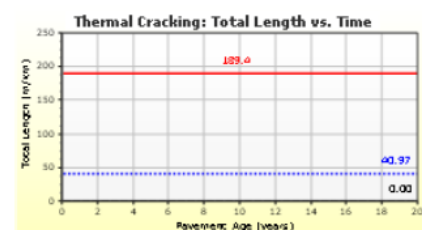
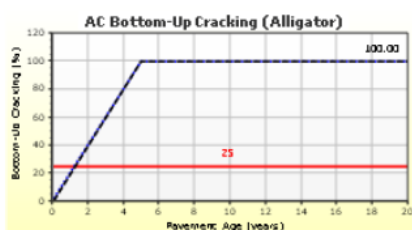
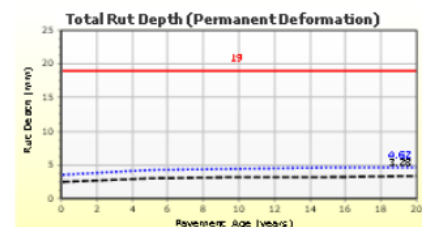
Age (year)	Heavy Trucks (cumulative)
2018 (initial)	1 000
2028 (10 years)	1 734 940
2038 (20 years)	3 469 880

Design Outputs

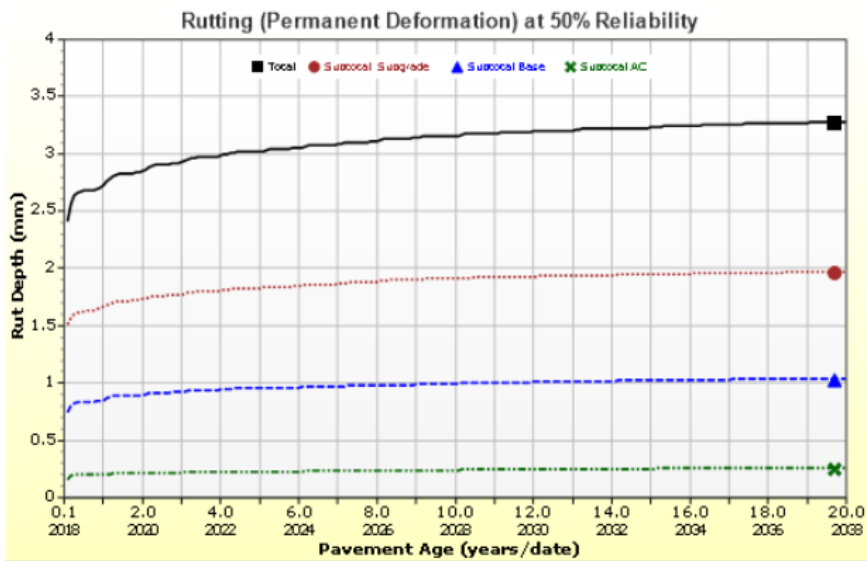
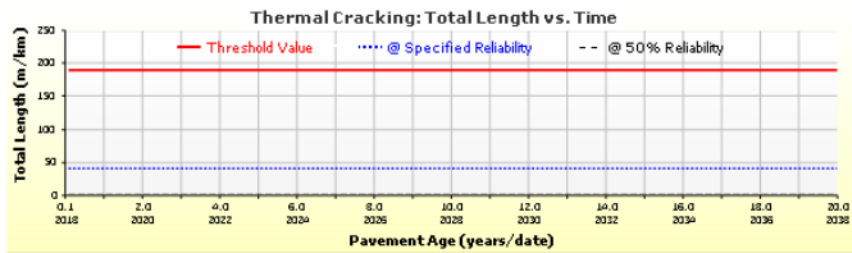
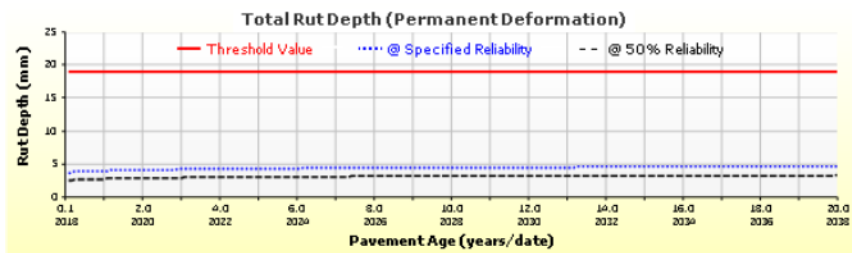
Distress Prediction Summary

Distress Type	Distress @ Specified Reliability		Reliability (%)		Criterion Satisfied?
	Target	Predicted	Target	Achieved	
Terminal IRI (m/km)	2.70	2.70	90.00	89.88	Fail
Permanent deformation - total pavement (mm)	19.00	4.62	90.00	100.00	Pass
AC bottom-up fatigue cracking (percent)	25.00	100.00	90.00	0.00	Fail
AC thermal cracking (m/km)	189.40	40.97	90.00	100.00	Pass
AC top-down fatigue cracking (m/km)	378.80	1436.33	90.00	14.77	Fail
Permanent deformation - AC only (mm)	6.00	0.50	90.00	100.00	Pass

Distress Charts



Analysis Output Charts



HS DRY ARIZONA Pavement ME Design PDF Output



HS_DRY_1ESAL_AZ

File Name: C:\Users\pc\Documents\Michele\Politecnico\TEST\Pavement ME\DESIGNS\HS_DRY_1ESAL_AZ.dgpx



Design Inputs

Design Life: 20 years Base construction: June, 2018 Climate Data: 33.5, -111.875
 Design Type: FLEXIBLE Pavement construction: June, 2018 Sources (Lat/Lon)
 Traffic opening: June, 2018

Design Structure

Layer type	Material Type	Thickness(mm)
Flexible	Default asphalt concrete	50.0
Flexible	Default asphalt concrete	50.0
NonStabilized	A-1-a	300.0
Subgrade	A-1-a	Semi-infinite

Volumetric at Construction:

Effective binder content (%)	11.6
Air voids (%)	7.0

Traffic

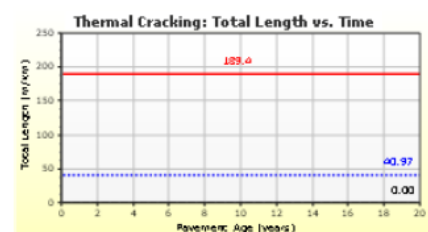
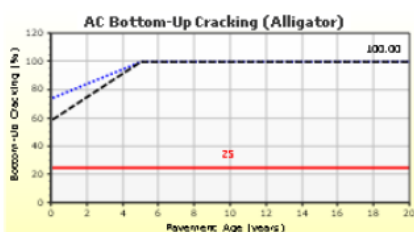
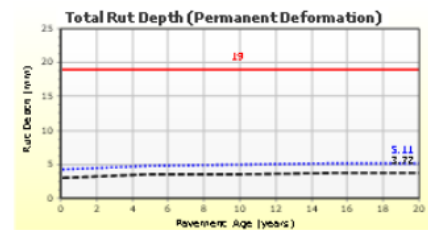
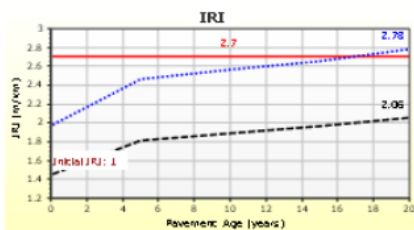
Age (year)	Heavy Trucks (cumulative)
2018 (initial)	4 000
2028 (10 years)	6 939 750
2038 (20 years)	13 879 500

Design Outputs

Distress Prediction Summary

Distress Type	Distress @ Specified Reliability		Reliability (%)		Criterion Satisfied?
	Target	Predicted	Target	Achieved	
Terminal IRI (m/km)	2.70	2.78	90.00	87.30	Fail
Permanent deformation - total pavement (mm)	19.00	5.11	90.00	100.00	Pass
AC bottom-up fatigue cracking (percent)	25.00	100.00	90.00	0.00	Fail
AC thermal cracking (m/km)	189.40	40.97	90.00	100.00	Pass
AC top-down fatigue cracking (m/km)	378.80	2365.85	90.00	0.15	Fail
Permanent deformation - AC only (mm)	6.00	0.78	90.00	100.00	Pass

Distress Charts



— Threshold Value @ Specified Reliability - - - @ 50% Reliability

